THE UNIVERSITY OF ASTON IN BIRMINGHAM

TITLE: FATIGUE PROPERTIES OF A HIGH STRENGTH ALUMINIUM ALLOY

NAME: JING-EN ZHOU

DEGREE: Ph.D. 1982

ABSTRACT

The initiation and propagation of fatigue cracks from notches under constant amplitude loading have been studied in a high strength aluminium alloy 7010-T736. The root radii of the notches varied from 0.11 mm to 5 mm with the depth varying from 5 mm to 10 mm. The various approaches to prediction of fatigue crack initiation from notches were compared. It was concluded that the modified stress intensity factor could be described by introducing a function of microstructural characteristic of material, notch geometry and crack length. This was applied to the prediction of fatigue crack initiation of notches and fatigue crack growth within the notch stress field.

The correlation between fatigue crack growth rates and fatigue striation spacings was established. An empirical equation relating striation spacings and the normalised ΔK was derived and used to predict failure life times.

The effects of shot peening on fatigue crack initiation and propagation from notches were evaluated and it was found that the beneficial effect of shot peening on crack initiation could be expected at low nominal loading level but the reverse was true at high loading levels.

The behaviour of alloy 7010-T736 under variable amplitude loading was investigated. The results suggested that the retardation in fatigue crack growth rates following multiple overloads mainly occurred in the near surface region and the crack growth rates could be retarded by a factor of 8 by a Hi-Lo multiple overload even if the overloads ratio was only 1.17. The fatigue crack propagation rate for alloy 7010-T736 under block spectrum loading was tested and the results were represented by the characteristic stress intensity approach.

KEY WORDS: fatigue, initiation, propagation, fatigue striation, shot peening.

CONTENTS

Page

Page

LIST OF TABLES

LIST OF FIGURES

Page

LIST OF PLATES

Page

ACKNOWLEDGEMENT

I am greatly indebted to Professor J.T.Barnby, my supervisor, for his valuable guidance, help and encouragement. I would like to express my thanks to Dunlop Company for supplying the material. I wish to express my gratitude to Dr.A.Nadkarni for his valuable suggestions and helpful discussion. I also wish to express my thanks to Miss Mary Le Breuilly for her help during the period of the experiments and to the staff of the Department of Metallurgy and Materials Engineering. Finally, my thanks to Mrs.A.Howell for typing this thesis.

1. INTRODUCTION.

Failure due to repeated loading, that is fatigue, has accounted for at least half of mechanical failures (1). Since the term fatigue was first introduced in 1830's (2), considerable effort has been expended in determining the nature of the fatigue damage problem and methods for coping with it in design.

Many criteria for fatigue design from so-called infinite life design to damage tolerant design have been gradually developed. The oldest criterion is one of the unlimited safety, which is based on S-N curves established by experiments. Although this criterion still has its place in engineering, it often leads to conservative designs. The more economical and reliable design criteria based on the developments of fracture mechanics require the knowledge of initiation and propagation of cracks. For intermediate crack propagation rates with typically 10^{-5} - 10^{-3} mm/cycle a good description is given by Paris - Erdogan (3) equation with the form

$$\frac{da}{dN} = A(\Delta K)^m \tag{1.1}$$

where A and m are material constants determined by experiments, and ΔK is stress intensity factor range. The validity of Eq.(1.1) has been confirmed by considerable amount of fatigue crack propagation data collected later, but it does not consider the case in which fatigue cracks initiate and grow from stress concentrator. In practice, however, stress concentration can not be avoided for most engineering components. When suchlike components are subjected to alternating load, fatigue cracks almost always initiate from the stress concentrator and grow in its stress field and then beyond the field to the critical crack length and final fracture. Thus the total lifetime of the components depends on three quantities which can be expressed by the following form

$$N_t = N_i + N_s + N_f \qquad (1.2)$$

where N_t = total number of cycles to failure.

N_i = number of cycles to initiating a crack or cracks from stress concentrator.

N_s = number of cycles of crack growth through the concentrator stress field.

N_f = number of cycles of crack growth to failure beyond the stress field of the concentrator.

The prediction of N_f has been described by Eq.(1.1) already. In recent years more attention has been paid on prediction of the first two terms N_i and N_s (4,5). Two approaches, local stress-strain approach and fracture mechanics approach, and a number of parameters (such as $K_t\Delta S$, $K_f\Delta S$, $\Delta\epsilon$, $\frac{\Delta K}{\sqrt{\rho}}$ and ΔK_n) have been proposed to deal with this problem. Although some success has been made in prediction of fatigue lives with these parameters, the validity of these prediction methods still need to be further evaluated.

The fractographic studies have shown that the size of the fatigue striations can be related to macroscopic crack growth rates and several empirical equations between the range of the stress intensity factor and striation spacings have been established (6,7) for several engineering metal alloys under constant amplitude loading. However, the application of the fractographic technique to study the behaviour of material under variable amplitude loading is relatively rarely reported.

The present project aims at investigating the initiation and propagation of fatigue crack emanating from the blunt notches under constant and variable amplitude cyclic loading. The following specific objectives are to be achieved:

i. To establish interrelationship between some of the mentioned parameters and fatigue crack initiation from notches and its propagation in notch stress field with the emphasis on fracture mechanics approach.

ii. To seek after relationship between fatigue crack growth rates and striation spacings of aluminium alloy 7010 - T736 by fractographic technique.

iii. To evaluate the effects of shot-peening on fatigue crack initiation and propagation.

iv. To study the behaviour of fatigue crack propagation of the material under consideration under variable amplitude loading.

2. HISTORICAL REVIEW OF FATIGUE INVESTIGATION.

The first fatigue investigations were carried out in 1829 by a German mining engineer, W.A.J.Albert (8). The term "Fatigue" was first employed in 1839 by J.V.Poncelet (2), but it was first introduced into literature in 1854 by Braithwaite. During the last fifty years of the nineteenth century the main progress in investigation of fatigue was as follows:

i. During the 1850s and 1860s the first systematic investigation of fatigue was carried out by Wöhler. He presented his results by stress versus life (S-N) diagrams and showed that fatigue failures could occur below the elastic limit, and that there was a certain stress amplitude below which fatigue failure would not occur. Thus Wöhler introduced the concept of the S-N diagram and the fatigue limit.

ii. During the 1870s and 1890s Goodman proposed a simplified theory concerning the influence of mean stress on fatigue.

iii. Bauschinger (9) observed that the limits of proportionality measured in static tension and compression tests could be changed by the application of an alternating stress, but they reached stable values after a few reversals of stress. He regarded the stable values as the "natural" elastic limits and suggested that these corresponded with the limiting fatigue range.

In 1900s the optical microscope was used to pursue the study of fatigue mechanisms. Using the microscope Ewing and Humfrer (10) observed the deformation caused by fluctuating stress and found localized slip lines and slip bands leading to the formation of microcracks.

In 1920s Gough and Hanson (11) considered that the repeated plastic deformation occurring during cyclic stressing gradually decreased owing to work - or strain - hardening. If the stress range was below the fatigue limit the deformation would finally stop, but if not, a limit to the strain hardening would be reached and a crack would be formed. In the same period Griffith (12) analysed the brittle fracture behaviour of components that contain sharp discontinuties and found that the strength of brittle material depended on the size of microscopic cracks. By this pioneering work on the importance of cracks linear elastic fracture mechanics (LEFM) has been established. It is LEFM that has assisted greatly in improving our understanding to fatigue.

Because the classical theory of elasticity was inapplicable to components containing sharp notches Neuber (13) introduced the elementary block concept in 1930s. It was considered that fatigue failure was governed not by the peak stress, but by the average stress over a small volume at the root of the notch.

The linear fatigue damage criterion, an important tool in fatigue life predictions, was formulated by Miner (14) in 1945.

In 1950s the introduction of closed-loop electrohydraulic test systems and the application of electron microscopy greatly pushed forward the investigation of fatigue mechanisms, and in 1957 Irwin (15) introduced the stress intensity factor, K_I, which has been accepted as the basis of LEFM and of fatigue crack propagation life predictions.

In 1960s the publications of the Manson-Coffin (16,17) relationship between plastic strain amplitude and fatigue life and the Paris law were probably the two main advances in the investigation of fatigue. Since then, the use of fracture mechanics as a powerful tool to fatigue has been thoroughly established through practice and through regulations.

3. CHARACTERISTICS OF FATIGUE FAILURE AND FUNDAMENTALS OF LEFM FOR APPLICATION TO FATIGUE.

3.1. Characteristics of Fatigue Failure.

The term "fatigue" refers to the behaviour of materials subjected to a repeated or fluctuating stress as distinguished from the behaviour of materials subjected to a monotonic or static stress. Precisely because of this difference in stress condition some essential characteristics of fatigue failure are observed. They are summarised as follows:

i. Fatigue failures occur at stresses much lower than the static breaking stress and even much lower than the static yield stress.

ii. Macroscopically fatigue failures exhibit lack of deformation in the region of the fractures although both initiation and propagation of fatigue cracks are the results of local plastic deformation and therefore substantially fatigue belongs to stable plastic rupture until fracture (18).

iii. Fatigue failure is a process of cumulative damage under the action of repeated stresses. Usually this process consists of three phases.

  a. The initiation of fatigue crack or cracks.

  b. The sub-critical propagation of fatigue crack.

  c. The final unstable fracture.

  The corresponding aspects of the three phases are exhibited on the fatigue fracture surfaces of typical fatigue failures, i.e. distinct crack initiation site or sites and beach marks or conchoidal marks indicative of crack growth and distinct final fracture region. Fatigue failures suddenly occur after many cycles of stress (e.g. 10^4, 10^5, 10^6 ....) rather than the process of elastic deformation, plastic deformation and fracture under monotonic load. Therefore fatigue failure is a kind of time dependent fracture.

iv. The resistance of materials against fatigue failure is more sensitive than that of materials against static load. The resistance to fatigue not only depends on the materials themselves, but also depends on configurations, sizes, surface conditions of components and environments in which the components operate.

v. Fatigue failure usually belongs to transcrystalline fracture.

In macroscopic respect the purpose of the investigation of fatigue is to pose parameters of materials and mechanical parameters to correlate with fatigue failure through analysis of stress-strain and testing and practical applications. The object is to establish criteria for selecting materials and engineering designs against fatigue failures. The study of fatigue process from microscopic respect can reveal the mechanisms of fatigue crack initiation and propagation and lead to establish models of fatigue failure. The object is to seek for approaches to improve the resistance of materials against fatigue failure. The recent tendency in the investigation is to comprehensively study fatigue process from the two respects.

3.2. Fundamentals of LEFM for Application to Fatigue.

As mentioned above in order to design a structure subjected to a repeated load and to ensure its safety during the service period, it has to be considered how long the pregnant period of initiating a detectable fatigue crack will be, how fast the crack will grow, and at what size of crack fracture will occur. LEFM provides a powerful tool in making these predictions and developing prediction methods. The initiation period, N_i, and the crack propagation rates $\frac{da}{dN}$, can be related to the applied stress intensity factor range, ΔK. The critical crack length at which fracture will occur can be estimated from critical stress intensity factor, K_c or K_{Ic}, called fracture toughness or plane strain fracture toughness. Thus LEFM plays an important role in dealing with fatigue problem and the essential concepts of LEFM are described in this section.

3.2.1. Stress Intensity Factor.

Once a crack is initiated in material, subsequent crack propagation may occur in several ways depending on the relative displacements of the two faces (surfaces) of the crack. Three basic modes of crack surface displacements illustrated in Fig.3.1. are Mode I : the opening mode, Mode II : the sliding mode, and Mode III : the tearing mode. In Mode I, the displacements of the crack

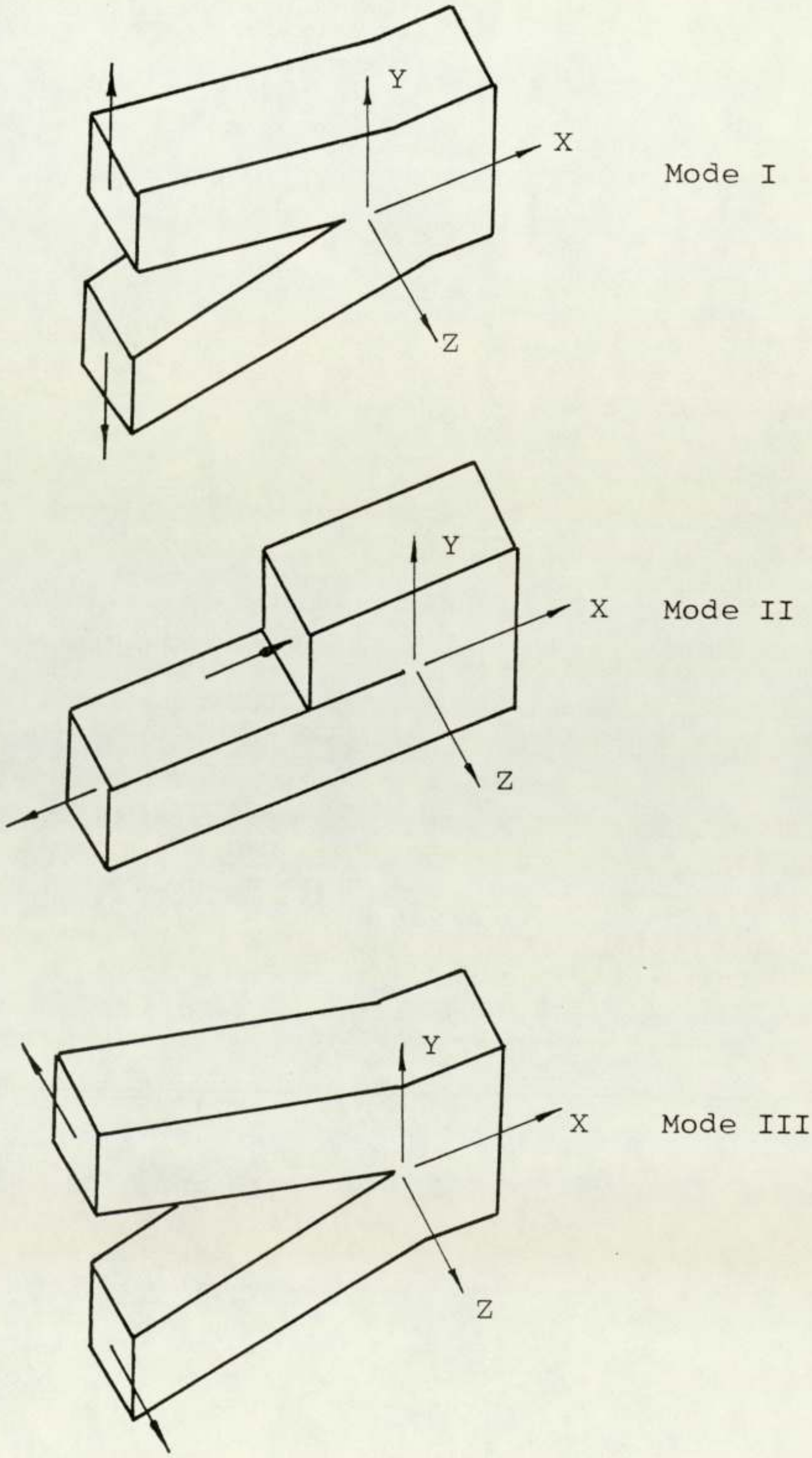

Figure 3.1 Three modes of crack extension.

surface are perpendicular to the plane of the crack. In Mode II, the crack surfaces move normal to the crack edge and remain in the plane of the crack. In tearing mode, Mode III, the crack surfaces move parallel to the crack edge and again remain in the plane of the crack. The most general cases of cracking can be described by superposition of the three basic modes. Mode I is the most common and technically the most important particularly in fatigue. The discussions in this section are confined to Mode I.

The basic equations of linear elastic fracture mechanics adequately describe the stress field at the tip of a crack through stress intensity factor K. Consider a through thickness sharp crack of length 2a in an infinite linear elastic isotropic plate, the plate is subjected to a tensile stress S at infinity. Such a two dimensional crack is schematically shown in Fig.3.2. A stressed element in the vicinity of the crack tip with coordinates r and θ relative to the crack tip and crack plane experiences normal stresses σ_x and σ_y in X and Y directions and a shear stress τ_{xy}. According to the analysis of LEFM these stresses can be described by (19)

$$\sigma_y = \frac{K_I}{\sqrt{2\pi r}} \cos\frac{\theta}{2}\left(1 + \sin\frac{\theta}{2}\sin\frac{3\theta}{2}\right)$$

$$\sigma_x = \frac{K_I}{\sqrt{2\pi r}} \cos\frac{\theta}{2}\left(1 - \sin\frac{\theta}{2}\sin\frac{3\theta}{2}\right)$$

$$\tau_{xy} = \frac{K_I}{\sqrt{2\pi r}} \cos\frac{\theta}{2}\sin\frac{\theta}{2}\cos\frac{3\theta}{2} \qquad (3.1)$$

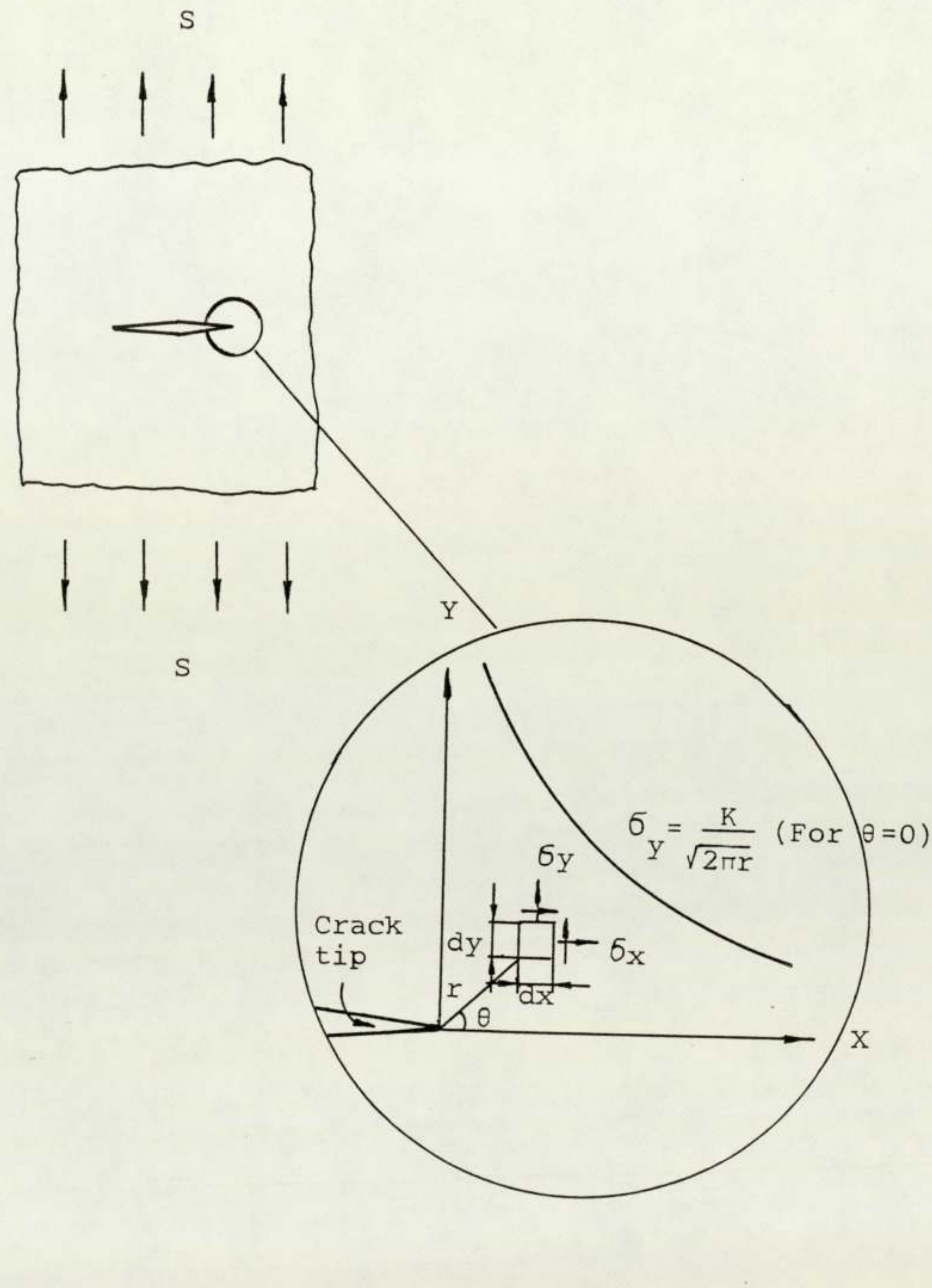

Figure 3.2 Elastic stresses near the crack tip

$\sigma_z = \tau_{xz} = \tau_{yz} = 0$ for plane stress

$\sigma_z = \mu(\sigma_x + \sigma_y)$
$\tau_{xz} = \tau_{yz} = 0$ for plane strain.

where μ is poisson's ratio.

The Eq.(3.1) indicates the elastic normal and shear stresses in the vicinity of the crack tip are dependent on r, θ and K only. The magnitudes of these stresses at a given point are thus dependent entirely on K. The factor K is called a stress field parameter or stress intensity factor. Its value depends on the load, body configuration and crack shape and size. The distribution of the stress σ_y as a function of r at $\theta = 0$ is illustrated in Fig.3.2. Eq. (3.1) are an elastic solution, which does not prohibit that the stresses become infinite at the crack tip. In reality this cannot occur, plastic deformation taking place at the crack tip keeps the stresses finite, so the elastic solution must be modified to account for crack tip plasticity. However, if the plastic zone size r_p at the crack tip is small relative to local geometry, little or no modification to the stress intensity factor, K, is needed as outside the plastic zone the stress field is still described by K, but when large plastic deformation occurs, the case will be different. Thus, an important restriction to the use of LEFM must be kept in mind; it is that nominal stresses in the crack plane must be less than the yield strength. In actual usage the nominal stress in the crack plane should be less than 80% of the yield strength (20).

Stress intensity factor for various loadings and configurations can be evaluated using the theory of elasticity involving both analytical and numerical calculation along with experimental methods. The solutions of K are now available for a wide range of geometrical configurations and many of them have been collected in reference books (21,22).

The most common reference value of K is for a two-dimensional centre crack of length 2a in an infinite plate subjected to a uniform tensile stress S. For this case, K is given by:

$$K = S\sqrt{\pi a} \tag{3.2}$$

The stress intensity factor for other crack geometries, configurations and loadings are generally expressed by the following form:

$$K = S\sqrt{\pi a}\,F\left(\frac{a}{w}\right) \quad \text{or} \quad S\sqrt{\pi a}\,Y \tag{3.3}$$

where Y or $F(\frac{a}{w})$ are dimensionless parameters and usually are given in the form of polynomials.

It should be noted that K is merely the measure of the intensity of stress-strain field at the tip of the crack rather than a property of materials. Thus, it cannot be used to estimate the ability of tolerant-flaws of materials but K can be related to fatigue crack growth rates.

3.2.2. Griffith Criterion.

The basic equation of the condition for the crack to extend was established in 1920 by Griffith. Griffith recognised that a solid containing even an infinitely sharp crack must have a finite strength since a finite amount of surface energy is created as the crqck grows. Thus, when an infinite plate of unit thickness with a through-thickness crack of length 2a is subjected to a uniform tensile stress S, the total potential energy of the system, U, can be written as:

$$U = U_o - U_a + U_\gamma \qquad (3.4)$$

where U_o = elastic energy of the uncrack plate

U_a = decrease in the elastic energy due to introducing the crack in the plate.

U_γ = increase in the elastic-surface energy due to the formation of the crack surfaces.

According to the stress analysis (23) U_a is given by:

$$U_a = \frac{\pi S^2 a^2}{E} \qquad (3.5)$$

where E is elastic module. The elastic surface energy, U_γ, is equal to the product of the specific elastic-surface energy of the material, γ_e, and the new surface area of the crack.

$$U = 2(2a\gamma_e) \qquad (3.6)$$

Consequently, Eq.(3.4) can be rewritten as follows:

$$U = U_o - \frac{\pi S^2 a^2}{E} + 4a\gamma_e \qquad (3.7)$$

Set the first derivative of U with respect to crack length a, equal to zero, result in

$$\frac{dU}{da} = \frac{d}{da}\left(U_o - \frac{\pi S^2 a^2}{E} + 4a\gamma_e\right) = 0$$

$$2\gamma_e = \frac{\pi S^2 a}{E} \qquad (3.8)$$

Eq.(3.8) is the equilibrium condition for crack extension.

The left-hand side of Eq.(3.8) represents the resistance of materials to crack extension, R. The right-hand side of the equation has been designated as the elastic energy release rate, G, i.e.

$$G = \frac{\pi S^2 a}{E} \tag{3.9}$$

The energy condition for crack extension in Eq.(3.8) now states that G must be at least equal to R before crack propagation can occur. Because γ_e is a material property, therefore the left-hand side of Eq.(3.8) is a constant. Hence the criterion for crack extension in brittle materials is that G must exceed a critical value G_{Ic}, i.e.

$$\frac{\pi S_c^2 a}{E} = G_{Ic} \quad \text{or} \quad S_c\sqrt{a} = \sqrt{\frac{EG_{Ic}}{\pi}} \tag{3.10}$$

From Eq.(3.2) and Eq.(3.10) the relationship between K and G is given by:

$$\frac{K_I^2}{E} = G_I \tag{3.11}$$

Eq.(3.11) is valid for plane stress and the following equations given by:

$$\frac{K_I^2(1-\nu^2)}{E} = G \quad \text{and} \quad \frac{K_{IC}^2(1-\nu^2)}{E} = G_{IC} \tag{3.12}$$

are valid for plane strain.

where K_{Ic} and G_{Ic} are plane strain fracture toughness and critical crack extension force or critical elastic energy release rate respectively.

3.2.3 Crack Tip Plastic Zone Size.

As mentioned in Section 3.2.1 the infinite high local stress at the very tip of the crack is physically impossible and in a real situation the stress cannot be higher than the yield stress (24). Plastic deformation must occur, thus creating a plastic zone surrounding the crack tip. Because the local plasticity at the crack tip controls both fracture and crack growth, the determination of plastic zone size by means of theoretical calculation and experimental measurement is of great importance. The simplest estimate of the plastic zone size on the crack plane (θ=0) can be obtained by setting σ_y equal to the yield strength σ_{ys} in the stress field Eq.(3.1), which result in:

$$r_p = \frac{1}{2\pi}\left(\frac{K_I}{\sigma_{ys}}\right)^2 \tag{3.13}$$

Since the load carried by a purely elastic stress distribution must be supported by material in the plastic zone at a constant stress level, this causes the plastic zone to increase to a value of about $2r_p$ (25). Irwin (26) suggested that the plastic zone size under plane strain conditions is smaller than that given by Eq.(3.13) under plane stress conditions because of the increase in the tensile stress for plastic yielding due to plane strain elastic constraint. The yield strength is estimated to increase by a factor of $\sqrt{2\sqrt{2}}$ (27,28). Consequently, the plane strain plastic zone size becomes

$$r_p = \frac{1}{4\sqrt{2}\pi}\left(\frac{K_I}{\sigma_{ys}}\right)^2 = \frac{1}{5.6\pi}\left(\frac{K_I}{\sigma_{ys}}\right)^2 \approx \frac{1}{6\pi}\left(\frac{K_I}{\sigma_{ys}}\right)^2 \tag{3.15}$$

The plastic zone at the tip of a through thickness crack is graphically presented in Fig.3.3.

Under cyclic loading a reversed plastic zone occurs when the tensile load is removed. Rice (25) suggested that the yield stress should be replaced by two times its value. Thus, the cyclic yield zone will be one quarter of the monotonic plastic zone. Lankford and his co-workers (29) experimentally measured the coefficient, α, relating to monotonic plastic zone size and $(K_I/\sigma_{ys})^2$, and the coefficient, α', relaring to cyclic plastic zone size and $(K_I/\sigma_{ys})^2$. The results were presented as follows:

$\alpha \approx 0.06$ to 0.1

$\alpha' \approx 0.014$

Thus, the ratio of monotonic plastic zone size to cyclic plastic zone size is about 4 to 7.

3.2.4 Fracture Toughness - K_c, K_{Ic}

Fracture toughness, K_c, refers to the critical value of K, which can be obtained under condition when a crack extends in a rapid manner without an increase in load or applied energy. K_c is given by:

$$K_c = S_c\sqrt{\pi a_c}\; F(\frac{a_c}{W}) \qquad (3.16)$$

where S_c = applied nominal stress at crack instability

a_c = crack length at instability.

K_c is called fracture toughness and depends on materials, temperature, strain rates, environment, thickness of specimen and crack length. The relationship between

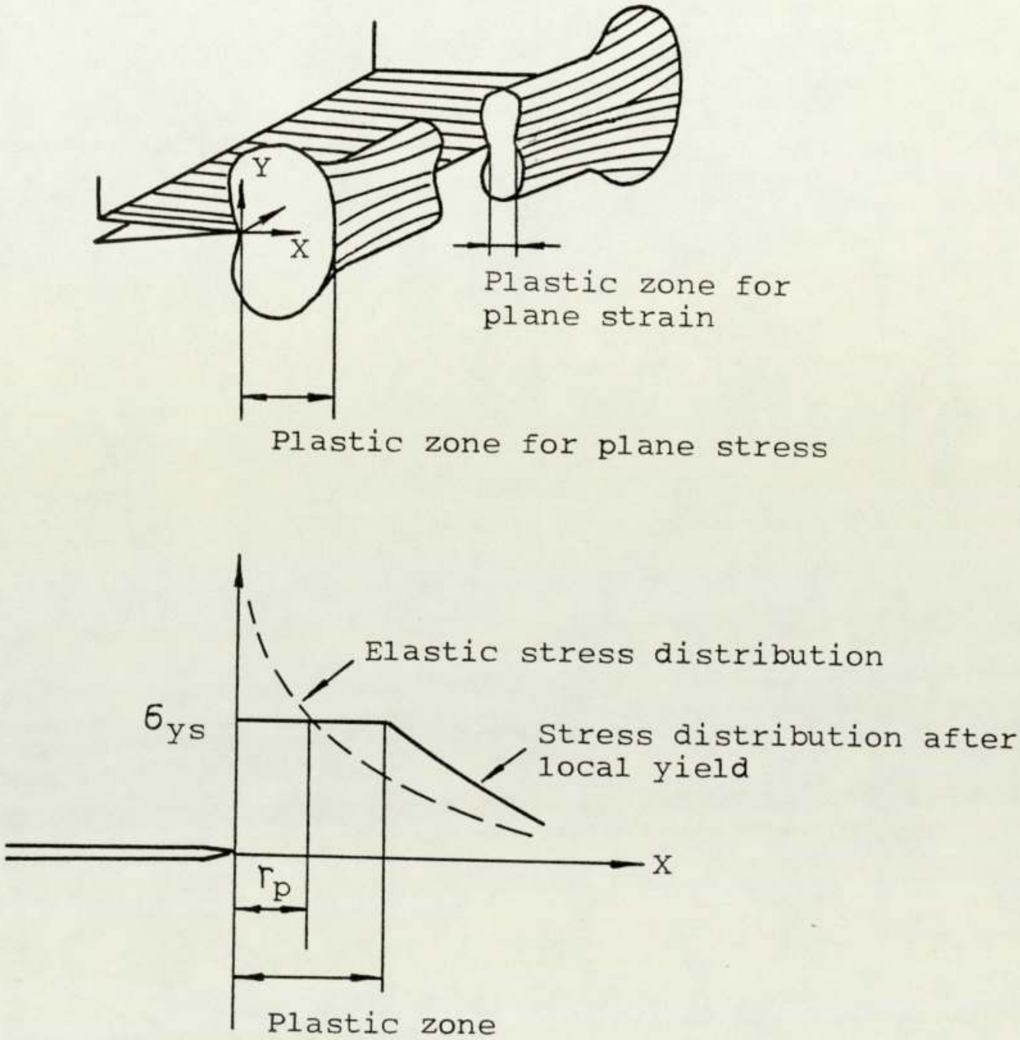

Figure 3.3 Plastic zone and the distribution of the stress component in the crack-tip region.

fracture toughness, K_c, and the thickness of specimens is schematically shown in Fig.3.4. It can be seen that K_c decreases as the thickness increases until a certain value is reached at which a further increase in thickness does not decrease the fracture toughness, i.e. K_c approaches an asymptotic minimum value. The minimum value of fracture toughness is called the "Plane strain fracture toughness", K_{Ic}. K_{Ic} is a property of materials. K_c and K_{Ic} can be used as a quantitative design criterion to prevent brittle fracture involving applied stress and crack size and the critical crack length for failure under cyclic loading can also be estimated using K_c and K_{Ic}.

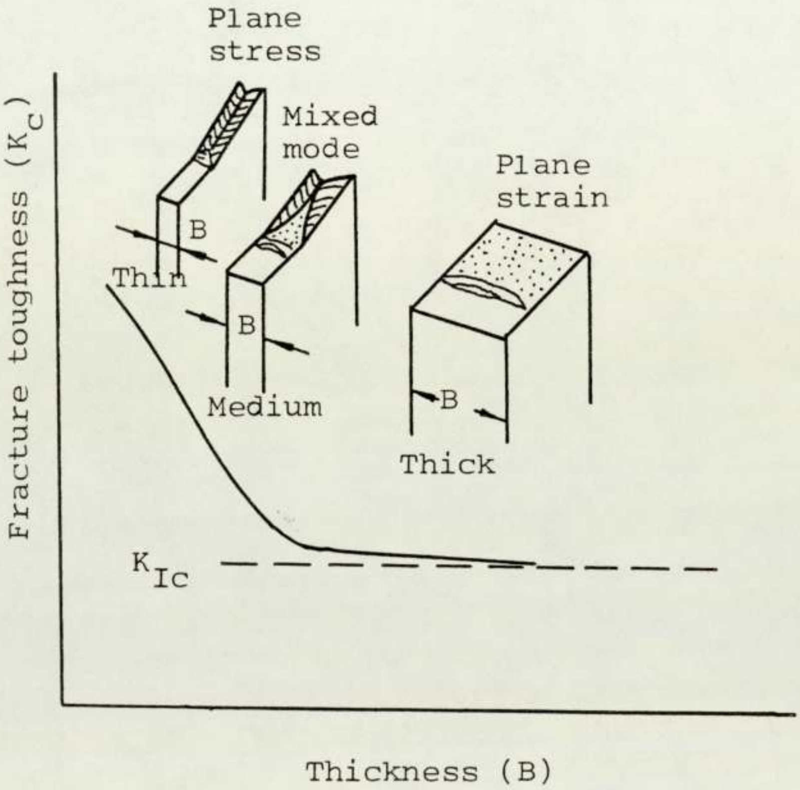

Figure 3.4 Effect of specimen thickness on fracture toughness.

4. CONSTANT AMPLITUDE FATIGUE.

4.1. Introduction.

The data from constant amplitude fatigue (CAF) is the basis for analysing the problems under real variable amplitude loads although the latter is more complex. The essential aspects of mechanisms of variable amplitude fatigue (VAF) are basically the same as CAF. Therefore the investigation of CAF is of primary importance.

As mentioned in Section 3.1 fatigue has been investigated from both microscopic and macroscopic aspects. The microscopic aspect implies that the study of fatigue is carried out from the viewpoints of physics and metallurgy and the macroscopic aspects means investigating fatigue from the viewpoints of applied mechanics and structures (30). The former involves the observation scale 10^{-9}m — 10^{-3}m, which belongs to materials science category; the latter involves the observation scale 10^{-4}m — 10^{2}m, which belongs to the engineering category (31).

4.2. Microscopic Aspect of Fatigue.

4.2.1. Multi-Stage Model of Fatigue.

The process of fatigue failure has been reviewed by a number of researchers (32-34). The multi-stage model of fatigue has been established. It can be summarised as follows:

Stage 1. Cyclic plastic deformation and slip band intrusion and extrusion occur and lead to the formation of persistent slip band (PSB) under cyclic loading.

Stage 2. Fatigue cracks initiate in PSB and propagate in a plane of maximum shear stress (fatigue crack propagation Stage I).

Stage 3. A fatigue crack propagation in a zig zag manner in a plane which is perpendicular to the maximum tensile stress (fatigue crack propagation Stage II).

Stage 4. Final fracture occurs at a critical size of crack due to the fact that the decreased remaining section either cannot support the load any longer or the correspondent stress intensity factor reaches the critical value (K_C or K_{IC}).

4.2.2. Initiation of Fatigue Cracks and Its Early Stage Propagation (Stage I).

The theory based on locally repeated slip for fatigue crack initiation has been widely accepted. In a polycrystalline metal some grains are oriented such that planes of easy slip are in the direction of the maximum applied shear stress. Slip first occurs in these grains under cyclic loading. A systematic accumulation of fine reverse slip movements of the order of 10^{-3} μm (35) leads to the formation of slip lines or bands and causes slip bands intrusion and extrusion. The processes of slip band intrusion and extrusion are schematically shown in Fig.4.1. The number of the slip lines or bands and the size of some of them increase as cyclic loading continues. The depths of the slip bands are different. Most of the slip bands can be eliminated by removing several microns (0.002 mm) from the surface by electropolishing. However, a few slip bands may become more distinct, and thus they have been called "persistent slip bands" (PSB). It has been found that the fatal microcracks occur in PSB due to slip band intrusion.

The process of crack nucleation described above is valid in ductile materials for low strain fatigue. At high cyclic strains, the slip band intrusion and extrusion no longer occur instead of slip step formation at the boundaries of grains on specimen surface and a microcrack may build up at these steps (33). In high strength or brittle metals fatigue cracks have been found to initiate at discontinuities such as inclusions or voids.

Once a crack forms it certainly grows in depth as cyclic loading continues. It is futile to physically make a division between initiation and Stage I crack propagation because both the physical processes involve reverse slip in a similar way. The only difference is that at the beginning reverse slip may produce a groove or pit or an extruded sliver of metal (36), but during crack propagation Stage I the extrusion ceases.

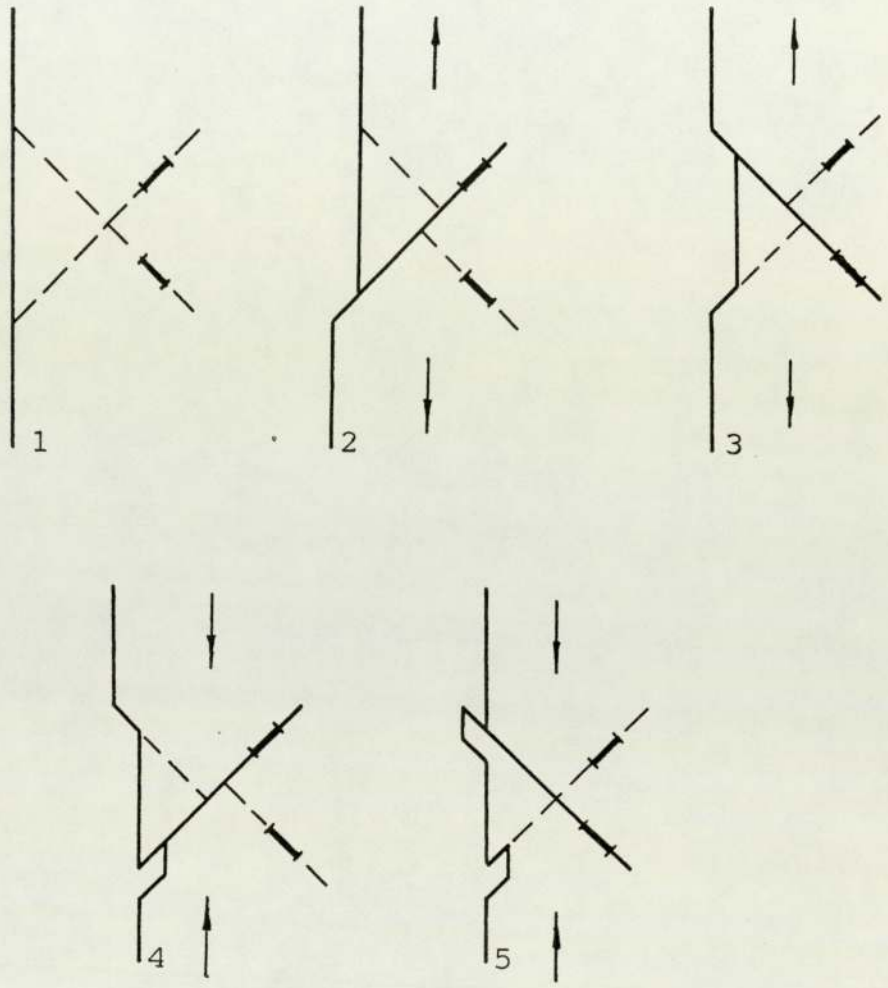

Figure 4.1 Slip band intrusion and extrusion

The initiation of cracks and Stage I crack propagation may occupy as much as 80% - 90% of total life for high cycle fatigue, especially in smooth specimens. However, it also may not exist at all for low cycle fatigue, especially in sharply notched specimens. Various factors can affect initiation of cracks and Stage I crack propagation. It is obvious that improving surface condition may increase the resistance to initiation of cracks. Fine grain size with no embrittled grain boundaries is of benefit to the resistance against initiation and Stage I crack propagation. The size and distribution of inclusions can also affect initiation of cracks. It has been found that in 2024 aluminium alloy the influence of the inclusions (Al_2CuMg and Al_7Cu_2Fe) on initiation of cracks rapidly decreases as the inclusion size is below 7 μm (37).

4.2.3 Fatigue Crack Propagation (Stage II).

4.2.3.1 Metallographic Characteristic of Fatigue Crack Propagation (Stage II) - Fatigue Striations.

One of the metallographic characteristics of fatigue crack propagation (Stage II) is the presence of many parallel plateaus or patches separated by longitudinal ridges. The plateaus are usually normal to the direction of maximum tensile stress. The most marked characteristic is fatigue striations which cover the largest area of the fatigue fracture surface. There are two types of striations commonly observed (38) : ductile striations and brittle striations. Although they have different forms (schematically shown in Fig.4.2), some common characteristics are present and can be summarised as follows:

i. Striations are parallel to each other in each plateau with slightly curved front and locally perpendicular to the direction of crack propagation.

ii. Within a certain range of crack propagation rates one striation represents one load cycle.

iii. Striation spacings vary with stress intensity amplitude.

iv. Mating striations on two mating fracture surfaces will have a peak-to-peak and a valley-to-valley match.

The above mentioned points have been supported by experimental evidence (39). Materials, environments and inclusions can affect the formation of striations. Generally speaking fatigue striations in F.C.C. metals such as aluminium and its alloys are more distinct than those in B.C.C. metals and H.C.P. metals. Wet air accelerates fatigue crack propagation and promotes the formation of striations. A corrosive environment promotes the occurrence of brittle striations. At lower crack propagation rates inclusions only slightly affect striation spacings. At high propagation rates static type fracture occurs due to the higher stress intensity factor and therefore mixed type fracture such as striation plus micro void coalescence has been observed (40). The relationship of single striation to single

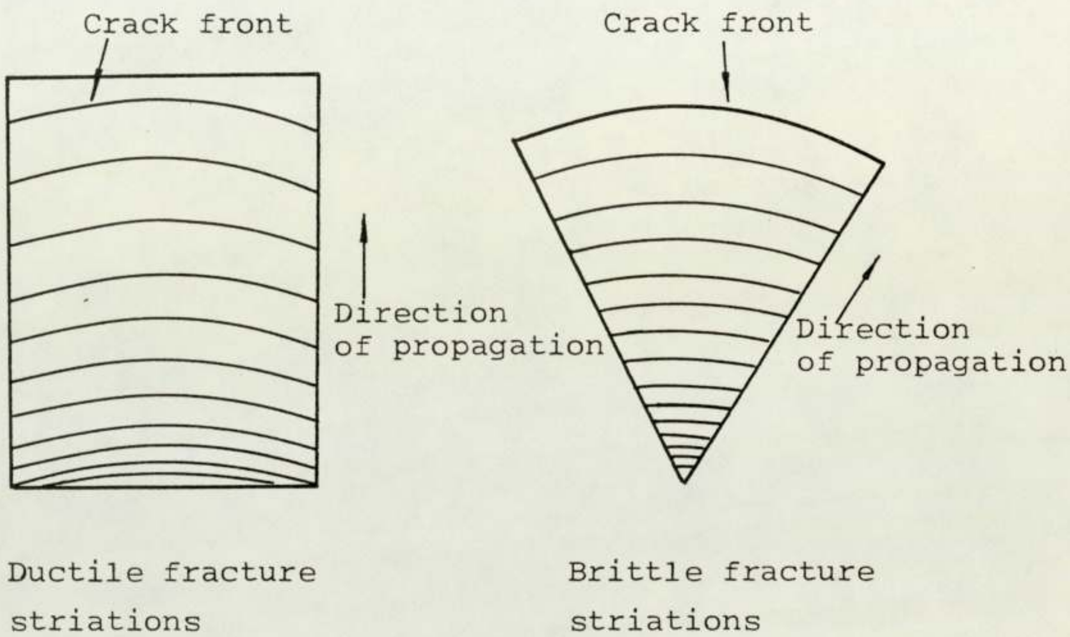

Figure 4.2 Schematic diagrams of two type striations

load cycle in a certain range of fatigue crack propagation rates has been confirmed to be useful in investigation of fatigue crack propagation (38, 39, 41).

4.2.3.2 Fatigue Crack Propagation Theories.

It should be noted that so far no theory which can explain the formations of both ductile and brittle striations exists although various theories have been proposed to deal with the problem of the propagation of fatigue crack during Stage II. In a comprehensive review Weertman (42) divided these theories into two categories. They have been termed accumulated damage or accumulated plastic work theory and shear sliding (geometric) and crack opening displacement theory respectively.

The first is based on the consideration that some sort of "damage" occurs in the plastic region ahead of the crack tip and that material near the tip no longer holds together when this damage has increased to a sufficiently large value. The second was originally proposed by Laird and Smith (43). It is basically a plastic blunting and resharpening model as that illustrated in Fig.4.3. A number of modified models have been formulated by other workers. Neumann (44), Pelloux (45) and Broek and Bowles (46) have made detailed examination of the slip processes. The shear slipping model is schematically illustrated in Fig.4.4. (47). A sharp crack in a tension stress field will initially open with shear slipping along a favourable slip plane (Stage 1, 2), which is

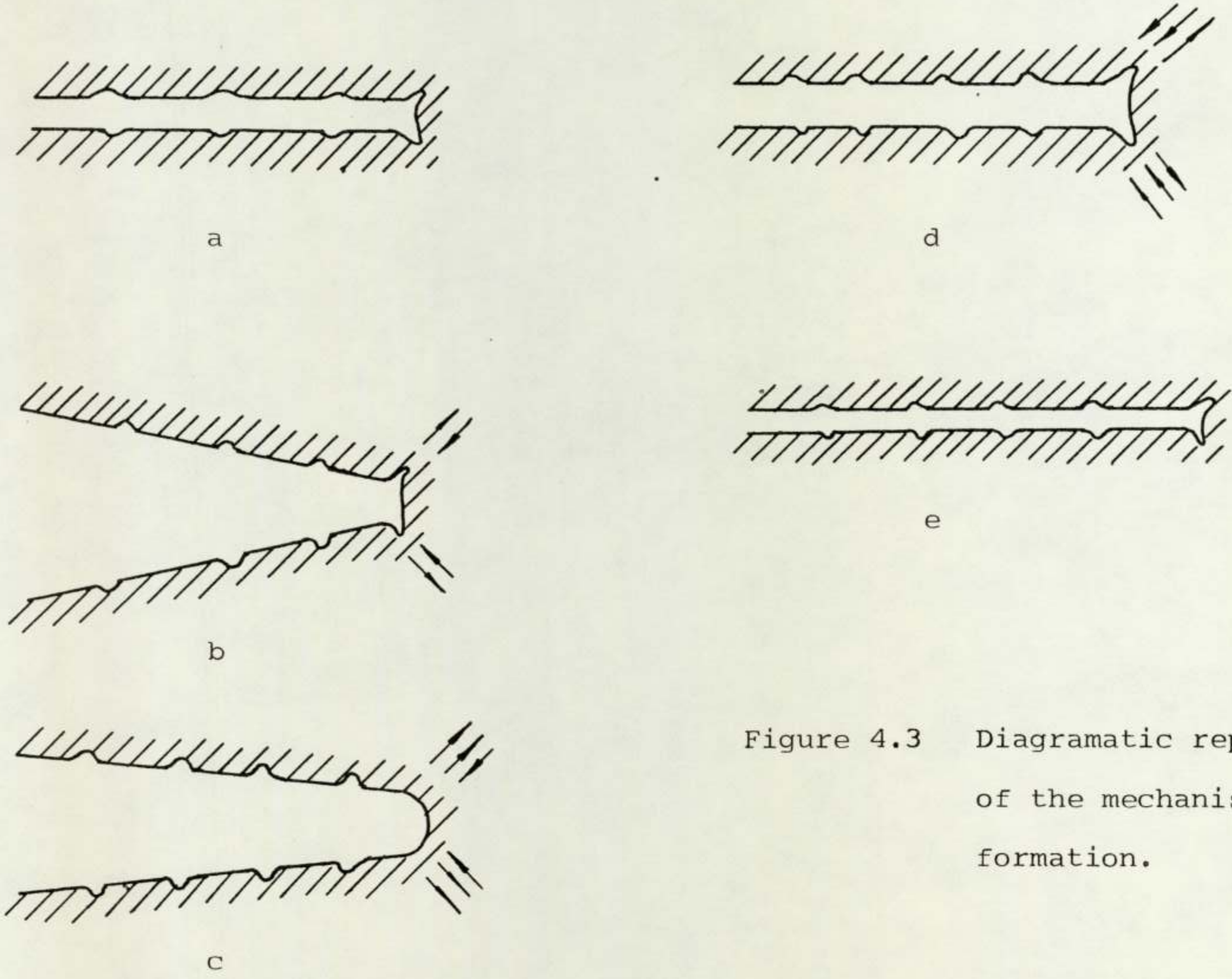

Figure 4.3 Diagramatic representation of the mechanism of striation formation.

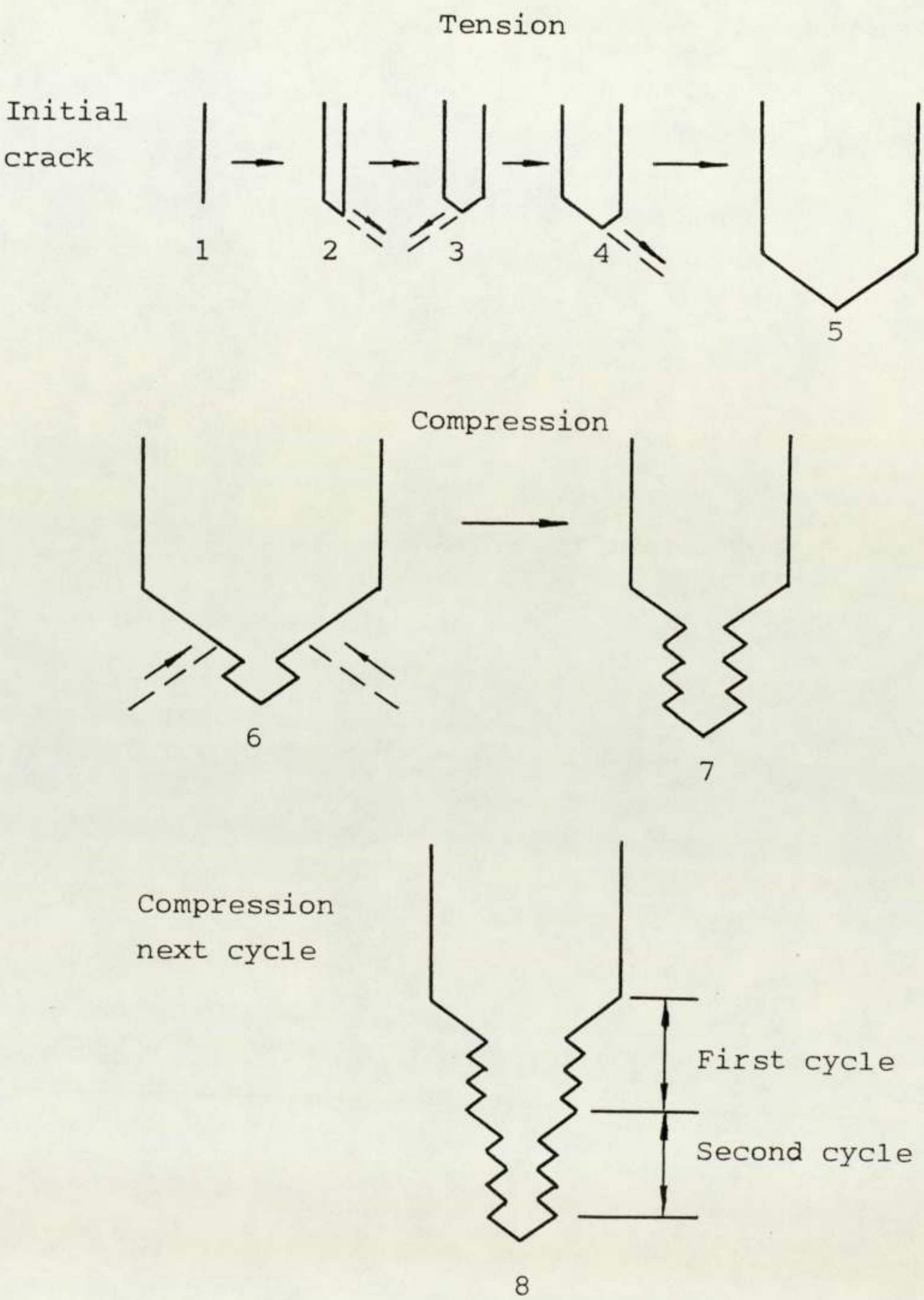

Figure 4.4 The shear slipping model for fatigue crack growth

followed by shear slipping on another favourable slip plane (Stage 3). Slip also may occur simultaneously on both slip planes. In this way the crack is blunted (Stage 4-5). Because plastic deformation has occurred in a small region embedded in elastic surroundings some compressive stresses will be given by the elastic surroundings to the small plastic deformation under a diminishing load, which will cause the reverse slip, but this may not take place on the original plane because of the new free surface oxidation, and slip will occur on a number of parallel planes. Thus, a series of fine slip steps apppear on the fracture surface and a large step or striation is produced during each stress cycle (Stage 6-8).

4.3. Macroscopic Aspects of Fatigue.

In engineering the estimations of crack initiation life and crack propagation rates are indispensible for successful fatigue design. A number of methods have been built up to deal with the predictions of both the periods although none of them is "exact".

4.3.1 Initiation of an Engineering Crack.

The initiation of an engineering crack has been defined to be one which can be easily detected at low magnification, such as 10 X to 25 X. This corresponds to a crack length of 0.127 mm to 0.25 mm (48-51). The early investigation of fatigue were based on the establishment of a S-N diagram. The S-N diagrams represent a dependence of stress on number of cycles to failure. Because almost the entire life is spent of forming a small crack defined as above in higher polished smooth fatigue specimens, especially for high strength materials the S-N diagrams are also considered to represent the dependence of stress on the number of cycles to initiate a crack.

The relationship between nominal stress, S, and the number of cycles or reversals, N or 2N, for failure or initiation of a crack in smooth fatigue specimens for high cycle fatigue (HCF) is given by Basquin's equation (52).

$$\frac{\Delta S}{2} = \sigma_f'(2N)^b \tag{4.1}$$

where $\frac{\Delta S}{2}$ = stress amplitude

σ_f' = fatigue strength coefficient, it is equal to the true stress required to cause fracture on the first reversal of cyclic loading.

b = fatigue strength exponent.

For HCF ($N > 10^5$ cycles) strain is essentially limited in elastic range. Thus, Eq.(4.1) can be rewritten in the following form:

$$\frac{\Delta \epsilon_e}{2} = \frac{\sigma_f'}{E}(2N)^b \tag{4.2}$$

where $\frac{\Delta \epsilon_e}{2}$ = elastic strain amplitude

E = modulus of elasticity.

For low cycle fatigue (LCF) the plastic strain must be considered and the relationship between plastic strain and life can be described by Manson and Coffin equation (16, 17).

$$\frac{\Delta\epsilon_p}{2} = \epsilon_f{}' (2N)^c \tag{4.3}$$

where ϵ_p = plastic strain amplitude

$\epsilon_f{}'$ = fatigue ductility coefficient, it is equal to the true strain required to cause fracture on the first reversal at cyclic loading.

c = fatigue ductility exponent.

The relationship between total strain and life is given by the combination of Eqs.(4.2) and (4.3). It is:

$$\frac{\Delta\epsilon}{2} = \frac{\Delta\epsilon_e}{2} + \frac{\Delta\epsilon_p}{2} = \frac{\sigma_f{}'}{E} (2N)^b + \epsilon_f{}' (2N)^c \tag{4.4}$$

Eq.(4.4) has been modified to account for the effect of mean stress S_m, result in

$$\frac{\Delta\epsilon}{2} = \epsilon_f{}'(2N)^c + \frac{\sigma_f{}' - S_m}{E} (2N)^b \tag{4.5}$$

Since the part of fatigue crack propagation for LCF can not be neglected Manson suggested a correlation between cycles to initiation N_i and cycles to failure N_f (53)

$$N_i = N_f - 4.0(N_f)^{0.6} \tag{4.6}$$

4.3.2 Propagation of Engineering Fatigue Crack.

Numerous fatigue crack propagation laws have been proposed in the last three decades. Hoeppner and Krupp listed as many as 33 laws for dealing with fatigue crack propagation in 1974 (54). Among them Paris-Erdogan law shown in functional form as Eq.(1.1) is preferred due to its relative simplicity and validity of fitting experimental results obtained in various materials. The Paris equation (Eq.(1.1)) usually is graphically represented by a straight line in a log-log plot of $\frac{da}{dN}$ versus ΔK. However, considerable results of experiments show that a typical complete curve in double logarithmic plot of $\frac{da}{dN}$ - ΔK has a sigmoidal shape rather than a straight line and it can be divided into three regions, as shown in Fig.4.5. Region I indicates the existence of a threshold ΔK_{th}, below which no experimentally detectable fatigue crack propagation can be observed. In region III the high growth rates are commonly observed and growth rates become increasingly sensitive to the stress intensity, which implies that K_{max} approaches K_c or K_{Ic} and that striation mechanisms are replaced by mixed mechanisms of striation plus static fracture modes. Region II represents Eq.(1.1).

The theory of fatigue crack growth based on accumulated damage or accumulated plastic work leads to a ΔK exponent of 4 in Eq.(1.1) and the theory based on crack opening displacement leads to a ΔK exponent of 2 in Eq.(1.1) respectively (33). Recently, based on energy balance concepts Irving, Lindley and McCartmey (58, 60) have derived the laws which predict the exponent of ΔK lying between 2 and 4 depending on the size of the reversed plastic zone.

A large amount of experimental results has shown that the exponent in Eq.(1.1) varies between 2 and 4 for steels varying in yield strength from 210 to 2070 Mpa

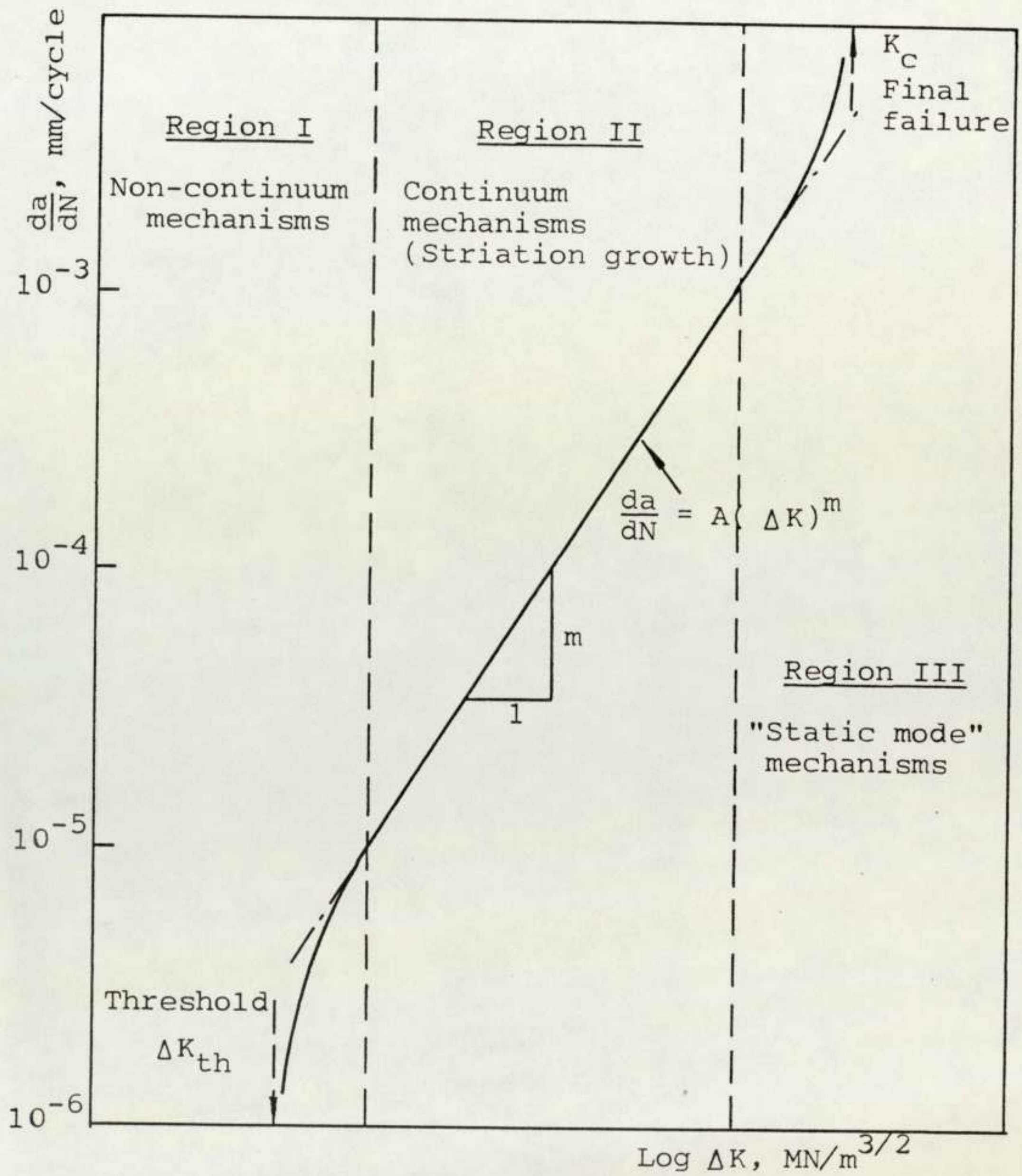

Figure 4.5 Schematic sigmoidal behaviour of fatigue crack growth rate versus ΔK

(30 to 300 Ksi)(55). However, it has been found that many exceptions exist and the values of m in Eq.(1.1) may range from about 2 to 7 (56). For different aluminium alloys the fatigue crack propagation rates in region II vary even more than in steels. For CAF in air the region II is not sensitive to microstructure of materials. The effects of frequency below 200 HZ and wave shape are not important yet. However, the range of threshold stress intensity ΔK_{th} and the behaviour of transition from region II to region III are strongly affected by the microstructure and property of materials. A positive mean stress increases fatigue crack propagation rates in all three regions although relatively less effect of mean stress on crack propagation behaviour in region II has been observed. The effects of mean stress on fatigue crack growth in region II and region III has been studied by a number of workers and Forman equation (55) has been generally accepted, which is in the form:

$$\frac{da}{dN} = \frac{A(\Delta K)^m}{(1-R)K_c - \Delta K} \qquad (4.7)$$

where R = stress ratio = $\frac{S_{min}}{S_{max}} = \frac{K_{min}}{K_{max}}$

The results of experiments have shown that the fatigue crack growth at threshold region is strongly influenced by mean stress. The data compiled by Lindley and McCartney (58) for mild and low alloy steels with lower yield or 0.2% proof stresses of less than about 600 Mpa demonstrate that threshold stress intensity range ΔK_{th} could decrease by a factor of about 2 to 4 for R increasing from zero to 0.9. The similar effect of R on

ΔK_{th} has been observed in aluminium alloy (59).

4.4. Notches and Their Effects on Initiation and Propagation of Fatigue Cracks.

Notches not only affect initiation of fatigue cracks, but also affect propagation of cracks within a certain growth extension. Traditionally the notch effects are evaluated using stress concentration factor K_t and fatigue notch factor K_f, which are defined as the ratio of the maximum stress related to the notch to the nominal stress based on the net section and the ratio of fatigue life on un-notched specimen to that of notched specimen, respectively. During the past two decades the local strain approach for initiation of fatigue cracks at a blunt notch root has been gradually established (61-66). More recently, the fracture mechanics approach has been developed to deal with the initiation of fatigue cracks from a notch root (67-72). Both approaches involve the determination of a characteristic parameter to describe the stress-strain field at the notch root. As for propagation of a fatigue crack emanated from a notch root, it seems that the fracture mechanics provides a most feasible approach as described in section 4.3.2 and later sections.

4.4.1 Prediction of Initiation of Fatigue Cracks from Blunt Notches.

4.4.1.1 Stress Concentration Approach.

On the basis of the assumption that the fatigue crack initiation at a notch root in a notched member is controlled by local elastic stress, the parameter $K_t \Delta S$ has been employed to deal with the prediction of fatigue crack initiation in the form (73)

$$N_i = B(K_t \Delta S)^n \tag{4.8}$$

where ΔS = nominal stress range

B, n = experimental constants.

In Eq.(4.8) K_t is elastic stress concentration factor and is calculated by elastic theory. Thus, it does not consider the effect of local yielding on stress distribution at the notch root. To take this effect into account an effective stress concentration factor or fatigue notch factor K_f is introduced and results in:

$$N_i = B(K_f \Delta S)^n \tag{4.9}$$

It seems that Eq.(4.9) could give better prediction of fatigue crack initiation life compared with Eq.(4.8). Unfortunately, it has been found that K_f depends on many factors such as the characteristics of materials, the nature of the load, the geometry of the notch and the investigated fatigue life range, and thus the difficulty in the determination of K_f limits the application of Eq.(4.9) in practice.

4.4.1.2 Local Strain Approach.

This approach is based on the assumption that as long as the local strain amplitude at a notch root is equal to the strain amplitude of a smooth specimen then the same fatigue life will be given. Thus, if the local strain amplitude can be determined then Manson-Coffin equation (Eqs.(4.4) or (4.5)) can be used to predict the life of initiation of cracks. This can be done by means of Neuber's rule. The severity of concentration of stress and strain caused by a notch is measured by the elastic stress concentration factor K_t. In fatigue, however, notches may be less effective than that predicted by K_t because of the local plastic deformation at the notch roots. Therefore, K_t should be replaced by K_f, the effective stress concentration factor or the fatigue notch factor.

According to Neuber's rule:

$$K_\epsilon K_\sigma = K_t^2 \qquad (4.10)$$

for monotonic loading.

For the case of fatigue Eq.(4.10) becomes:

$$K_\epsilon K_\sigma = K_f^2 \qquad (4.11)$$

due to the consideration discussed above.

where $K_\sigma = \frac{\Delta\sigma}{\Delta S}$ = stress concentration factor

$K_\epsilon = \frac{\Delta\epsilon}{\Delta e}$ = strain-concentration factor

ΔS and Δe = nominal stress and strain amplitude

and $\Delta\sigma$ and $\Delta\epsilon$ = local stress and strain amplitude at notch root.

result in

$$K_f = \left(\frac{\Delta\sigma}{\Delta S} \frac{\Delta\epsilon}{\Delta e} \right)^{\frac{1}{2}} \qquad (4.12)$$

$$K_f(\Delta S \Delta e\, E)^{\frac{1}{2}} = (\Delta\sigma \Delta\epsilon E)^{\frac{1}{2}} \qquad (4.13)$$

Usually the nominal stress and strain are limited to the elastic region for fatigue, hence Eq.(4.13) becomes the following simple form:

$$K_f \Delta S = (\Delta \sigma \Delta \epsilon E)^{\frac{1}{2}} \quad (4.14)$$

Combining Eq.(4.14) and the equation of strain-stress curve, which is represented by

$$\frac{\Delta \epsilon}{2} = \frac{\Delta \epsilon_e}{2} + \frac{\Delta \epsilon_p}{2} = \frac{\Delta \sigma}{2} + \left(\frac{\Delta \sigma}{2K'}\right)^{1/n'} \quad (4.15)$$

where n' = cyclic strain hardening exponent

K' = cyclic strength coefficient

the solution of $\Delta \sigma$ and $\Delta \epsilon$ can be obtained.

Substituting the value of $\Delta \epsilon$ into Eq.(4.4) or (4.5) the life of initiation of cracks can be predicted.

Again, the difficulty arises due to the requirement of K_f. Many attempts have been made to determine the value of K_f analytically. Two similar formula have been proposed by Neuber and Peterson (74).

They are:

$$K_f = 1 + \frac{K_t - 1}{1 + \sqrt{\frac{a^*}{\rho}}} \quad (4.16)$$

and

$$K_f = 1 + \frac{K_t - 1}{1 + \frac{\rho^*}{\rho}} \quad (4.17)$$

where ρ = radius of notch root

a^* and ρ^* = materials constants.

The values of a^* and ρ^* for a number of materials can be found in Ref.(74) and (75).

4.4.1.3 Fracture Mechanics Approach.

The theoretical basis of fracture mechanics approach for prediction of fatigue crack initiation was given by a dislocation model developed by Bilby and Heald in 1967 (76). On the basis of an analysis of the plastic relaxation at a crack tip they assumed that crack initiation will occur when the summation of the plastic displacement ϕ per cycle reaches a critical value ϕ_c. This results in an expression:

$$N_i = \frac{2\gamma G}{\pi(\Delta K)^2} \tag{4.18}$$

where γ = plastic work done per unit area of fracture and $\gamma = \phi_c \sigma_y$

G = elastic shear modulus.

Eq.(4.18) demonstrates that N_i should be inversally proportional to the square of the range of stress intensity factor.

Bilby and Heald obtained ϕ_c by linear summation of the individual displacements. Jack and Price (68) argued that the critical displacements ϕ_c should be obtained by the summation of the square of the individual displacements and then they suggested that the relationship between N_i and ΔK should be taken the form:

$$N_i \propto (\Delta K)^{-4} \tag{4.19}$$

and for the case of a blunt notch ΔK should be substituted by the effective stress intensity factor range, ΔK_{eff} which is given by:

$$\Delta K_{eff} = \Delta K \left(\frac{\rho_o}{\rho'}\right)^{\frac{1}{2}} \tag{4.20}$$

where ρ_o = critical value of notch root radius below which notches can be treated as a crack

ρ' = effective root radius and

$\rho' = \rho$ when $\rho > \rho_o$

$\rho' = \rho_o$ when $\rho < \rho_o$

results in

$$N_i = B\left(\Delta K\sqrt{\frac{\rho_o}{\rho'}} \right)^{-4} \tag{4.21}$$

where B = constant involving materials and applied stresses.

Other fracture mechanics parameters proposed to deal with initiation of fatigue cracks are the relative stress-intensity factor range $\frac{\Delta K}{K_a}$ (69) and $\frac{\Delta K}{\sqrt{\rho}}$ (77). Forman (69) defined K_a as the apparent fracture toughness in the form

$$K_a = \left(\frac{r_n}{r_p}\right) K_c \quad . \tag{4.22}$$

where r_p = plastic zone size for a sharp crack when stress intensity factor is equal to K_c.

r_n = Plastic zone size for a blunt notch with a depth being equal to the sharp crack and at the same stress.

Then he used $\frac{\Delta K}{K_a}$ as a parameter to represent the experimental results. Many workers employed $\frac{\Delta K}{\sqrt{\rho}}$ as a parameter to describe the behaviour of fatigue crack initiation at notch tips and similar results have been reported in various materials (67, 72, 51, 78).

Despite the fact that some success has been made for the three fracture mechanics parameters in the prediction of fatigue crack initiation, there is still argument in using these parameters as the K - calibration for cracks emanating from notches fall to zero at the notch tip. Recently, Barnby and Nadkarni (79) have developed a function to deal with this problem. They considered that the slip band could be taken as a short crack at the notch tip. Thus, the equations proposed by Jergeus (71) can be modified for prediction of initiation of fatigue cracks at notches. The original Jergeus' equation for K - calibration in notch stress field is in the form

$$K = 1.122S\sqrt{\pi a} \tag{4.23}$$

where $$a = a_o(1 - \exp(-4(1 + \sqrt{\frac{a_o}{\rho}})C / \sqrt{a_o\rho})) + C \tag{4.24}$$

a_o = notch depth

and C = crack length

If Eqs.(4.23) and (4.24) are generally re-written in the following form

$$K = YS\sqrt{a} \tag{4.25}$$

then for a long crack beyond the notch stress field a is equal to $a_o + C$ and Y is equal to the standard K - calibration factor Y_L. For a short crack within the notch stress field if a is still equal to $a_o + C$ then $Y(Y_n)$ is given by

$$Y_n = Y_L\left[(a_o(1 - \exp(-4(1 + \sqrt{\frac{a_o}{\rho}})\frac{C}{\sqrt{a_o\rho}})) + C) / (a_o + C)\right]^{\frac{1}{2}} \tag{4.26}$$

Eq.(4.26) was modified (79) to

$$Y_n = Y_L\left[(a_o \tanh(2\sqrt{1 + \frac{a_o}{\rho}}\ (C + C_B) / \sqrt{a_o\rho}) + (C + C_B)) / (a_o + C)\right]^{\frac{1}{2}} \tag{4.27}$$

where C_B is material parameter which was considered to be grain size or mean free path (50). Eqs.(4.25) and (4.27) can be used to calculate the effective stress intensity factor for a blunt notch to describe the fatigue crack initiation and fatigue crack propagation in the notch stress field.

4.4.2 Propagation of Fatigue Crack in Notch Stress Field.

It has been found that fatigue crack growth rates decrease as the crack length increases within a certain distance from the notch tip in a notched member (67). The discrepancy with the traditional fracture mechanics concept of fatigue crack propagation for which stress intensity and crack growth rates increase continuously with increasing crack length is attributed to the effect of the notch stress field. It is obvious that this effect of the notch will reduce gradually as the crack propagates and at a critical crack length C_o, the effect will no longer exist and the notch can be treated as a crack which has the same length as the notch.

Many attempts have been made to establish the relationship between the contribution of notches and stress intensity factors. Smith and Miller (80, 81) suggested an equivalent crack to account for the contribution of a notch. For an elliptical edge notch they defined the equivalent crack L with the length given by:

$$L = e + C \tag{4.28}$$

$$e = 7.69\sqrt{\frac{a_o}{\rho}}\, C \tag{4.29}$$

result in

$$L = \left(1 + 7.69\sqrt{\frac{a_o}{\rho}}\right) C \tag{4.30}$$

for $C < C_o$

where e = contribution of the notch to the crack length.

C = length of a crack emanating from the notch root.

Eq.(4.30) suggests a linear dependence of notch contribution on crack length. A more complicated dependence on the contribution of the notch to the crack length was proposed by Jergeus (71), which is:

$$e = a_o(1 - \exp(-4(1 + \sqrt{\frac{a_o}{\rho}}\,)C / \sqrt{a_o\rho}\,)) \qquad (4.31)$$

It is noteworthy that in Eq.(4.27) the contribution of a notch was included in a function of the K - calibration factor rather than an equivalent crack. However, if the standard function of K - calibration factor is preferred, the dependence on the contribution of a notch to the crack length can also be derived. It is:

$$e = a_o \tanh(2\sqrt{1 + \frac{a_o}{\rho}}\,(C + C_B) / \sqrt{a_o\rho}) + C_B \qquad (4.32)$$

By comparison of Eqs.(4.30), (4.31) and (4.32), it can be seen only Eq.(4.32) overcomes the difficulty of stress intensity factor K falling to zero at the notch tip and therefore it can be used for prediction of initiation of fatigue cracks from a blunt notch as discussed in the last section.

The critical crack length C_o has been estimated by a number of workers. The suggested values are listed in Table 4.1.

Table 4.1

Values of Crack Length C_o Which Indicates the Extent of Notch Stress Field as Suggested by Different Investigators.

C_o	Investigator	Ref.
$0.13\sqrt{a_o\rho}$	Smith	(82)
0.2ρ	Dowling	(66)
$0.5\sqrt{a_o\rho}$	Jergeus	(71)
$0.25\sqrt{a_o\rho}$	Novak and Barsom	(83)
$(w - a_o)\,\xi_o$	Yamamoto	(70)
$\xi_o = 1 - \exp\left(-\frac{0.5\sqrt{a_o\rho}}{w - a_o}\right)$		

4.5 Effects of Shot-Peening on Fatigue Resistance of Materials.

It is well known that compressive self-stresses on the surface of parts are beneficial to fatigue strength. The compressive self-stresses can be introduced by two processes: mechanical methods and thermal processes. Probably, shot-peening is one of the most widely used mechanical methods for producing suchlike self-stresses. In practice shot-peening has been applied to many automative components such as valve springs, suspension springs and other steel parts. In aerospace industry shot-peening is limited to improve fatigue resistance of high strength aluminium alloys.

According to Ref(84) fatigue strength of a number of high strength aluminium alloys can be increased by a factor of 23% to 34% due to shot-peening. Nordmark (85) tested welded 5456-H321 aluminium alloy and found that the fatigue resistance was improved significantly by peening the weld and the heat affected zone. Similar conclusion was drawn by Campbell (86). The beneficial effects of shot-peening on the resistance to fatigue and stress-corrosion cracking of 7075-T6 aluminium alloy has been reported by Was and Pelloux (87) and Sprowls and Brown (88) respectively. Other investigator (89) pointed out that the heavier peening processes can result in a substantial reduction in fatigue properties whilst the more gentle processes will generally result in improved fatigue properties. Most of these results are referred to smooth specimens and welded workpieces. Little work has been done on the effects of shot-peening on crack initiation from a stress concentrator.

The effectiveness of shot-peening depends on the property of materials which are to be peened and several inter-dependent parameters employed in the peening process. The relationship between these parameters is schematically illustrated in Fig.4.6. Among the parameters intensity is most important for quality control of shot-peening. The intensity is expressed by the arc height of standard test trips,which are made of cold rolling spring steel, under full coverage conditions. During the peening process the test strip is firmly attached to the strip hold and exposed to the shot stream in exactly the same manner as the specimens. When it is then removed from the hold, it will be curved convex toward the peened side. The arc height of the curved strip then is measured using Almen gauge and it is used to represent the peening intensity (90). Usually the appropriate intensity is the lowest peening intensity capable of producing the desired effect. Exceeding intensity will induce folds or other defects on the surface or produce high tensile stress in the core material and thus the beneficial effect of the compressive self-stresses at surface will be partly or completely cancelled.

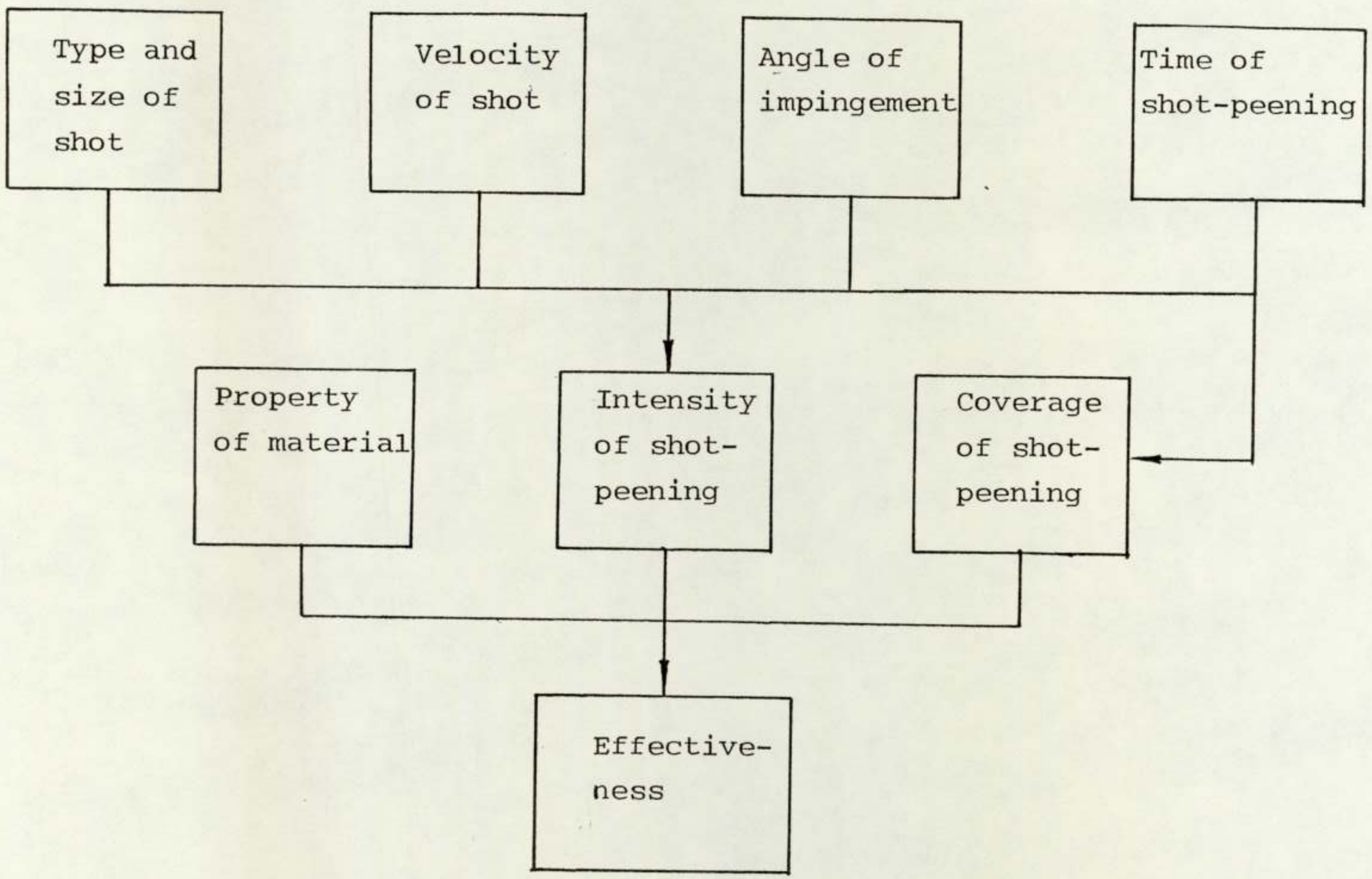

Figure 4.6 Interdependency of parameters of shot-peening

5. FATIGUE CRACK GROWTH UNDER VARIABLE AMPLITUDE CYCLIC LOADING.

5.1. Introduction.

Real engineering structures are usually subjected to irregular cyclic loading histories. The variations in load history parameters may affect the life of suchlike components significantly. In order to develop accurate prediction methods of variable amplitude fatigue lives the thorough understanding of the effects of loading variables on crack initiation and propagation is essential. Unfortunately, the state-of-the-arts have not reached this stage yet despite the fact that some techniques of analysis for fatigue from real load histories are available in literature.

5.2 Brief Review of the State-of-the-Arts.

The results of traditional S-N approach and Miner's linear damage law are still employed to deal with crack initiation and early stage of fatigue process under variable amplitude load fluctuations in engineering design (91-94). The fracture mechanics investigations of variable amplitude fatigue have concentrated on the later stage of fatigue process, i.e. the fatigue crack propagation behaviour of materials. Some significant results of the investigations from both microscopic and macroscopic aspects are summarized as follows:

i. The variations of loading variables affect both crack initiation and crack propagation (95, 96).

ii. The effects of loading sequences on crack initiation are different from that on crack propagation (95).

iii. Overloads within certain amounts result in the lengthening of crack initiation life and the retardation of crack propagation (96).

iv. Underloads accelerate crack propagation rate and therefore decrease crack growth life (97).

v. The effects of overloads on crack growth can be explained by crack closure and compressive residual stresses around crack tip, which are induced by the overloads (98, 99).

On the basis of the above-mentioned observations and findings many models for prediction of fatigue crack growth life under spectrum loading have been proposed. These models can be generally divided into two categories: calculating the crack propagation cycle-by-cycle and calculating the crack propagation by characteristic stress intensity factor (98, 100). Although a number of new models (101, 102, 103) have been proposed for cycle-by-cycle prediction method in recent years, three models formulated in the early 1970s by Wheeler (104), Willenborg (105) and Elber (106) are still the basic models for dealing with fatigue crack propagation under variable amplitude loading. The idea of Wheeler's model and Willenborg's model can be briefly described as follows. The tensile overload induces a large plastic zone in front of the crack tip. If the overload is followed by a smaller load, smaller plastic zone embedded in the prior larger plastic zone will be induced by the current load. The compressive residual stresses developed in the overload plastic zone, which are caused by the restoration of the elastic surroundings give some reduction of the effective mean stress or stress ratio R and, thus the growth is retarded. This effect of retardation will maintain as long as the crack tip is in the plastic zone induced by the overload. The Elber's crack closure model is based on the following findings. It was found that following a high stress peak the crack did close before the load applied became zero,and when smaller amplitudes followed, that it did not open until the load reached a certain level above zero. Elber assumed that crack extension occurred only when the applied stress was greater than the crack opening stress. Thus the controlling stresses in crack growth process should be the maximum stress and the crack opening stress within a cycle and in this way the effective stress range $\Delta\sigma_{eff}$ was introduced by

$$\Delta\sigma_{eff} = \sigma_{max} - \sigma_{op} \qquad (5.1)$$

where σ_{op} is the crack tip opening stress determined experimentally. The effective stress ratio U and the closure factor C_i were defined by

$$U = \frac{\Delta\sigma_{eff}}{\Delta\sigma} \qquad (5.2)$$

and $$C_i = \frac{\sigma_{op}}{\sigma_{max}} \qquad (5.3)$$

result in

$$\Delta\sigma_{eff} = U\,\Delta\sigma = U(\sigma_{max} - \sigma_{min}) \qquad (5.4)$$

and $\Delta \sigma_{eff} = \Delta \sigma_{max} (1 - C_i)$ (5.5)

Substituting $\Delta \sigma_{eff}$ given by Eq.(5.4) or Eq.(5.5) into stress intensity factor solutions the effective stress intensity factor range ΔK_{eff} can be calculated and then Paris equation given by

$$\frac{da}{dN} = A(\Delta K_{eff})^m \qquad (5.6)$$

can be used for computation. The results later published by a number of investigators (107-112) showed that crack closure is complex phenomenon and depends on many factors. The values of U and C_i are not constants and, therefore difficulties occur for the use of crack closure model. This will return in a later section. The other calculation method for fatigue crack growth prediction is the use of Forman equation (57), for which the effect of retardation by high tensile loads is neglected.

The validity of the above mentioned methods was surveyed by Schütz (100). It is concluded that none of the models proposed by Wheeler, Willenborg and Elber have reliably shown convincing improvements compared with the Forman model. Moreover, the former three models require substantial numerical calculations with high speed computers and can be quite expensive. However, when the load histories are consisted of infrequent overloads with high overload ratio and minor loads, the effects of retardation caused by the overloads cannot be neglected. For this case the Forman model is not applicable and one of the mentioned three models could be employed to deal with this situation although the accuracy of the prediction is not often satisfactory.

The characteristic stress intensity factor method is based on the idea of finding a constant stress intensity amplitude ΔK_{equ} . which is equivalent (with regard to crack propagation) to the real service stress intensity amplitudes. The root mean square (r.m.s.) of the realistic sequence was thought by some to be that equivalent (113). Obviously, no interaction effect of loading sequences can be taken into account in this way. However, if the real history is in random sequence with a narrow frequency band or the real history can be replaced by a number of blocks of constant maximum and minimum load with random sequence and no severe changes in loading variables between the blocks exist, the method of characteristic stress intensity factor, say ΔK_{rms} , probably could be expected to give an applicable prediction of fatigue crack growth since in the two cases there will be no definable sequence, or no significant sequences. It should be noted that in many cases the collection and monitoring, data analysis and simulation of real service loading may dominate the accuracy of the prediction rather than the prediction method employed itself.

The efforts have been spent on the investigation of fatigue crack propagation process under spectrum loading and crack closure phenomenon by electron microscope fractography (99, 114). It was shown that the retardation and acceleration in fatigue crack propagation rates can be illustrated through fatigue striation measurements and that the crack opening stress intensity factor can be determined by fractographic technique. Since the relationship of one cycle and one striation only exists within a certain range of fatigue crack growth rates and no identifiable striations can be observed for some materials, this technique has some limitations when it is employed to study fatigue failure process, but obvious advantages of the technique still exist, for example no other method can study fatigue cycle-by-cycle.

6. THE HIGH-STRENGTH ALUMINIUM ALLOY 7010.

The alloy 7010 is one of the 7XXX series of high strength aluminium alloys, in which zinc, magnesium and copper are the main alloying elements and high Zn : Mg ratio enables the alloy to produce a high level of strength after heat treatment. The higher amount of copper in 7010 compared with other 7XXX series alloys improves the resistance to stress corrosion cracking.

Compared with the well established alloy 7075 other important features of its composition are considered to be (115, 116)

i) By using a high purity base aluminium, which has a controlled and low iron and silicon contents, the volume fractions of undissolved second phases is minimized and thus the toughness of the material is improved.

ii) The introduction of 0.14% zirconium in place of 0.2% chromium makes it less sensitive to quench rates, which allows the increase in thickness of a useful material without the loss of tensile properties in thick sections.

The composition of alloy 7010 is shown in Table 6.1.

Two tempers are usually supplied to alloy 7010. When higher strength and less stress corrosion resistance are required temper DTD 5120 (T76) can be used. When higher stress corrosion resistance is required temper DTD 5130 (T73) is recommended and this is particularly

Table 6.1

The Composition Limits of Alloy 7010 (Wt %)

	Composition limits	Nominal composition
Zn	5.7/6.7	6.2
Mg	2.2/2.7	2.35
Cu	1.5/2.0	1.7
Zr	0.11/0.17	0.13
Fe	$\ngtr$ 0.15	
Si	$\ngtr$ 0.12	
Mn	$\ngtr$ 0.10	
Cr	$\ngtr$ 0.05	
Ti	$\ngtr$ 0.05	
Others total	$\ngtr$ 0.15	
Al	balance	remainder

appropriate for thicker plate.

7. THE ELECTRICAL POTENTIAL METHOD FOR MONITORING FATIGUE CRACK GROWTH.

Probably the electrical potential method is the most popular method of monitoring crack growth because it has the advantages of versatility, sensitivity and continuous monitoring capabilities. This method relies on the fact that the potential distribution in the vicinity of a crack changes with crack growth when a D.C. current passes through specimens. This can be detected and then the measurements of electrical potential can be converted to crack lengths by pre-established calibration curves (117-120).

The calibration curves can be obtained by theoretical method or experimental method. For central cracked and edge cracked specimen the theoretical solutions were given by Gilbey and Pearson (119). If the edge cracked configuration which is shown in Figure 7.1 is considered, the potential between probe g and crack plane will depend on the current application mode and for the case of uniform input of current the solution is given by

$$V' = \text{Imaginary part of } \left[K_1 \cos^{-1} \frac{\cos(\pi Z/2W)}{\cos(\pi a/2W)} \right] \quad (7.1)$$

where

V' = potential between probe and crack plane

Z = complex number $(x + iy)$

a = crack length

W = specimen width

K_1 = proportional constant.

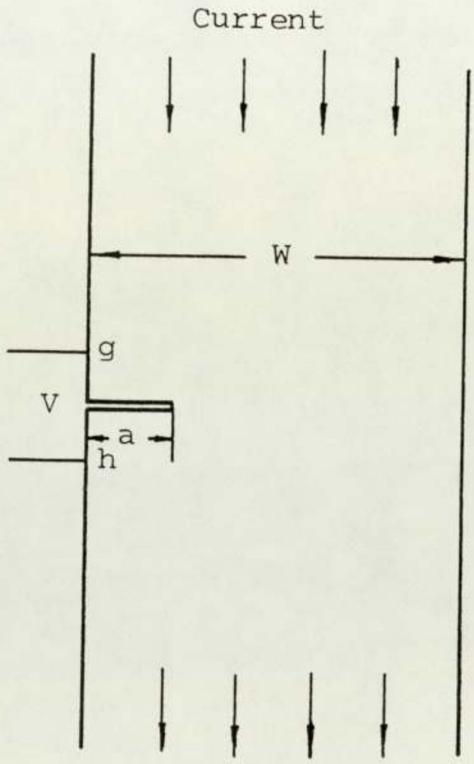

Figure 7.1 Electrical potential system in edged cracked plate

set $a = o$ result in $K_1 = \frac{2V_oW}{\pi}$

where V_o is the potential gradient of a uncracked specimen. The potential drop V between probes should be equal to 2V' as the probes are placed at symetrical points across the crack plane. Thus, the dependence of crack length a on V is given by

$$a = \frac{2W}{\pi} \cos^{-1} \frac{\cosh(\pi y/2W)}{\cosh(\pi V/4V_oW)} \tag{7.2}$$

For the case of point input of current the theoretical solution can be found in (120).

The above mentioned theoretical solution was derived on a finite plate with single edge crack. In practice usually the members with blunt notch from which the fatigue crack initiates have to be considered and obviously the theoretical solution given by Eq. (7.2) does not hold for suchlike cases. Thus, the establishment of an experimental calibration using actual size specimens is essential for the study of fatigue crack initiation and propagation when the potential technique is employed.

It has been found that the calibration of potential depends on various factors. To obtain the reliable calibration curves the effects of the following factors have to be considered : positions of probes, specimen geometry, materials, magnitude of current and its input mode and the equipment used for measuring potential. The effects of these factors on the sensitivity of potential method were reviewed by Holder (73). Choosing the location of potential probes involves satisfying the requirements of sensitivity and reproducibility. For the edge crack member shown in Figure 7.1 if the probes are moved first along the specimen face towards the crack and then along the crack faces towards the crack tip, the sensitivity increases continuously as the probes approach the crack tip (121), but the reproducibility is degraded due to the increase of the probe location-sensitivity. Considering the requirements of the sensitivity and reproducibility the most suitable position of potential probes is on the top face of the specimen across the open mouth of the crack or notch. The notch geometry in a finite specimen may affect the calibration of potential significantly (121). The higher sensitivity can be expected for a sharp notch due to the steeper potential gradient at the notch root. The potential difference between probes is directly proportional to the resistivity of the material and the magnitude of the electrical current. For a given material the maximum magnitude of the electrical current should be used when the specimen heating effect is taken into account. The magnitudes of the current between 10 amperes and 50 amperes are suitable for most materials. For materials with high resistivity low magnitude of electrical current should be used,for materials with low resistivity like aluminium the upper limit is recommended. Under the condition mentioned above the potential developed across the crack faces has the order of one hundred to several hundreds microvolts. To obtain the required detection sensitivity of the order of a few microvolts a voltage offset source therefore is needed so that the small potential increase due to fatigue crack growth can be detected by the chart recorder which has a full scale of 50 μv.

It should be noted that problems arise when the potential technique is employed to monitor initiation and early growth of fatigue cracks from notches. The electrical potential method can not tell the exact length at different points along the front of a small thumbnail crack. However, such a crack is a common case for a blunt notched specimen. Cooke and Robinson (120) compared a number of potential readings taken across a crack at various points in the through thickness surface and found the measured potential varied less than 5% for the sets of potential leads regardless of the form of the crack front. It seemed to indicate that the measured potential is the characteristic of crack area rather than crack length. Thus it implies that only an equivalent through thickness crack length converted from the area of fatigue crack can be measured. The effect of plastic deformation on potential measurements during initiation and early propagation of fatigue crack has been considered by a number of investigators (120,122). Plumbridge analysed the influence of the plastic zone at the notch tip developed in the pre-growth period on the subsequent measurement of crack length. It was pointed out that the build up of plastic zone at the notch tip changed the resistivity of material within the plastic zone. Therefore the measured increment of electrical potential consisted of two parts. One is contributed by crack growth and the other is contributed by the increase of resistivity. The latter part cannot be ignored at small growth rates and low temperatures. However, Cooke and Robinson found that no significant influence of the elastic and plastic deformation on the measurements of electrical potential was observed (120).

8. EXPERIMENTAL PROCEDURE.

8.1 The Material and Heat Treatment.

The high strength Al-Zn-Mg-Cu alloy 7010 was employed in the present investigation. The chemical composition of the material is shown in Table 8.1. The heat treatment was carried out on the whole block measuring 300mm x 415mm x 50mm by Temper T736, which was equivalent to T73651 (DTD 5130) but the 2% cold stretch in the present treatment was omitted. The details were as follows:

1) The solution treatment was carried out by heating at the temperature of 475 $\pm$ 5^{o}C for 5 hours and quenching in hot water with the original temperature of 62^{o}C and the final temperature of 70^{o}C after the quenching.

2) Two-step ageing was employed, which was carried out by heating at the temperature of 110 $\pm$ 2^{o}C for 10 hours, followed with cooling to room temperature, by further heating at the temperature of 178 $\pm$ 2^{o}C for 12 hours, followed by air cooling.

8.2 Mechanical Properties of the Material.

The mechanical properties of the material are presented in Table 8.2. The universal tensile properties were obtained using Hounsfield No.12 tensile specimens tested in Instron at a cross head speed of 0.05 cm/min. The fracture toughness was determined using slow-bend specimens with the dimensions of 10mm x 22mm x 100mm under three-point bending for which the ratio of span to width

Table 8.1

The Chemical Composition of the Alloy 7010

(Wt %)

Zn	Mg	Cu	Fe	Si	Zr	Al
6.04	2.52	1.50	0.13	0.06	0.14	Balance

Table 8.2

The Mechanical Properties of the Alloy 7010-T736 *

σ_{ys} MN/m^2	σ_{UTS} MN/m^2	El %	RA %	K_c $MN/m^{3/2}$
412	471	16.6	50	37.6

* The data listed in Table 8.2 are the average values of three specimens.

was 4 : 1, following the standard method (123) except the specimen size.

8.3 The Specimens.

The specimen blanks were cut from the two inch thick (50mm) plate in L-S orientation such that the crack propagates in short transverse direction and then machined to be 100mm long x 22mm wide x 10mm thick with a central edge notch. Fig.8.1 shows the orientation of the specimen blanks in the plate.

The selected size of the specimens was to satisfy the conditions of plane strain under cyclic loading. The requirement of plane strain is that the plastic zone size at the crack tip should be less than 2% of the thickness. The monotonic plastic zone size is given by

$$r_p \approx \frac{1}{5.6\pi} \left(\frac{K_I}{\sigma_{ys}} \right)^2 \qquad (8.1)$$

If the cyclic plastic zone size is taken as one-fourth of the monotonic plastic zone size and K_I is replaced by K_c the maximum cyclic plastic zone size can be evaluated by

$$r_p^{\,c} = \frac{1}{4 \times 5.6\pi} \left(\frac{K_c}{\sigma_{ys}} \right)^2 \qquad (8.2)$$

K_c and σ_{ys} are 37.6 $MN/m^{3/2}$ and 412 MN/m^2 and then the requirement of minimum thickness for plane strain is about 6mm. Usually the stress intensity factor range during fatigue tests will not reach K_c and thus the conditions of plane strain can be met by the dimensions of the specimen.

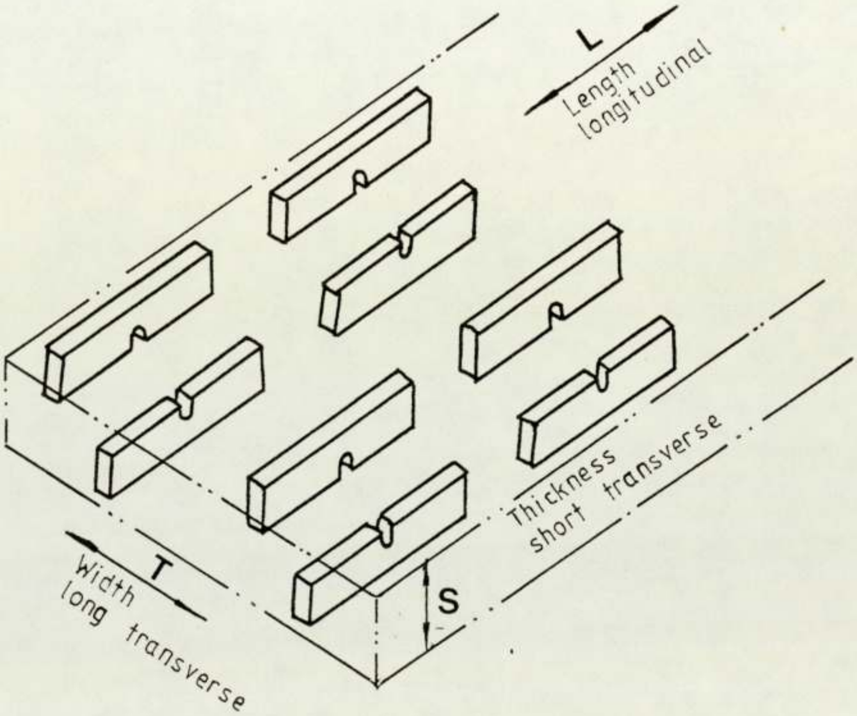

Figure 8.1 The orientation of the specimen blanks in the plate

Various geometry of notches was designed to represent the range of stress concentrations usually encountered in engineering practice. The notches were essentially of U - or semi-circle shapes. Fig.8.2 shows the dimensions of the four types of notches designated as 2XX, 5XX, 35XX and 30XX respectively. The stress concentration factors were calculated by Wood and Richards (124), using finite element technique. The dimensions of the specimens and stress concentration factors are presented in Table 8.3.

The depths and widths of all notches were measured and the profiles of the notch roots were examined and traced using a projection microscope. By taking the form of the notch root region as a part of the circle then the notch root radii were calculated by

$$\rho = \frac{p^2 + q^2}{2qM} \tag{8.3}$$

where M is the magnification of the tracing and ρ, p and q are shown in Fig.8.3

8.4 The Equipment and Test Conditions.

The tests for constant amplitude fatigue were carried out in three point bending, at a frequency 20 HZ, in laboratory air, at room temperature with a stress ratio of 0.1 and using sinusoidal wave form and an electro-hydraulic fatigue machine (Servo test 177-F8) with a capacity of $\pm$50KN was employed. Fatigue cracks were monitored by the electrical potential method. The constant current was supplied by a FARNELL Stabilised Power Supply Type H30/100 with a maximum output 60 amps.

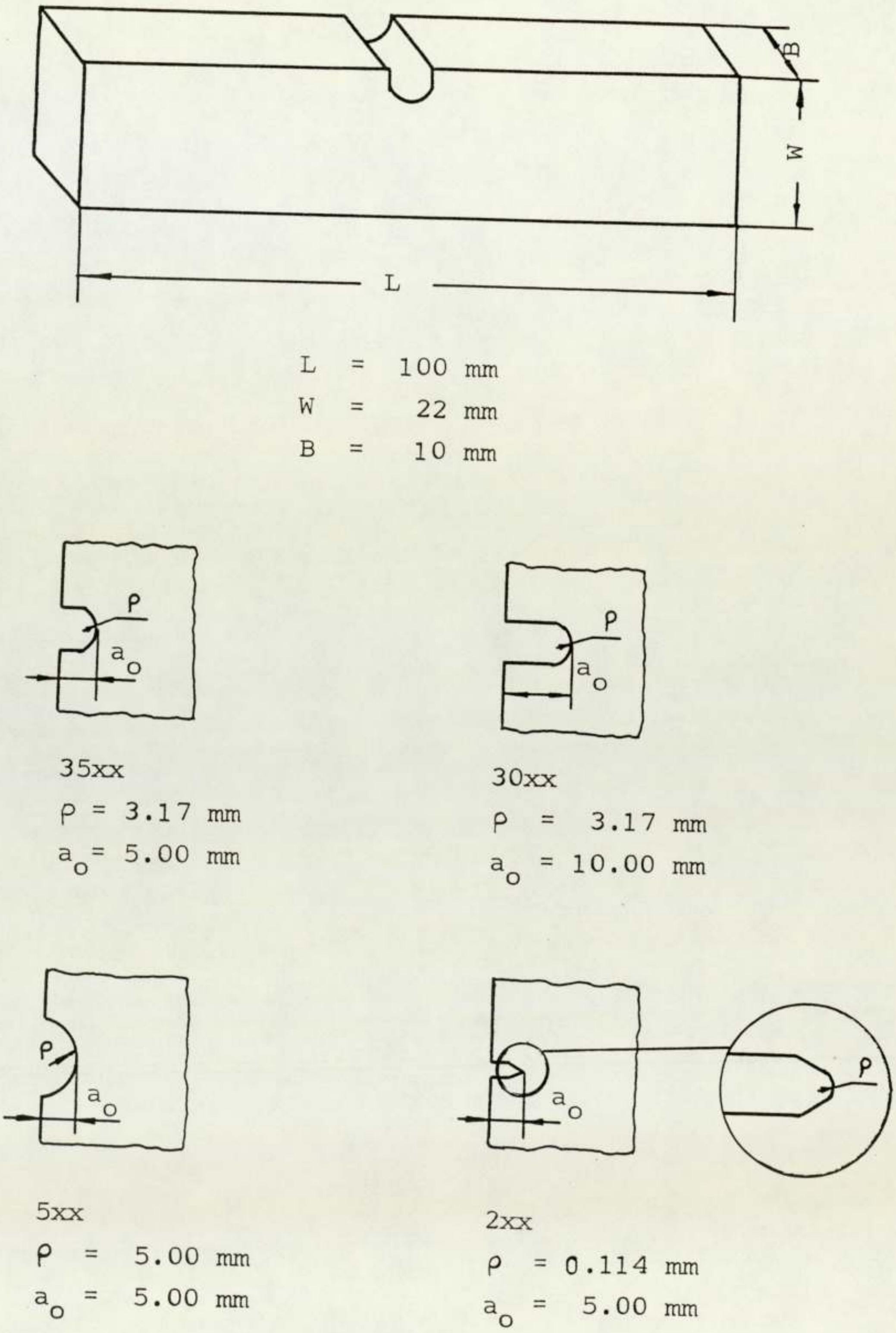

Figure 8.2 Dimensions of specimens

Table 8.3

Notch Dimensions and Stress Concentration Factors.

Notch Root Radius, ρ, mm	Notch Depth a_o, mm	Notch Width W, mm	K_t
0.11	5.00	2.00	7.75
3.17	5.00	6.34	1.75
3.17	10.00	6.34	1.69
5.00	5.00	10.00	1.56

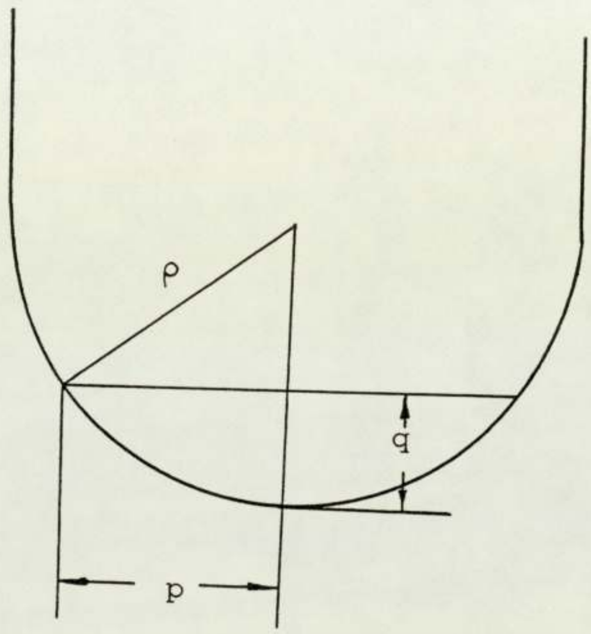

Figure 8.3 Schematic diagram of the measurement for notch root radius

The general view of the equipment is shown in Plate 8.1.

A 100KN Dartec servo-controlled electrohydraulic test machine with computor control unit was used for the tests of variable amplitude loading. The machine is composed of load frame, hydraulic power supply, load cell, actuator, control console and computer control unit. The designed actuator can be allowed to operate fatigue testing at frequencies from 0.1 HZ to 100 HZ but the actual maximum frequency is about 70 HZ due to the power required at high frequency. The accuracy of the load cell is better than 1% of reading down to $^{1}/_{100}$th of its capacity under room temperature. That means that the accuracy of the load measurement is expected within 10 newtons. A load indicator and an oscilloscope are available in the control panel for continuous monitoring of load during tests. The current, minimum and maximum values of load, the number of elapsed repeats of loading spectrum, the number of elapsed cycles and other test information can be displayed on the screen of the computer unit and they can also be output through a printer. The test machine system is shown in Plate 8.2.

The other test conditions for variable amplitude fatigue were basically the same with that of constant amplitude fatigue except that four-point bending was employed instead of three-point bending and that a different D.C. stable power supply source (FARNELL F2111) with an output variable between zero and fifty amps was used in the

Plate 8.1 The general view of the test machine and the potential drop equipment.

Plate 8.2 The general view of Dartec fatigue test machine.

application of the electrical potential technique to monitor crack propagation. The closer views of specimens in the three - and four - point bend rigs are shown in Plate 8.3 and Plate 8.4 respectively. All tests were carried out in load control mode.

8.5 The Electrical Potential Calibration.

The circuit diagram of electrical potential method for monitoring fatigue crack is shown in Fig.8.4. The specimen was electrically insulated from the test machine and a constant current of 50 amp or 44 amp was introduced into and through the specimen from its two ends by toolmakers clamps covered with 1 mm thick annealed electrical purity copper. The potential was picked up by 0.15 mm Nichrome wires spot-welded at the edge surface across the notch. The nominal distance between the probes was 10 mm. It was found that the potential difference developed between the probes depends on the notch geometry, e.g. for a notch depth of 5 mm and root radius of 0.11 mm, the potential difference was about 147 μv and for a notch with the depth of 10 mm and the root radius of 3.17 mm this value is about 308 μv. To obtain the maximum sensitivity the potential drop between the probes was backed off by a D.C.voltage calibration unit (Time electronics Type 2003, % 0.006) and then fed into a chart recorder (Teckman 200) which had a maximum sensitivity of 0.5 μv and 50 μv full scale deflection. The tests were not performed until the current had been passed through the specimens for at

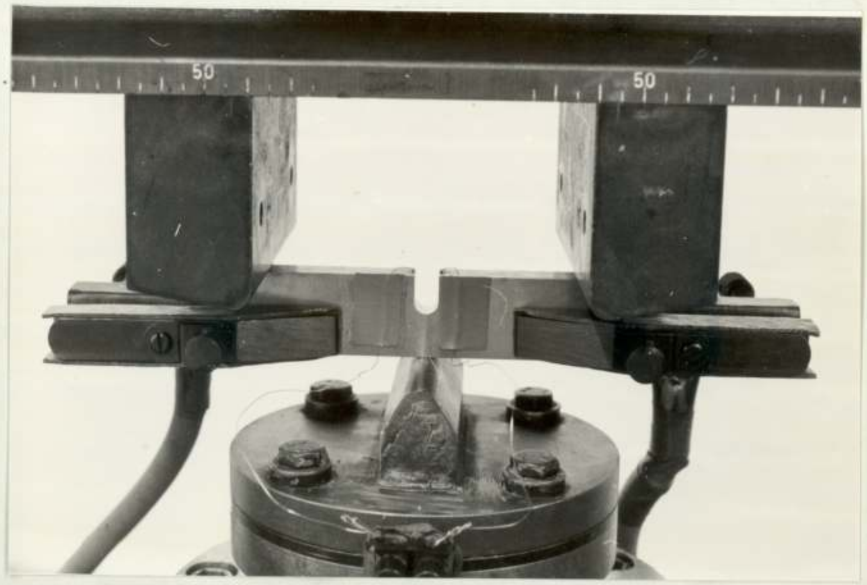

Plate 8.3 Specimen located in
three-point bending rig.

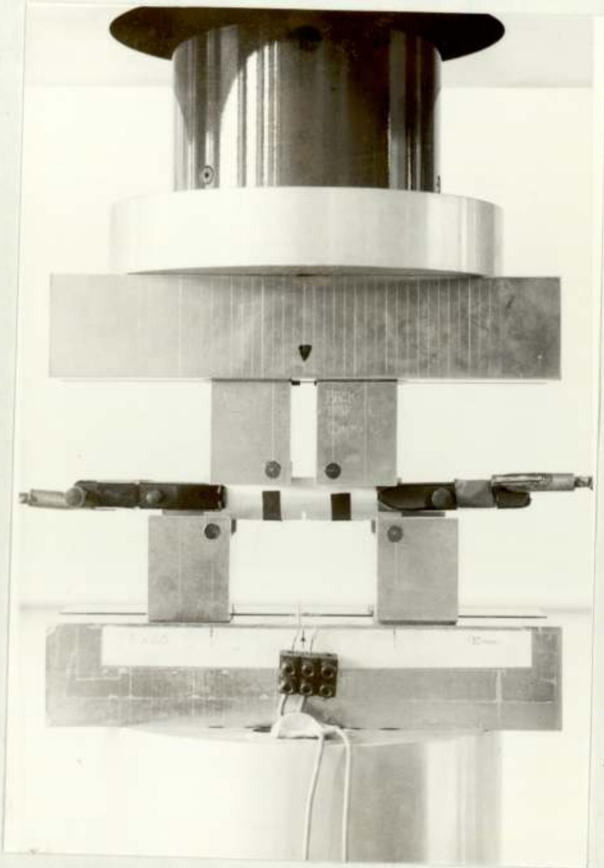

Plate 8.4 Specimen located in four-point bending rig.

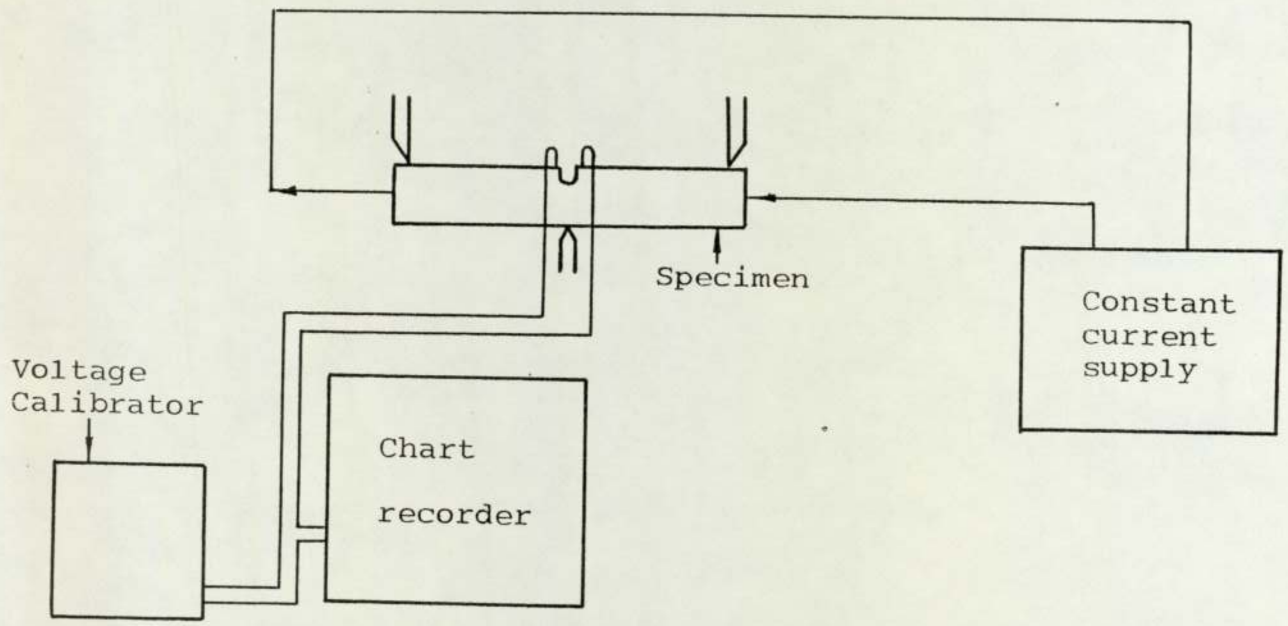

Figure 8.4 Circuit diagram for electrical potential difference measurement system

least half an hour and the Teckman chart recorder was switched on with the fatigue machine to ensure the thermal and electrical stabilization before the start of any tests. During the tests the back off voltage and chart speed were adjusted as the increase of crack growth rates so that the slope of 1.0 to 1.7 for the graph of voltage against time, which was recorded on the chart recorder, can be obtained. A number of specimens for each type of notch were fatigue cracked to potential increments of 2 μv, 5 μv, 10 μv, 20 μv, 40 μv, 80 μv and 160 μv etc. and then the tests were stopped and the specimens were broken open in fast fracture.

The graphs of fatigue fracture surfaces were traced by a contour projector at a magnification of 10. The area of the graphs were measured and divided by the thickness of the specimen to establish the equivalent crack lengths. Eq.(7.2) suggests that $\frac{a}{W}$ is a function of $\frac{V}{V_o W}$ at a given location of potential probes. Thus the results were plotted in terms of $\frac{a}{W}$ against $\frac{V}{V_o W}$, where a is equal to notch depth plus crack length and V is the corresponding potential difference between the probes. The regression analysis was employed to fit the experimental data and to establish the calibration functions which were used in the later study of the initiation and propagation of fatigue cracks.

8.6 The Design of Experimental Program and Test Methods.

8.6.1 Constant Amplitude Fatigue.

8.6.1.1 Fatigue Crack Initiation.

Two problems have to be solved before the start of the tests of fatigue crack initiation. One is the definition of crack initiation and another is to estimate the minimum and maximum applied loads. The crack initiation can be defined as a predeterminal deviation from the steady potential across the notch on chart recorder or defined as a predetermined crack length. In practice for any engineering definition of crack initiation some fraction of crack propagation can not be avoided but to a reasonable definition of crack initiation this fraction should be the same for different notch geometry. Obviously, the first definition mentioned above cannot ensure the same crack length at initiation for various notch geometry and therefore the different fraction of crack propagation will be included in the initiation phase. For this reason the occurrence of a crack with a certain length, which is defined as crack initiation, is preferred and the presence of the equivalent crack length 0.127 mm was taken as the definition of crack initiation in present investigation.

The minimum and maximum applied loads for initiation tests were estimated by stress concentration method. For a finite life of crack initiation the applied loads must be chosen such that the local stress range at the notch roots will be higher than the uniaxial fatigue endurance limit of the material. After the examination of S-N curve obtained previously (115) it was decided that the majority of the tests should have a finite life of crack initiation less than 10^6 cycles for which the corresponding applied stress is higher than the endurance limit by a factor of about 10%. The minimum applied load range then can be estimated as follows:

$$K_f \ \Delta S_{min} = 1.1\, \sigma_{limit} \tag{8.4}$$

where the values of K_f for different notches were calculated by Eq.(4.16) in which the Neuber's length estimated was 0.45 mm (75). σ_{limit} is the uniaxial fatigue limit of the material under consideration, which is about 220 MN/m^2 (32 Ksi) (115). ΔS_{min} is the nominal minimum applied stress range which was calculated by:

$$\Delta S_{min} = \frac{6\, \Delta P_{min}\, W}{B\, (W - a_o)^2} \tag{8.5}$$

where ΔP_{min} = required minimum applied load range

W = specimen width

B = specimen thickness

a_o = notch depth

result in

$$\Delta P_{min} = \frac{1.1\, \sigma_{limit}\, B\, (W - a_o)^2}{6\, K_f\, W} \tag{8.6}$$

The maximum load adopted was such that the nominal stress S less than the net section general yield stress. When the notch constrain factor was taken into account, the maximum applied load can be calculated using the following equation

$$P_{max} = 1.216\, S_{ys} \frac{B(W - a_o)^2}{4W} \qquad (8.7)$$

For the four type notched specimens the minimum values of the load range calculated by Eq.(8.6) were approximately 1700N to 3800N and the maximum values of the load range given by Eq.(8.7) were 8000N to 16000N respectively. The two limits of the load range have been determined. The intermediate values of the load range were selected such that a predetermined increment of load range maintained from the lower limit to the higher limit.

To start the tests the potential probes were spot-welded to the specimen at a fixed position and then the current clamps were placed at the ends of the specimen. The specimen was placed on the bearing rig of the machine and small load was supplied. The specimen was then positioned with the aid of the pre-made marks on the specimen so that it was centrally located in the bending rig. The free ends of the potential probes were clamped in the terminal block and through it the probes were connected to the chart recorder and the D.C voltage calibrator. The voltage on the calibrator then was adjusted so that the difference recorded on the chart was about 10 μv. It was found that 30 minutes were necessary to stabilize the potential after the connection of the probes. When the potential was stabilized, the required mean load was applied to the specimen and the button "GEN RUN" was then switched on and the machine began to cycle the load. Because of the machine drift the mean load and the amplitude were adjusted in the initial few seconds of the tests so that the required load variables can be guaranteed. The minimum load was selected to maintain the stress ratio R value of 0.1 for all tests. The tests were continued until the potential across the notch had increased to the predetermined values.

8.6.1.2 Fatigue Crack Propagation

Seven specimens with a notch of 5 mm depth and 0.11 mm root radius were used to obtain the baseline data of the fatigue crack propagation. In order to eliminate the effect of the notch stress field on the experimental results the data were collected after the fatigue cracks had grown to the length more than 1 mm from the notch root. The identical test procedure as described in the last section was followed. The applied load ranges, ΔP, were different for each specimen so that the crack growth rates over different ranges can be obtained. Each specimen was tested at a constant ΔP and all tests were carried out at a fixed set of loading variables which had been described in Section 8.4. The test was not interrupted for each specimen until the crack grew to the predetermined length to avoid the transient effect on the measurement of crack growth rates. After the tests the crack growth rates were expressed as a function of the stress intensity factor range, ΔK, i.e. the results were presented by Eq.(1.1) in which the constant A and m were obtained by regression analysis.

8.6.1.3 Shot-Peening Tests.

Two groups of 5XX type specimens were employed for the shot-peening tests. The specimens of group A were peened on top as well as sides. For specimens of group B only the top was peened. The appearance of the shot-peened specimens are shown in Plate 8.5. To ensure the whole surface and edges under consideration can be uniformly peened the notch edges were machined to a 2 mm chamfer and therefore the experimental potential calibration curve had to be re-established.

The shot-peening process was carried out in Metal Improvement Company using the shot type MI330. The intensity was 0.012 – 0.014 A measured by Almen gauge. The Almen gauge and the peened strip was shown in Plate 8.6. The shot-peened specimens were then tested under the same conditions as described in Section 8.4.

8.6.2 Variable Amplitude Fatigue.

8.6.2.1 The Loading History.

The loading history used to investigate the behaviour of crack growth under variable amplitude loading consists of 24 blocks of constant amplitude loads. The maximum overload ratio between the blocks is 1.17. The stress ratio R varies from 0.41 to 0.64 among these blocks except two blocks of static loads. The amplitude-

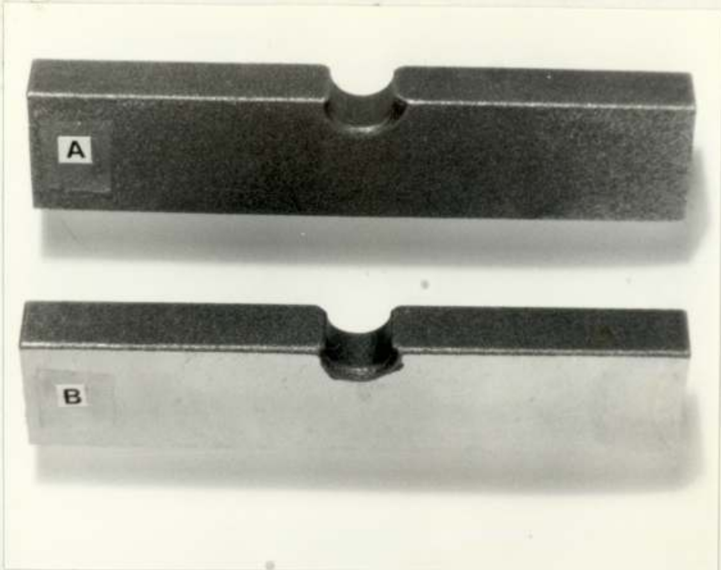

Plate 8.5 The shot-peened specimens.

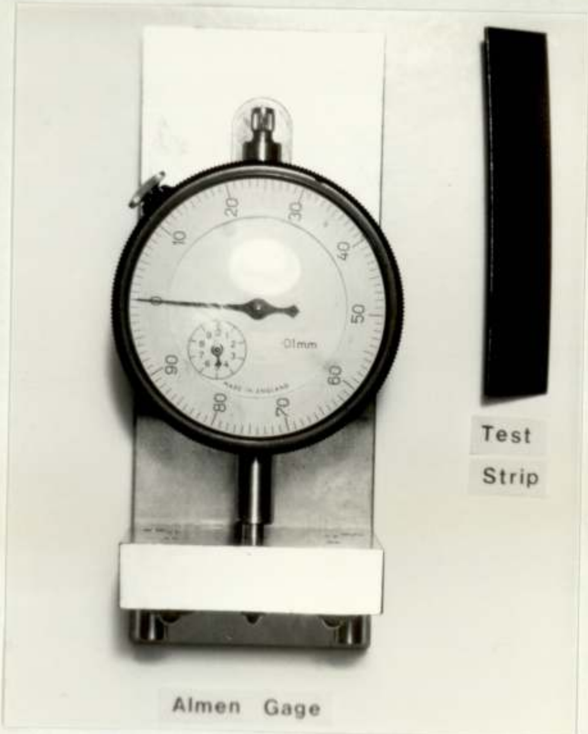

Plate 8.6 The Almen gauge and the shot-peened test strip.

time display of the loading programme is schematically illustrated in Fig.8.5. For the convenience of discussion the loading programme is indicated as programme 1.

8.6.2.2 The Measurements of Crack Opening Stress Intensity Factor.

With the aid of a specially designed loading programme the crack opening stress intensity factor was measured by a fractographic technique. The principle of the technique was based on the correlation between crack tip opening displacement and the amount of crack extension per cycle. According to the model of shear sliding of fatigue crack growth originally proposed by Laird and Smith (43) and modified later by others the crack increment per cycle was expected to be proportional to the crack tip opening displacement (CTOD), i.e.

$$\frac{da}{dN} = \beta \ \Delta\,(CTOD) \qquad (8.8)$$

where β was a constant whose value depends on the orientation of the slip planes on which shear sliding occurs. Following Dugdale's equation the relationship of CTOD and stress intensity factor K is given by

$$CTOD = \frac{\pi S^2 a}{E\,\sigma_{ys}} = \frac{K^2}{E\,\sigma_{ys}} \qquad (8.9)$$

where σ_{ys} = yield strength of the material

a = crack length

S = nominal stress

E = modulus of elasticity.

In fatigue cases Eq.(8.9) becomes

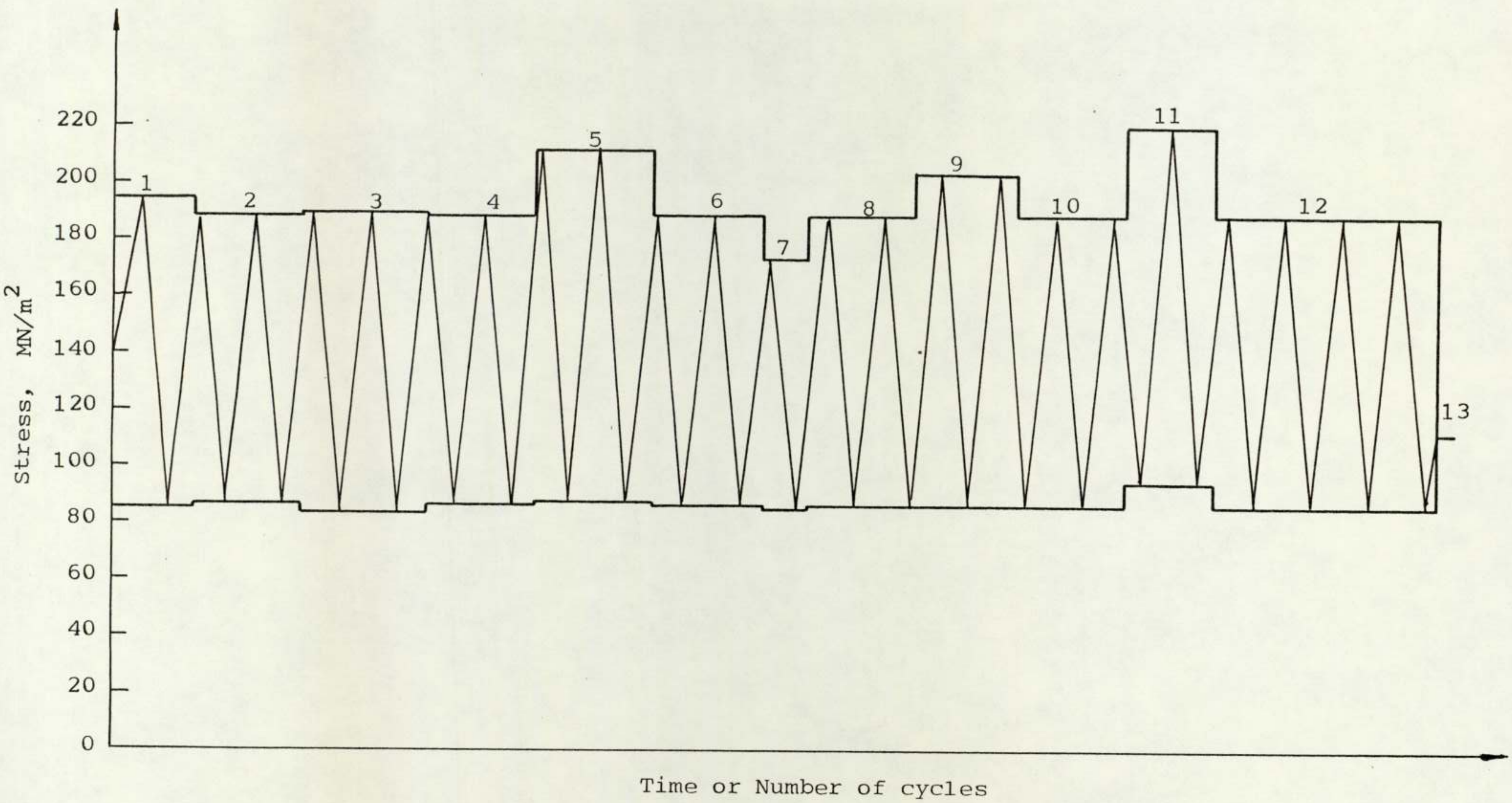

Figure 8.5 Profile of programmed load spectrum (Programme 1)

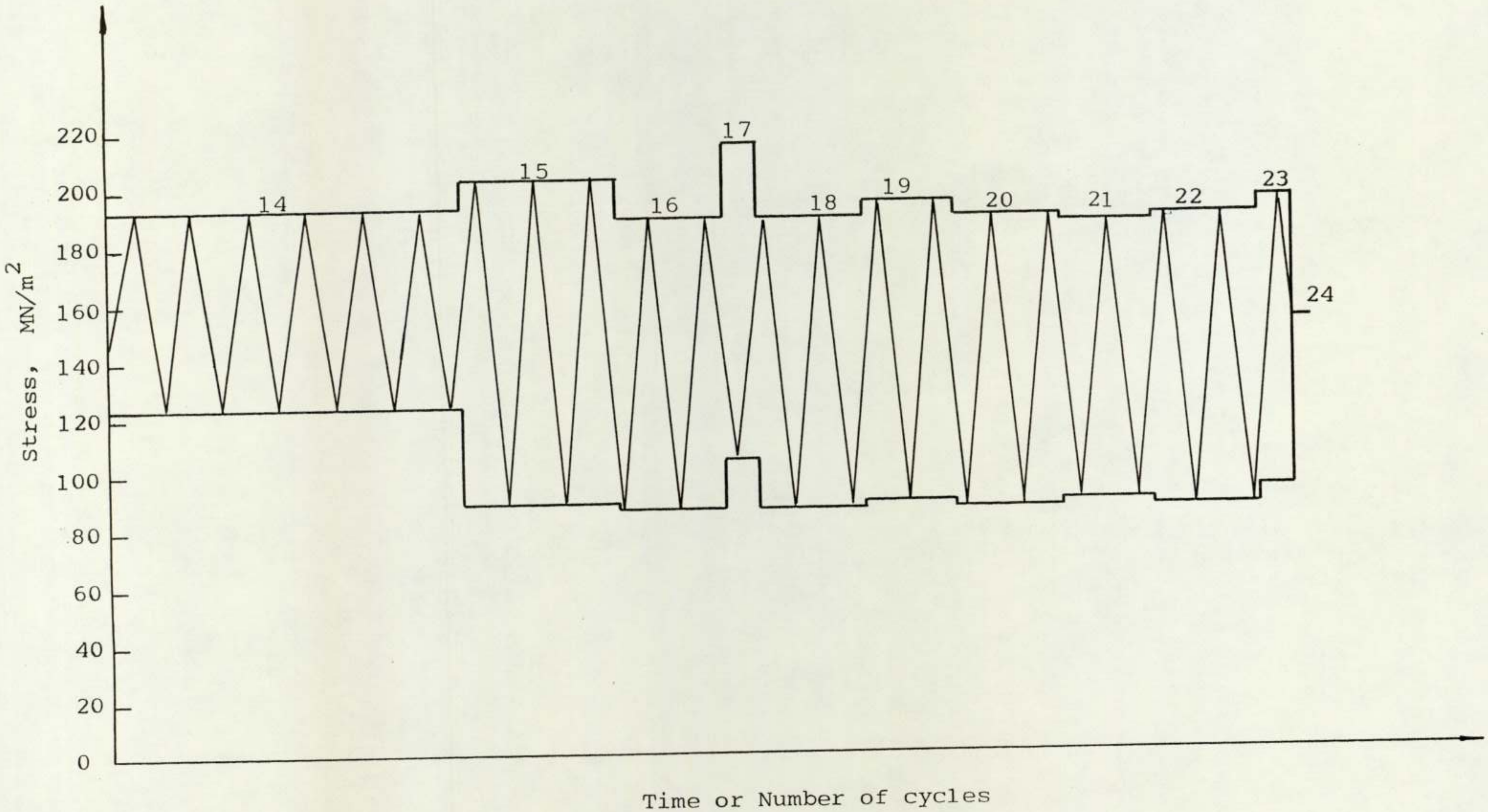

Figure 8.5 (Cont.)

$$\Delta(\text{CTOD}) = \frac{\Delta K^2}{2E\sigma_{ys}} \qquad (8.10)$$

Combining Eq.(8.8) and (8.10) leads to the expression

$$\frac{da}{dN} = \beta\ \Delta(\text{CTOD}) = \beta\ \frac{\Delta K^2}{2E\sigma_{ys}} \qquad (8.11)$$

Since only effective stress intensity factor range is responsible for crack growth the Eq.(8.11) is re-written to the following form:

$$\frac{da}{dN} = \beta\ \Delta(\text{CTOD}) = \beta\ \frac{(\Delta K_{eff})^2}{2E\,\sigma_{ys}} \qquad (8.12)$$

where $\Delta K_{eff} = K_{max} - K_{op}$ if $K_{op} > K_{min}$

$\Delta K_{eff} = \Delta K = K_{max} - K_{min}$ if $K_{op} \leq K_{min}$

In practice the measurement of CTOD is very difficult, however, the relative ratios of CTOD can be obtained by the measurements of striation spacings and, thus crack opening stress intensity factor K_{op} can be calculated through the relationship expressed in Eq.(8.12). This is further explained as follows. A number of loading blocks were designed to form a programmed load indicated as program 2, which was shown in Fig.8.6. The maximum loads maintained constant and the minimum loads were various. The blocks with minimum load ratio and those with higher load ratio (R0.2 to R0.8) were alternatively arranged. The block 1 and block 15 were designed so that the blocks 2 to 14 could be easily identified on the fracture surface by electron microscope. For the convenience of discussion the even number and odd number blocks were indicated as block B and block A respectively. The stress ratio $R_A = (\frac{S_{min}}{S_{max}})$ was 0.1 for

Figure 8.6

Load programme for the measurement of crack opening stress intensity factor (programme 2)

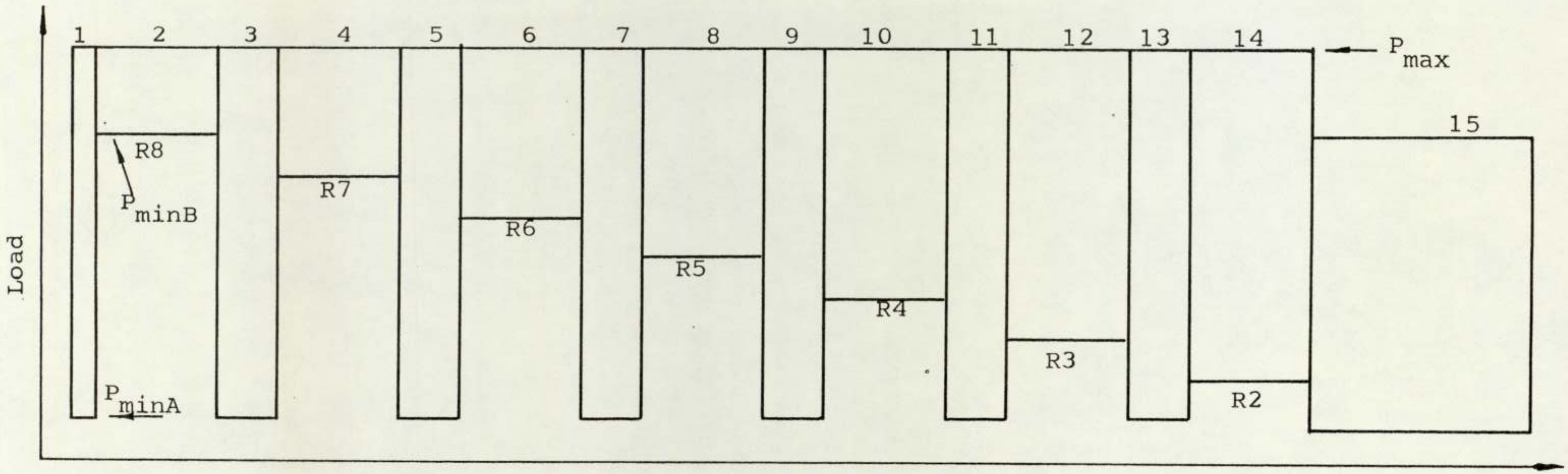

Block No.	P_{max} KN	P_{min} KN	R	N	F
1	3.4	0.34	0.1	4	1
2	3.4	2.72	0.8	20	1
3	3.4	0.34	0.1	10	1
4	3.4	2.38	0.7	20	1
5	3.4	0.34	0.1	10	1
6	3.4	2.04	0.6	20	1
7	3.4	0.34	0.1	10	1
8	3.4	1.70	0.5	20	1
9	3.4	0.34	0.1	10	1
10	3.4	1.36	0.4	20	1
11	3.4	0.34	0.1	10	1
12	3.4	1.02	0.3	20	1
13	3.4	0.34	0.1	10	1
14	3.4	0.68	0.2	20	1
15	2.7	0.27	0.1	50	2

$$R = \text{Stress ratio} = \frac{P_{min}}{P_{max}}, \quad N = \text{Number of cycles}, \quad F = \text{Frequency}$$

block A and it was assumed that S_{minA} should be less than S_{op} (i.e. $K_{minA} < K_{op}$). If $(\Delta K)_B$ was such that $K_{minB} < K_{op}$ there would be no fractographic difference in striation spacing between adjacent block A and block B. If $(\Delta K)_B$ was such that $K_{minB} > K_{op}$ the K_{op} could be determined from the measurement of striation spacing of adjacent block A and block B.

Eq.(8.12) directly resulted in

$$\frac{(S_p)_A}{(S_p)_B} = \frac{(\frac{da}{dN})_A}{(\frac{da}{dN})_B} = \frac{(CTOD)_A}{(CTOD)_B} = \left(\frac{\Delta K_{eff}}{\Delta K_B} \right)^2 \qquad (8.13)$$

and

$$\frac{(S_p)_A}{(S_p)_B} = \left(\frac{K_{max} - K_{op}}{K_{max} - K_{minB}} \right)^2 = X \qquad (8.14)$$

and

$$\sqrt{X} = \frac{1 - \frac{K_{op}}{K_{max}}}{1 - \frac{K_{minB}}{K_{max}}} = \frac{1 - \frac{K_{op}}{K_{max}}}{1 - R_B} \qquad (8.15)$$

$$\frac{K_{op}}{K_{max}} = 1 - \sqrt{X}\,(1 - R_B) \qquad (8.16)$$

K_{max} and R_B were the known quantity and X was obtained by measurements of striation spacings and then K_{op} was calculated.

8.6.2.3 The Effects of Multiple Overloads on Crack Growth.

The load history used to investigate the overload retardation effects on crack growth was shown in Fig.8.7, which was indicated as programme 3. This programme consisted of basically constant amplitude cycles with

Figure 8.7

Profile of the programmed load spectrum for the study of the effect of load sequences (Programme 3)

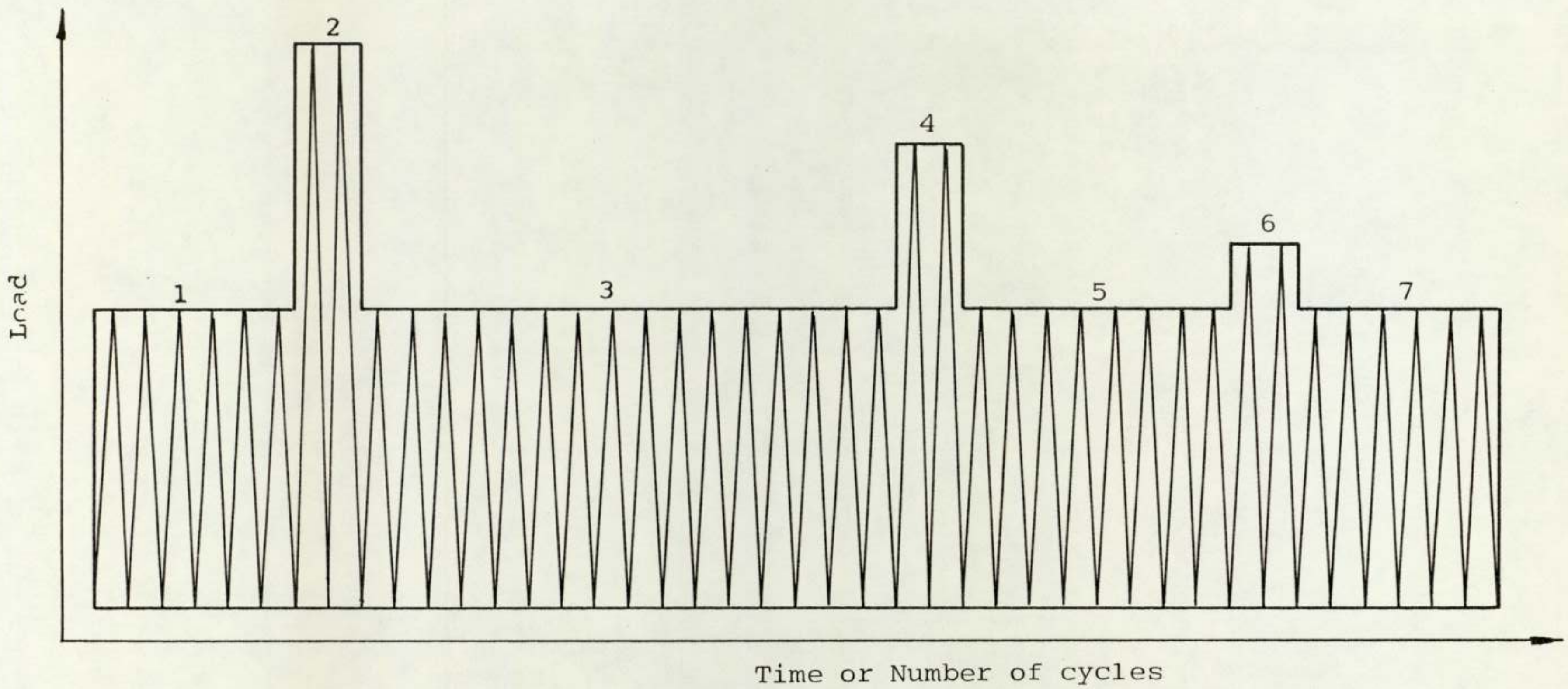

Specimen 227						Specimen 228					
Block No.	P_{max} KN	P_{min} KN	N	F	Rol	Block No.	P_{max} KN	P_{min} KN	N	F	Rol
1	2.5	0.25	500	5		1	2.5	0.25	9000	5	
2	4.5	0.25	10	5	1.8	2	4.5	0.25	10	5	1.8
3	2.5	0.25	8900	5		3	2.5	0.25	11450	5	
4	3.75	0.25	10	5	1.5	4	3.75	0.25	10	5	1.5
5	2.5	0.25	3000	5		5	2.5	0.25	4000	5	
6	3.0	0.25	10	5	1.2	6	3.0	0.25	10	5	1.2
7	2.5	0.25	500	5		7	2.5	0.25	4000	5	

three blocks of overloads at different overload ratios (R_{ol} = 1.2, 1.5 and 1.8). The overload ratio 1.2 was designed since the maximum overload ratio in programme 1 was at the same level ($(R_{ol})_{max}$ = 1.17). The retardation effects of overloads at R_{ol} 1.5 and 1.8 were also examined for comparison.

8.7 Metallography and Fractography.

8.7.1 The Examinations of Microstructure and the Measurements of Grain Dimensions.

A number of samples were cut in longitudinal, transverse and short transverse sections from the tested specimens. The samples were then ground on 180 to 1200 grade abrasive papers and polished on 6 μ diamond Brasso and finally 1 μ diamond.

The mechanically polished samples were then divided into two groups. The first group of the samples were etched in Keller's reagent (2ml HF, 3ml HCl, 5ml HNO_3 and 190ml water) and then used for the examination of the microstructure. The second group of the samples were anodised in Baker's reagent (5g HBF_4 per 200ml H_2O) at a potential 26 volts and with the limit current set at 0.5 amp for 50-60 seconds. The anodised samples were then employed to measure the grain dimensions by optical microscope under polarized illumination. This was carried out using linear intercept procedure at five or more random chosen areas on each section.

Some specimens, which were fatigued to initiate a crack but not fractured open, were used to examine the influence of microstructure on crack propagation. The metallographic samples were cut from the notch part of these specimens and a number of sections of the samples were examined under optical microscope, which was accomplished by gradually mechanically grinding and polishing the samples.

8.7.2 The Examination of Fracture Surfaces.

The features of the crack initiation sites and the fracture surfaces from slow crack growth region to final fast fracture region were examined using a scanning electron microscope (SEM S-150). The striation spacings were quantitatively measured and the procedure of the measurement are described as follows.

In the early stage of the investigation the examination of the striation spacings was conducted on the fracture surfaces of sharp notched specimens to establish the relationship between the striation spacings and the macroscopic crack growth rates. The selection of sharp notched specimens for the study was due to the relatively uniform propagation of the fatigue crack through thickness in these specimens and thus the results obtained from the interior region on the fracture surfaces can be directly related to the macroscopic crack growth rate $\frac{da}{dN}$. To measure the striation spacings the micrographs were taken from the interior region at different sites in the crack growth direction and then the average spacings of 5 to 51 successive striations were measured in the direction perpendicular to the striations on the micrographs or on the projections of the negatives. The striation spacings were calculated using the following formula

$$S_p = \frac{L}{N_s M} \frac{\cos\alpha}{\cos\theta} \cos\beta \qquad (8.17)$$

where S_p = striation spacing

L = unit length

M = magnification

N_s = number of striations per unit length

θ = tilting angle of specimen

α = tilting correction angle

β = angle between the local crack growth direction and the macro-crack growth direction.

After the relationship between S_p and $\frac{da}{dN}$ was established, the technique was extended to study the growth rates at short crack lengths in blunt notch specimens.

For variable amplitude fatigue when the striations can not be identified clearly by SEM, the transmission electron microscope (TEM) was employed for the study. The replicas for TEM were prepared by standard two-stage replica technique for which the shadowing direction was opposite the fatigue crack growth direction.

9. RESULTS

9.1 The Electrical Potential Calibration

The experimental results of electrical potential calibration are shown in Fig.9.1, in which the curves are presented in terms of $\frac{V_a}{V_o W}$ versus $\frac{a_o+c}{W}$, where V_a is the potential drop with the unknown crack length, a_o+c, which is to be measured, and W is the specimen width and V_o, the potential drop per unit length of the uncracked specimen, was obtained by the following method. The potential probes with the interval 10mm were placed on the side of each specimen midway between the specimen end and the notch and the potential drop between the two probes was recorded. The measured potential drop was then divided by the interval to obtain V_o. The position of the probes is shown in Fig.9.2. It was found that the measured V_o was different for specimens with various notch geometry due to the influences of the notches. The average values of V_o of 7 to 8 specimens for each type notch are listed in Table 9.1.

To check the influence of the notch geometry the un-notched specimen with the dimension of 100mm long X 22mm width X 9.6mm thick was used to measure the potential drop by placing the potential probes on the side of the specimen midway between the two ends of the specimen with an interval 10.275mm. Then the conductivity of the material was converted from the measured potential drop

Figure 9.1 Experimental electrical potential calibration curves. The dot line curves represent the theoretical calibration (Gilbey and Pearson (119)).

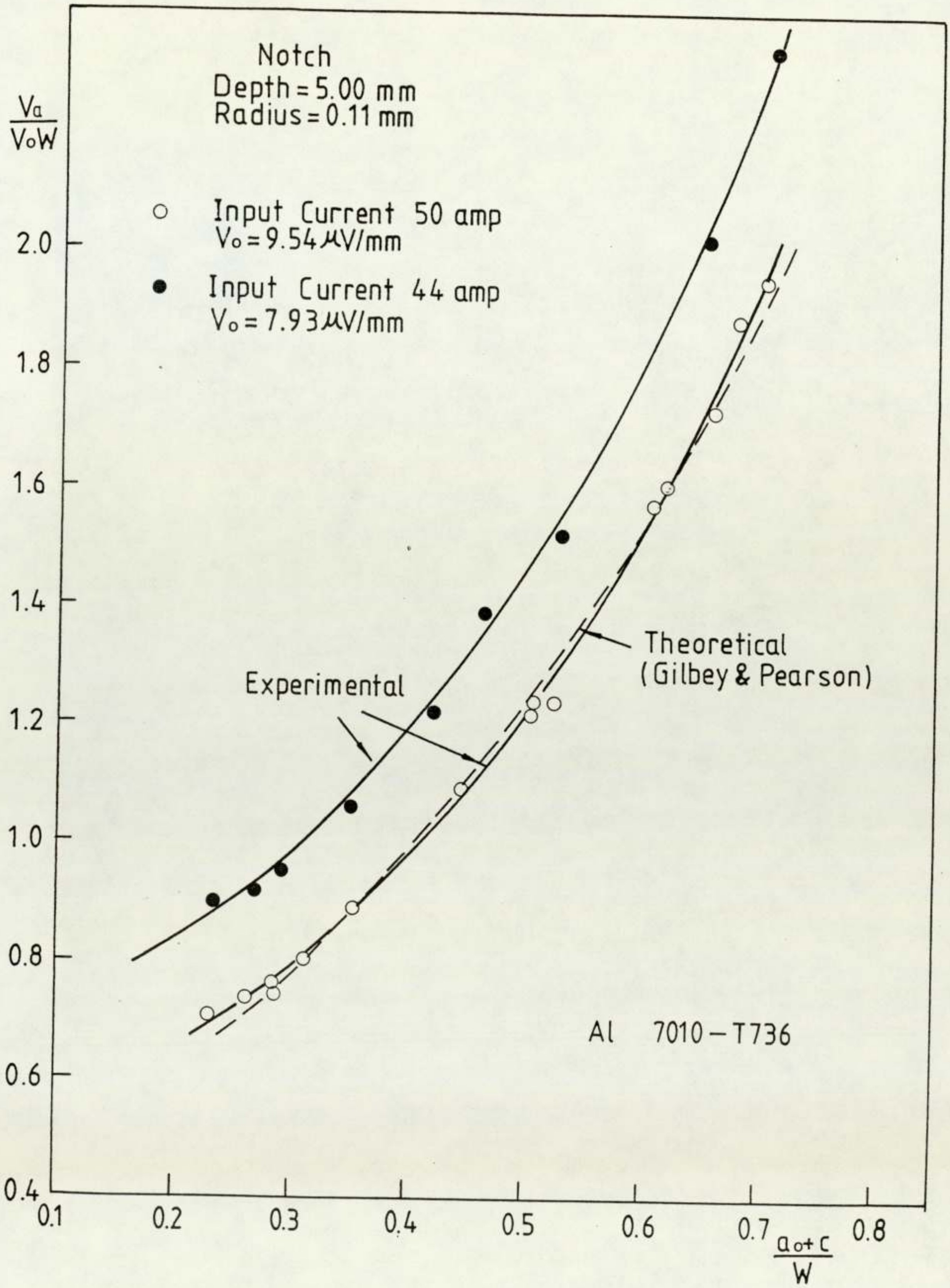

Figure 9.1a Notch geometry, a_o = 5.00mm

ρ = 0.11mm

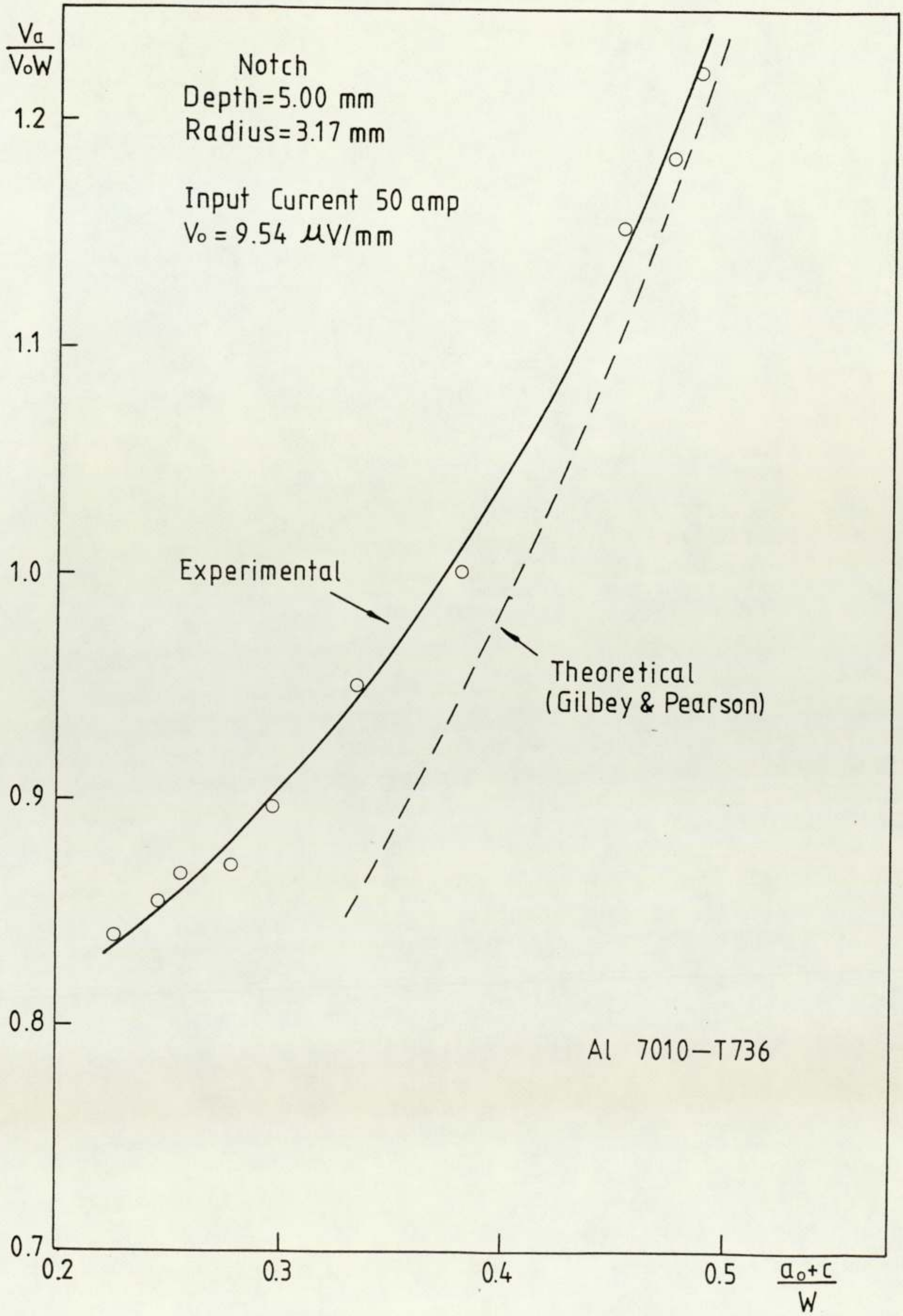

Figure 9.1b Notch geometry, a_o = 5.00mm

ρ = 3.17mm

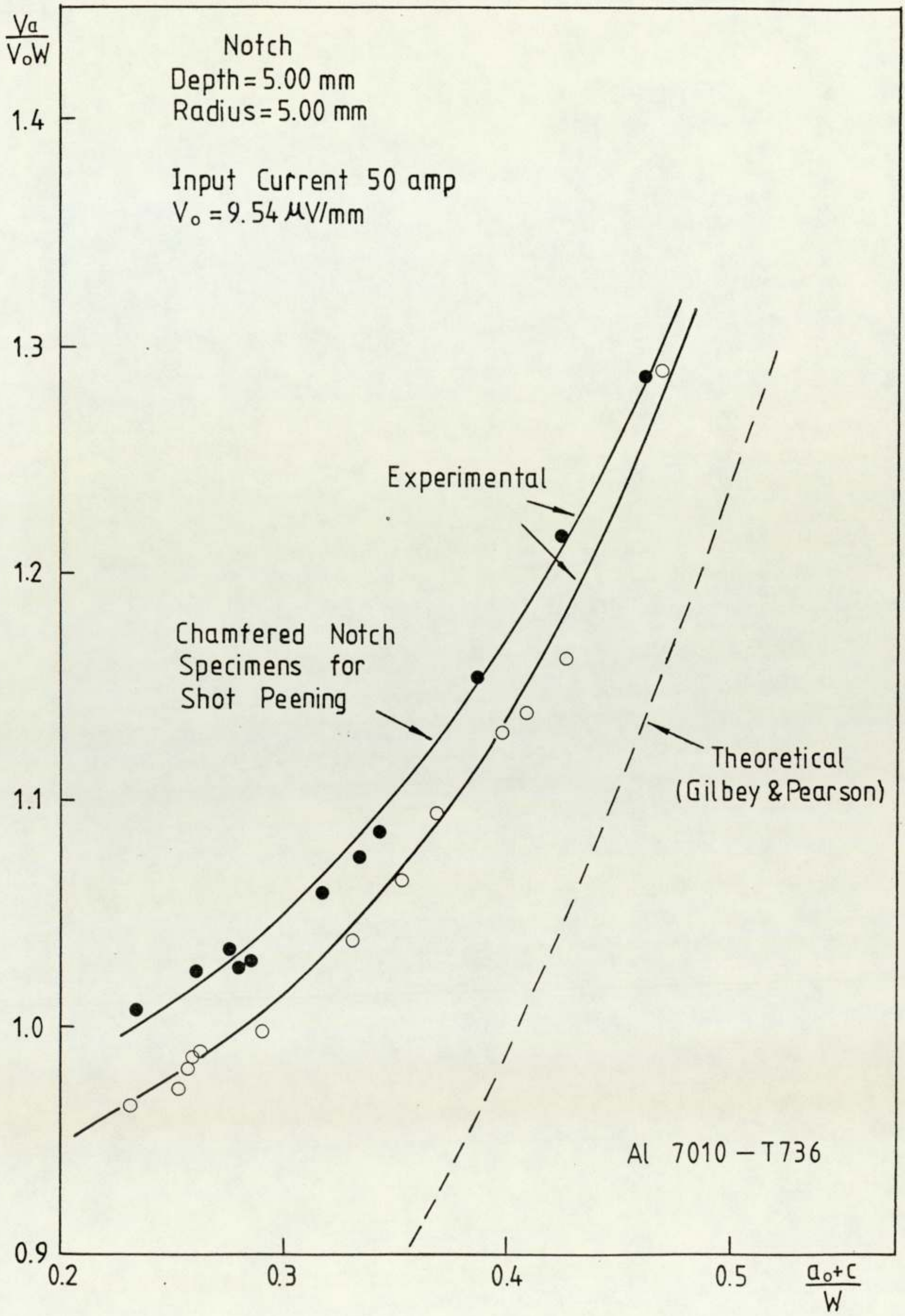

Figure 9.1c Notch geometry, a_o = 5.00mm

ρ = 5.00mm

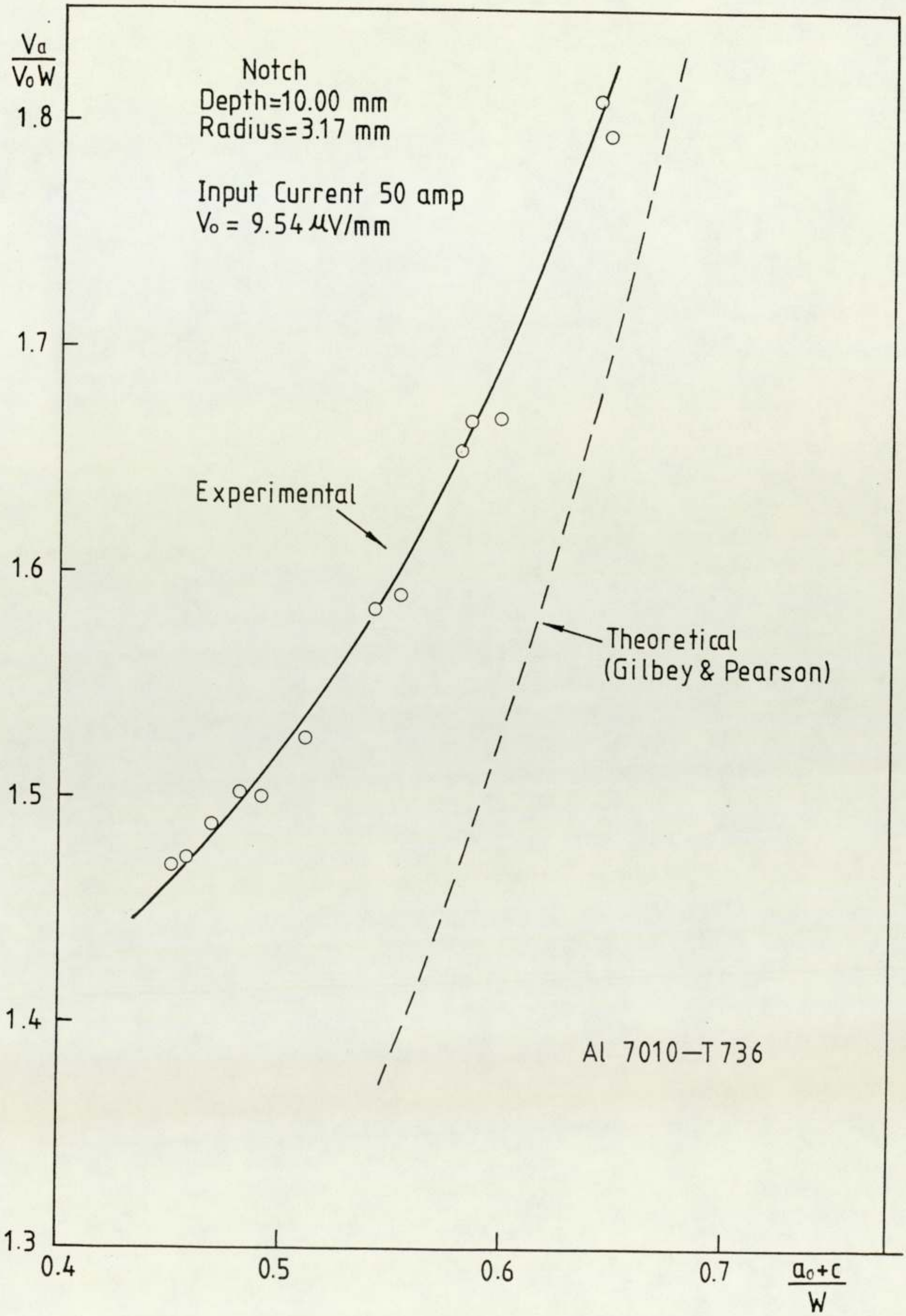

Figure 9.1d Notch geometry, a_o = 10.00mm

ρ = 3.17mm

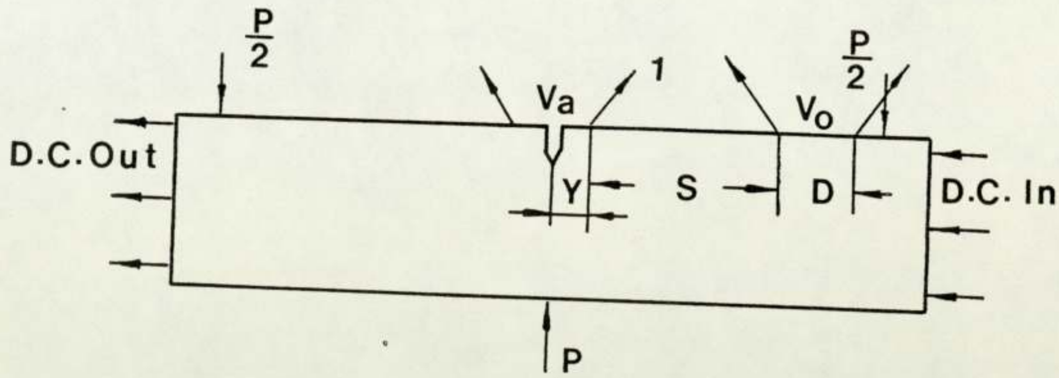

Y = 5.00 mm

S = 25.00 mm

D = 10.00 mm

Figure 9.2 The positions of potential probes for measuring V_a and V_o

Table 9.1

Average Values of V_o (Measured on 7 to 8 Specimens)

(*Input Current 50 amp)

Notch Type	ρ mm	a_o mm	V_o μv/mm
2XX	0.11	5.00	9.54
35XX	3.17	5.00	9.21
30XX	3.17	10.00	8.96
5XX	5.00	5.00	8.86

* For the 2XX group of specimens at input current 44 amp the V_o is 7.93 uv/mm.

and the value of V_o was calculated. The conductivity obtained by this method was 4.137 x 10^{-5} ohm.mm and the calculated value of V_o was 9.45 μv/mm for the specimen of 22mm width and 10mm thick at a D.C. input current 50 amp. Comparing this value with that listed in Table 9.1 and considering the error of experiments the effect of sharp notch geometry on the measurement of V_o could be neglected. Thus the average value of V_o measured using sharp notch specimens was employed in the calculation of $\frac{V_a}{V_o W}$. For the case of a D.C. input current 44 amp the measured value of V_o was 7.93 μv/mm.

In present work the current was input from the ends of the specimen therefore the theoretical solution for uniform current input given by Eq.(7.2) was plotted in Fig.9.1 for comparison with the experimental results. It can be seen that the theoretical calibration curve is remarkably in agreement with the experimental calibration curve of the sharp notch specimens (Fig.9.1a). However, no such agreement exists for the blunt notch specimens (Figs 9.1b,c & d) because the theoretical solution is based on the assumption of the existence of a sharp crack.

The polynomials of 2, 3, 4 and 5 degrees were used to fit the curves in Fig.9.1. The results showed that the best fit can be given by the 3 degree polynomial. Thus, the curves in Fig.9.1 could be functionally expressed by

$$\frac{a_o+c}{W} = K_0 + K_1 \left(\frac{V_a}{V_o W}\right) + K_2 \left(\frac{V_a}{V_o W}\right)^2 + K_3 \left(\frac{V_a}{V_o W}\right)^3 \quad (9.1)$$

The constants in Eq.(9.1) are presented in Table 9.2. It was found that the cracks were semi-elliptical cracks rather than through thickness cracks for blunt notch specimens until the crack lengths were approximately 2.9mm, 2.96mm or 2.7mm, which depends on the notch geometry. Therefore the measured crack lengths only represent the equivalent through thickness crack lengths rather than real crack lengths when the crack lengths are less than a certain length for blunt notch specimens. Plates 9.1 to 9.4 show the contours of fatigue cracks of various notch geometry specimens. The increments of potential drop and the corresponding equivalent through thickness crack lengths are listed in the tables below the plates.

The through thickness crack lengths in sharp notch specimens were estimated by measuring the crack length at 5 positions along the crack front with a travelling microscope and then the average crack length was compared with the equivalent crack length. This comparison is presented in Table 9.3. It can be seen that the difference between them is less than 4%. Thus the measured crack lengths in the present work were related to the areas of cracks for both sharp notch specimens and blunt notch specimens.

Table 9.2

Constants in Eq.(9.1) for Various Notch Geometry

(* Input Current 50 amp)

Constants	Notch Geometry, mm				
	$a_o = 5.00$ $\rho = 0.11$	$a_o = 5.00$ $\rho = 3.17$	$a_o = 5.00$ $\rho = 5.00$	$a_o = 10.00$ $\rho = 3.17$	$a_o = 5.00$ $\rho = 5.00$ chamfered
K_0	-0.415	-4.611	-6.627	-5.972	-6.607
K_1	1.263	12.392	15.367	9.614	14.952
K_2	-0.525	-10.457	-11.258	-4.746	-10.719
K_3	0.087	3.053	2.800	0.804	2.615

* For the 2XX group ofspecimens (a_o = 5.00mm, ρ = 0.11mm) at input current 44 amp the constants are as follows: $K_o = -0.385$, $K_1 = 1.223$, $K_2 = -0.515$, $K_3 = 0.084$

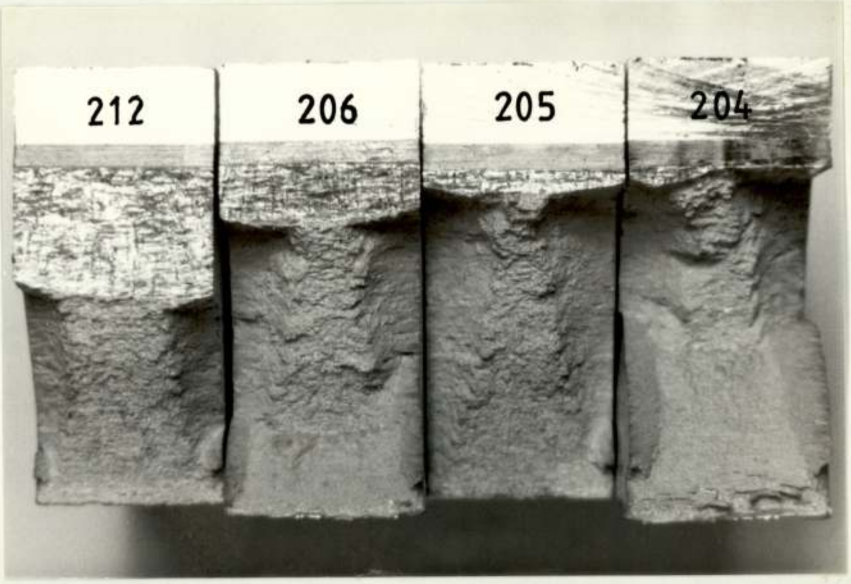

Specimen No	a_o mm	ρ mm	Δ P KN	C mm	ΔV µv
204	5.34	0.11	1.80	0.339	2.5
205	5.26	0.12	2.52	0.950	10.0
206	5.00	0.12	2.88	2.730	40.0
212	5.00	0.11	2.25	6.175	114.0

Plate 9.1 Macrograph of fatigue fracture surface for sharp notch specimens (a_o = 5.00mm, ρ = 0.11mm)

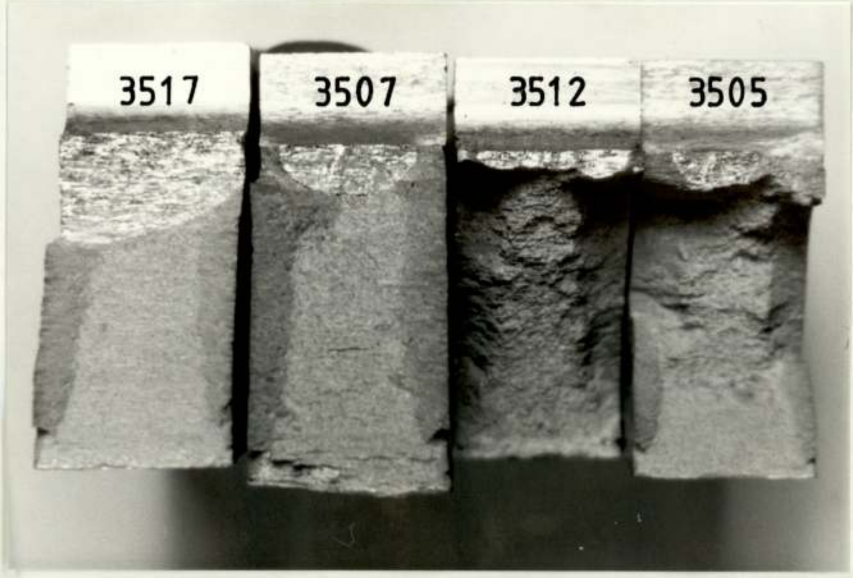

Specimen No	a_o mm	ρ mm	ΔP KN	C mm	ΔV μv
3505	4.88	3.29	4.68	0.681	3.5
3512	5.04	3.13	8.10	0.640	2.5
3507	5.00	3.20	5.22	1.511	10.0
3517	5.04	3.12	5.40	4.915	65.0

Plate 9.2 Macrograph of fatigue fracture surface for blunt notch specimens (a_o = 5.00mm, ρ =3.17mm)

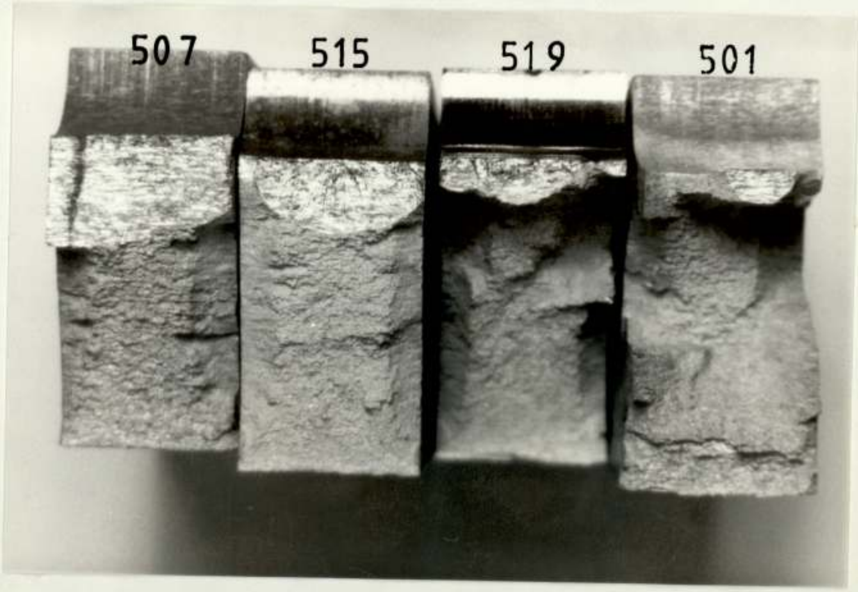

Specimen No	a_o mm	ρ mm	ΔP KN	C mm	ΔV μv
501	5.06	5.09	5.76	0.523	2.5
519	5.15	5.10	8.64	1.459	7.0
515	5.14	5.07	5.76	2.966	25.5
507	4.96	4.92	5.76	5.335	64.5

Plate 9.3 Macrograph of fatigue fracture surface for blunt notch specimens (a_o = 5.00mm, ρ = 5.00mm)

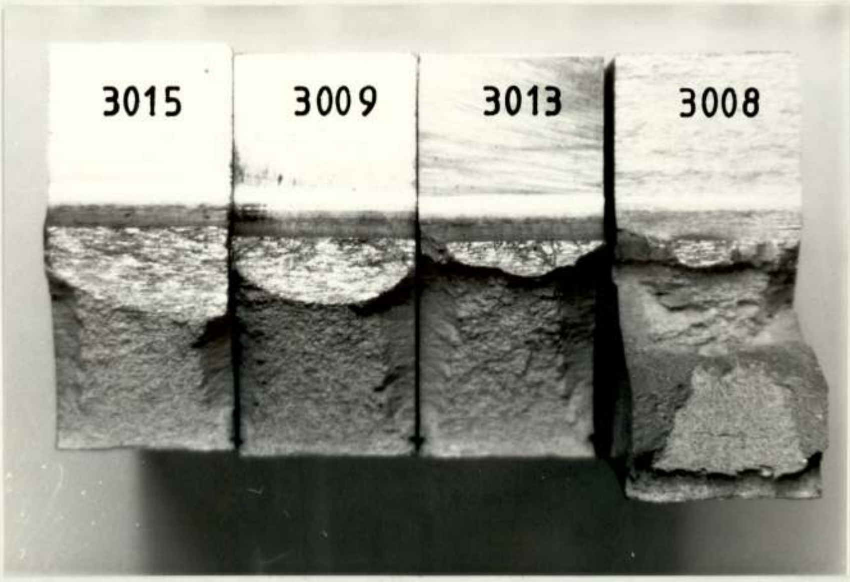

Specimen No	a_o mm	ρ mm	ΔP KN	C mm	ΔV μv
3008	9.95	3.18	3.96	0.216	1.7
3013	9.97	3.16	5.58	1.039	7.5
3009	9.95	3.15	3.83	2.902	41.0
3015	9.89	3.11	3.78	4.287	70.0

Plate 9.4 Macrograph of fatigue fracture surface for blunt notch specimens (a_o = 10.00mm, ρ = 3.17mm)

Table 9.3

Comparison of Measured Crack Lengths Using Different Methods

Increment of Potential Drop µV	Average Length mm	Equivalent Crack Length mm
2.5	0.329	0.339
10.0	0.930	0.950
10.5	1.230	1.323
20.0	1.566	1.759
40.0	2.671	2.729
87.5	4.802	4.808
112.5	5.990	6.077
113.5	6.331	6.486
114.0	6.119	6.175
182.0	8.295	8.413
194.5	8.561	8.656
219.0	9.459	9.501
249.5	9.878	9.818
264.0	10.385	10.429

9.2 Constant Amplitude Fatigue

9.2.1 The Initiation of Fatigue Crack

The dimensions of specimens which were employed to investigate the crack initiation are listed in Table 9.4. The experimental results are presented in Table 9.5 in which the definitions of the individual terms are described as follows. In order to give the similar lengths at initiation for various notch geometry the crack lengths at initiation for 2XX group and 30XX group specimens are defined as a crack which corresponds to 2 μv increment of potential drop and for 35XX group and 5XX group specimens the crack corresponds to 1 μv increment of potential drop. ΔS is nominal stress amplitude. K_t is stress concentration factor given in Table 8.3. K_f is fatigue notch factor calculated by Eq.(4.16). The equation is rewritten as follows:

$$K_f = 1 + \frac{K_t - 1}{1 + \sqrt{\frac{a^*}{\rho}}}$$

where ρ is notch root radius

a^* is Neubers length.

The estimated value of a^* is equal to 0.45mm in the present work (75). The calculated K_f are listed in Table 9.6 in which the K_t are also listed for comparison. ΔK is the stress intensity factor amplitude which is calculated with an imaginary crack whose length is the same as the notch depth. ΔK_n is the notch stress intensity factor amplitude calculated using Eqs.(4.27) and (4.25). The equations are rewritten as follows:

Table 9.4

Dimensions of Specimens

Specimen No	Width mm	Thickness mm	Notch Depth mm	Notch Root Radius mm
201	21.99	10.02	5.00	0.11
202	21.97	9.99	4.94	0.11
203	22.01	10.00	5.11	0.14
204	22.01	9.98	5.34	0.11
205	21.98	9.99	5.26	0.12
206	21.99	9.94	5.00	0.12
207	22.00	10.03	4.95	0.11
208	21.99	10.02	4.94	0.13
209	21.97	10.02	5.00	0.12
210	22.00	9.96	5.05	0.10
211	22.00	10.02	5.03	0.11
212	22.00	10.02	5.00	0.11
213	22.00	10.00	4.98	0.10
214	21.99	9.99	5.07	0.13

Table 9.4

(Contd.)

Specimen No	Width mm	Thickness mm	Notch Depth mm	Notch Root Radius mm
3516	22.03	9.99	5.00	3.18
3505	21.98	9.98	4.88	3.29
3506	21.98	9.98	4.91	3.23
3507	22.01	9.99	5.00	3.20
3517	22.00	9.99	5.04	3.12
3510	22.00	10.00	4.96	3.25
3509	22.00	10.00	5.05	3.27
3511	22.00	9.98	4.91	3.17
3512	22.00	10.00	5.04	3.13
3518	22.00	9.98	5.06	3.23

Table 9.4

(contd.)

Specimen No	Width mm	Thickness mm	Notch Depth mm	Notch Root Radius mm
517	21.99	10.01	5.00	5.10
510	22.00	10.03	5.22	5.06
508	21.97	10.03	5.15	5.26
506	21.96	10.00	4.91	5.22
501	21.97	10.03	5.06	5.09
505	21.99	10.04	5.16	5.21
507	21.98	9.99	4.96	4.92
511	21.99	10.01	5.02	4.96
502	22.00	10.01	5.15	5.07
504	21.99	10.03	5.19	5.02
509	21.99	10.02	5.07	5.08
519	21.96	10.01	5.15	5.10

Table 9.4

(Contd.)

Specimen No	Width mm	Thickness mm	Notch Depth mm	Notch Root Radius mm
3012	22.01	10.06	9.88	3.13
3010	21.98	9.99	9.97	3.22
3017	21.98	10.02	9.90	3.16
3015	21.97	10.01	9.89	3.11
3016	21.97	10.02	9.91	3.22
3014	22.00	10.06	9.87	3.16
3009	22.00	10.03	9.95	3.15
3008	21.99	10.02	9.95	3.18
3007	21.98	10.02	9.88	3.13
3006	21.99	10.01	9.88	3.13
3004	21.97	10.03	9.93	3.15
3005	21.97	9.99	9.90	3.22
3011	21.97	10.00	9.87	3.16
3013	21.99	10.03	9.97	3.16

Table 9.5

The Representation of Fatigue Crack Initiation Data

Table 9.5a

(Notch Geometry $a_o = 5.00mm$ $\rho = 0.11mm$)

Specimen No	Crack Length at initiation mm	Load Range KN	$K_t \Delta S$ MN/m^2	$K_f \Delta S$ MN/m^2	$\frac{\Delta K}{\sqrt{\rho}}$ MN/m^2	ΔK_n $MN/m^{3/2}$	N_i Cycles
204	0.13	1.80	664.3	297.4	615.9	6.54	702600
202	0.14	1.98	698.2	293.7	638.9	6.87	97200
209	0.14	1.98	701.3	295.0	622.9	6.90	69670
211	0.14	2.25	797.7	335.5	761.2	7.86	60800
210	0.14	2.25	804.4	338.4	778.7	7.92	34700
212	0.14	2.25	794.8	334.5	740.9	7.83	35400
201	0.14	2.25	795.4	334.5	731.3	7.83	42330
205	0.13	2.52	922.2	287.9	839.9	9.07	18940
203	0.14	2.70	967.5	406.8	779.5	9.51	17700
208	0.14	2.70	947.8	398.7	815.9	9.33	15520
206	0.14	2.88	1026.4	431.6	923.6	10.10	9888
207	0.14	3.06	1073.6	451.5	1001.3	10.57	7764
213	0.14	3.06	1080.6	454.4	1041.1	10.64	8160
214	0.14	3.42	1222.8	514.4	1044.2	12.02	3792

Table 9.5b

(Notch Geometry a_o = 5.00mm, ρ = 3.17mm)

Specimen No	Crack Length at Initiation mm	Load Range KN	$K_t \Delta S$ MN/m^2	$K_f \Delta S$ MN/m^2	$\frac{\Delta K}{\sqrt{\rho}}$ MN/m^2	ΔK_n $MN/m^{3/2}$	N_i Cycles
3504	-	4.32	342.9	301.7	256.9	4.12	>1002690
3516	0.12	4.50	359.3	316.2	275.4	6.83	182020
3505	0.12	4.68	370.1	325.7	278.6	6.97	119500
3506	0.12	4.86	385.7	339.4	293.0	7.29	90260
3507	0.11	5.22	417.4	367.3	318.6	7.91	85040
3517	0.11	5.40	434.1	382.0	335.6	8.27	35300
3510	0.11	5.58	443.9	390.7	336.1	8.38	75560
3509	0.11	5.76	463.1	407.5	349.7	8.69	20160
3511	0.12	5.94	470.9	414.3	361.3	8.97	19640
3512	0.12	8.10	650.5	572.4	502.2	12.39	18350
3518	0.12	8.64	696.9	613.3	529.7	13.13	9840

Table 9.5c

(Notch Geometry a_o = 5.00mm, ρ = 5.00mm

Specimen No	Crack Length at Initiation mm	Load Range KN	$K_t \Delta S$ MN/m^2	$K_f \Delta S$ MN/m^2	$\frac{\Delta K}{\sqrt{\rho}}$ MN/m^2	ΔK_n $MN/m^{3/2}$	N_i Cycles
518	-	5.04	362.3	332.1	242.9	4.25	> 1003290
517	0.14	5.13	365.4	335.0	248.7	7.15	89950
510	0.14	5.22	380.6	348.9	259.9	7.40	93960
508	0.13	5.40	391.3	358.7	261.8	7.54	114400
506	0.14	5.58	394.5	361.7	265.2	7.69	60120
501	0.14	5.76	413.0	378.6	281.0	8.06	62700
505	0.14	5.76	416.9	382.1	280.4	8.06	64240
507	0.13	5.76	409.5	375.4	283.1	8.10	58980
511	0.13	5.85	417.7	382.9	287.8	8.23	49610
502	0.13	5.94	430.4	394.5	293.3	8.39	67300
504	0.13	6.30	458.1	419.9	313.7	8.93	57000
509	0.13	8.64	616.3	564.9	416.6	12.06	22080
519	0.14	8.64	627.8	575.5	426.8	12.19	18428

Table 9.5d

(Notch Geometry $a_o = 10.00$mm, $\rho = 3.17$mm)

Specimen No	Crack Length at Initiation mm	Load Range KN	$K_t\Delta S$ MN/m^2	$K_f\Delta S$ MN/m^2	$\frac{\Delta K}{\sqrt{\rho}}$ MN/m^2	ΔK_n $MN/m^{3/2}$	N_i Cycles
3012	0.12	3.24	488.5	433.6	359.5	8.22	808790
3010	0.13	3.60	556.8	494.2	402.8	9.24	109530
3017	0.12	3.69	562.5	499.2	410.9	9.43	75880
3015	0.12	3.78	576.5	511.7	424.8	9.73	57700
3016	0.12	3.78	577.8	512.9	418.1	9.61	67200
3014	0.12	3.78	569.7	505.6	417.2	9.56	69760
3009	0.13	3.83	585.9	520.0	428.9	9.81	110000
3008	0.13	3.96	607.9	539.6	442.8	10.14	122560
3007	0.13	4.14	629.0	558.3	462.7	10.59	46060
3006	0.13	4.14	628.8	558.1	452.8	10.59	43440
3004	0.13	4.32	661.9	587.5	484.2	11.09	37860
3005	0.13	4.32	661.3	587.0	479.0	11.03	45968
3011	0.13	5.40	821.7	729.3	601.6	13.79	20940
3013	0.12	5.58	858.6	762.1	626.7	14.35	10660

Table 9.6

The Fatigue Notch Factor and Stress Concentration Factor

Specimen Type	Notch Depth mm	Notch Root Radius mm	K_f	K_t
2XX	5.00	0.11	3.26	7.75
35XX	5.00	3.17	1.54	1.75
30XX	10.00	3.17	1.50	1.69
5XX	5.00	5.00	1.43	1.56

$$K_n = \frac{6\,\Delta P\, Y_n \sqrt{a_o + C}}{BW} \tag{9.3}$$

$$Y_n = Y_L \sqrt{\frac{a_o \tanh\left(\frac{2\sqrt{1 + a_o/\rho}\;(C + C_B)}{\sqrt{a_o \rho}}\right) + (C + C_B)}{a_o + C}} \tag{9.4}$$

where C_B is grain size obtained by measuring the average intercepts in three sections of the grains. The procedure will be described in a later section. N_i is the number of cycles to initiation. The results are graphically presented in Figs.9.3-9.6 and can be represented in the form

$$N_i = B_1\,(K_t \Delta S)^{n_1} \tag{9.5}$$

$$N_i = B_2\,(\Delta K/\rho^{\frac{1}{2}})^{n_2} \tag{9.6}$$

$$N_i = B_3\,(K_f \Delta S)^{n_3} \tag{9.7}$$

$$N_i = B_4\,(\Delta K_n)^{n_4} \tag{9.8}$$

The values of B_1-B_4 and n_1-n_4 obtained from the best fit for the specimens with various notch geometry are given in Tables 9.7-9.10. It should be noted that the data for which the initiation lines exceeded 5×10^5 cycles were not used for the regression analysis.

The following observations can be made. The exponents n_1-n_4 are almost the same for the correspondent group of the specimens when the four parameters are used to represent the crack initiation data, but the coefficients are considerably different. For parameters $K_t \Delta S$, $\Delta K/\rho^{\frac{1}{2}}$ and $K_f \Delta S$ the coefficients in Eqs.(9.5)-(9.7) vary as

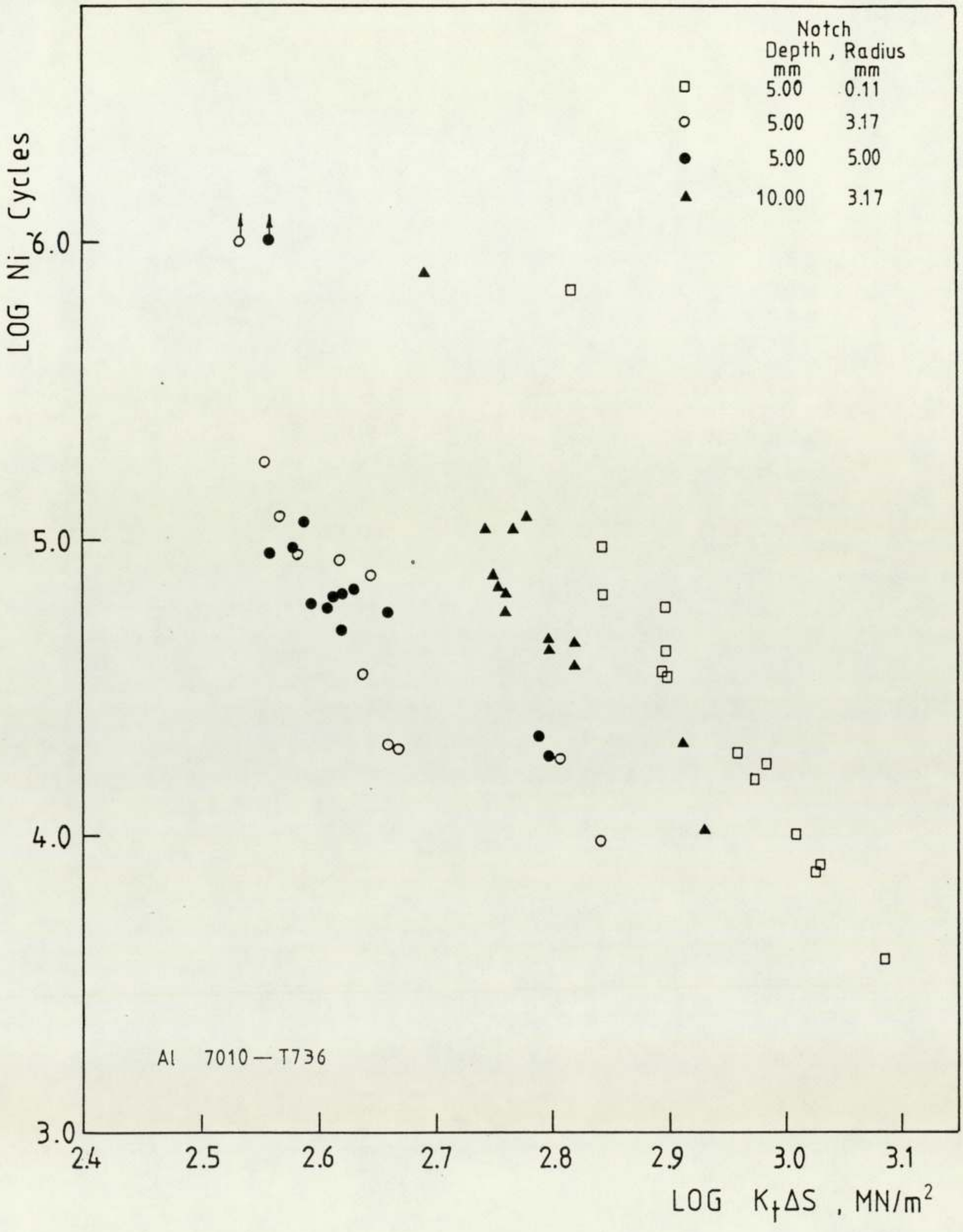

Figure 9.3 Fatigue crack initiation data for alloy 7010 - T736 (N_i versus $K_t\Delta S$)

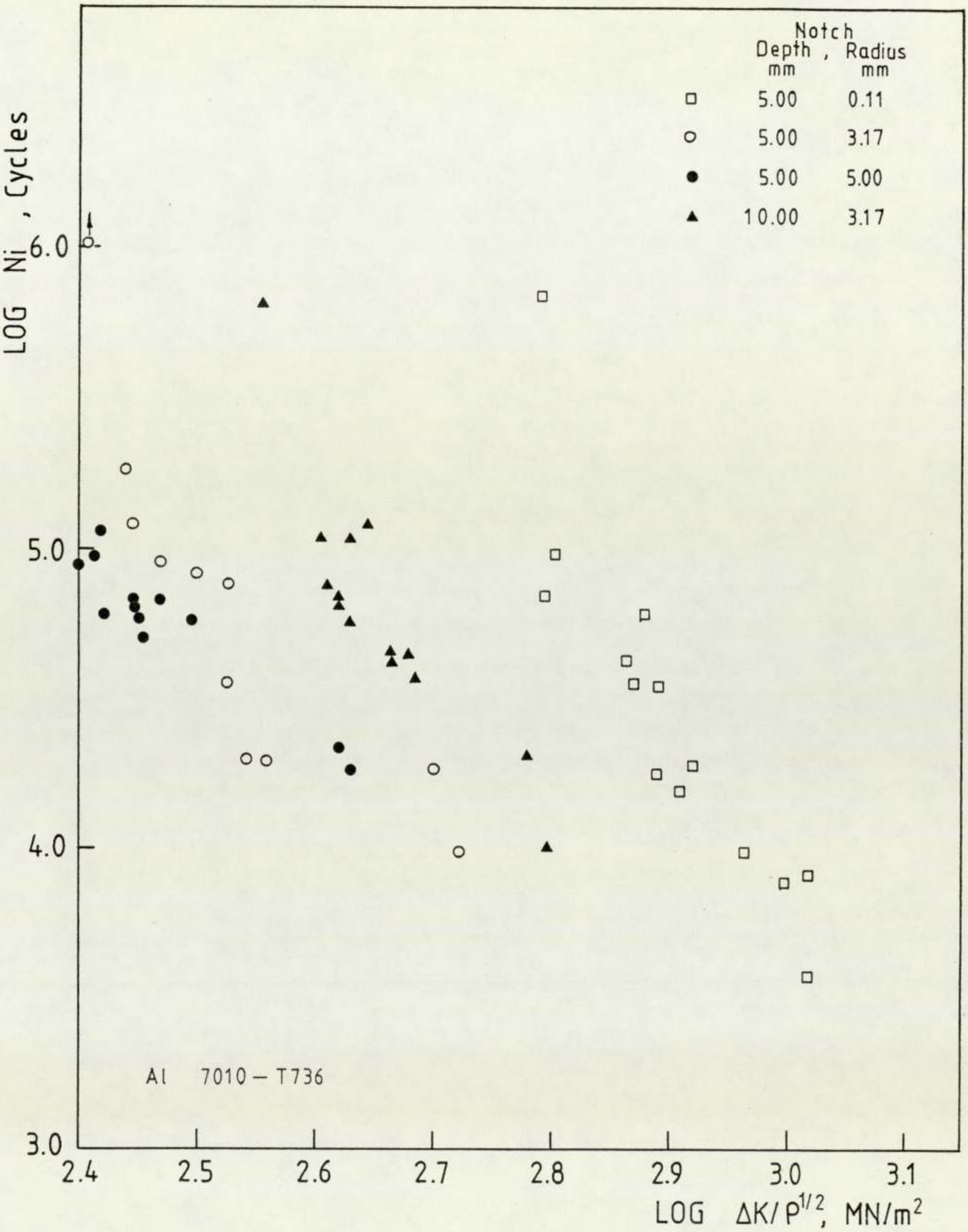

Figure 9.4 Fatigue crack initiation data for alloy 7010 - T736 (N_i versus $\Delta K/\rho^{\frac{1}{2}}$)

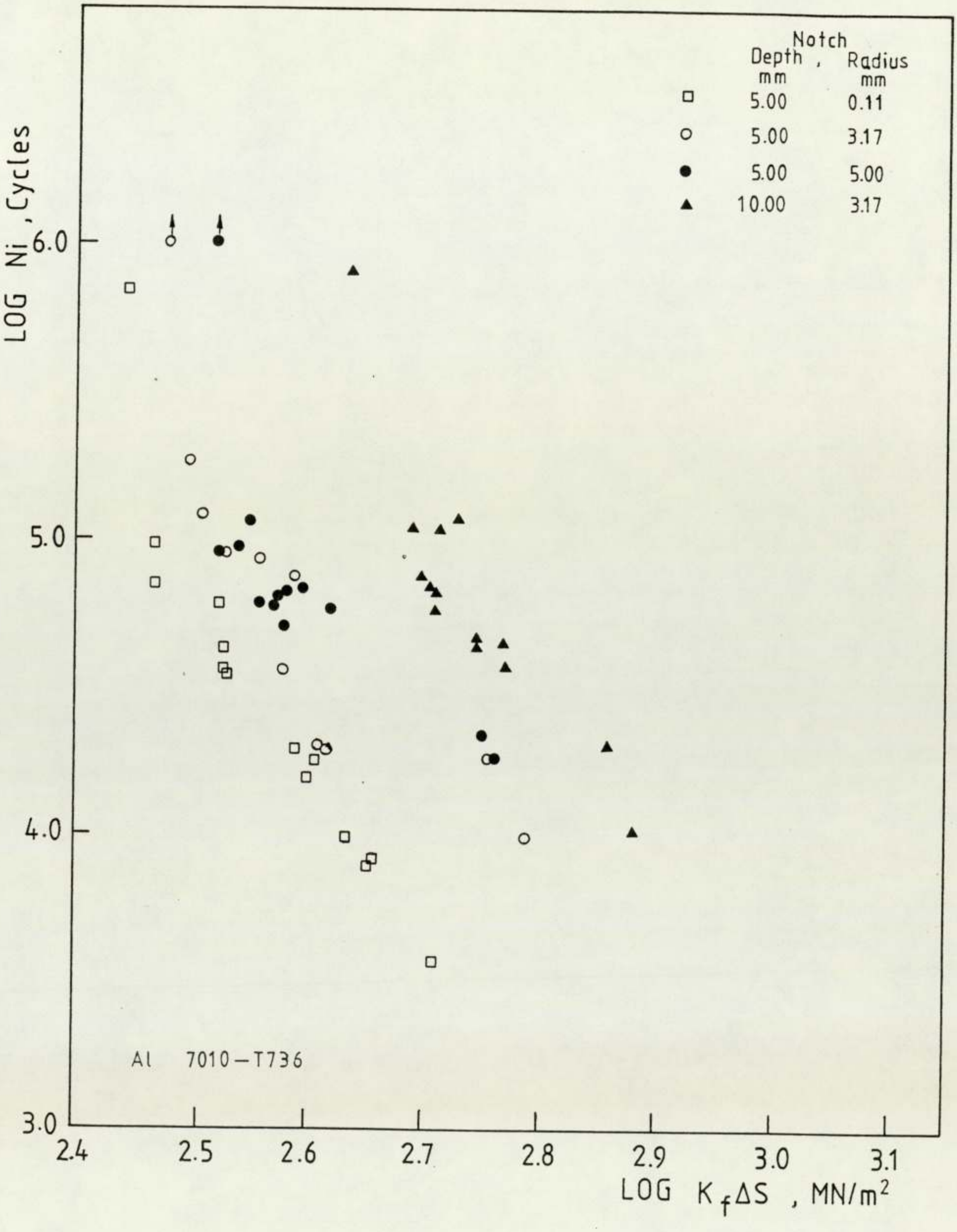

Figure 9.5 Fatigue crack initiation data for alloy 7010 - T736 (N_i versus $K_f\Delta S$)

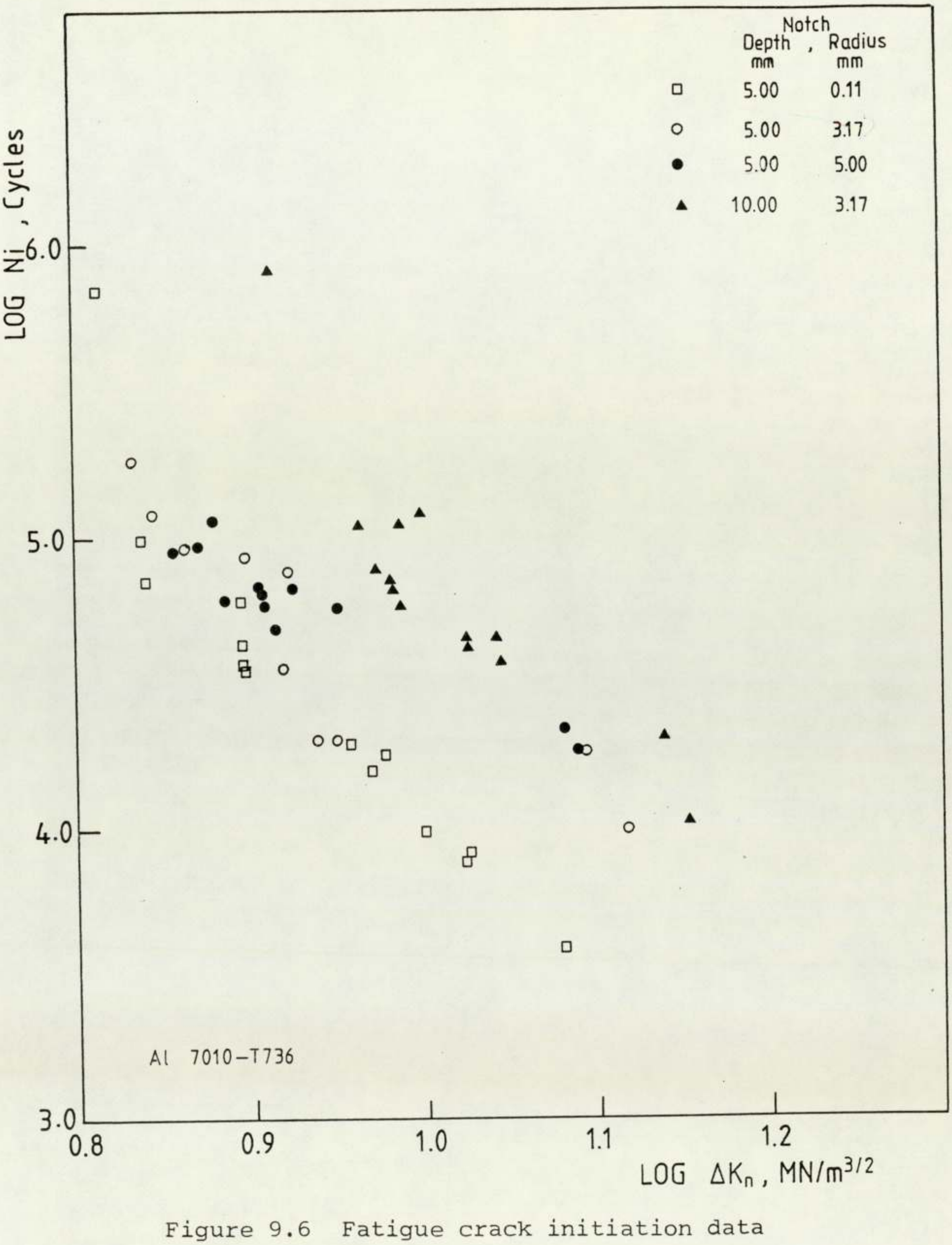

Figure 9.6 Fatigue crack initiation data for alloy 7010 - T736 (N_i versus ΔK_n)

Table 9.7

Constants of Initiation Equation (9.5)

for Alloy 7010 - T736

Specimen Type	Notch Geometry		$N_i = B_1 (K_t \Delta S)^{n_1}$	
	ρ mm	a_o mm	B_1	n_1
2XX	0.11	5.00	3.64×10^{20}	-5.49
30XX	3.17	10.00	1.82×10^{17}	-4.48
35XX	3.17	5.00	7.30×10^{14}	-3.84
5XX	5.00	5.00	2.54×10^{12}	-2.90

Table 9.8

Constants of Initiation Equation (9.6)

for Alloy 7010 - T736

Specimen Type	Notch Geometry		$N_i = B_2\ (\Delta K/\rho^{\frac{1}{2}})^{n_2}$	
	ρ mm	a_o mm	B_2	n_2
2XX	0.11	5.00	1.79×10^{20}	-5.47
30XX	3.17	10.00	4.56×10^{16}	-4.48
35XX	3.17	5.00	2.00×10^{14}	-3.79
5XX	5.00	5.00	8.28×10^{11}	-2.90

Table 9.9

Constants of Initiation Equation (9.7)

for Alloy 7010 - T736

Specimen Type	Notch Geometry		$N_i = B_3 (K_f \Delta S)^{n_3}$	
	ρ mm	a_o mm	B_3	n_3
2XX	0.11	5.00	3.18×10^{18}	-5.50
30XX	3.17	10.00	1.06×10^{17}	-4.48
35XX	3.17	5.00	4.47×10^{14}	-3.84
5XX	5.00	5.00	1.98×10^{12}	-2.90

Table 9.10

Constants of Initiation Equation (9.8)

for Alloy 7010 - T736

Specimen Type	Notch Geometry		$N_i = B_4 (\Delta K_n)^{n_4}$	
	ρ mm	a_o mm	B_4	n_4
2XX	0.11	5.00	3.57×10^9	-5.51
30XX	3.17	10.00	2.21×10^9	-4.50
35XX	3.17	5.00	1.83×10^8	-3.85
5XX	5.00	5.00	3.00×10^7	-2.93

much as 10^8 times for the sharp notch specimens to the blunt notch specimens. However, much less change can be observed when the crack initiation data was represented by the parameter ΔK_n. The regression analysis showed that the all crack initiation data presented in Fig.9.6 for the four groups of the specimens could be represented by one strainght line and described by Eq.(9.8) with the following constants:

$$B_4 = 3.32 \times 10^7$$
$$n_4 = 3.03$$

9.2.2 The Propagation of Long Fatigue Crack

As described previously the propagation rate of engineering crack can be represented by Paris law which is given in the form

$$\frac{da}{dN} = A\ (\Delta K)^m \tag{9.9}$$

The experimental results of long fatigue crack growth rate (LFCGR) are graphically represented in Fig.9.7. The constants A and m in Eq.(9.9) were obtained by least-square regression and this can be presented in a convenient form

$$\frac{da}{dN} = 4.3926 \times 10^{-8} \times (\Delta K)^{3.015} \tag{9.10}$$

The data presented here was obtained by the method described in Section 8.6.1.2. The details of the data analysis is as follows. A number of readings of potential

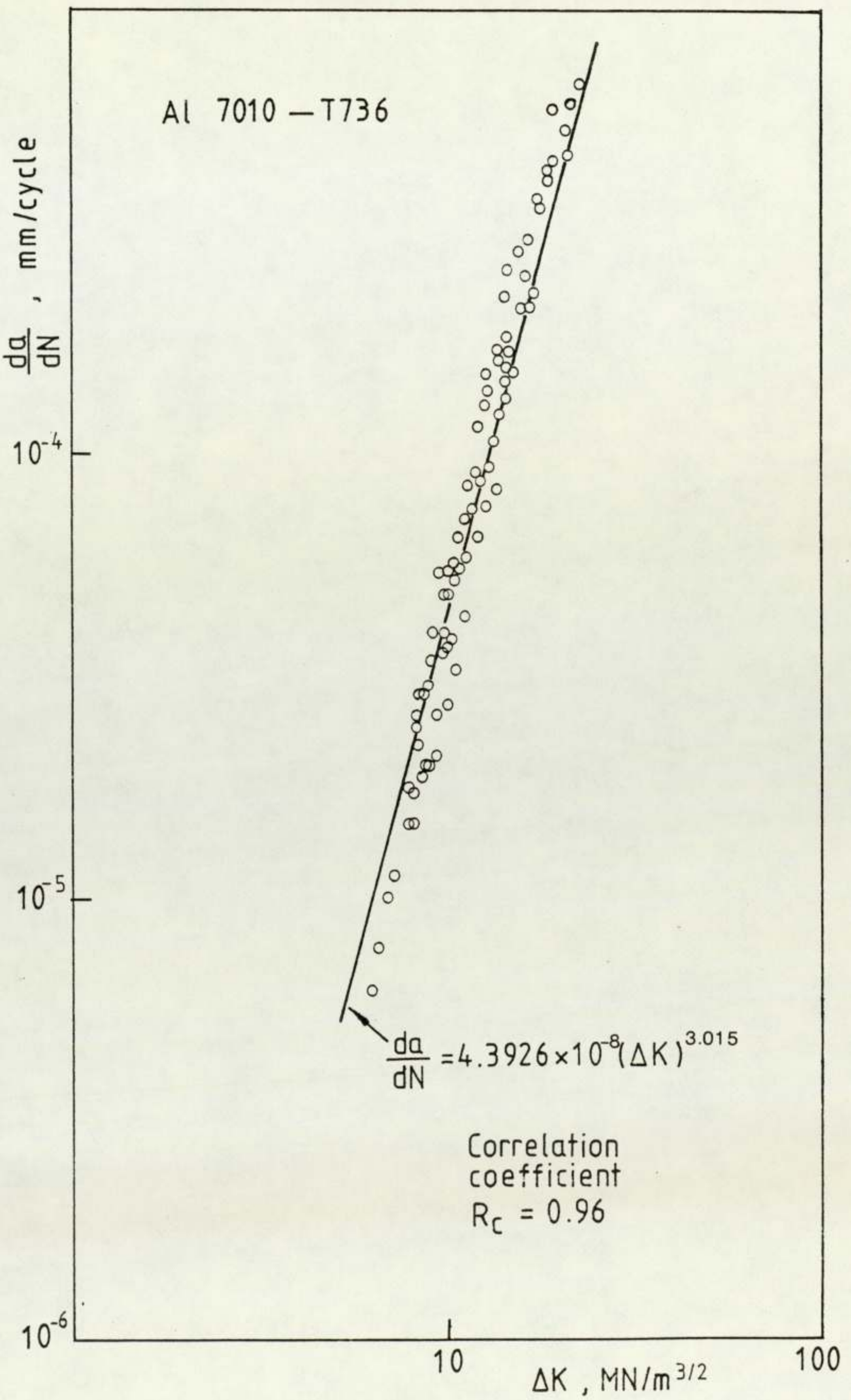

Figure 9.7

FCGR data $\frac{da}{dN}$ versus ΔK

drop were taken from the chart recorder. The initial increment of two successive readings was 2 μv until the change of potential drop was up to 10 μv, then the increment was maintained at 5 μv for the change of potential drop less than 120 μv after which it was 20 μv. In this way the proper Δa - increments were obtained and the minimum error for calculating $\frac{da}{dN}$ could be guaranteed. This will be discussed in a later section. The values of potential drop taken in this way were then substituted into Eq.(9.1) to calculate the corresponding crack length a_i and the corresponding number of cycles N_i for each potential drop readings were counted from the chart recorder. Two adjacent data pairs of a_i and N_i were used to produce the crack growth rate data using secant methods. This could be expressed in the form of

$$\left(\frac{da}{dN}\right)_{\bar{a}} = \frac{a_i - a_{i-1}}{N_i - N_{i-1}}$$

where $\bar{a}$ was the average value of two adjacent crack lengths a_i and a_{i-1}, i.e. $\bar{a} = \frac{1}{2}(a_i + a_{i-1})$, and it was used to calculate stress intensity factor range ΔK using the following equation (125)

$$K = \frac{6\,\Delta P\, Y_L \sqrt{a}}{BW} \tag{9.11}$$

where

$$Y = \frac{1.99 - 2.15(\frac{a}{W}) + 6.08(\frac{a}{W})^2 - 6.63(\frac{a}{W})^3 + 2.7(\frac{a}{W})^4}{(1 + 2\frac{a}{W})\,(1 - \frac{a}{W})^{3/2}} \tag{9.12}$$

It was found that the increment of 10 μv of potential drop corresponded to the crack length of 1mm. Thus, the data of $\frac{da}{dN}$ and ΔK computed after this increment of potential drop was used to determine the constants A and m by regression analysis so that the influence of the notch stress field on the results can be avoided. This procedure described above was carried out using a computer programme in which the input merely involves the data pairs of potential drop readings V_i and the corresponding number of cycles N_i, the load amplitude ΔP and the dimension parameters of the specimen. In the present work the upper and lower limits on $\frac{da}{dN}$ are 10^{-3} mm/cycle and 5×10^{-6} mm/cycle and the unit of ΔK is $MN/m^{3/2}$.

9.2.3 The Propagation of Short Fatigue Crack in Notch Stress Field.

As described in the previous section (Section 4.4) the propagation of fatigue crack emanating from notch root is affected by the notch stress field within a certain length. Following the same procedure described in the last section the crack growth rates in blunt notch stress field were determined and the results are shown in Figs. 9.8-9.10.

Using the measured crack growth rates and the constants A and m the stress intensity factor range ΔK_n in notch stress field were experimentally calibrated. This can be expressed in the form

$$\Delta K_{cal} = \left(\frac{da}{dN} \frac{1}{A}\right)^{\frac{1}{m}} \qquad (9.13)$$

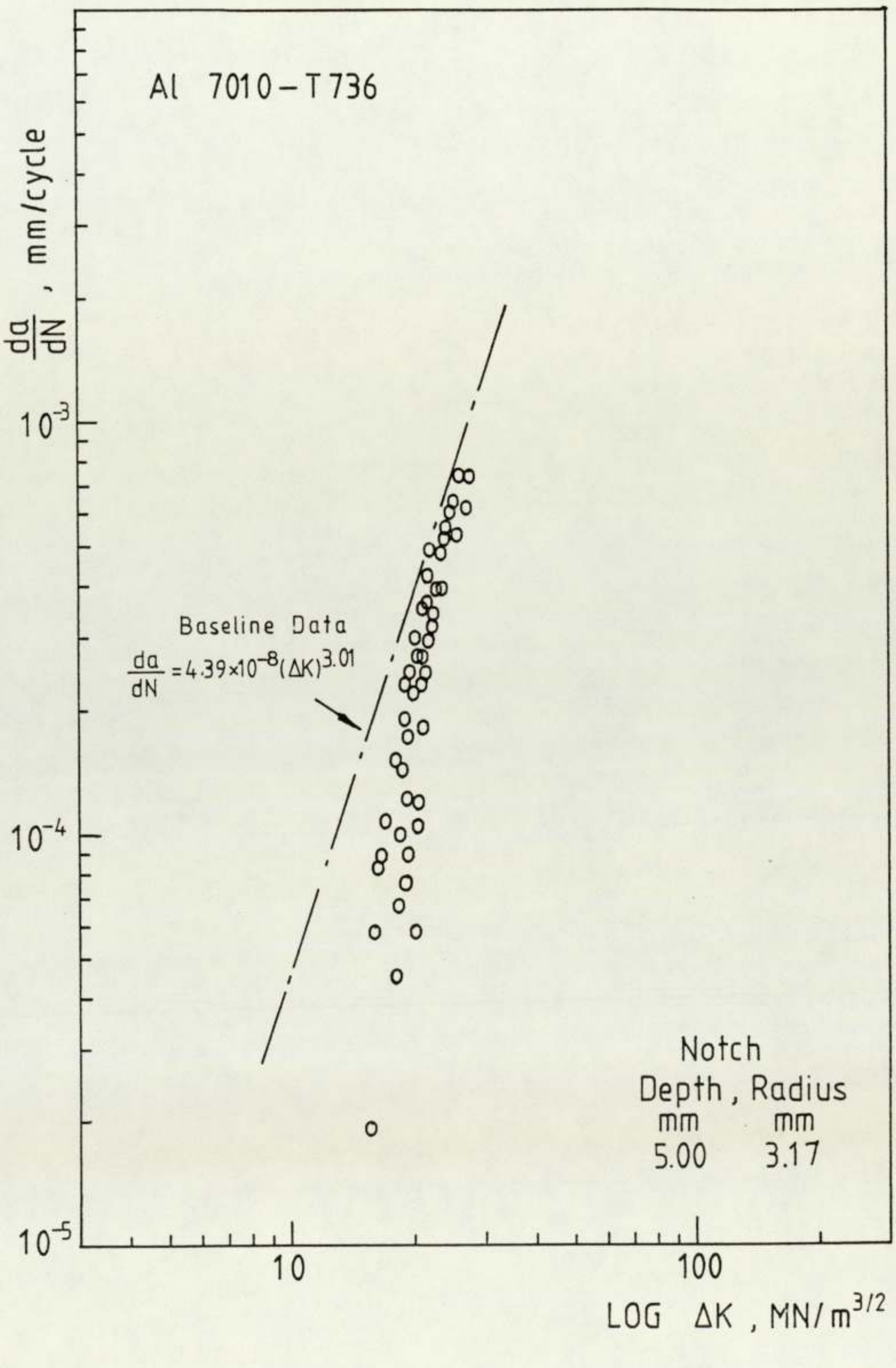

Figure 9.8 Short crack growth rate in notch stress field for alloy 7010 - T736 (a_o = 5.00mm, ρ = 3.17mm)

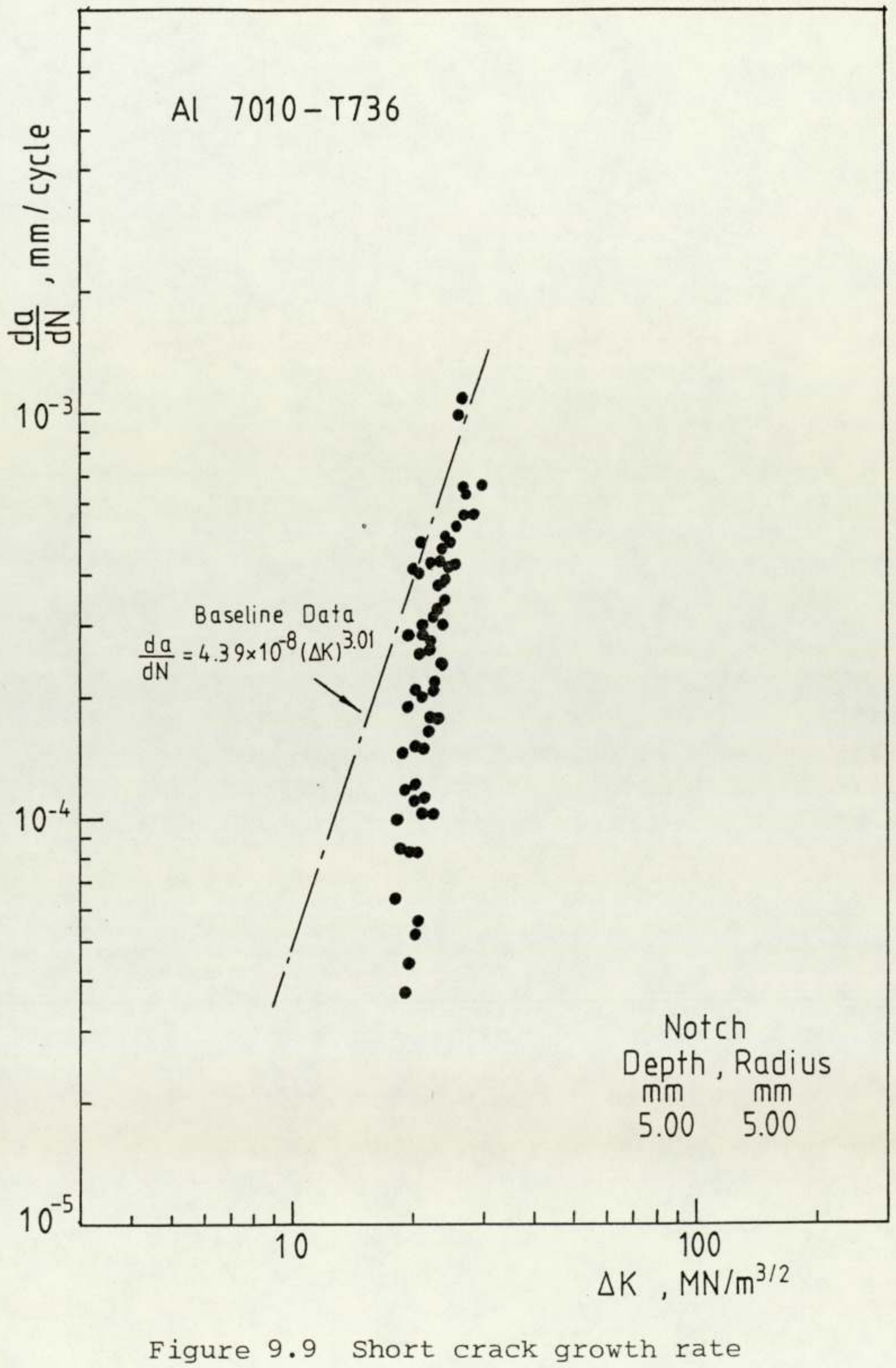

Figure 9.9 Short crack growth rate in notch stress field for alloy 7010 - T736 (a_o = 5.00mm, ρ = 5.00mm)

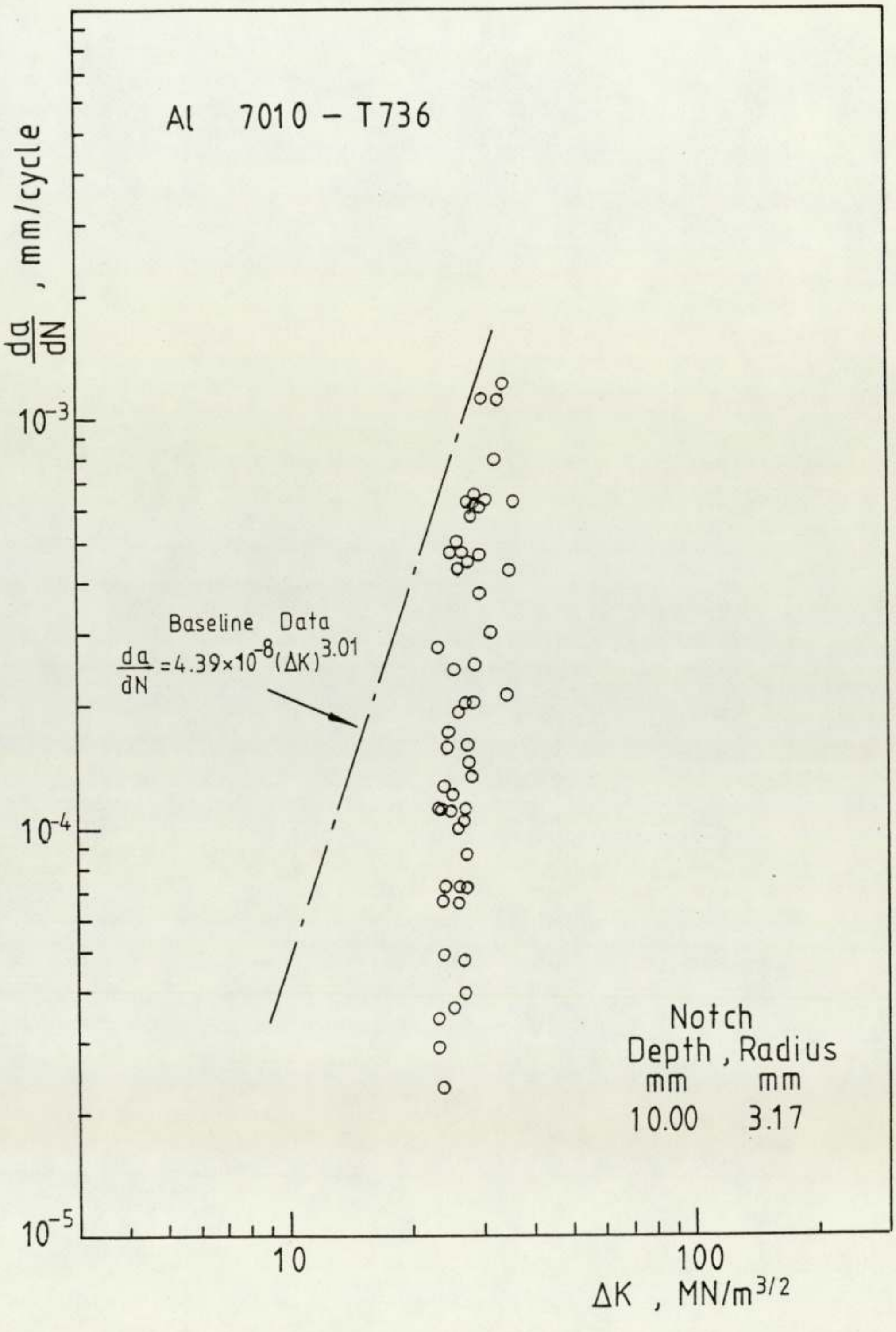

Figure 9.10 Short crack growth rate in notch stress field for alloy 7010 - T736 (a_o = 10.00mm, ρ = 3.17mm)

Since ΔK_n is also given by

$$\Delta K_n = \Delta S \, Y_n \sqrt{a_o + C} \qquad (9.14)$$

the ratio of the dimension less parameter Y_n for short crack to Y_L is given by

$$\frac{Y_n}{Y_L} = \frac{\left(\frac{da}{dN} \; \frac{1}{A}\right)^{\frac{1}{m}}}{Y_L \, \Delta S \, \sqrt{a_o + C}} \qquad (9.15)$$

The experimental results of $\frac{Y_n}{Y_L}$ are graphically presented in Figs. 9.11-9.13 in which the calculated results using Jergeus' (71) equation are also plotted for comparison.

It can be seen the values of Y_n/Y_L asymptotically increase to 1 as cracks grow to a critical length C_o. In present investigation C_o were experimentally estimated by taking C_o as the crack lengths at which Y_n/Y_L reach stable values that correspond to the values from 0.85 to 0.95 depending on individual specimen. The results are shown in Table 9.11 in which some calculated values of C_o are also presented. It seems that Jergeus' equation ($0.5\sqrt{a_o \rho}$) and Yamaamoto's equation $(W - a_o)\xi_o)$ could give more reasonable estimation of C_o than others.

9.2.4 The Initiation and Propagation of Fatigue Crack from the Shot-Peened Blunt Notches.

The dimensions of the shot-peened specimens are listed in Table 9.12. The experimental results of fatigue crack initiation are presented in Table 9.13 and graphically shown in Figs. 9.14-9.17 in which the data of unshot-peened specimens are also plotted for comparison.

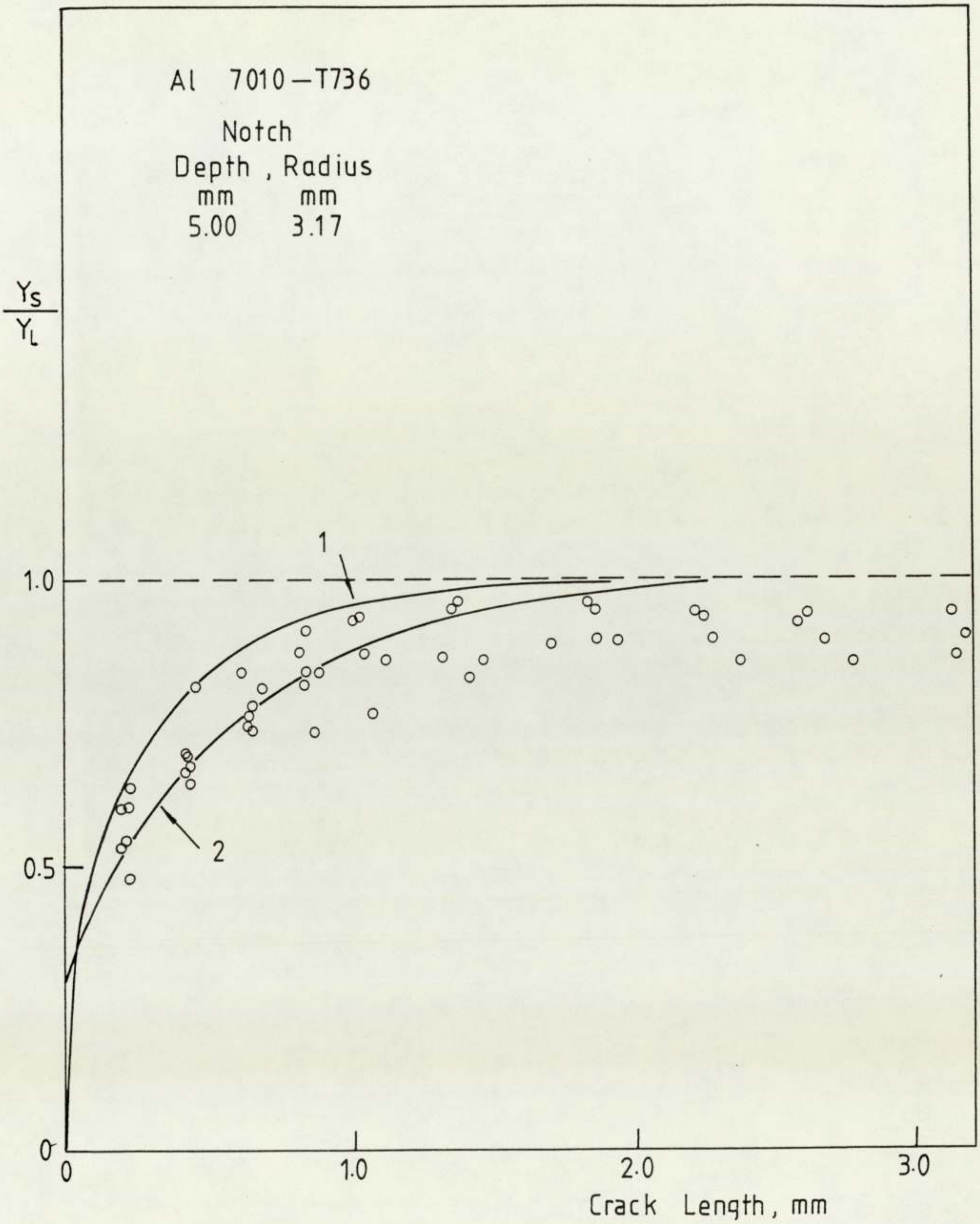

Figure 9.11 Correlation of stress intensity factor coefficients for short crack to long crack. (a_o = 5.00mm, ρ = 3.17mm)

Curve 1 represents Eq.(4.26) (Jergeus (71)).

Curve 2 represents Eq.(4.27) (Nadkarni (50)).

The same in Figs.9.12 and 9.13

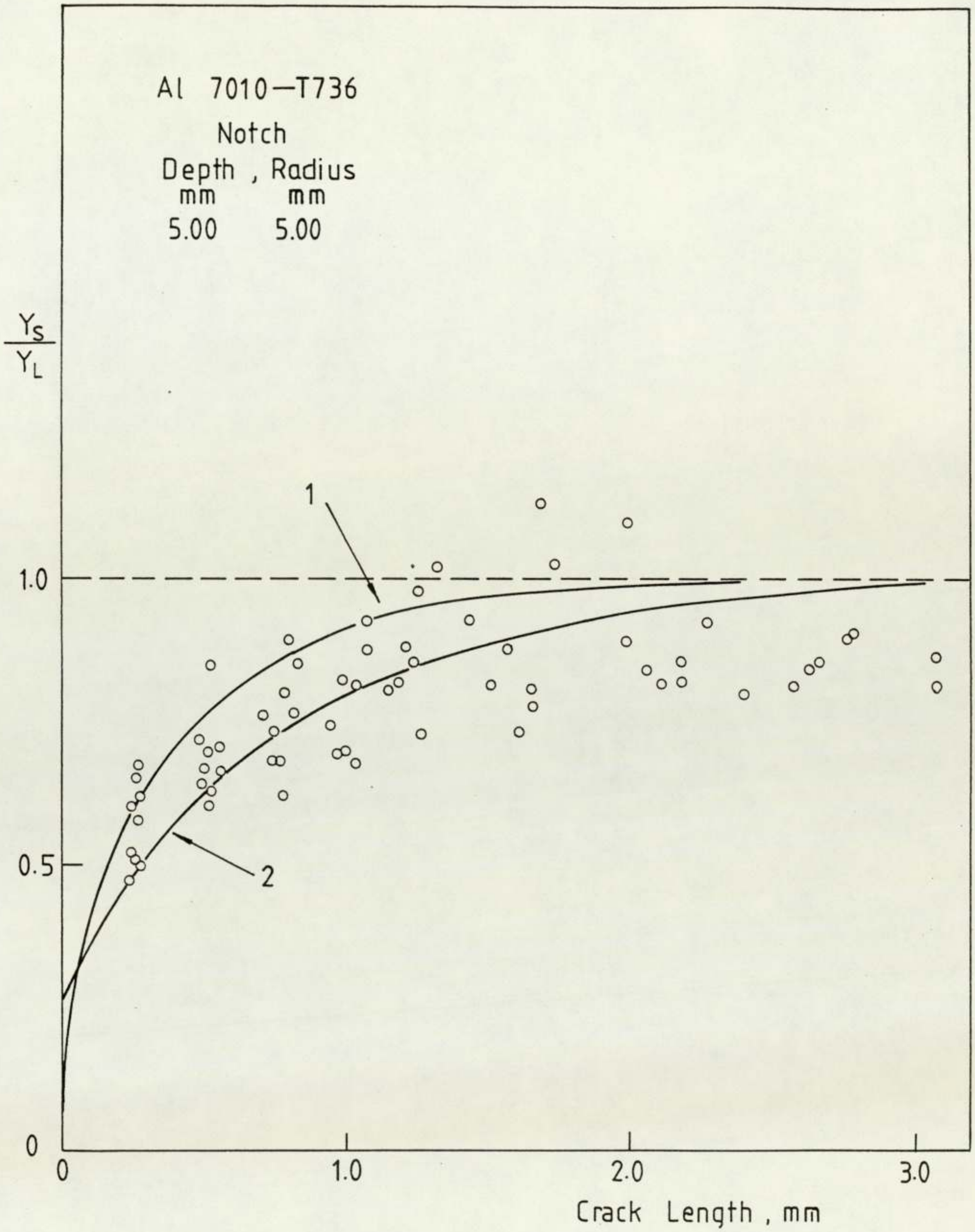

Figure 9.12 Correlation of stress intensity factor coefficients for short crack to long crack (a_o = 5.00mm, ρ = 5.00mm)

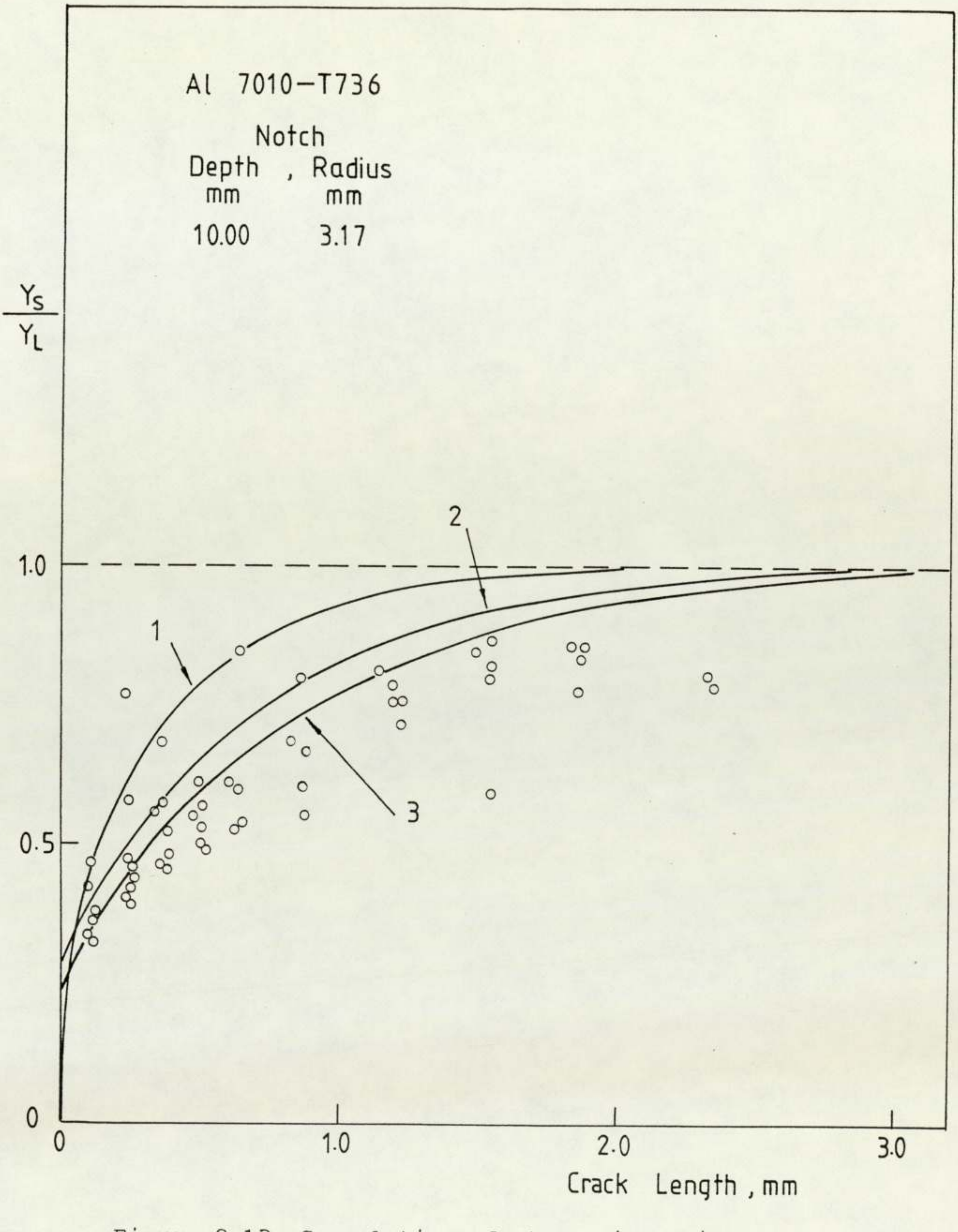

Figure 9.13 Correlation of stress intensity factor coefficients for short crack to long crack (a_o = 10.00mm, ρ =3.17mm)

Table 9.11

Comparison of the Experimental C_o and the Calculated C_o

Specimen	Notch Geometry		Calculated C_o, mm				Experimental
Type	a_o, mm	ρ mm	$0.13\sqrt{a_o \rho}$	0.2ρ	$0.5\sqrt{a_o \rho}$	$(W-a_o)\xi_o$	C_o, mm
30XX	10.00	3.17	0.73	0.634	2.18	2.59	-
5XX	5.00	5.00	0.65	1.00	2.50	2.32	2.25
35XX	5.00	3.17	0.518	0.634	1.99	1.88	1.50
2XX	5.00	0.11	0.098	0.023	0.38	0.37	-

Table 9.12

Dimensions of the Shot-Peened Specimens*

Specimen No	Width mm	Thickness mm	Notch Depth mm	Notch Root Radius mm
53A	21.99	10.00	5.15	4.86
54A	21.96	10.01	5.30	4.89
55A	21.98	10.01	5.05	5.08
56A	22.00	10.00	5.40	4.87
57A	21.94	9.98	5.10	4.92
58A	21.96	9.99	5.30	4.96
59A	21.96	9.95	5.20	5.00
51B	21.99	10.01	5.15	4.87
52B	22.00	10.02	5.15	4.89
53B	21.98	9.98	5.20	4.97
54B	22.00	9.99	5.35	4.91
55B	21.98	10.03	5.10	4.93

* The specimens of group A were shot-peened on top and sides.

The specimens of group B were shot-peened on top only.

Table 9.13

The Representation of Fatigue Crack Initiation Data for Shot-Peened Specimens

(a_o = 5.00mm, ρ = 5.00mm)

Specimen No	Crack Length at Initiation mm	Load Range KN	$K_t\Delta S$ MN/m^2	$K_f\Delta S$ MN/m^2	$\Delta K/\rho^{\frac{1}{2}}$ MN/m^2	ΔK_n MN/m^2	N_i Cycle
53A	0.14	5.00	362.9	332.6	252.9	7.2	144000
57A	0.13	5.31	385.3	353.2	266.3	7.4	108000
59A	0.14	5.40	397.2	364.1	272.6	7.7	65100
58A	0.13	5.72	424.0	388.7	291.8	8.2	67800
56A	0.14	6.57	490.9	450.0	341.4	9.4	28200
55A	0.14	6.66	477.5	437.7	325.4	9.3	30000
54A	0.14	8.05	595.6	546.0	413.2	11.6	19800
51B	0.14	5.22	378.5	346.9	263.0	7.4	107400
52B	0.14	5.77	417.6	382.8	290.0	8.1	68400
53B	0.14	5.85	428.3	392.5	295.0	8.3	83510
54B	0.13	6.71	498.9	457.3	345.2	9.8	23160
55B	0.14	8.10	583.1	534.5	403.2	11.3	9400

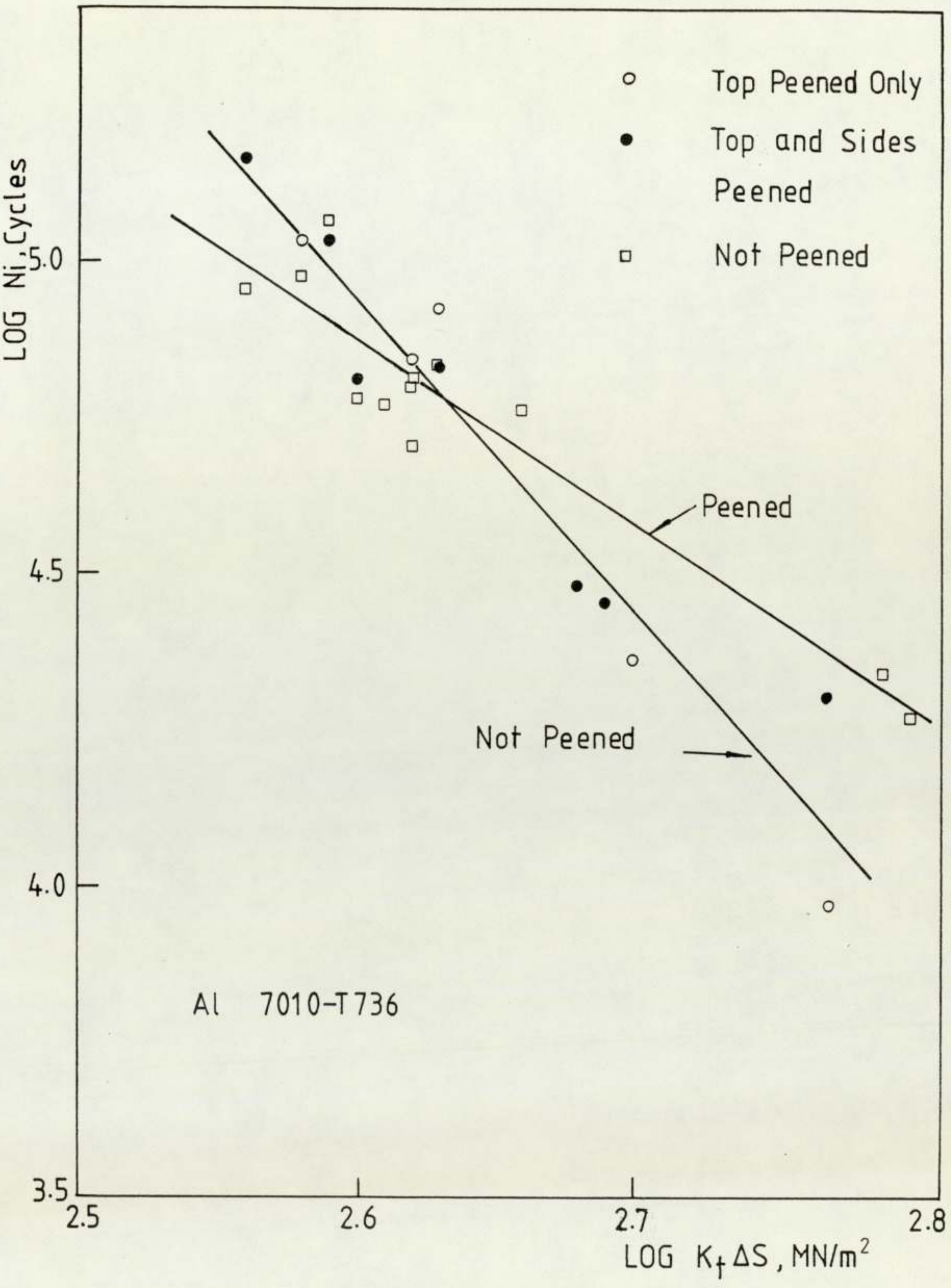

Figure 9.14 Comparison of initiation data for shot peened and unshot peened specimens (N_i versus $K_t \Delta S$)

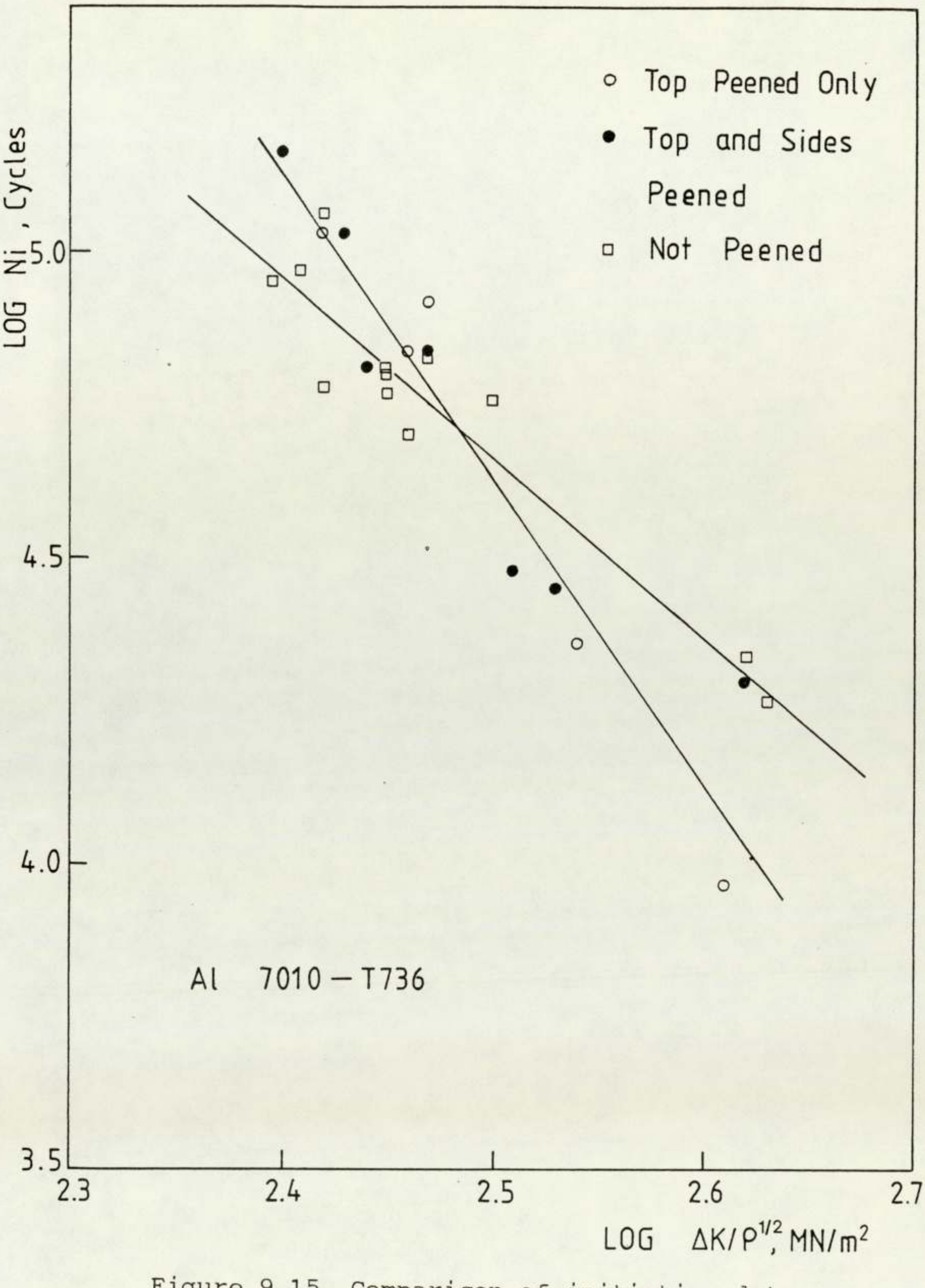

Figure 9.15 Comparison of initiation data for shot peened and unshot peened specimens (N_i versus $\Delta K/\rho^{\frac{1}{2}}$)

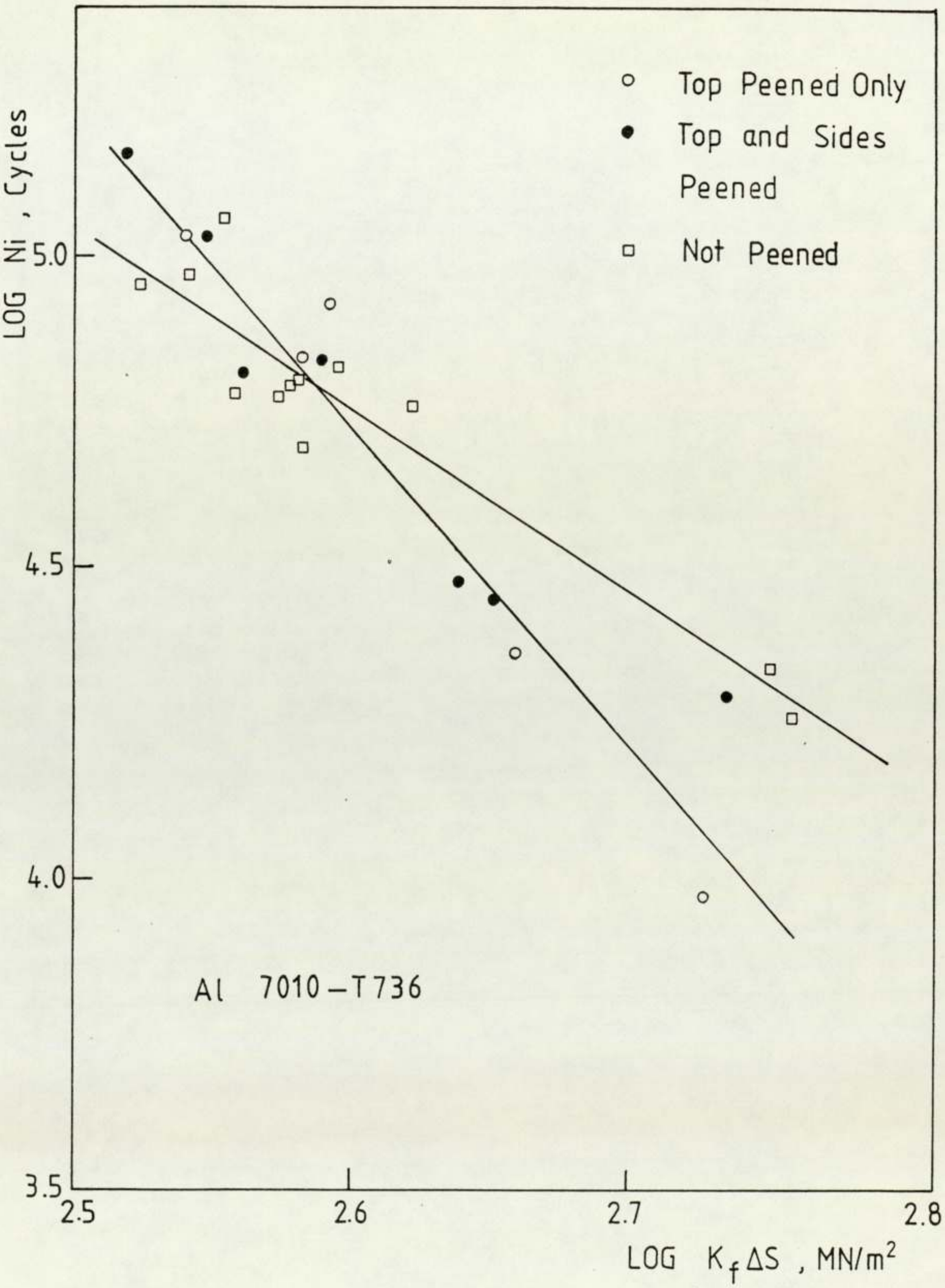

Figure 9.16 Comparison of initiation data for shot peened and unshot peened specimens (n_i versus $K_f \Delta S$)

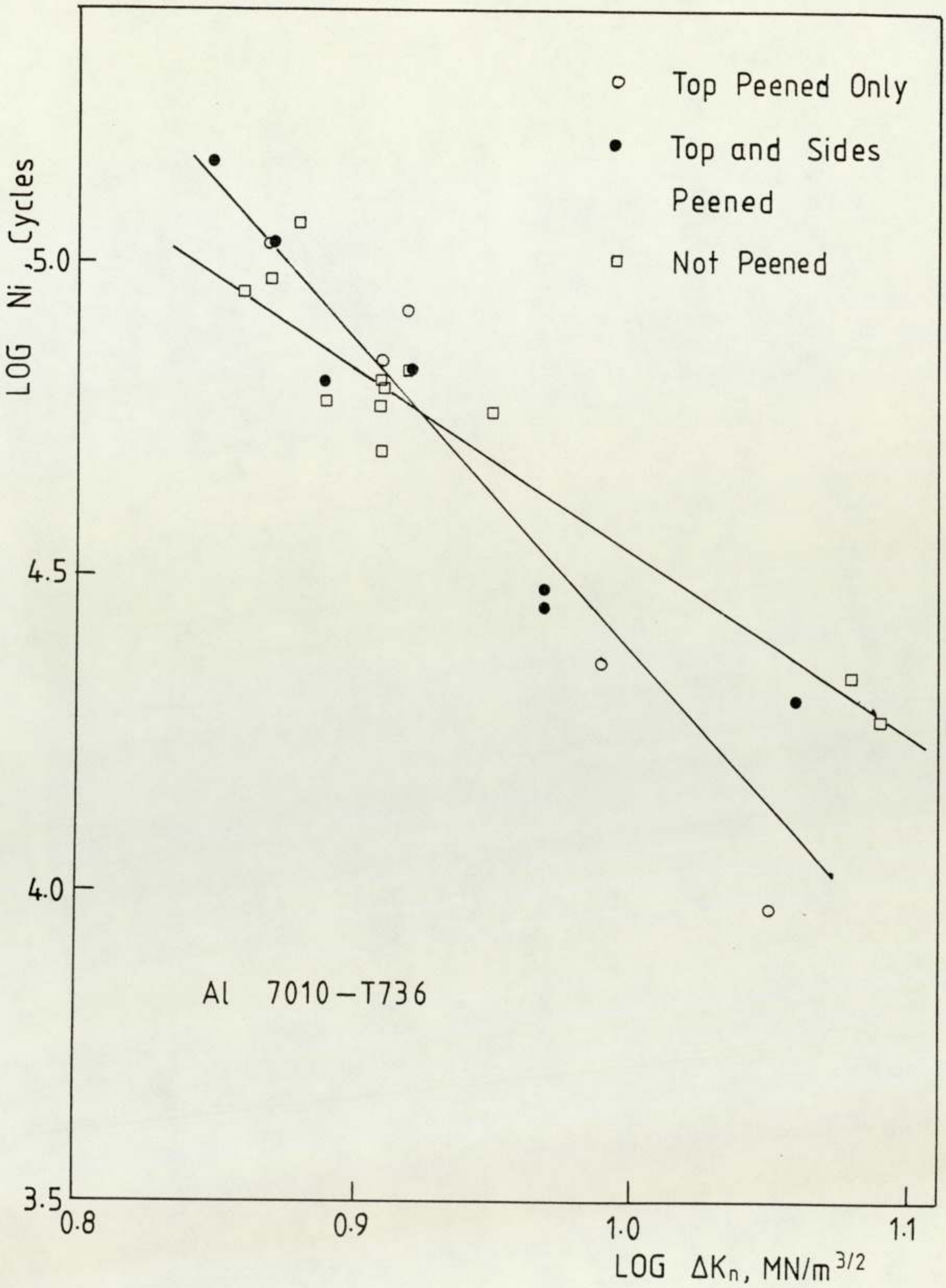

Figure 9.17 Comparison of initiation data for shot peened and unshot peened specimens (N_i versus ΔK_n)

The initiation criterion and the definitions of the terms in Table 9.13 were the same as that described previously. The results can be represented by Eqs.(9.5)-(9.8) and the constants B_1-B_4 and n_1-n_4 for both unshot-peened specimens and shot-peened specimens are shown in Table 9.14. The dependence of short crack growth rates on stress intensity factor range in notch stress field is shown in Fig.9.18. The effects of shot-peening on short crack growth rates is shown in Fig.9.19.

The following findings can be observed from the results

i) No significant difference in the effects of shot-peening on fatigue initiation and propagation can be seen for group A and group B specimens. This means that the shot-peening ways under consideration are not important as long as the peening intensity remains at the same level.

ii) The intersection of best fit lines of shot-peened and unpeened specimens in Figs 9.14-9.17 can be observed and it suggests that shot-peening could slightly improve the resistance to fatigue at lower load level, however, probably worse effect will occur due to shot-peening at high load level.

iii) After the crack initiation the fatigue crack growth rates of shot-peened specimens were higher than that of unpeened specimens until the crack grew to about 1.2mm and after that the influence of shot-peening on crack growth vanished.

Table 9.14

Comparison of the Constants of Initiation Eqs.(9.5) - (9.8) for Unshot-Peened Specimens and Shot-Peened Specimens

(a_o = 5.00mm, ρ =5.00mm)

Constants	Unshot-Peened Specimens	Shot-Peened Specimens
B_1	2.54×10^{12}	3.86×10^{17}
n_1	-2.90	-4.87
B_2	8.28×10^{11}	6.05×10^{16}
n_2	-2.90	-4.86
B_3	1.98×10^{12}	2.51×10^{17}
n_3	-2.90	-4.87
B_4	3.00×10^{7}	2.12×10^{9}
n_4	-2.93	-4.94

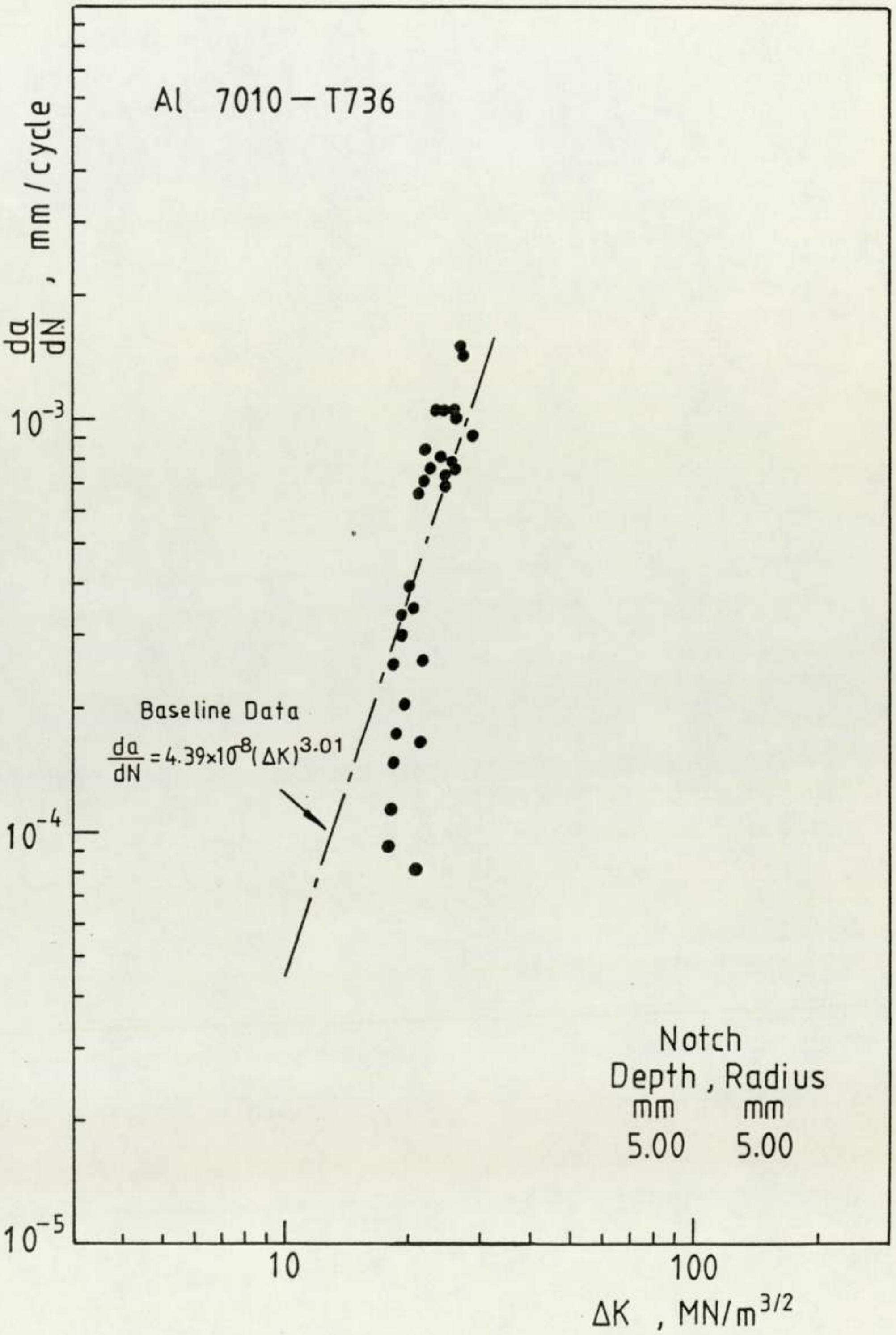

Figure 9.18 Short crack growth rate data in notch stress field for shot peened specimens.

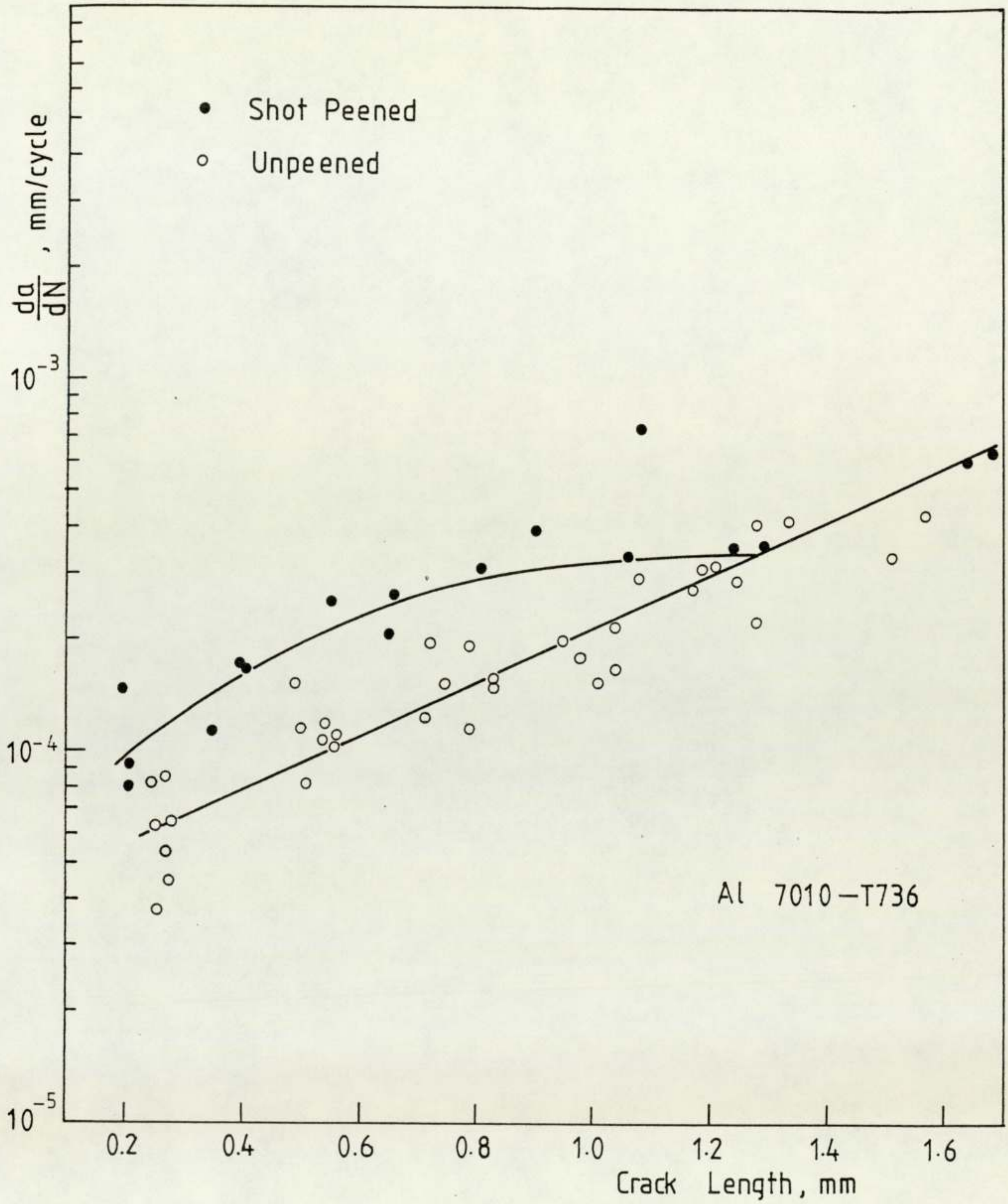

Figure 9.19 Comparison of short crack growth rates for shot peened and unshot peened specimens

9.2.5 Metallography and Fractography

9.2.5.1 The Measurements of Grain Dimensions

The grain structure on three section is shown in Plates 9.5-9.7 and the grain arrangement in specimen and the grain shape in space are schematically shown in Fig.9.20. The measured average intercept sizes in three directions $\bar{l}_s$, $\bar{l}_t$ and $\bar{l}_L$ are 0.08mm, 0.44mm and 1.52mm respectively. The fatigue crack initiation from notch root in present work should be mainly correlated to the value of $\bar{l}_s$. Thus, C_B was taken as $\bar{l}_s$ in Eq.(9.4) for the calculation of ΔK_n.

9.2.5.2 The Examination of Microstructure

The microstructure of the alloy 7010 - T736 is illustrated in Fig.9.21. It showed mixed granular structure, i.e. the structure constituted by aggregates of sub-grains and by randomly distributed recrystallised grains of rather reduced size. The analysis of x-ray microprobe suggested that the secondary phases, which were shown as dark particles in Fig.9.21, were mainly Al-Cu-Fe compounds and, to a much less degree, Al-Mg-Si compounds. It seems that the secondary phases may promote the procedure of recrystallisation.

9.2.5.3 The Examination of Macro-Fatigue Crack Growth

Two types of crack contour were observed during its early propagation stage. For sharp notch specimens (a_o = 5.00mm, ρ = 0.11mm) fatigue crack emanating from notch root is basically a through thickness crack even at the very beginning of the crack growth (Plate 9.1).

Plate 9.5 Grain structure in normal cross section. Etching in Barker's reagent, X27

Plate 9.6 Grain structure in transverse section. Etching in Barker's reagent, X27

Plate 9.7 Grain structure in longitudinal section. Etching in Barker's reagent, X27

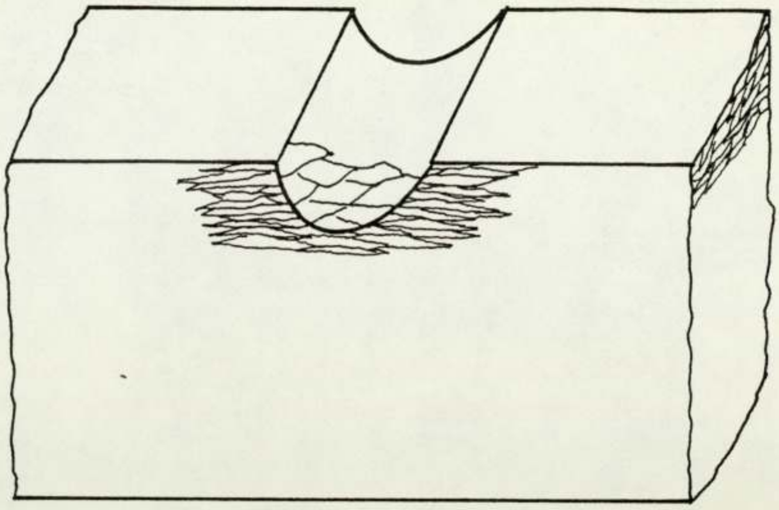

(a)

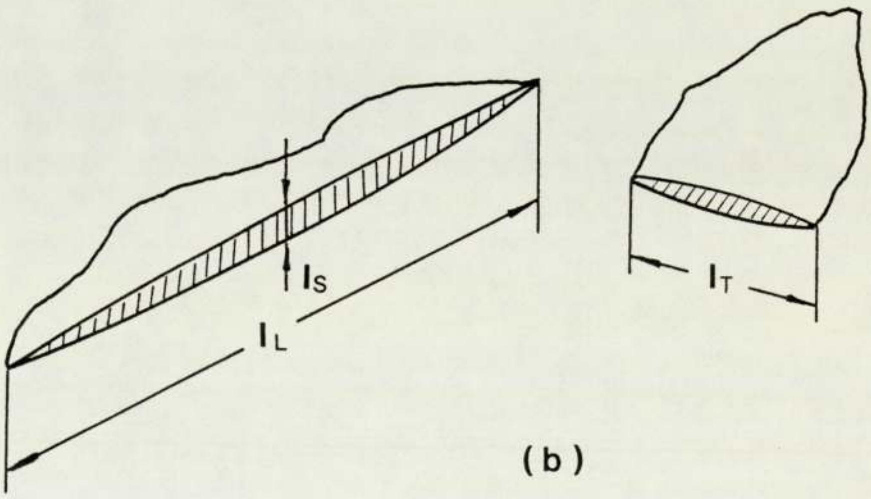

(b)

Figure 9.20 Schematical diagrams of grain arrangement in specimen and its shape in space.

a) Diagrams of grain arrangement in specimen.

b) Diagrams schematically showing the grain shape in space.

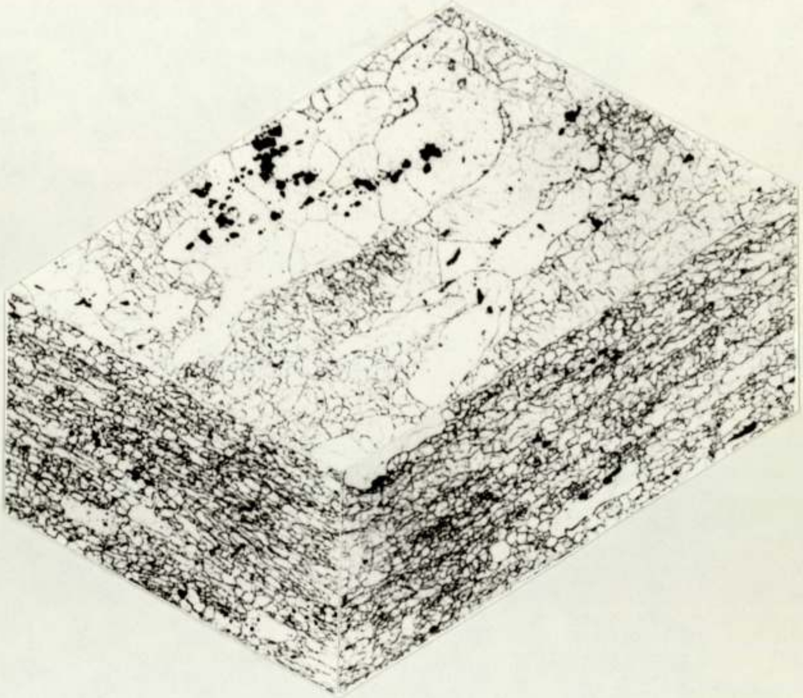

Figure 9.21 Three dimensional optical micrograph showing the subgrain structure of alloy 7010 - T736. Etching in Keller's reagent, X150

This type of crack was also observed in blunt notch specimens subjected to higher load(Plate 9.2, specimen 3512, Plate 9.3, specimen 519 and Plate 9.4, specimen 3013). The growing fatigue cracks in most blunt notch specimens prevail the semi-elliptical shape until a certain equivalent length C_c, the cracks break through the side-surfaces and then grow as a through thickness crack (Plates 9.2, 9.3 and 9.4).

Fig.9.22 is the graphic representation of the growing fatigue crack contours traced from the broken specimens (scale 10:1). The half major axis b and the half minor axis a of the semi-elliptical cracks are shown in Table 9.15. At present experiments the critical crack length C_c, is 2.9mm for 30XX group specimens (a_o = 10.00mm, ρ = 3.17mm), 2.97 for 5XX group specimens (a_o = 5.00mm, ρ = 5.00mm) and 2.7mm, an estimated value, for 35XX group specimens (a_o = 5.00mm, ρ =3.17 mm), respectively. The ratio of a to b is also shown in Table 9.15. It lies in the range from 0.72 to 0.97.

9.2.5.4 The Examination of Crack Initiation Sites.

Plates 9.8-9.15 show typical crack initiation site or sites. The arrows, R, in the plates indicate the crack initiation site or sites. Generally, multiple crack initiation sites were observed for sharp notch specimens and resulted in a through thickness macro-crack. The existance of some kind of discontinuous straight lines, which were indicated by arrow S in Plate 9.8, suggested

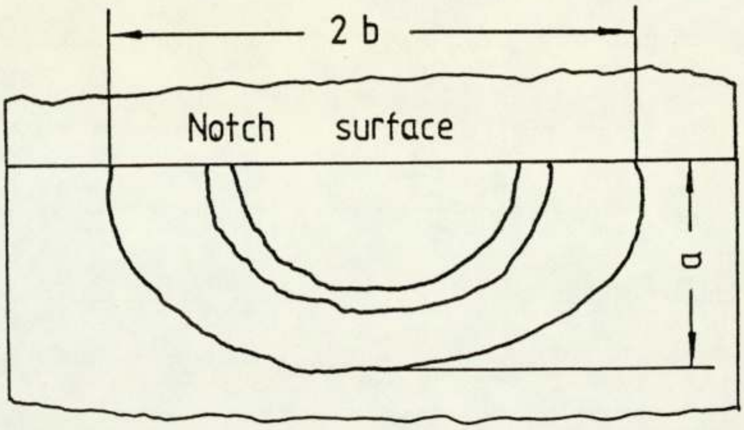

a) Notch depth = 5.00 mm
Notch root radius = 3.17 mm

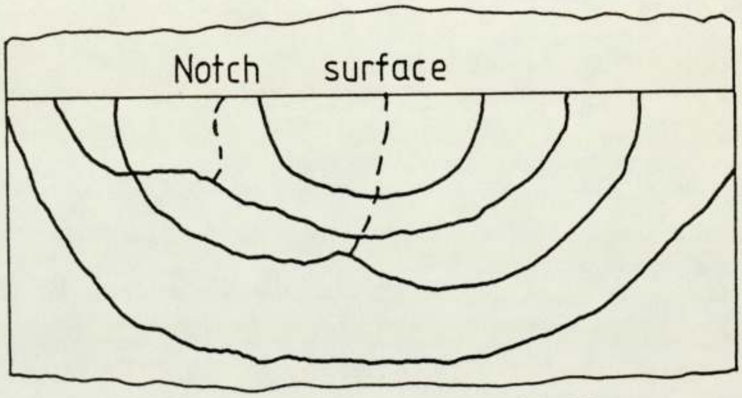

b) Notch depth = 10.00 mm
Notch root radius = 3.17 mm

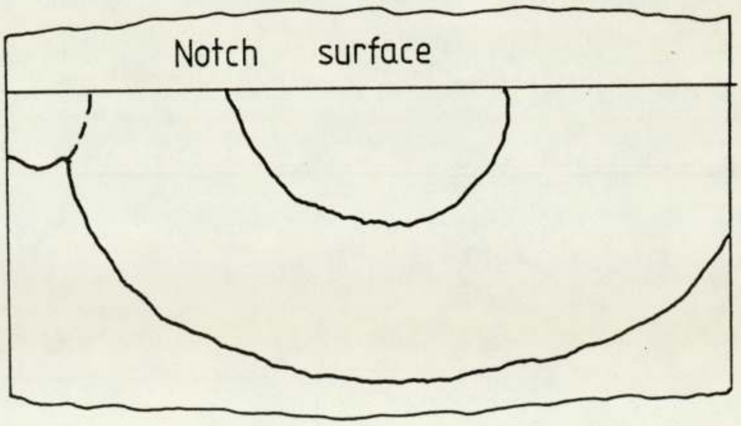

c) Notch depth = 5.00 mm
Notch root radius = 5.00 mm

Figure 9.22 Crack front contours traced from the fracture surface of broken specimens at magnification X10. The dot lines indicate the initiation of cracks on different planes.

Table 9.15

Dimensions of Semi-Elliptical Fatigue Cracks

Specimen No	Notch Dimensions ρ mm	a_o, mm	Load Range KN	a mm	2b mm	$\frac{a}{b}$	Eqv. Crack Length mm	Remarks
3506	3.23	4.91	4.86	1.70	3.80	0.89	0.451	
3503	3.29	4.88	4.68	2.00	4.55	0.88	0.681	Fig.9.22 a
3507	3.20	5.00	5.22	2.75	7.20	0.76	1.510	
3008	3.18	9.95	3.96	1.35	3.00	0.90	0.341	
3004	3.15	9.93	4.32	1.90	4.80	0.79	0.898	Fig.9.22 b
3005	3.22	9.90	4.32	2.60	7.00	0.74	1.357	
3009	3.15	9.95	3.83	3.60	10.00	0.72	2.902	
501	5.09	5.06	5.76	1.80	3.70	0.97	0.523	Fig.9.22 c
515	5.07	5.14	5.76	3.85	10.0	0.77	2.966	

Plate 9.8 SEM micrograph showing multiple crack initiation sites (a_o = 5.00mm, ρ = 0.11mm)

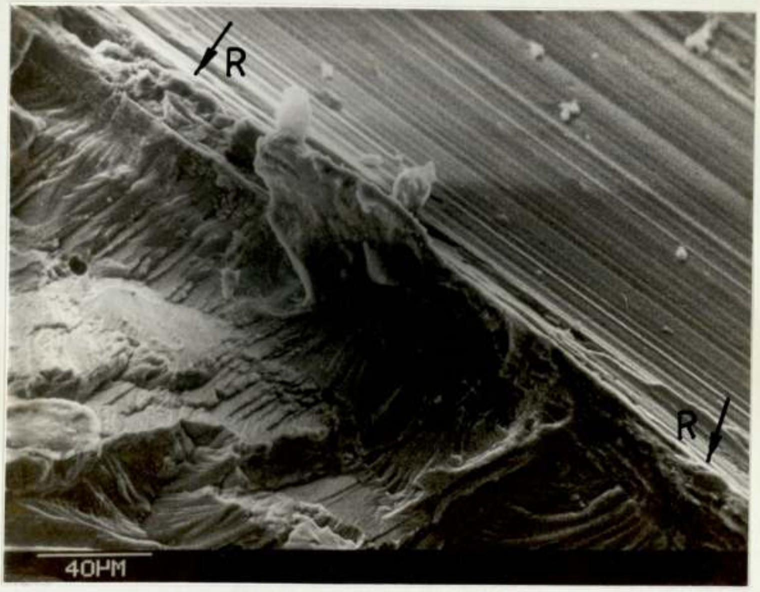

Plate 9.9 SEM micrograph showing the initiation sites in Plate 9.8 at high magnification (a_o = 5.00mm, ρ =0.11mm)

Plate 9.10 SEM micrograph showing crack initiation site in blunt notch specimen
(a_o = 5.00mm, ρ =3.17mm)

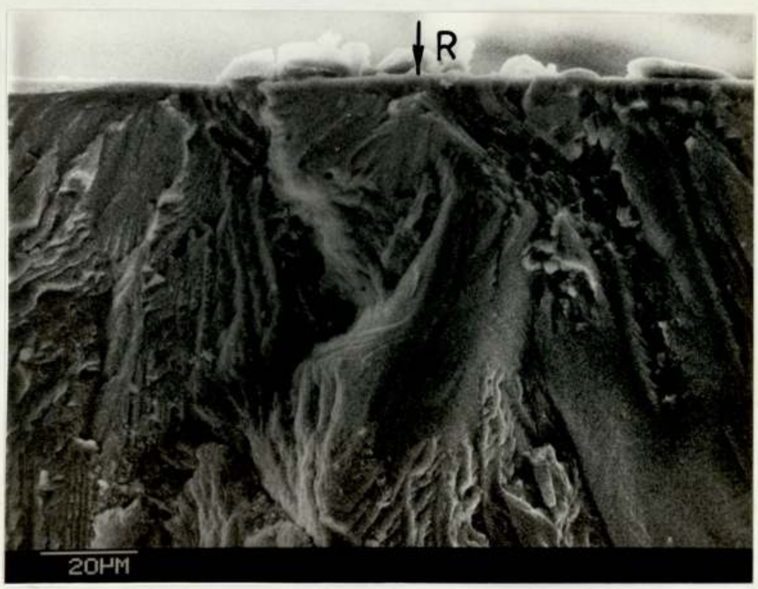

Plate 9.11 SEM micrograph showing the initiation site in Plate 9.10 at high magnification
(a_o = 5.00mm, ρ = 3.17mm)

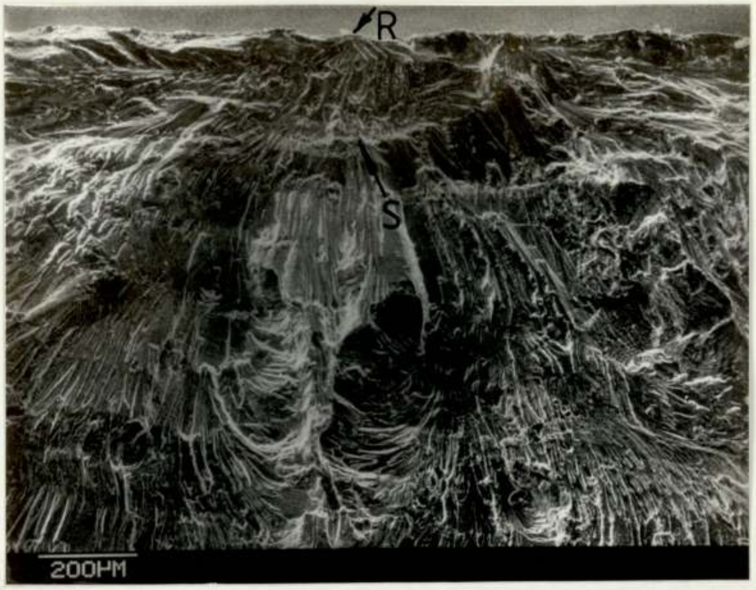

Plate 9.12 SEM micrograph showing crack initiation site in blunt notch specimen (a_o = 5.00mm, ρ =5.00mm)

Plate 9.13 SEM micrograph showing the initiation site in Plate 9.12 at high magnification (a_o = 5.00mm, ρ = 5.00mm)

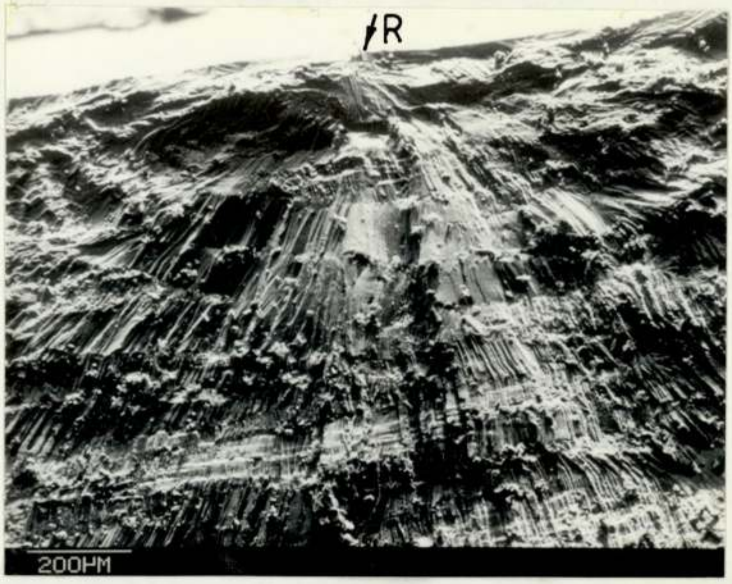

Plate 9.14 SEM micrograph showing crack initiation site in blunt notch specimen (a_o = 10.00mm, ρ = 3.17mm)

Plate 9.15 SEM micrograph showing the initiation site in Plate 9.14 at high magnification (a_o = 10.00mm, ρ = 3.17mm)

that the crack growths were relatively uniform through thickness for sharp notch specimens. The distances between the straight lines were of the order of grain dimension (0.08mm), which suggested that the direction of crack growth locally changed from one grain to another grain.

For blunt notch specimens the crack was predominately initiated at one site (Plate 9.10, 9.12 and 9.14).Although the case of multiple crack initiation sites was also observed in blunt notch specimens, these initiation sites were not on the same crack plane. The marks indicated by arrow S in Plates 9.10, 9.12 and 9.13 suggested that the crack growth was basically in a semi-elliptical form at the early stage of the crack growth, which was coincident with the macro-crack contour usually observed in blunt notch specimens.

9.2.5.5 The Quantitative Investigation of Fatigue Striations

The method for measuring fatigue striation spacings has been described in Section 8.7.2. This can be frimly explained by the examples shown as follows.
The notations in Eq.(8.17) are shown in Plate 9.16.
The calculation of striation spacings is demonstrated by

$$S_p = \frac{21}{21 \times 3750} \times \frac{\cos 0^{\circ}}{\cos 55^{\circ}} \times \cos 0^{\circ} = 4.65 \times 10^{-4}\text{mm}$$

for Plate 9.16a,

$$S_p = \frac{40.5}{28 \times 3750} \times \frac{\cos 0^{\circ}}{\cos 55^{\circ}} \times \cos 30^{\circ} = 5.82 \times 10^{-4}\text{mm}$$

for Plate 9.16b, and

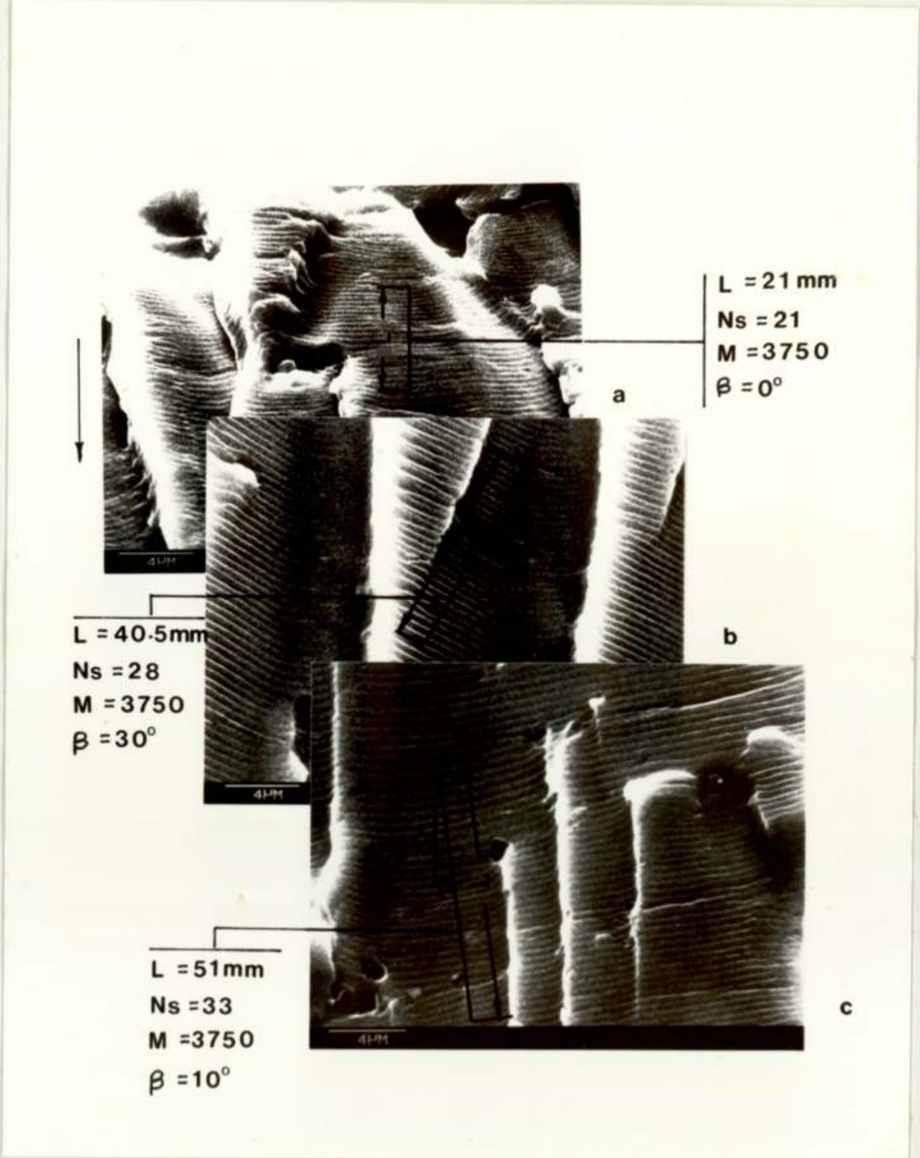

Plate 9.16 SEM fractographs showing fatigue striations under constant amplitude loading, notch depth 4.98mm, load range 3.06 KN. Tilt 55^{o}, no correction

a) Taken from a site 5.99mm from notch root.
b) Taken from a site 6.51mm from notch root.
c) Taken from a site 7.08mm from notch root.

$$S_p = \frac{51}{33 \times 3750} \times \frac{\text{Cos } 0^o}{\text{Cos } 55^o} \times \text{Cos } 10^o = 7.08 \times 10^{-4} mm$$

for Plate 9.16c.

The measured striation spacings, the corresponding crack lengths, macrocrack growth rates and the stress intensity factor ranges are listed in Table 9.16 and Table 9.17, in which the corresponding electron fractographs are shown in Plate 9.17 to Plate 9.48. The correlation between the striation spacings and the macrocrack growth rates is shown in Fig.9.23. Fig.9.24 illustrates the dependence of striation spacing against stress intensity factor range. The values obtained at high stress ratio using TEM are also presented in Fig. 9.24 for comparison. This will be returned to in a later section.

It can be seen that the relationship of single striation to single-load-cycle does exist within the range of crack growth rates from 0.1 μm/cycle to 1.0 μm/cycle. The corresponding stress intensity factor range are from $13MN/m^{3/2}$ to $28MN/m^{3/2}$ for the material under consideration . However, this relationship was not observed when the crack growth rates were less than 0.1 mm/cycle as the correspondent lower stress intensity factor could not produce enough increment of crack extension for the one load cycle to form distinct striation or as the resolution of the SEM is not powerful enough to distinguish the striations. It was noteworthy that the striations were discontinuous for the crack growth rates

Table 9.16

Comparison of Striation Spacings and Crack Growth Rates at Low ΔK

Specimen No	Crack Length mm	S_P 10^{-4}mm	$\frac{da}{dN}$ 10^{-4}mm	ΔK $MN/m^{3/2}$	Remarks
208	0.50	2.30	0.32	8.9	-
	1.00	3.63	0.37	9.3	-
	2.27	2.80	0.36	9.3	Plate 9.17
	3.78	1.91	0.60	11.0	Plate 9.19
210	3.80	1.26	0.60	11.0	Plate 9.20
	4.48	2.41	0.77	11.9	Plate 9.21
	4.55	2.49	0.79	12.0	Plate 9.22

Table 9.17

Comparison of Striation Spacings and Crack Growth Rates at Higher ΔK

Specimen No.	208			
Notch Geometry	a_o = 4.94mm,	ρ = 0.13mm		
Load Range	ΔP = 2700 N			
Crack Length mm	S_P 10^{-4}mm	$\frac{da}{dN}$ 10^{-4}mm	ΔK $MN/m^{3/2}$	Remarks
4.04	1.21	1.04	14.7	-
4.39	1.67	1.18	15.3	Plate 9.23
4.92	1.78	1.43	16.4	Plate 9.24
5.23	2.29	1.61	17.1	Plate 9.25
5.40	2.72	1.72	17.6	Plate 9.26
5.51	2.01	1.80	17.8	Plate 9.27
5.93	1.89	2.12	18.9	Plate 9.28
6.97	3.48	3.33	22.2	Plate 9.29

Table 9.17 (contd.)

Specimen No	207
Notch Geometry	a_o = 4.95mm, ρ = 0.11mm
Load Range	ΔP = 3060 N

Crack Length mm	S_P 10^{-4}mm	$\frac{da}{dN}$ 10^{-4}mm	ΔK $MN/m^{3/2}$	Remarks
3.90	2.24	2.75	16.3	-
3.96	1.66	2.81	16.5	Plate 9.30
4.34	3.00	3.18	17.3	Plate 9.31, 9.32
4.72	2.96	3.65	18.2	Plate 9.33
5.00	3.41	4.00	18.8	-
5.02	4.13	4.03	18.9	Plate 9.34
5.23	4.35	4.36	19.5	-
5.47	4.72	4.76	20.1	Plate 9.35
5.58	6.00	4.95	20.4	Plate 9.36
5.63	5.10	5.03	20.6	Plate 9.37

Table 9.17 (contd.)

Specimen No.	213
Notch Geometry	a_o = 4.98mm, ρ = 0.10mm
Load Range	ΔP = 3060 N

Crack Length mm	S_P 10^{-4}mm	$\frac{da}{dN}$ 10^{-4}mm	ΔK $MN/m^{3/2}$	Remarks
5.99	5.43	4.45	22.0	Plate 9.38
6.51	5.59	5.12	23.5	Plate 9.39, 9.40
7.08	6.19	6.66	25.8	Plate 9.41, 9.42
7.80	6.21	7.14	28.9	Plate 9.43, 9.44
8.92	8.14	11.12	35.1	Plate 9.45, 9.46
9.39	8.26	11.76	38.2	Plate 9.47, 9.48

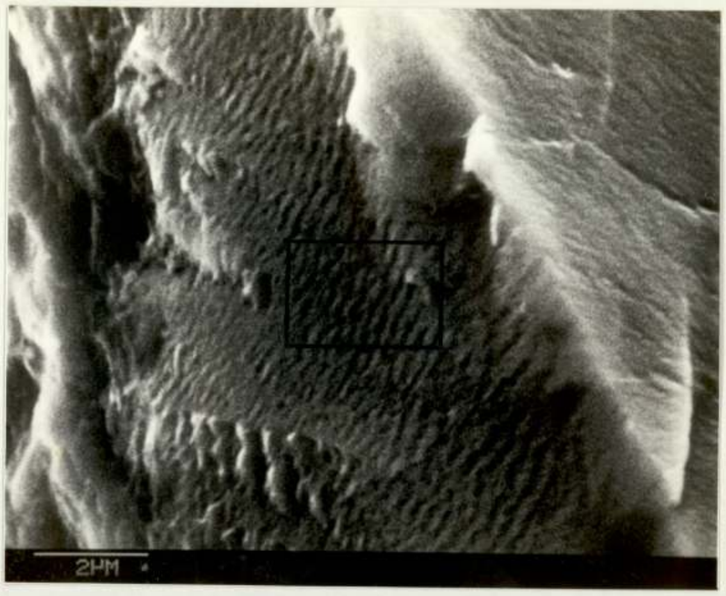

Plate 9.17 SEM *fractograph taken from a site 2.27mm from the notch root.

* The fractographs of Plate 9.17 - 9.48 were taken at 55^{o} tilt unless stated otherwise.

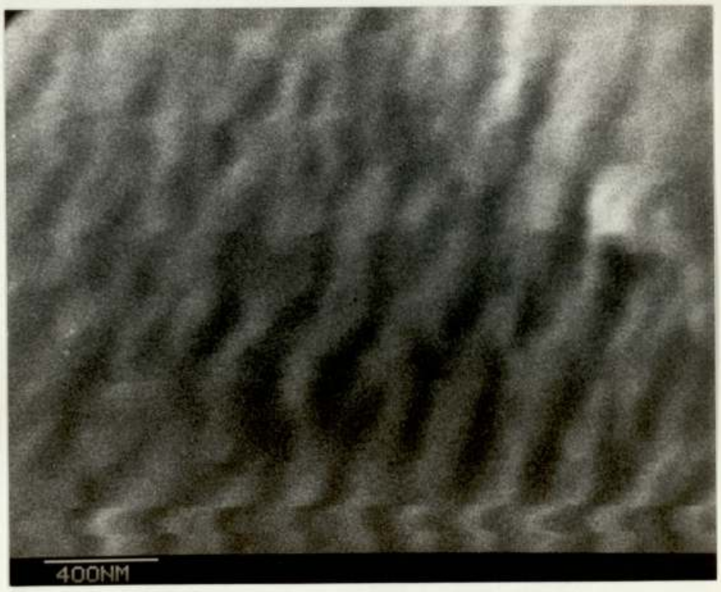

Plate 9.18 Higher-magnification view of the region outlined by the rectangle in Plate 9.17

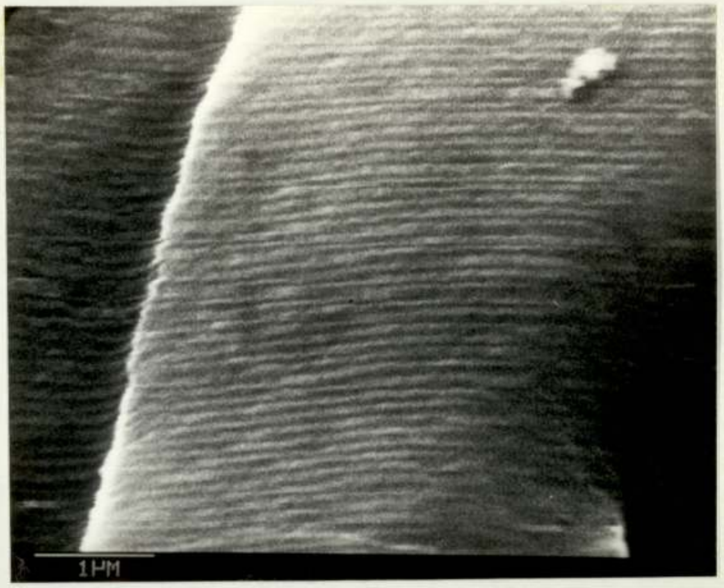

Plate 9.19 SEM fractograph taken from a site 3.78mm from the notch root

Plate 9.20 SEM fractograph taken from a site 3.80mm from the notch root

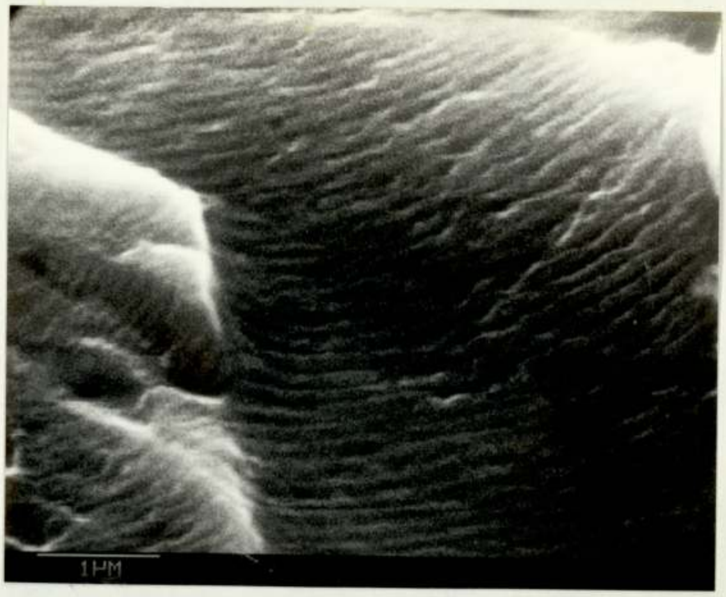

Plate 9.21 SEM fractograph taken from a site 4.48mm from the notch root

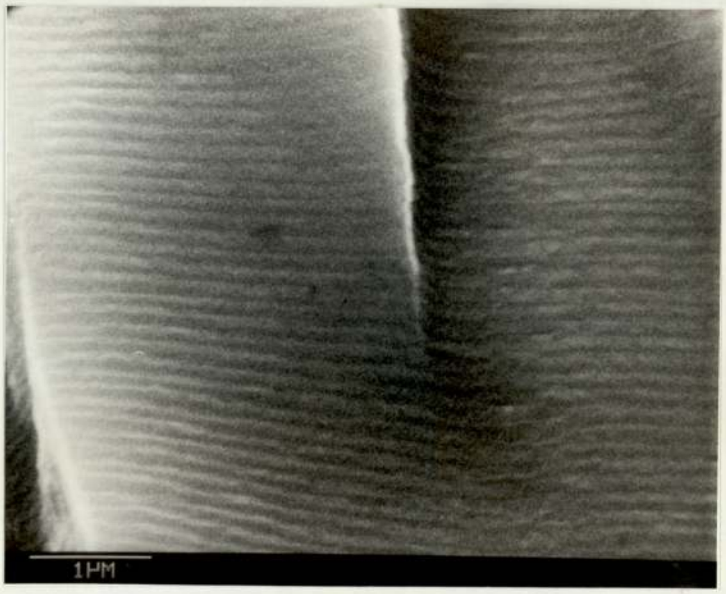

Plate 9.22 SEM fractograph taken from a site 4.55mm from the notch root.

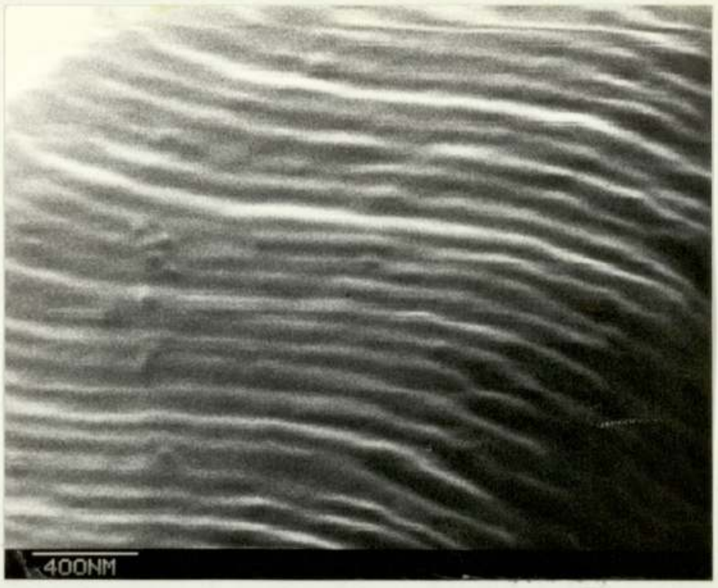

Plate 9.23 SEM fractograph taken from a site 4.39mm from the notch root.

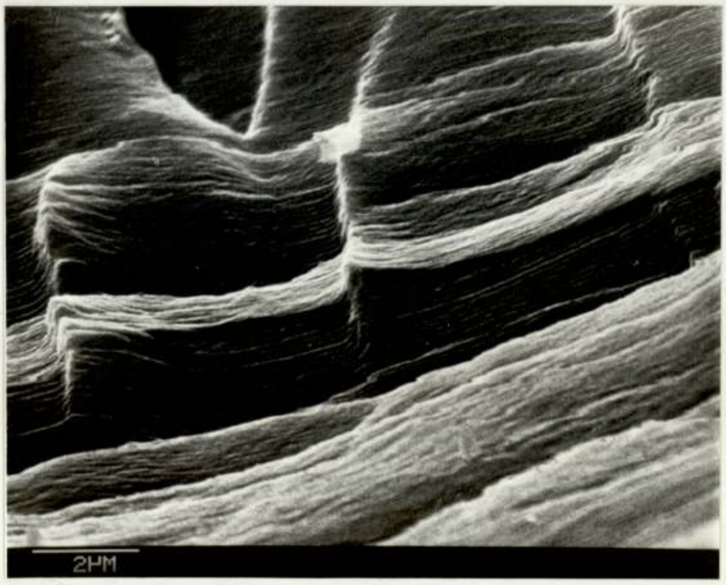

Plate 9.24 SEM fractograph taken from a site 4.92mm from the notch root.

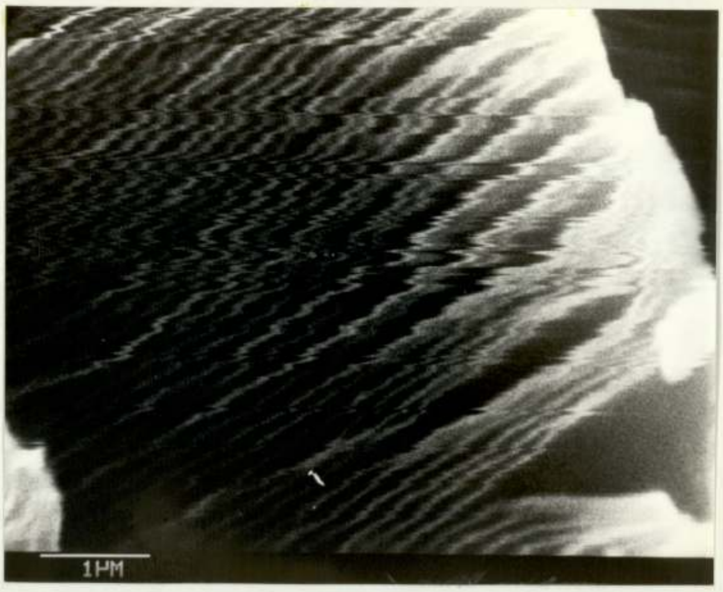

Plate 9.25 SEM fractograph taken from a site 5.23mm from the notch root.

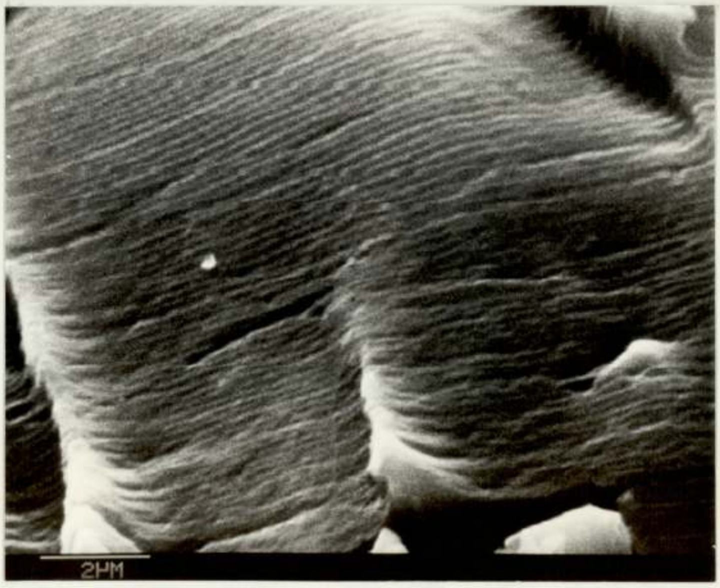

Plate 9.26 SEM fractograph taken from a site 5.40mm from the notch root.

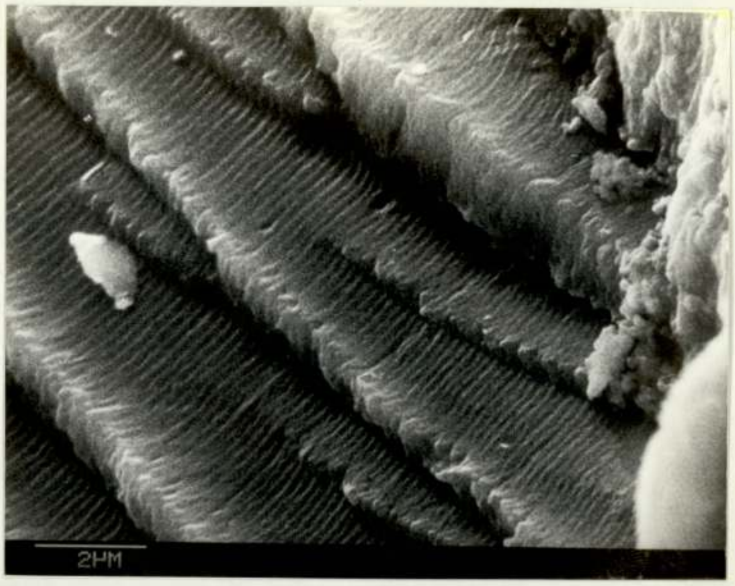

Plate 9.27 SEM fractograph taken from a site 5.51mm from the notch root.

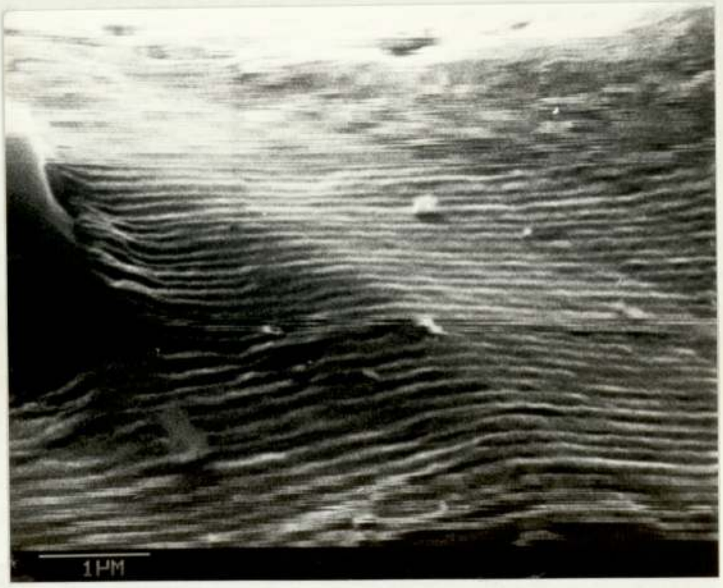

Plate 9.28 SEM fractograph taken from a site 5.93mm from the notch root.

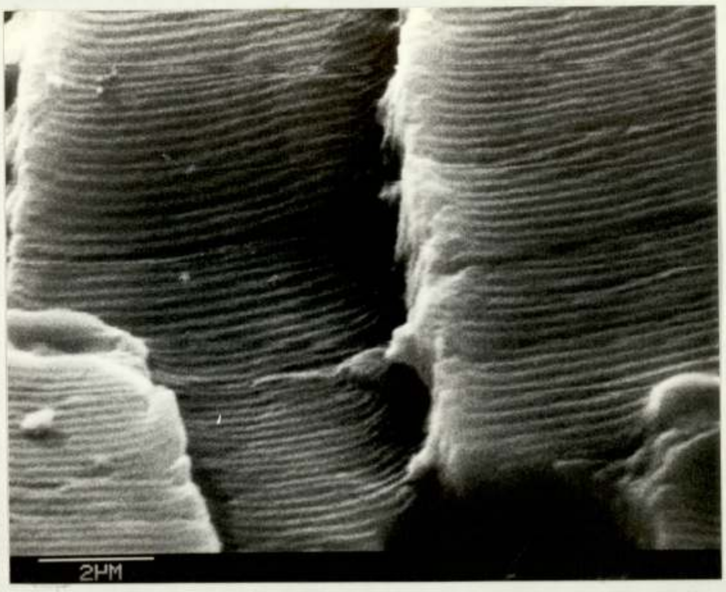

Plate 9.29 SEM fractograph taken from a site 6.97mm from the notch root

Plate 9.30 SEM fractograph taken from a site 3.96mm from the notch root.

Plate 9.31 SEM fractograph taken from a site 4.34mm from the notch root, 55^{o} correction.

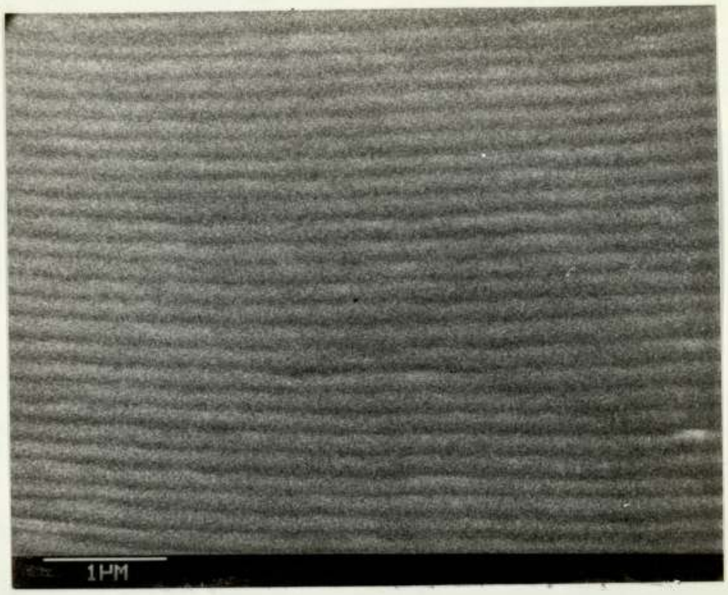

Plate 9.32 SEM fractograph taken from a site 4.34mm from the notch root.

Plate 9.33 SEM fractograph taken from a site 4.72mm from the notch root

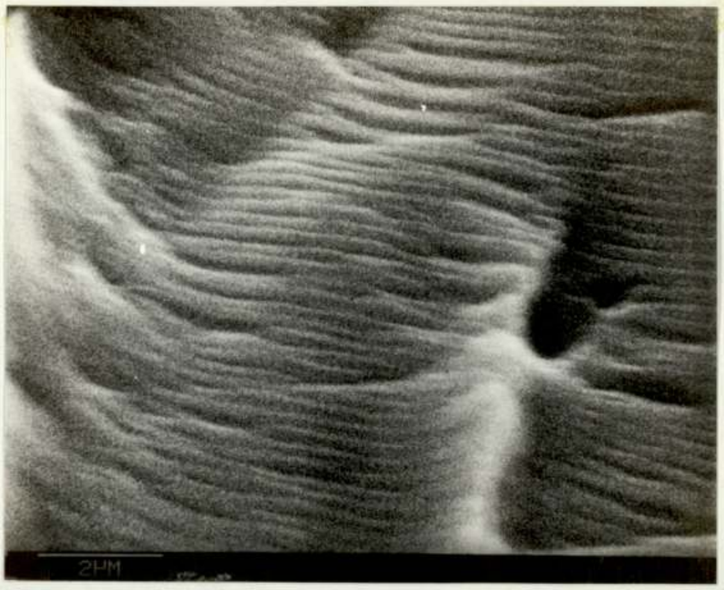

Plate 9.34 SEM fractograph taken from a site 5.02mm from the notch root

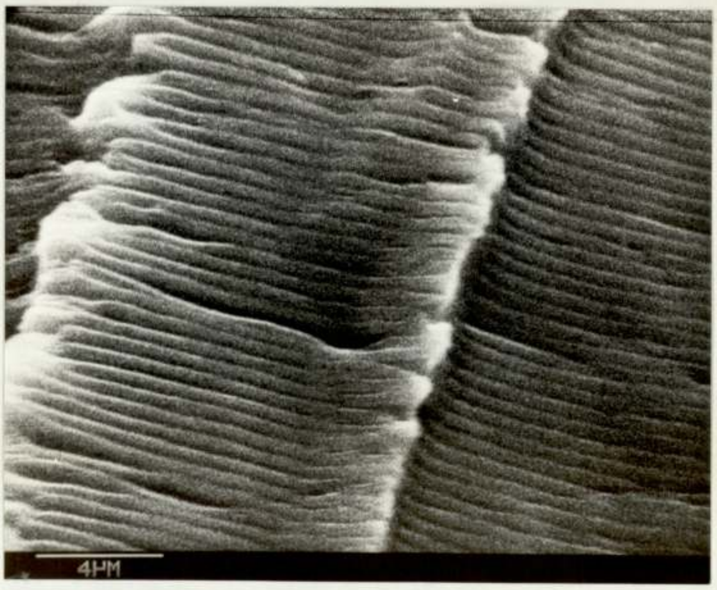

Plate 9.35 SEM fractograph taken from a site 5.47mm from the notch root.

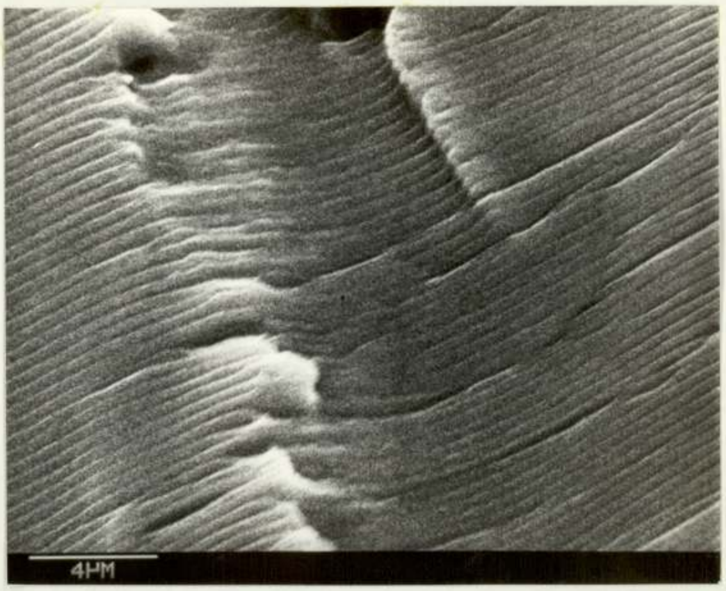

Plate 9.36 SEM fractograph taken from a site 5.58mm from the notch root.

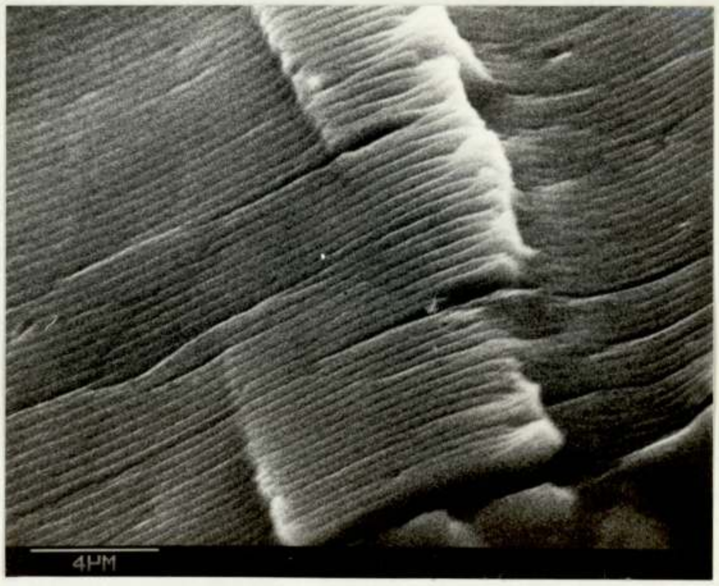

Plate 9.37 SEM fractograph taken from a site 5.63mm from the notch root.

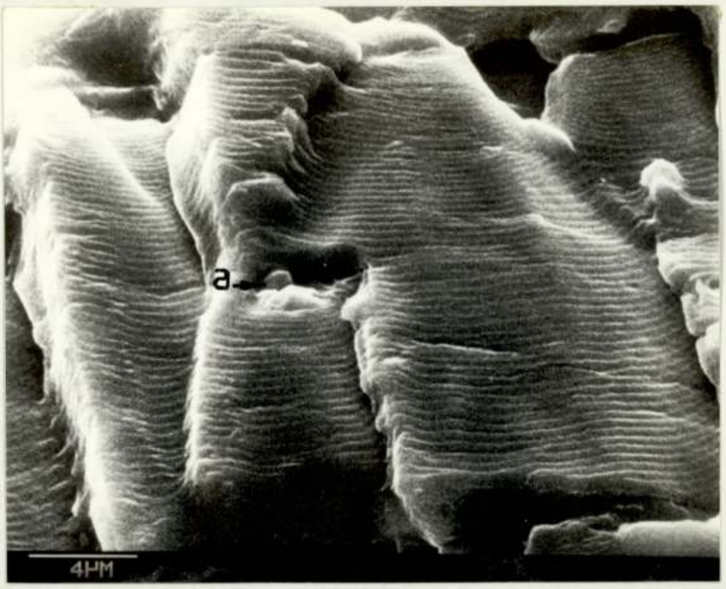

Plate 9.38 SEM fractograph taken from a site 5.99mm from the notch root.

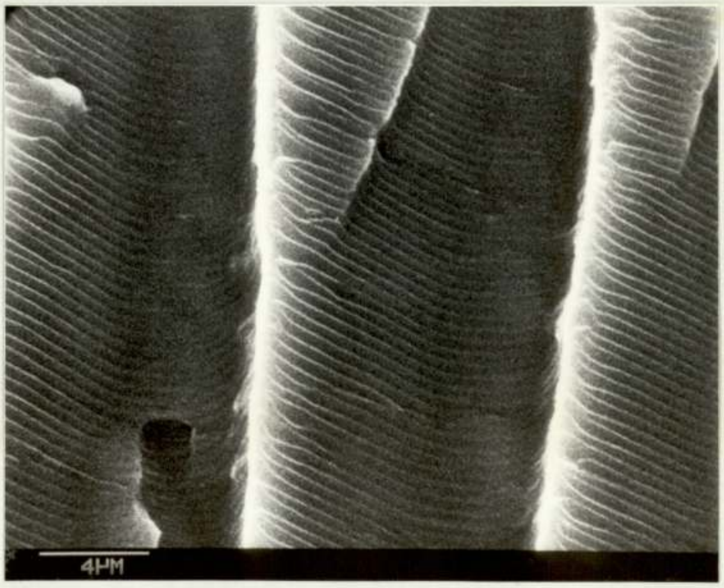

Plate 9.39 SEM fractograph taken from a site 6.51mm from the notch root.

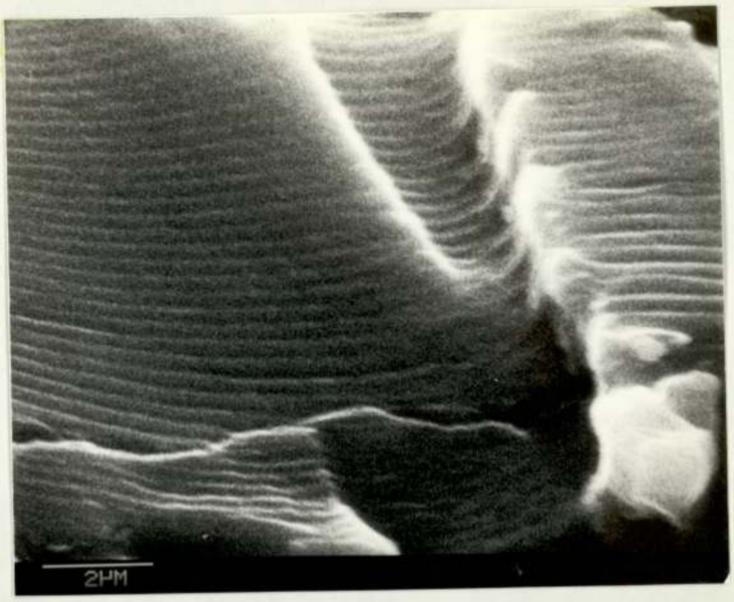

Plate 9.40 SEM fractograph taken from a site 6.51mm from the notch root.

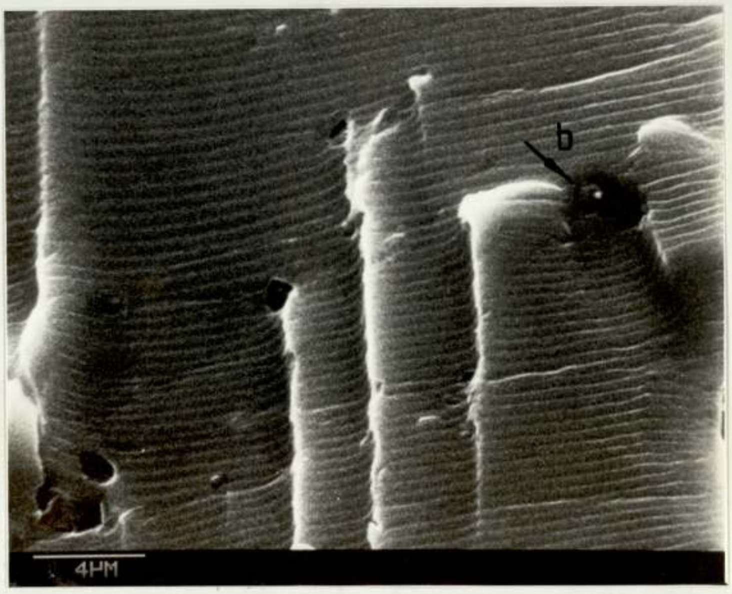

Plate 9.41 SEM fractograph taken from a site 7.08mm from the notch root.

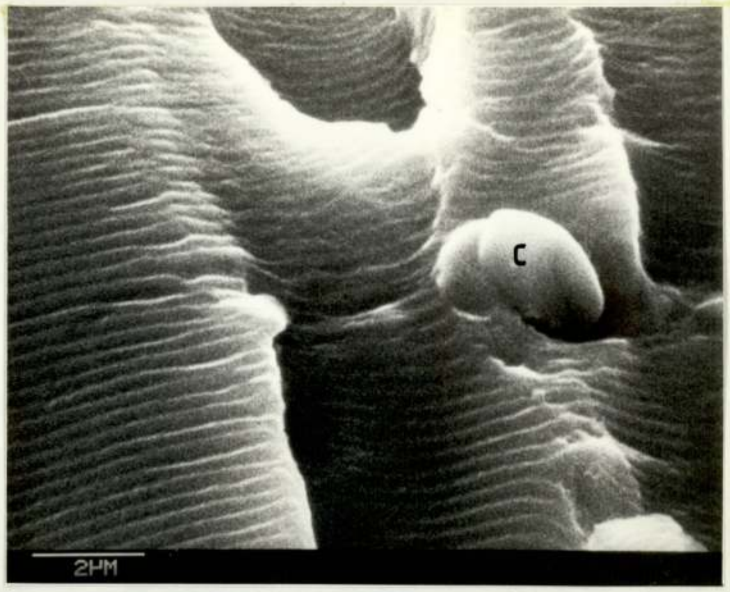

Plate 9.42 SEM fractograph taken from a site 7.08mm from the notch root.

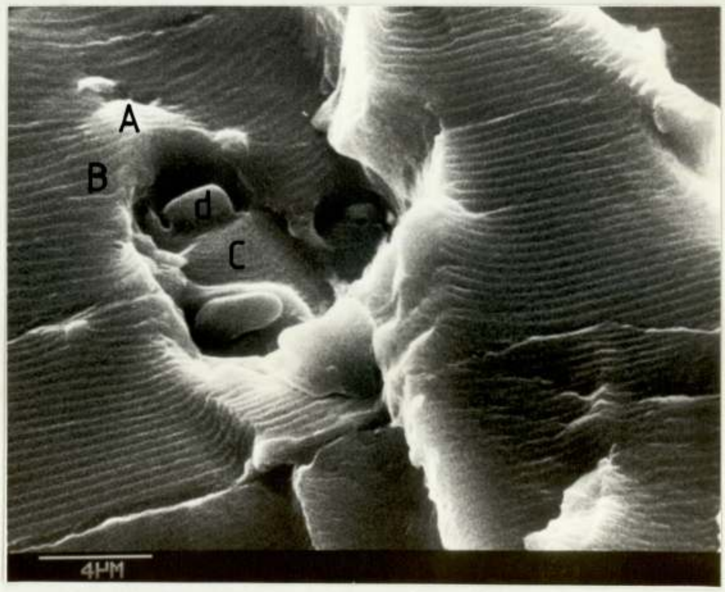

Plate 9.43 SEM fractograph taken from a site 7.80mm from the notch root.

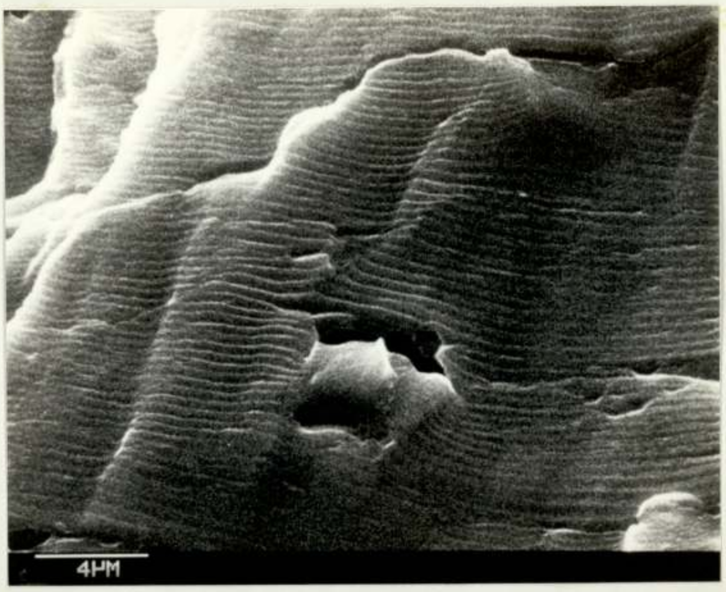

Plate 9.44 SEM fractograph taken from a site 7.80mm from the notch root.

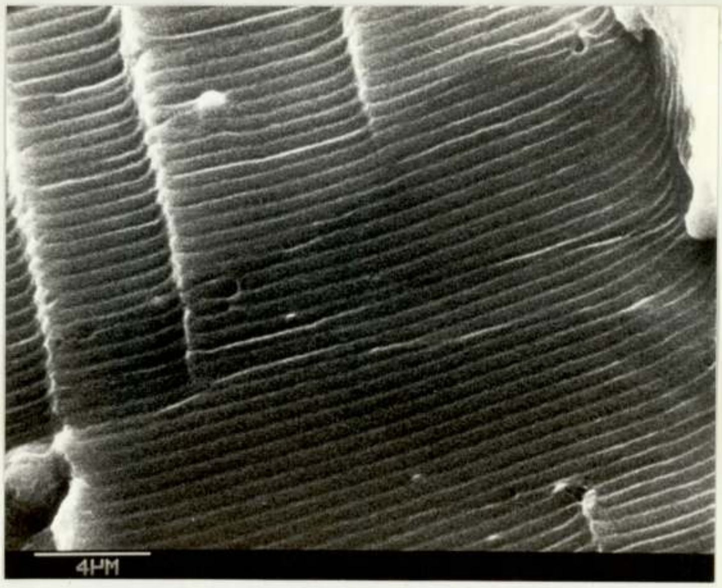

Plate 9.45 SEM fractograph taken from a site 8.92mm from the notch root.

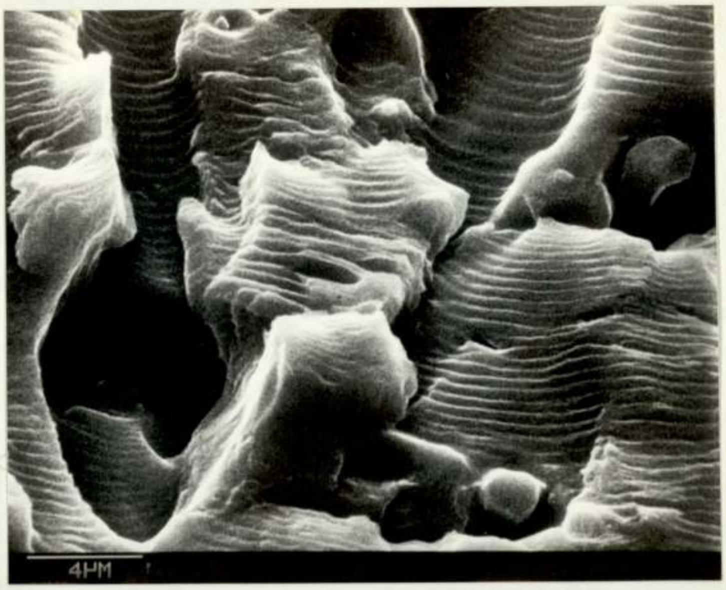

Plate 9.46 SEM fractograph taken from a site 8.92mm from the notch root.

Plate 9.47 SEM fractograph taken from a site 9.39mm from the notch root, 55^{o} correction.

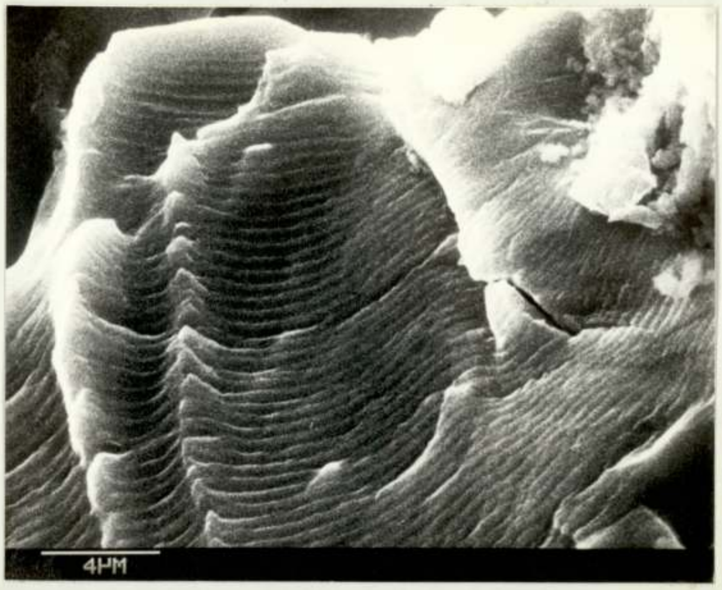

Plate 9.48 SEM fractograph taken from a site 9.39mm from the notch root.

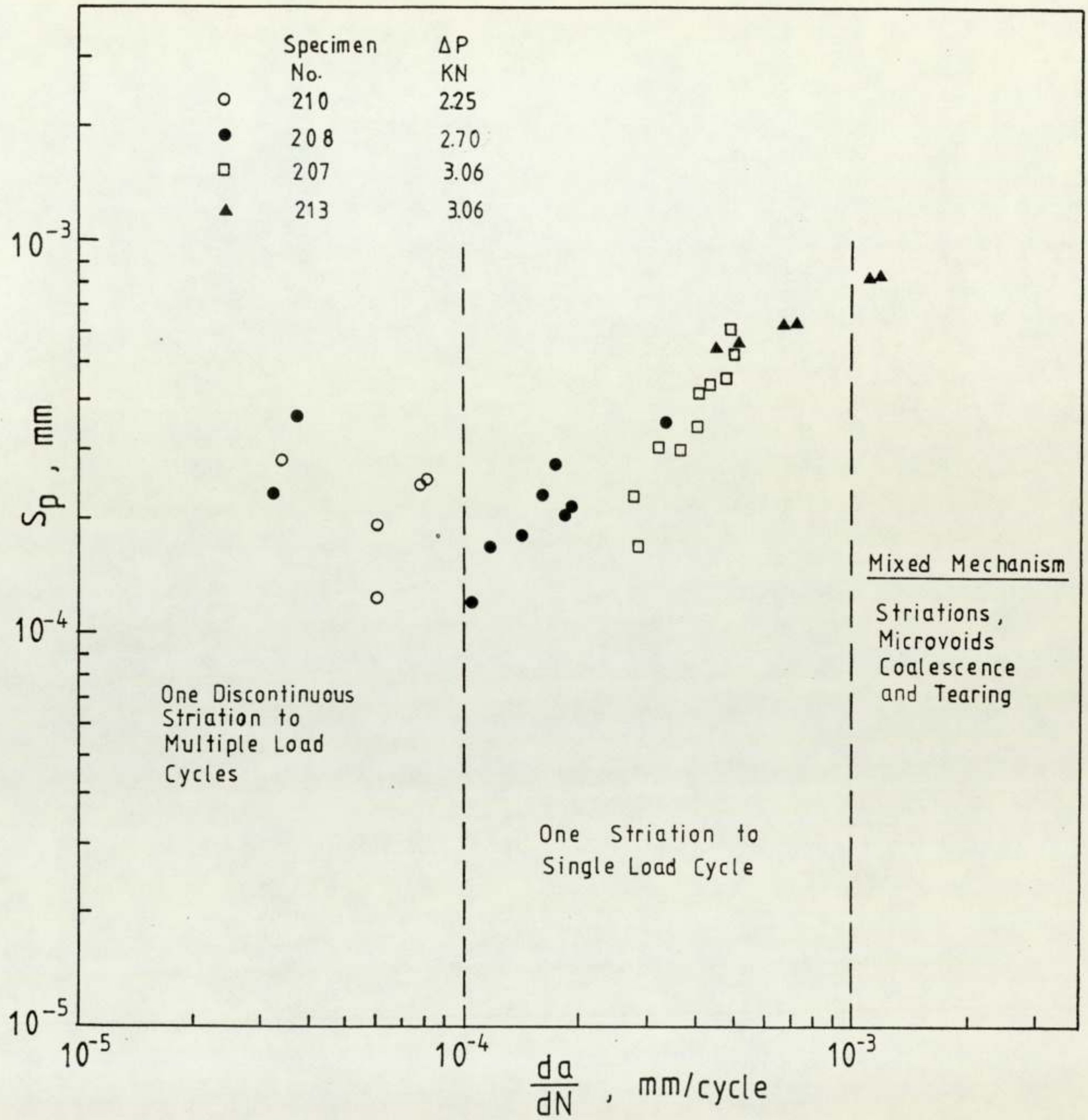

Figure 9.23 Correlation between striation spacings and macrocrack growth rates in aluminium alloy 7010 - T736

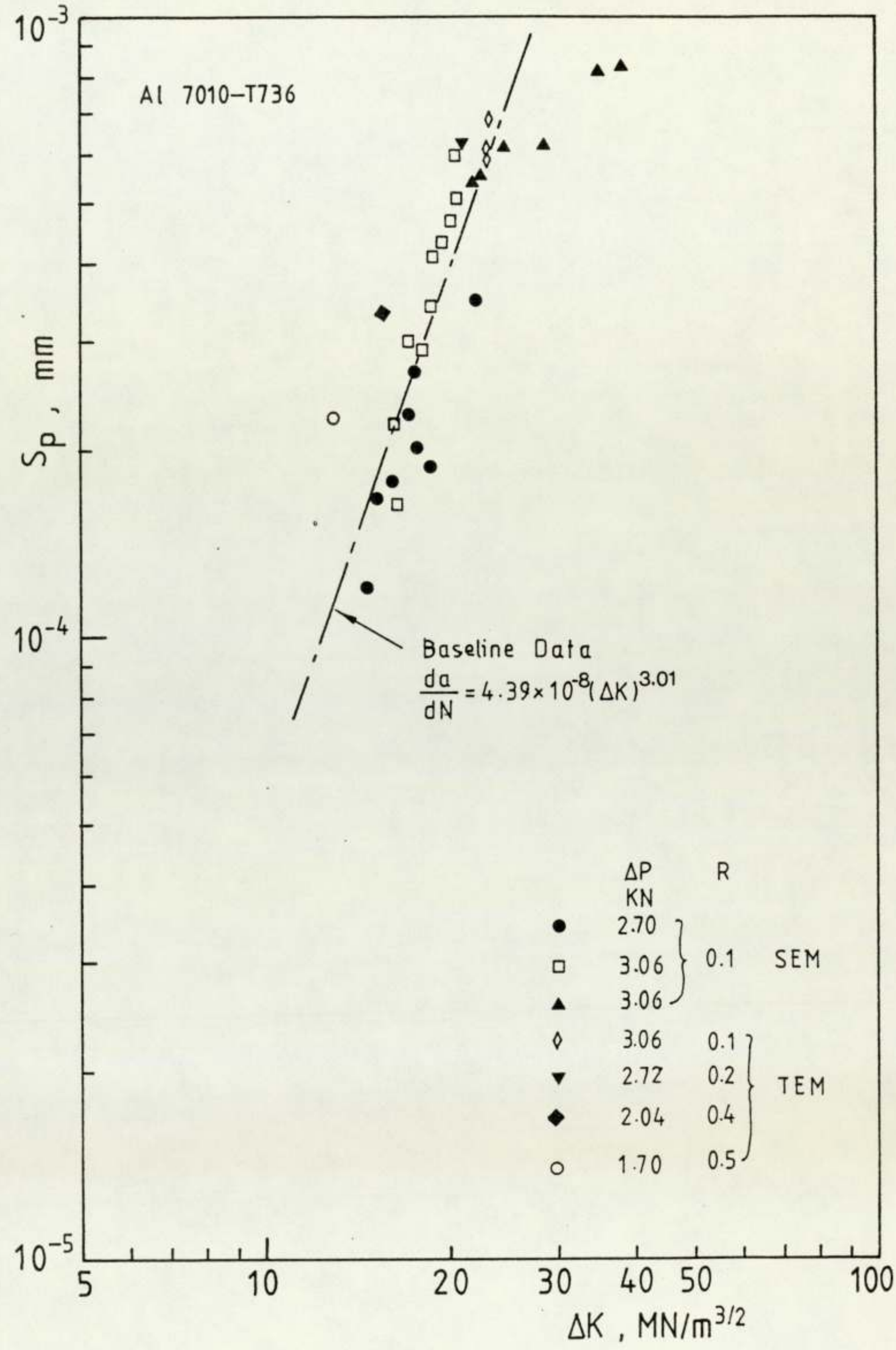

Figure 9.24 Dependence of striation spacing against stress intensity factor range in aluminium alloy 7010 - T736

$\frac{da}{dN} < 10^{-4}$ mm/cycle (Plates 9.17 - 9.22) and that the lower the crack growth rate was, the larger the difference between the measured striation spacings and the macrocrack growth rates could be observed (Fig.9.23). This suggested that the "discontinuous striations" were not produced by one-load-cycle at lower stress intensity factor.

The fatigue fracture surfaces of blunt notch specimens were carefully examined and three regions were observed before fatigue failure occurs. The three regions are the initiation site (or sites), the cleavage-like fracture zone around the initiation site (or sites) and the striation fracture zone. The three regions are schematically shown in Fig.9.25 and Fig.9.26.

The shape of the cleavage-like fracture zone is nearly a semi-circle in which no striations could be observed under SEM. The correspondent equivalent through thickness crack length converted from the area of this zone is about 0.5mm to 0.8mm. Beyond this zone the existence of distinct striations and the relationship of single striation to single-load-cycle can be allowed to do the quantitative analysis. The striation spacings were measured at the places which are nearly symmetrical about the initiation site. The measured striation spacings were then used to calculate the local stress intensity factors by Paris' law, i.e.

$$\frac{da}{dN} = S_P = A\,(\Delta K)^m$$

$$\Delta K = \left(\frac{S_P}{A}\right)^{\frac{1}{m}} \qquad (9.16)$$

Figure 9.25 Diagram of fatigue fracture surface for a blunt notch specimen (a_o = 5.00mm, ρ = 3.17mm). The fractographs display the features of local fracture. The figures in the diagram show the local stress intensity factor range, ΔK, obtained by measuring striation spacings.

The same in Fig.9.26.

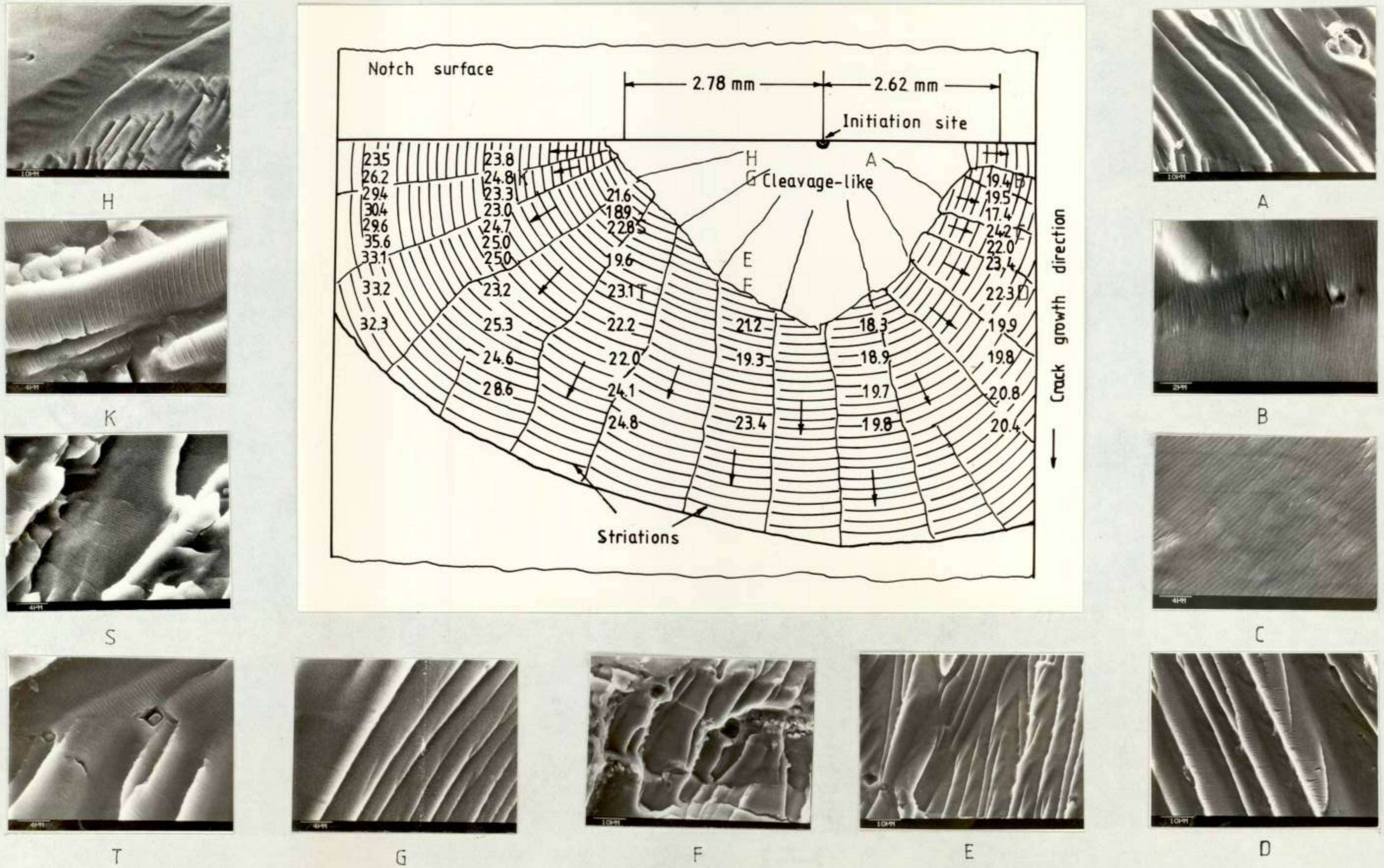
Notch surface
2.78 mm
2.62 mm
Initiation site
Cleavage-like
Striations
Crack growth direction
23.5
26.2
29.4
30.4
29.6
35.6
33.1
33.2
32.3
23.8
24.8
23.3
23.0
24.7
25.0
25.0
23.2
25.3
24.6
28.6
21.6
18.9
22.8
19.6
23.1
22.2
22.0
24.1
24.8
21.2
19.3
23.4
18.3
18.9
19.7
19.8
19.4
19.5
17.4
24.2
22.0
23.4
22.3
19.9
19.8
20.8
20.4
H
K
S
T
G
F
E
D
C
B
A

Figure 9.25

Figure 9.26 Diagram of fatigue fracture surface for a blunt notch specimen (a_o = 5.00mm, ρ = 3.17mm).

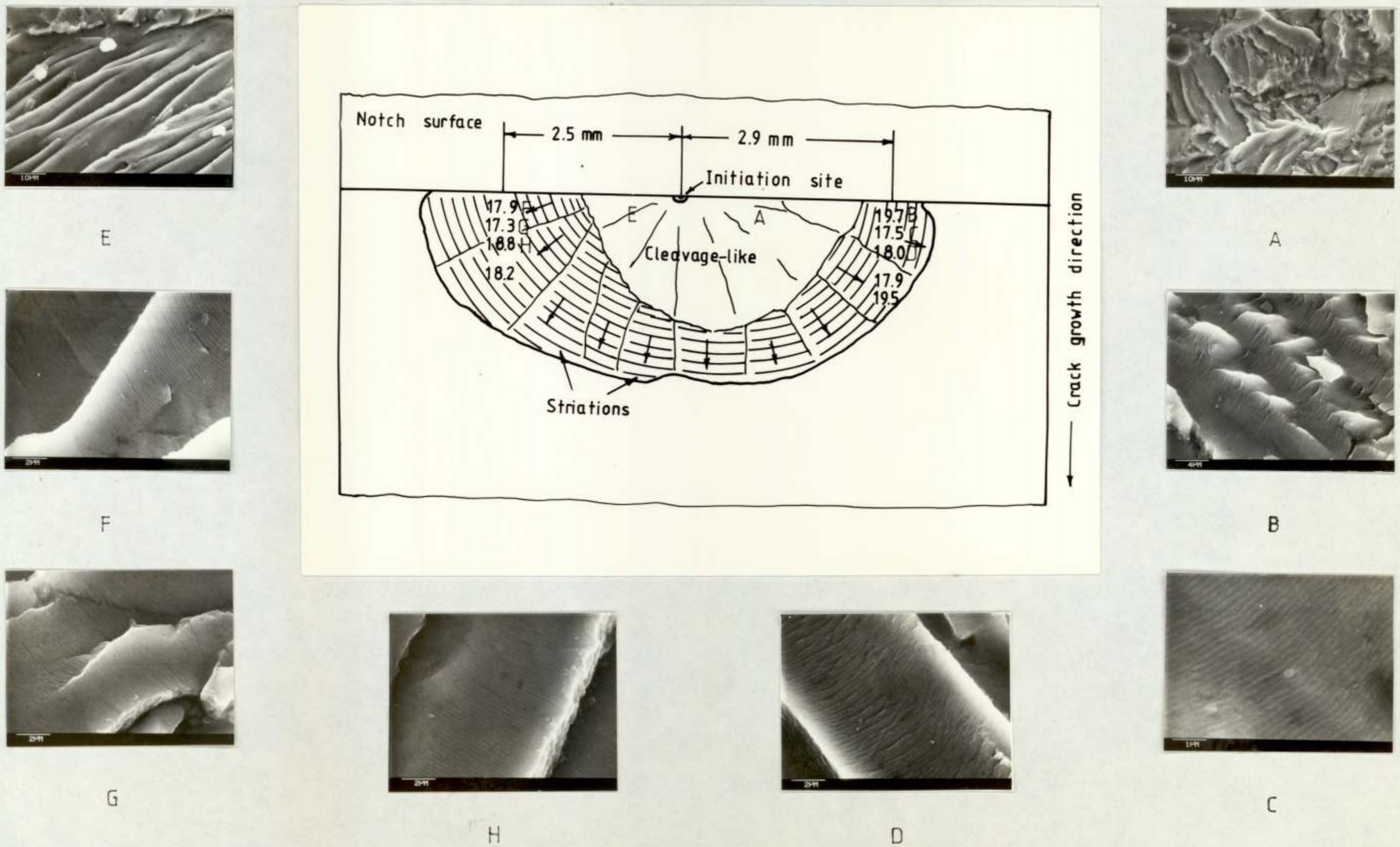

Notch surface
2.5 mm
2.9 mm
Initiation site
E
A
Cleavage-like
17.9 F
17.3 G
18.8 H
18.2
19.7 B
17.5 C
18.0 D
17.9
19.5
Striations
Crack growth direction
E
F
G
H
D
A
B
C

Figure 9.26

where S_p is the measured striation spacings. Fig.9.25 and Fig.9.26 present the results. It can be seen that the local stress intensity factor amplitudes are basically symmetrical about the initiation site. This is in agreement with the semi-elliptical contour of crack growth.

9.3 Variable Amplitude Fatigue

9.3.1 The Measurements of Crack Opening Stress Intensity Factor

It was found that the striations could not be resolved by fractographic techniques when the stress ratio R was greater than 0.5 for loading programme 2 shown in Fig.8.6 due to the corresponding smaller stress intensity factor range. Thus, the crack opening stress intensity factor was measured with block 7 to 14 in programme 2, and the corresponding stress ratios were 0.5 to 0.2. The results are presented in Table 9.18.

The striation spacings presented in Table 9.18 were measured on Plate 9.49 and Plate 9.50 and K_{op}/K_{max} were calculated by Eq.(8.16)

9.3.2 The Effects of Multiple Overloads on Crack Growth.

Figs.9.27 and 9.28 represent the dependence of crack length versus the number of applied cycles, illustrating the effect of multiple overloads on crack growth. The curves of crack growth rates against crack length are presented in Figs. 9.29 and 9.30. After the application

Table 9.18

Representation of K_{op}/K_{max}

Block No	Striation Spacing S_p, X 10^{-4}mm	Corresponding Stress Intensity Range ΔK, $MN/m^{3/2}$	Stress Ratio R	$\frac{K_{op}}{K_{max}}$
7	5.90	23.5	0.1	0.19
8	2.25	13.1	0.5	
9	6.16	23.5	0.1	0.186
10	3.35	15.7	0.4	
13	6.80	23.5	0.1	0.17
14	6.35	21.1	0.2	

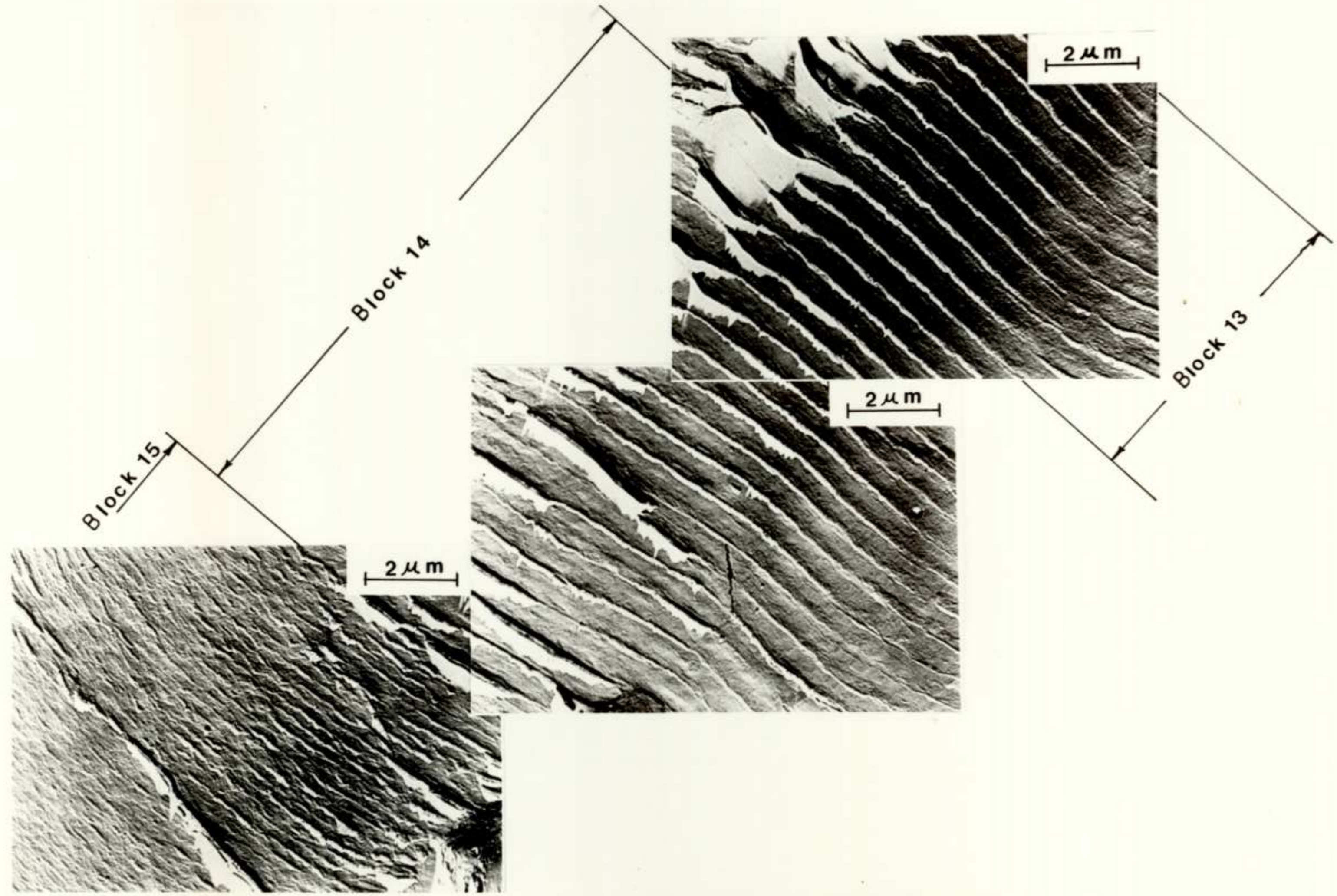

Plate 9.49 TEM fractographs showing the striations of block 13, 14 and 15 in load programme 2 in alloy 7010 - T736

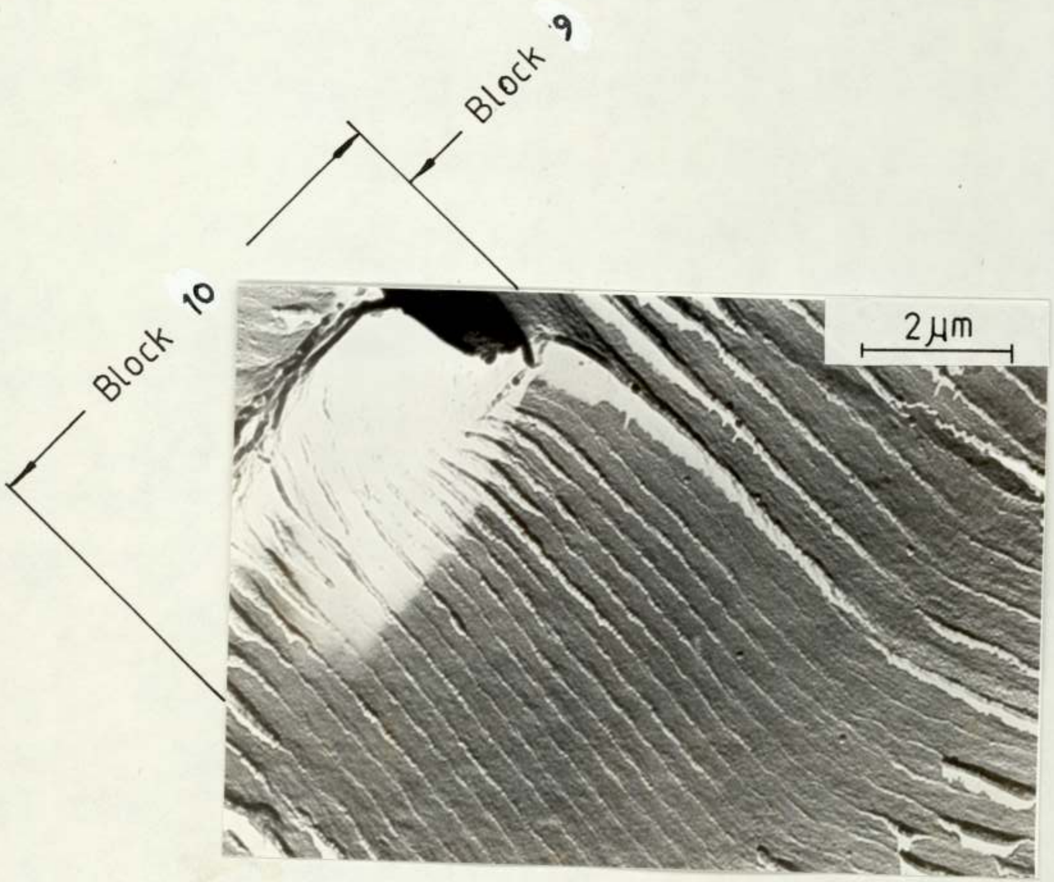

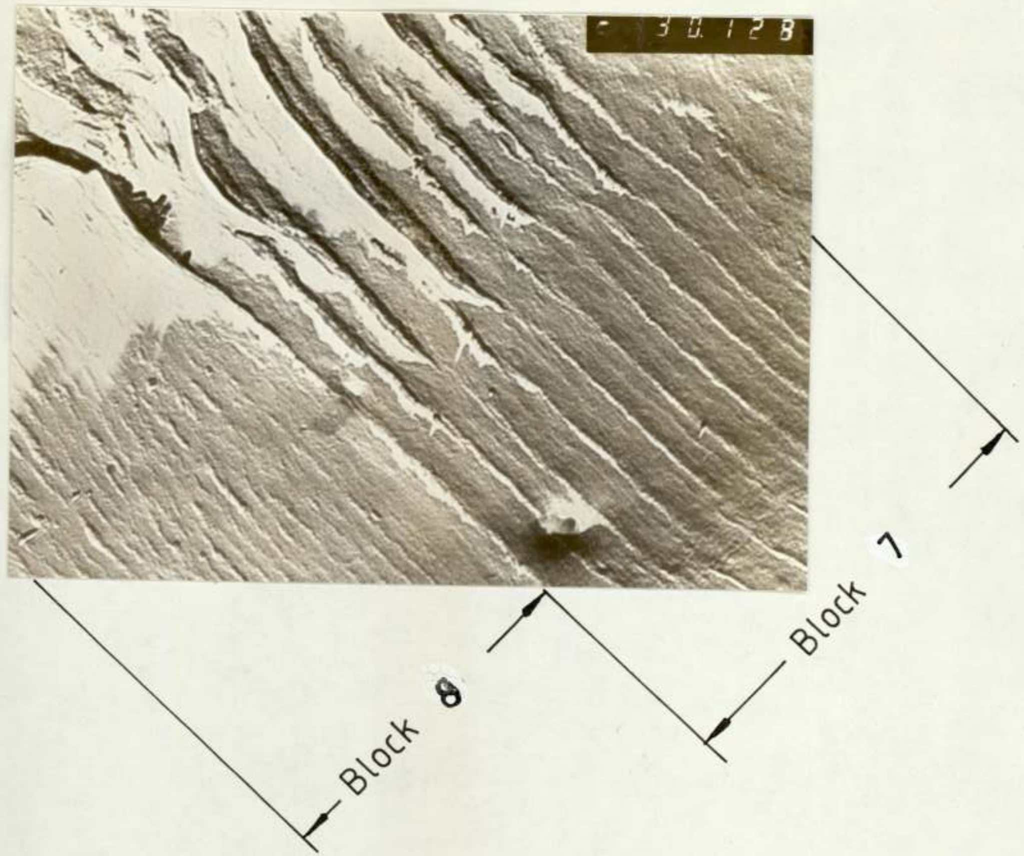

Plate 9.50 TEM fractographs showing the striations of block 9, 10, 11 and 12 in load Programme 2 in alloy 7010 - T736

Figure 9.27 Fatigue crack growth rates resulting from the applications of multiple overloads in alloy 7010 - T736. (Specimen 227)

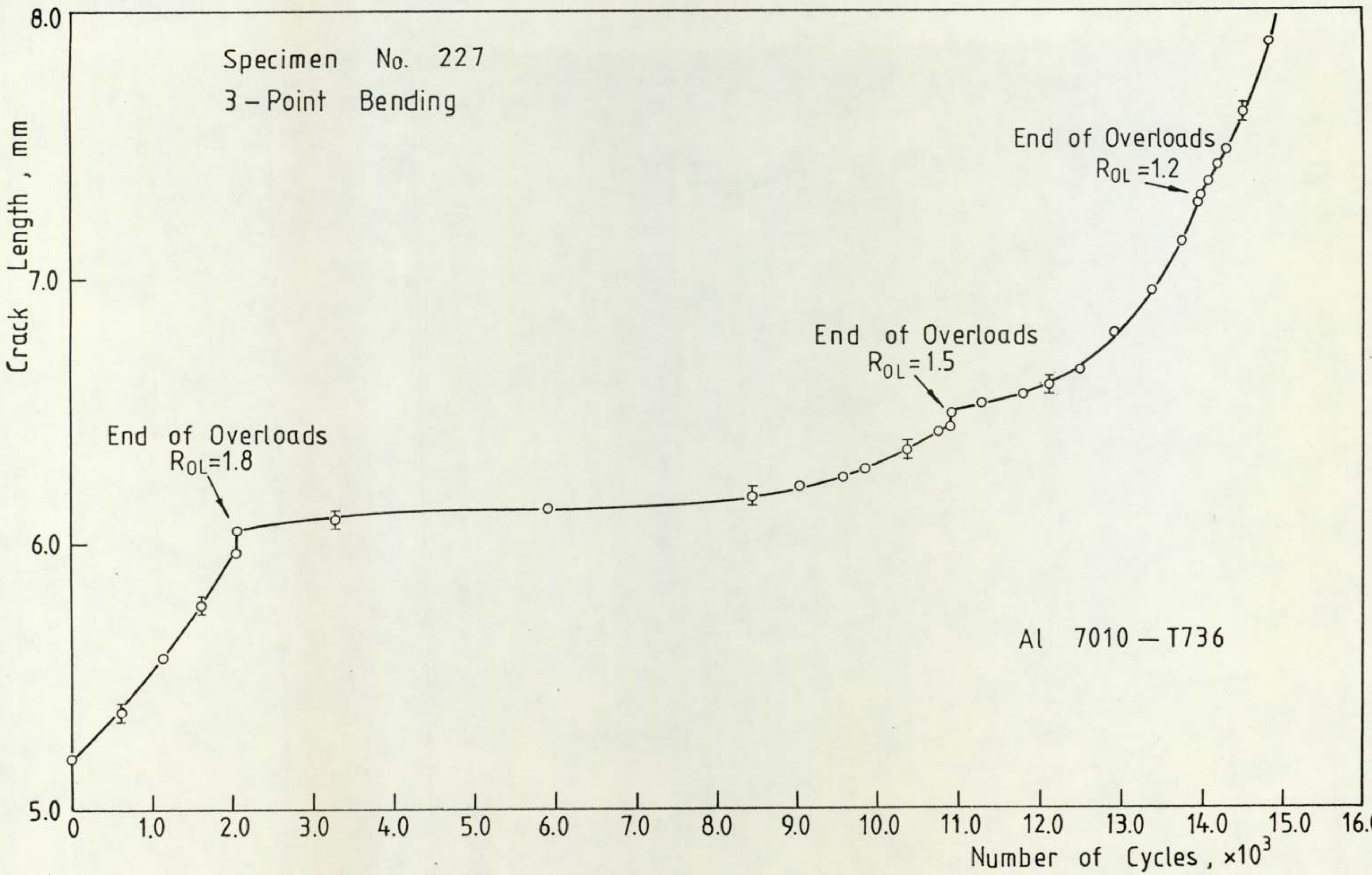
Specimen No. 227
3 – Point Bending
Crack Length , mm
8.0
7.0
6.0
5.0
End of Overloads
R_{OL}=1.8
End of Overloads
R_{OL} = 1.5
End of Overloads
R_{OL} =1.2
Al 7010 — T736
0
1.0
2.0
3.0
4.0
5.0
6.0
7.0
8.0
9.0
10.0
11.0
12.0
13.0
14.0
15.0
16.0
Number of Cycles , $\times10^3$

Figure 9.27

Figure 9.28 Fatigue crack growth rates resulting from the applications of multiple overloads in alloy 7010 - T736. (Specimen 228)

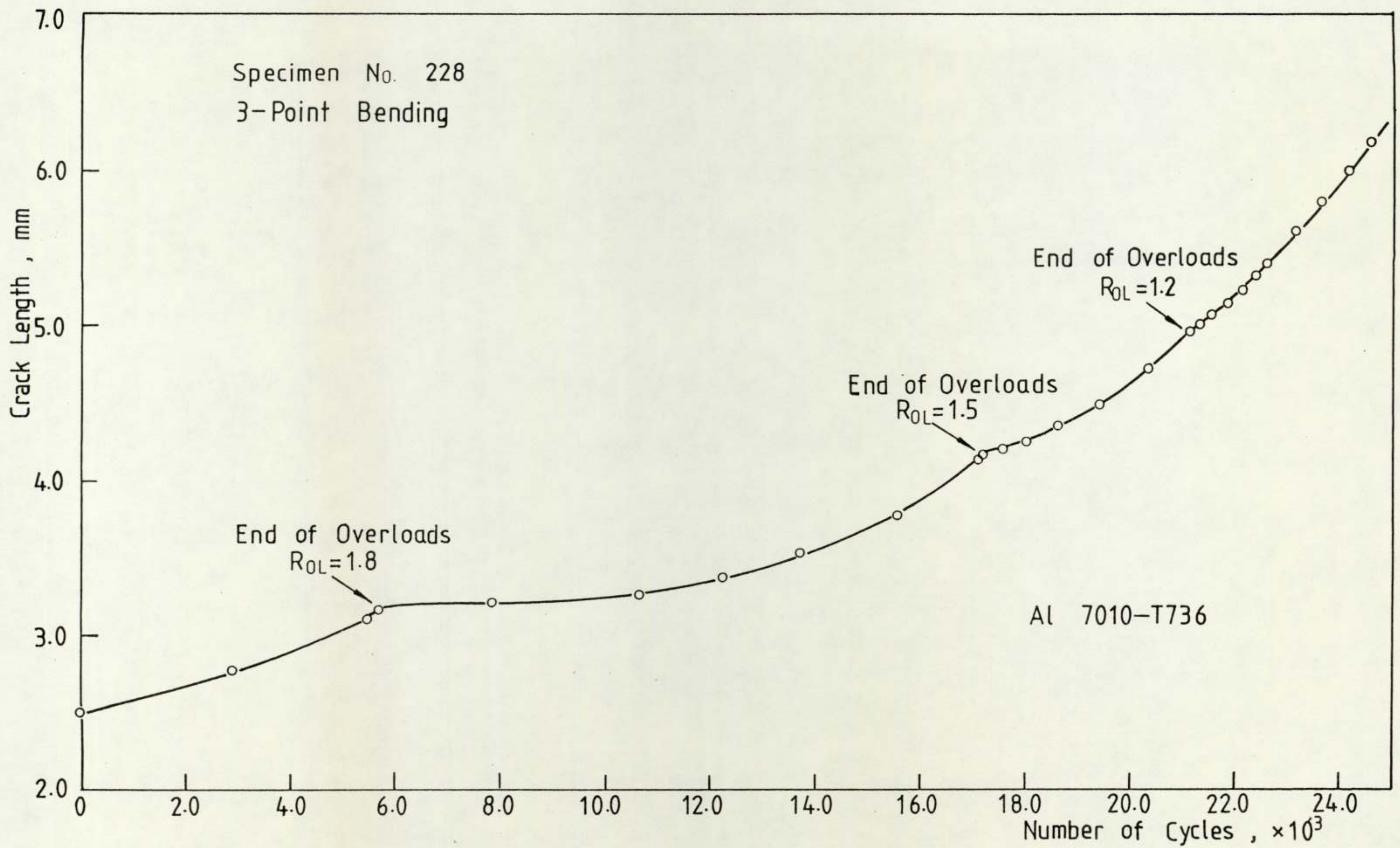

Specimen No. 228
3-Point Bending
End of Overloads
R_{OL}=1.8
End of Overloads
R_{OL}=1.5
End of Overloads
R_{OL}=1.2
Al 7010-T736
Crack Length , mm
Number of Cycles , $\times 10^3$
7.0
6.0
5.0
4.0
3.0
2.0
0
2.0
4.0
6.0
8.0
10.0
12.0
14.0
16.0
18.0
20.0
22.0
24.0

Figure 9.28

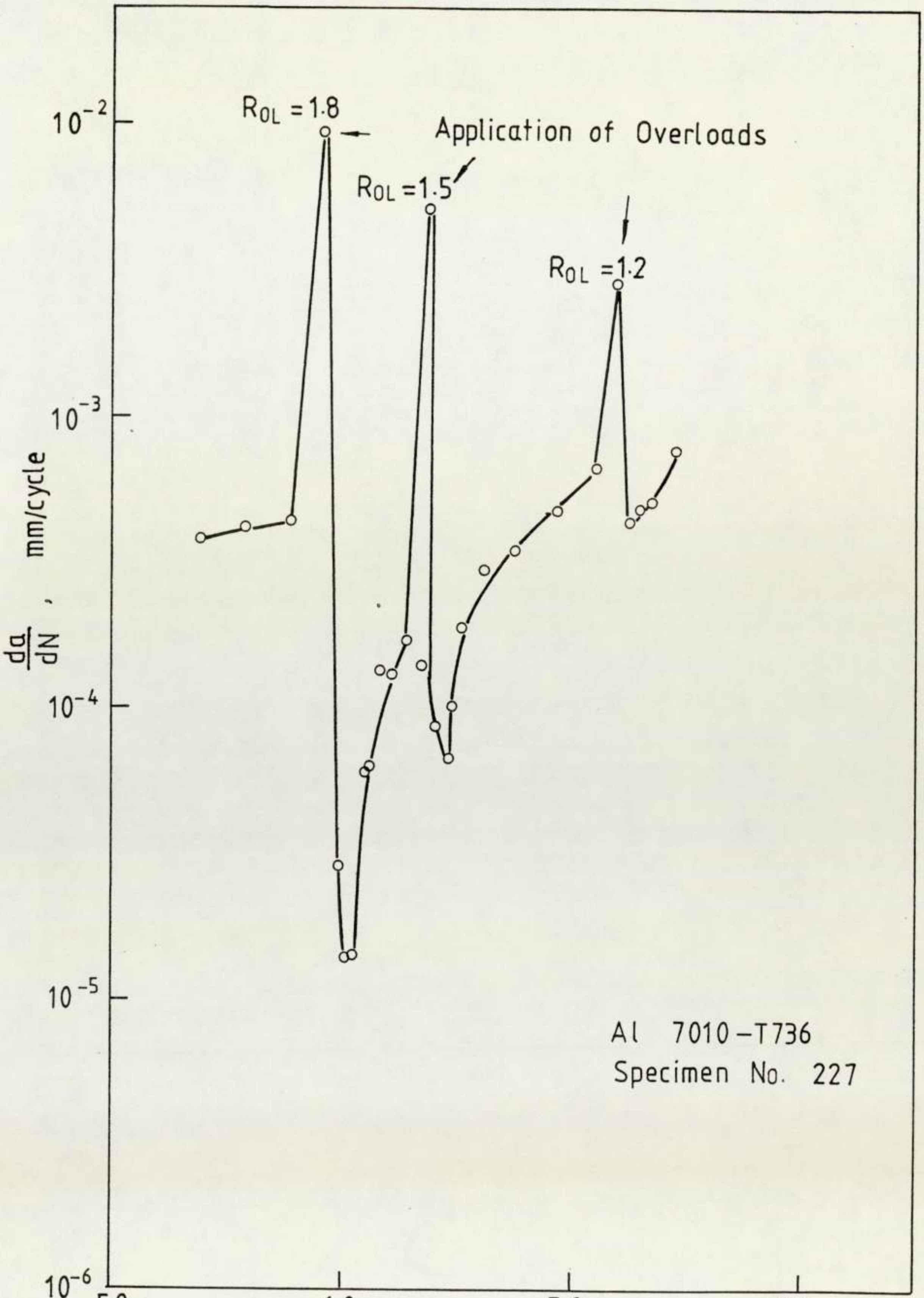

Figure 9.29 Crack extension through overloads affected region in alloy 7010 - T736.

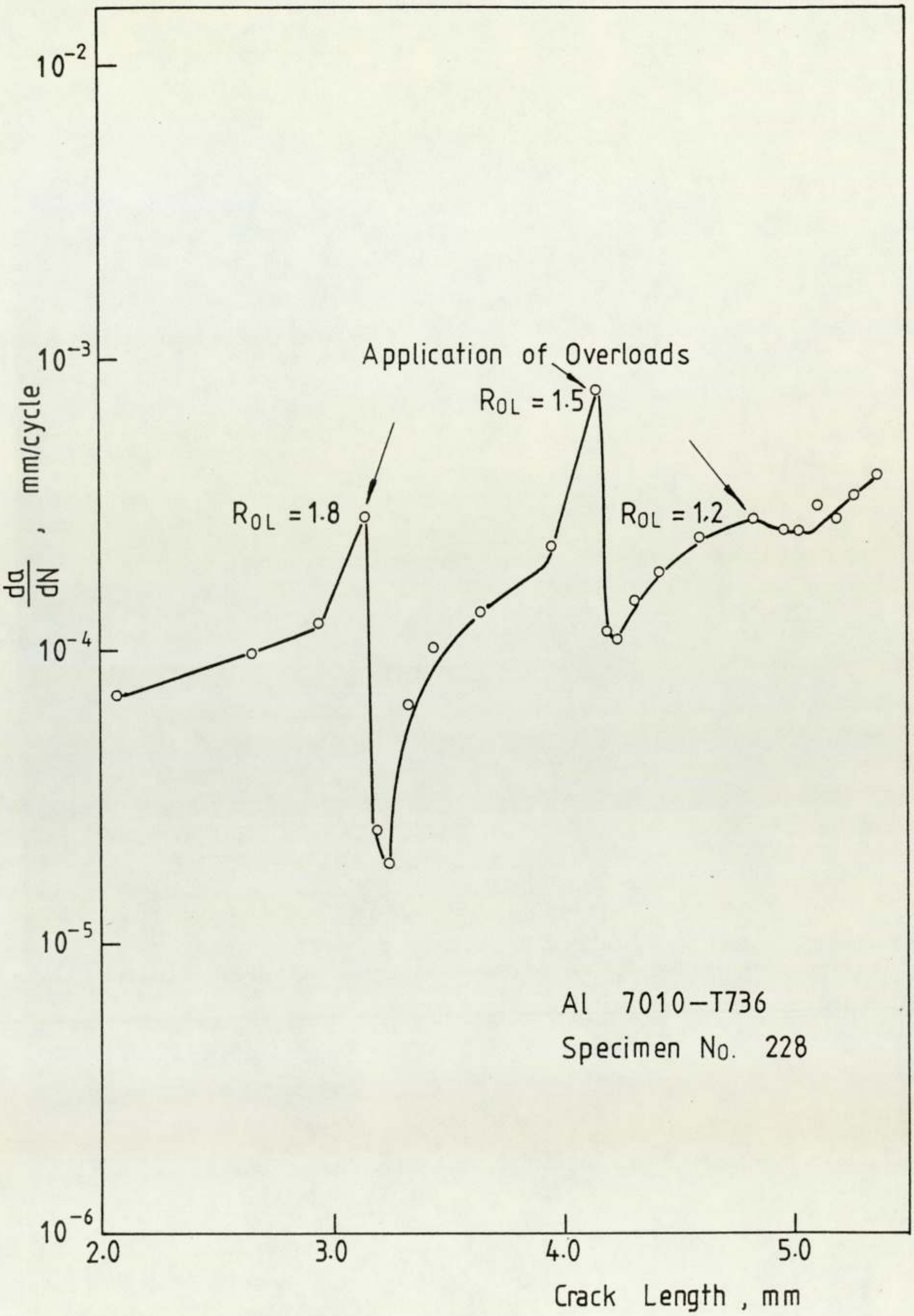

Figure 9.30 Crack extension through overloads affected region in alloy 7010 - T736

of the overloads with R_{ol} = 1.8, 1.5 and 1.2, the crack lengths were 6.06mm, 6.44mm and 7.27mm for specimen 227 and the corresponding plastic zone sizes induced by the overloads were 0.66mm, 0.51mm and 0.43mm. For specimen 228 the crack lengths were 3.1mm, 4.14mm and 4.96mm and the corresponding plastic zone sizes were 0.31mm, 0.26mm and 0.21mm. Usually the period of crack growth retardation N_r is defined as the number of cycles during which the crack growth rate following an overload application is restored to the unretarded crack growth rate just before the overload application. The values of N_r are given in Table 9.19.

The results indicate that the problem of crack growth retardation following overloads is complex. The overload ratio is the main factor which affects the degree of crack growth retardation. N_r reaches up about 10,000 cycles following the higher overloads (R_{ol} = 1.8) but less than 400 cycles of N_r can be expected for the lower overloads (R_{ol} = 1.2) under present experimental condition. The retardation effects also depend upon other factors such as crack length at which overloads are applied and the intervals between occurances of the overloads. At same overload ratio (R_{ol} = 1.2), when the overloads occurred at longer crack (7.27mm), indicating the higher stress intensity factor, the period of crack growth retardation was longer. If the overload or overloads are applied before the exhaustion of the prior retardation process the beneficial effect offered by the

Table 9.19

Comparison of Crack Growth Retardation after the Applications of Multiple Overloads at Different Overload Ratios.

Specimen No	Crack Length at Overloads mm	Amount of Overloads KN	Overload Ratio R_{o1}	Plastic Zone Size mm	N_r Cycles
227	6.06	4.50	1.8	0.66	> 8800
	6.44	3.75	1.5	0.51	1500
	7.27	3.00	1.2	0.43	350
228	3.10	4.50	1.8	0.31	9800
	4.14	3.75	1.5	0.26	3000
	4.96	3.00	1.2	0.21	240

current overload or overloads are reduced. For specimen 228 the period of crack growth retardation at $R_{ol} = 1.5$ was 3,000 cycles, but for specimen 227 it was only half of the value since the overloads ($R_{ol} = 1.5$) in specimen 227 occurred within the plastic zone induced by the prior overloads ($R_{ol} = 1.8$); however, it was not the case in specimen 228.

The effect of overloads at $R_{ol} = 1.2$ on crack growth was studied by fractographic technique using scanning electron microscope with specimen orientation at 50^{o}. The fractographs presented in Plate 9.51 - Plate 9.62 demonstrate the striation spacing prior to and after the overloads. The locations from which the fractographs were taken are schematically illustrated in Fig.9.31. The striation spacings measured in near surface region and interior region are presented in Table 9.20 and the corresponding macroscopic crack growth rates $\frac{da}{dN}$, are also listed for comparison.

The following observations can be made in the effects of overloads on crack growth.

i) The fatigue crack growth rate in near surface region was reduced by a factor of 65% following the overloads at $R_{ol} = 1.2$. However, no such reduction was observed in the interior of the specimen. Comparing the average striations measured in near surface region with the macroscopic fatigue crack growth rates $\frac{da}{dN}$, the agreement between the two is good.

Plate 9.51 SEM fractograph showing the effect of 20% multiple overloads on crack growth in near surface region in alloy 7010 - T736.

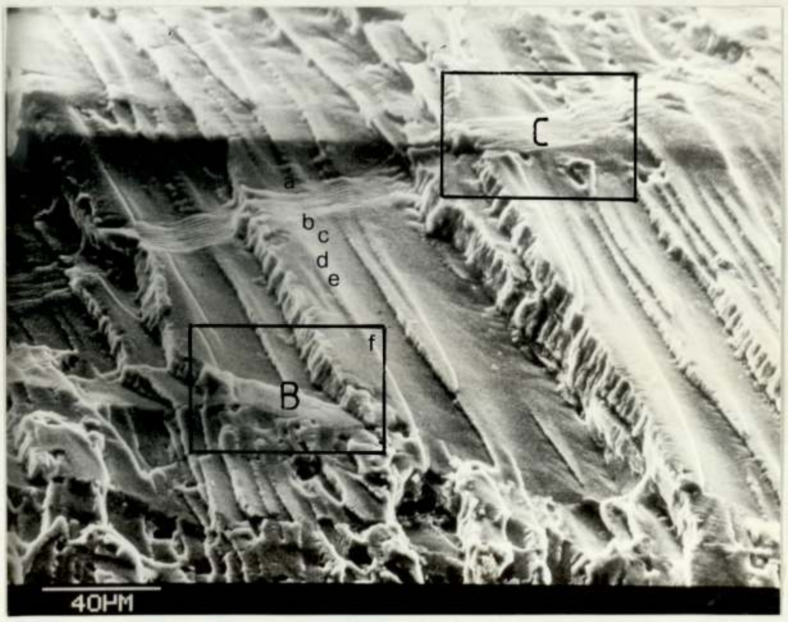

Plate 9.52 Higher-magnification view of the region outlined by the rectangle in Plate 9.51.

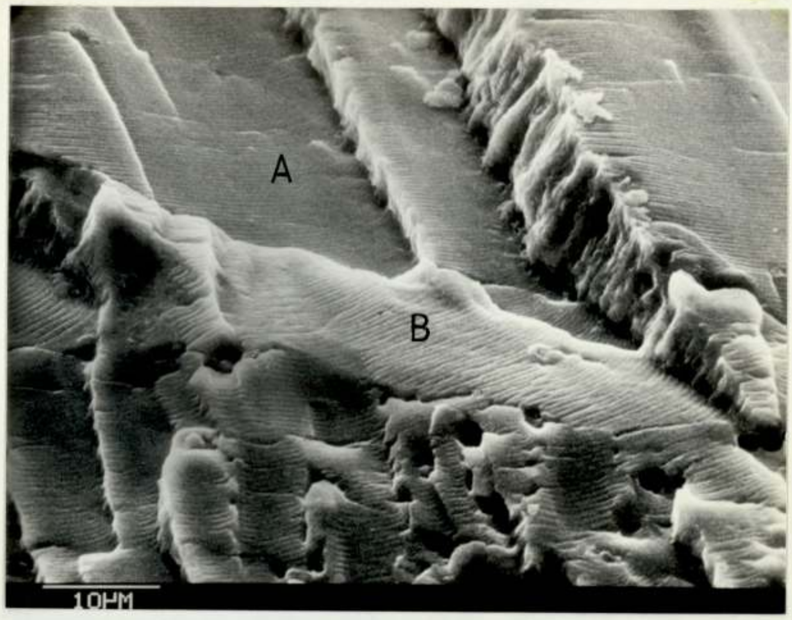

Plate 9.53 Higher-magnification view of the region outlined by the rectangle B in Plate 9.52

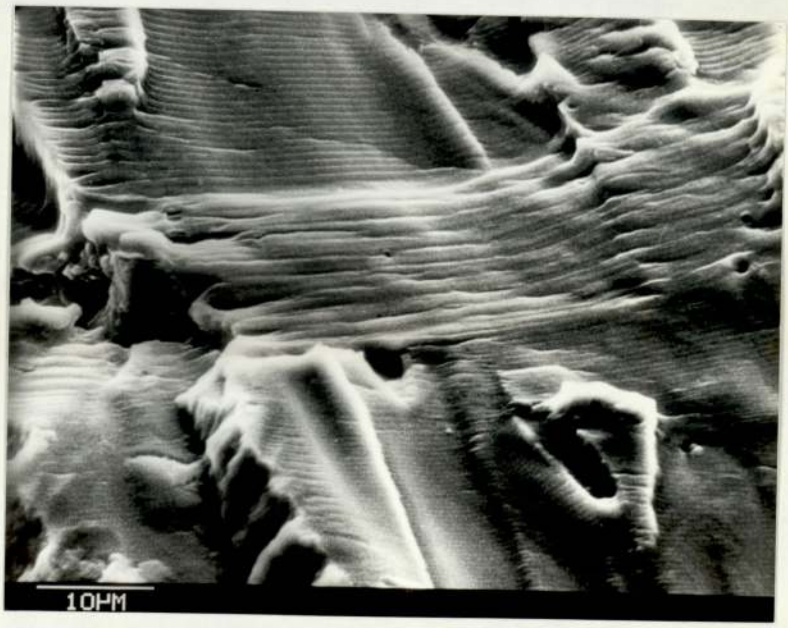

Plate 9.54 Higher-magnification view of the region outlined by the rectangle C in Plate 9.52

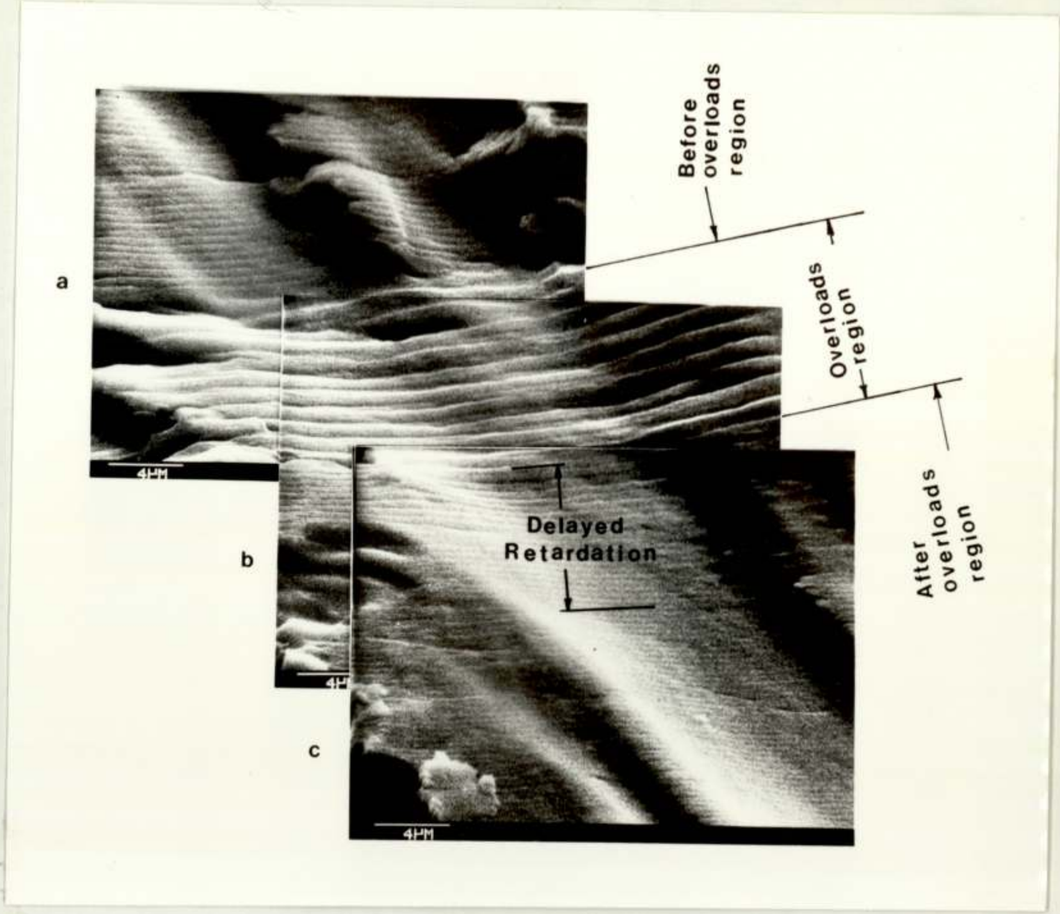

Plate 9.55 SEM fractographs taken from the locations marked with the letters a, b and c in Fig.9.31 and Plate 9.52

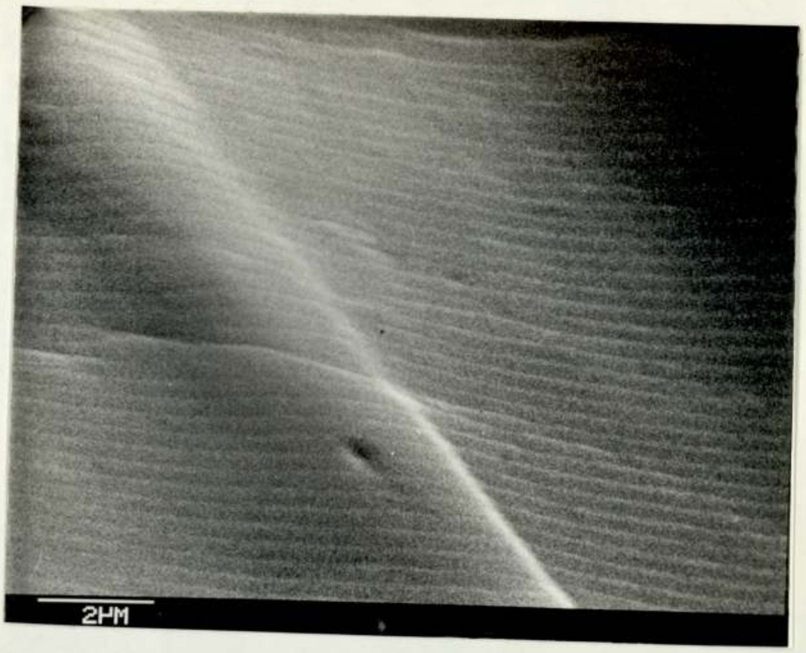

Plate 9.56 SEM fractograph taken from the site 0.05mm after the overloads, which is marked with the letter d in Plate 9.52

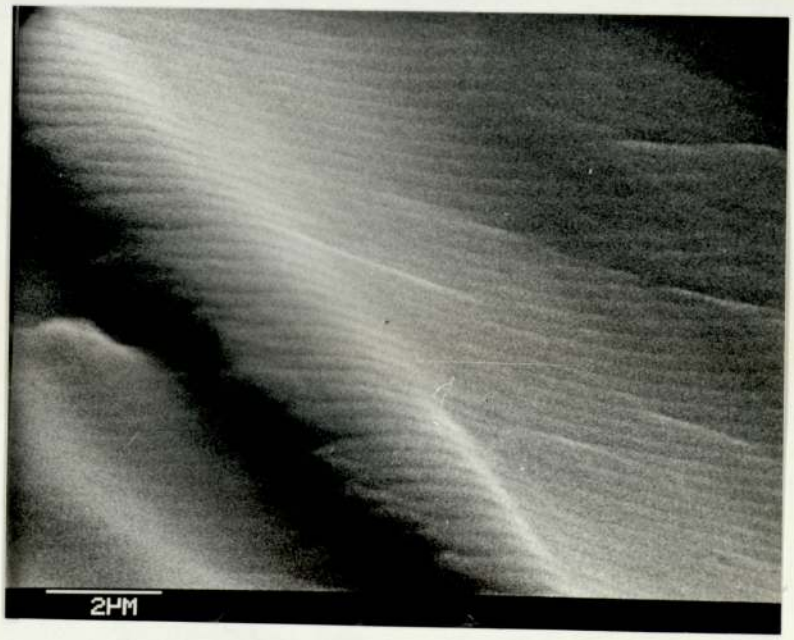

Plate 9.57 SEM fractograph taken from the site 0.07mm after the overloads, which is marked with the letter e in Plate 9.52.

Plate 9.58 SEM fractograph taken from the site 0.1mm after the overloads, which is marked with the letter f in Plate 9.52

Plate 9.59 SEM fractograph taken from the interior of the specimen before overloads. The site is marked with the letter g in Fig.9.31.

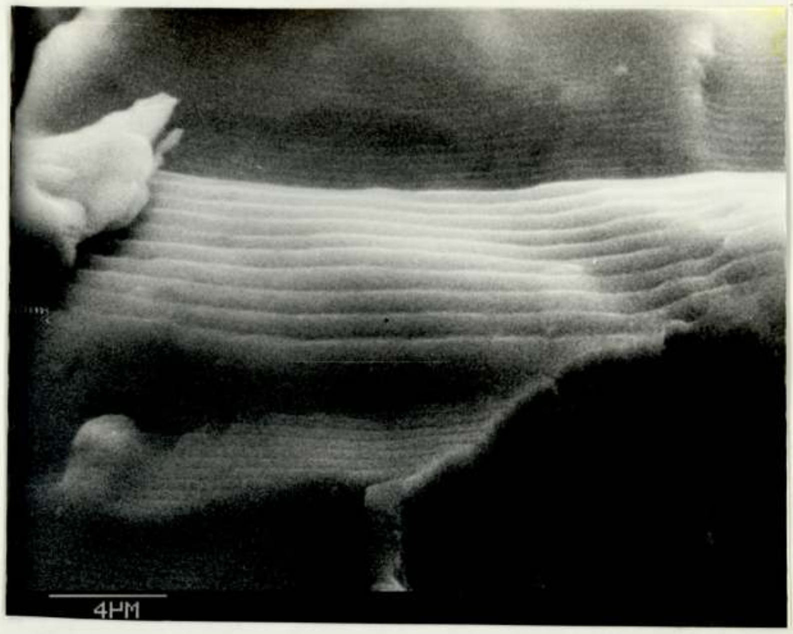

Plate 9.60 SEM fractograph taken from the site marked with the letter h in Fig.9.31.

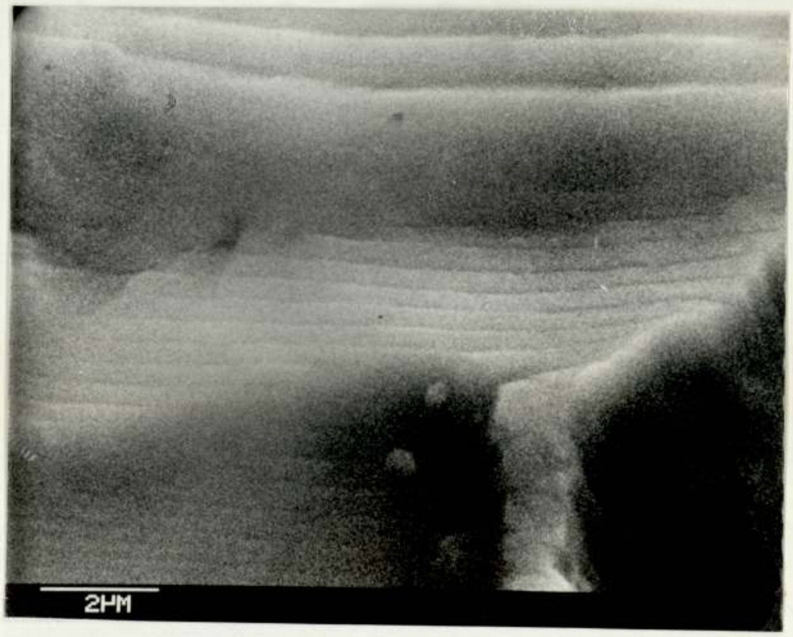

Plate 9.61 SEM fractograph taken from the site marked with the letter i in Fig.9.31.

Plate 9.62 SEM fractograph taken from the site marked with the letter j in Fig.9.31

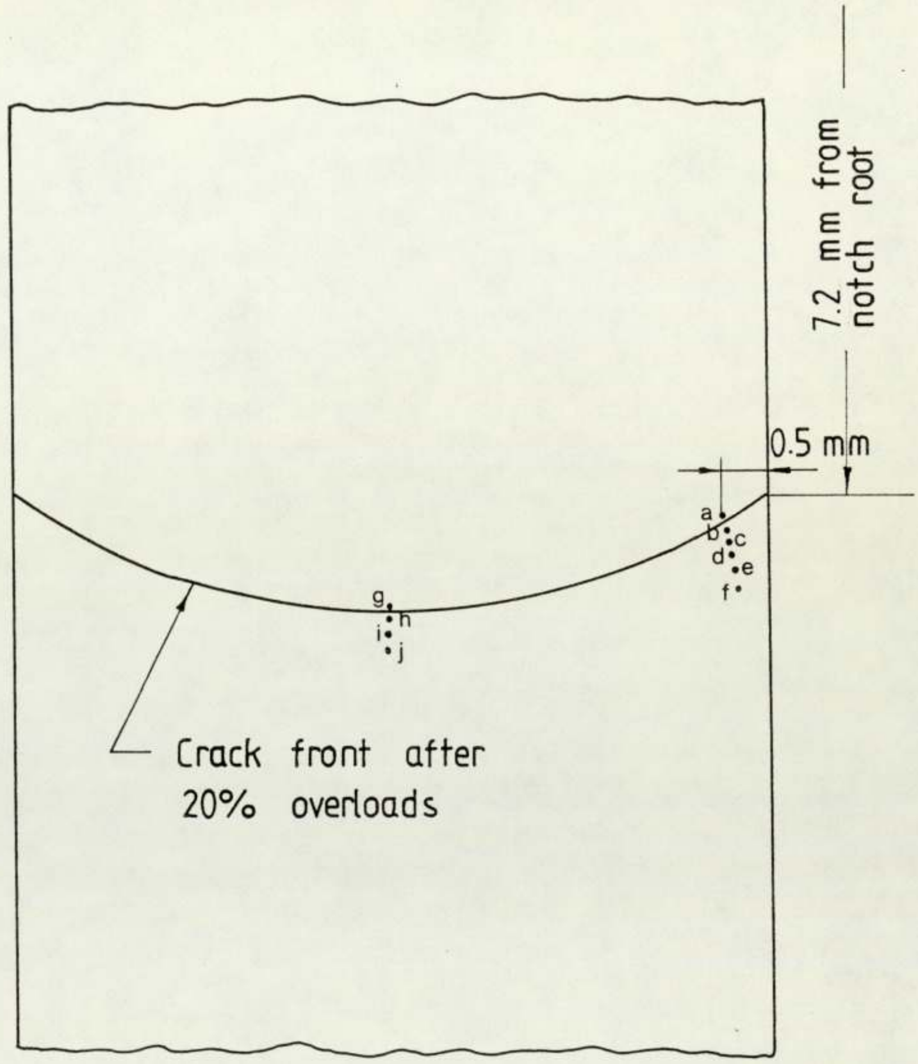

Figure 9.31 Locations of striations shown in Plate 9.51 to Plate 9.62

Table 9.20

Comparison of Striation Spacings with $\frac{da}{dN}$ Prior to and After the Application of 20% Multiple Overloads

*Location of Striations	Average Striation Spacing $\times 10^{-4}$ mm	$\frac{da}{dN}$ $\times 10^{-4}$ mm/cycle	Remarks
B.O.	6.86	6.81	
O.L.	16.00	28.90	
D.R.	6.22		
A.O.-0.05	4.45		In Near
A.O.-0.07	4.37		Surface
A.O.-0.10	4.71	4.24	Region
B.O.	5.52		In Interior
D.R.	5.62		Region
A.O.-0.05	5.28		

* B.O. - before overloads

O.L. - occurrence of overloads

D.R. - delayed retardation

A.O.-0.05 - after overloads, the figure indicating the distance from the crack front of the last overload cycle.

This implies that the crack growth retardation primarily occurred in the plane stress region.

ii) The delayed retardation can be studied by the fractographic technique and it was found that it occurred within about 20 cycles (0.01mm) following the overloads at $R_{01} = 1.2$ (Plate 9.55).

iii) Crack growth rate was locally accelerated when the crack extended through the affected region of the overloads. From Plate 9.51 - 9.54 it can be seen that the striations in region B are wider than that in Region A and voids appear in region B, indicating that static fracture took place.

9.3.3 Fatigue Crack Growth Under Block Spectrum Loads.

The characteristic stress intensity factor approach was employed to represent the experimental data. Root-mean-square stress intensity range ΔK_{rms} was taken as the characteristic stress intensity parameter for the representation. ΔK_{rms} was calculated by the following procedure. The specimen under 4-point bending was shown in Fig.9.32. The stress intensity was given by (126)

$$\Delta K = \frac{6\Delta M}{BW^2} \sqrt{\pi a} \; F\left(\frac{a}{W}\right) \qquad (9.17)$$

where

$$M = \frac{PS}{2} = 0.68 \; PW \qquad (9.18)$$

result in

$$\Delta K = \frac{4.08 \; \Delta P}{BW} \sqrt{\pi a} \; F\left(\frac{a}{W}\right) \qquad (9.19)$$

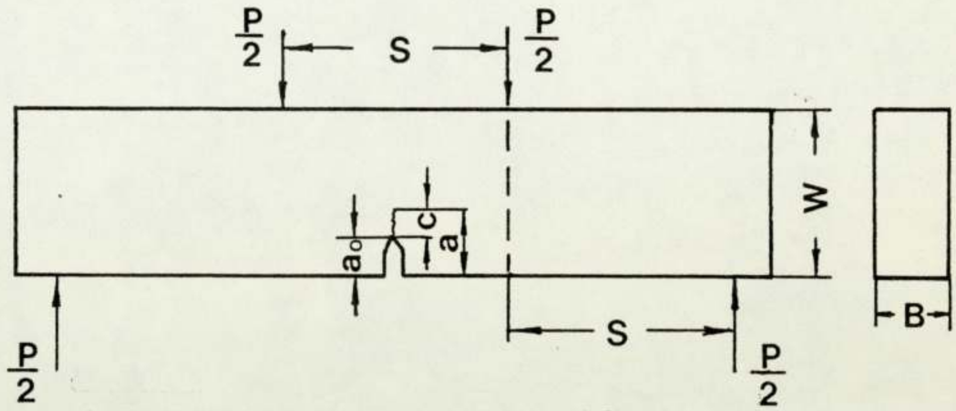

$W = 22.00$ mm

$S = 30.00$ mm

$B = 10.00$ mm

$a_o = 5.00$ mm

Figure 9.32 4 - point bending specimen configuration where

$$F(\frac{a}{W}) = \sqrt{\frac{2W}{\pi a} \tan \frac{\pi a}{2W}} \left(\frac{0.923 + 0.199(1-\sin\frac{\pi a}{2W})^4}{\cos \frac{\pi a}{2W}} \right)$$

The ΔK_{rms} was calculated by

$$\Delta K_{rms} = \sqrt{\frac{\Sigma \Delta K_i^2}{n}} \qquad (9.20)$$

where ΔK_i was the stress intensity factor range for individual block in load programme 1 and n is the number of blocks. The results are presented in Figs.9.33 and 9.34 in terms of $\frac{da}{dN}$ versus ΔK_{rms} and $\frac{da}{dR}$ (crack extension per repeat of load programme 1) versus ΔK_{rms} respectively. The curves can be represented by the following equations given by least-square fit.

$$\frac{da}{dN} = 1.36 \times 10^{-6} (\Delta K_{rms})^{1.84} \qquad (9.20)$$

$$\frac{da}{dR} = 1.98 \times 10^{-3} (\Delta K_{rms})^{1.84} \qquad (9.21)$$

Plate 9.63 shows crack initiation and its propagation in early stage. The black arrows indicate the multiple initiation sites. Some "striations" can be observed, illustrating crack growth per repeat of the load spectrum. Plate 9.64 is the "assembly" of SEM fractographs which were successively taken in one repeat, illustrating the striations from block 11 to block 16. The striation spacings, S_p, stress intensity factor ranges, ΔK and, stress ratios, R, for the individual block and the overload ratios between successive blocks are presented in Table 9.21.

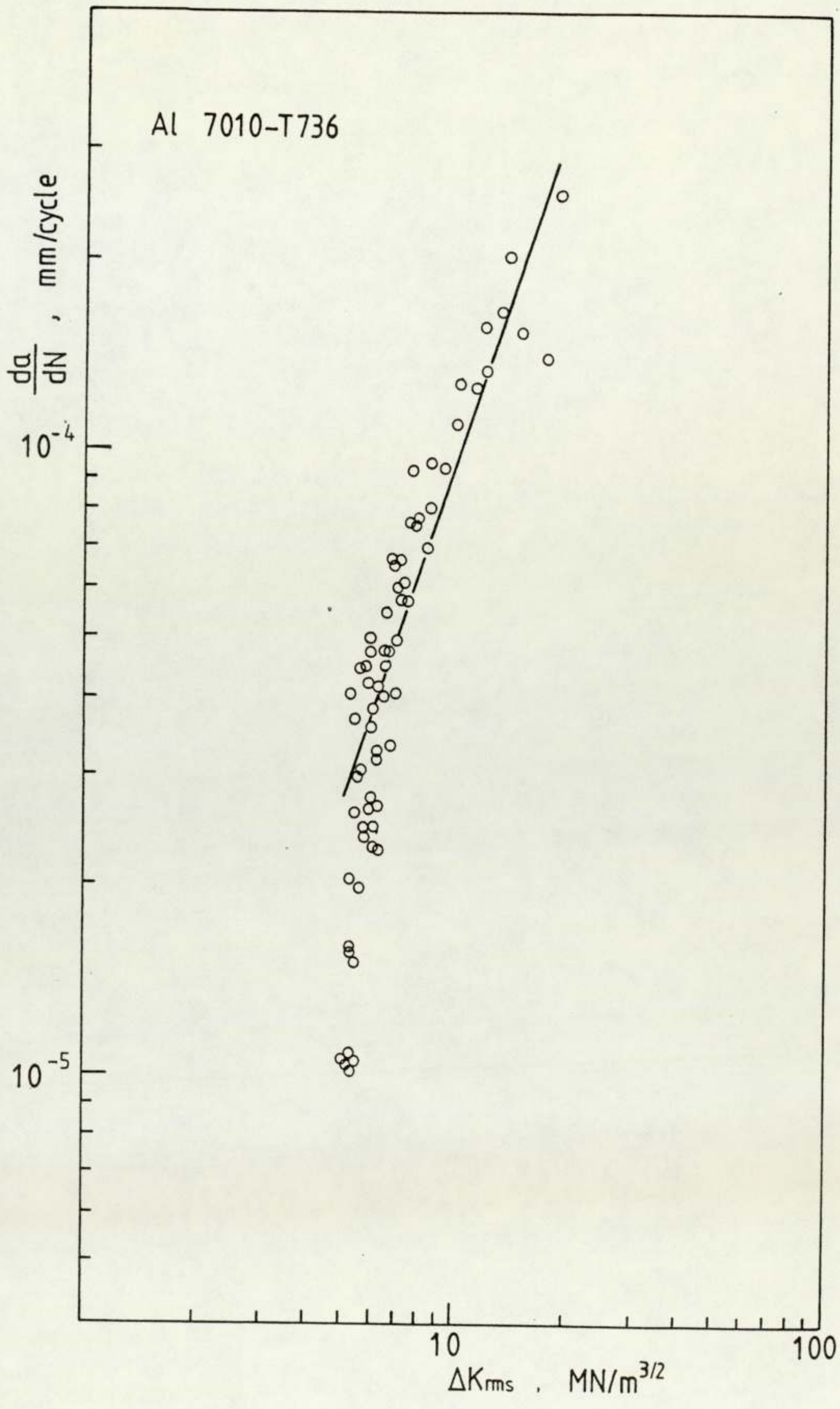

Figure 9.33 Fatigue crack growth rates as a function of the root-mean-square stress intensity factor range in alloy 7010 - T736

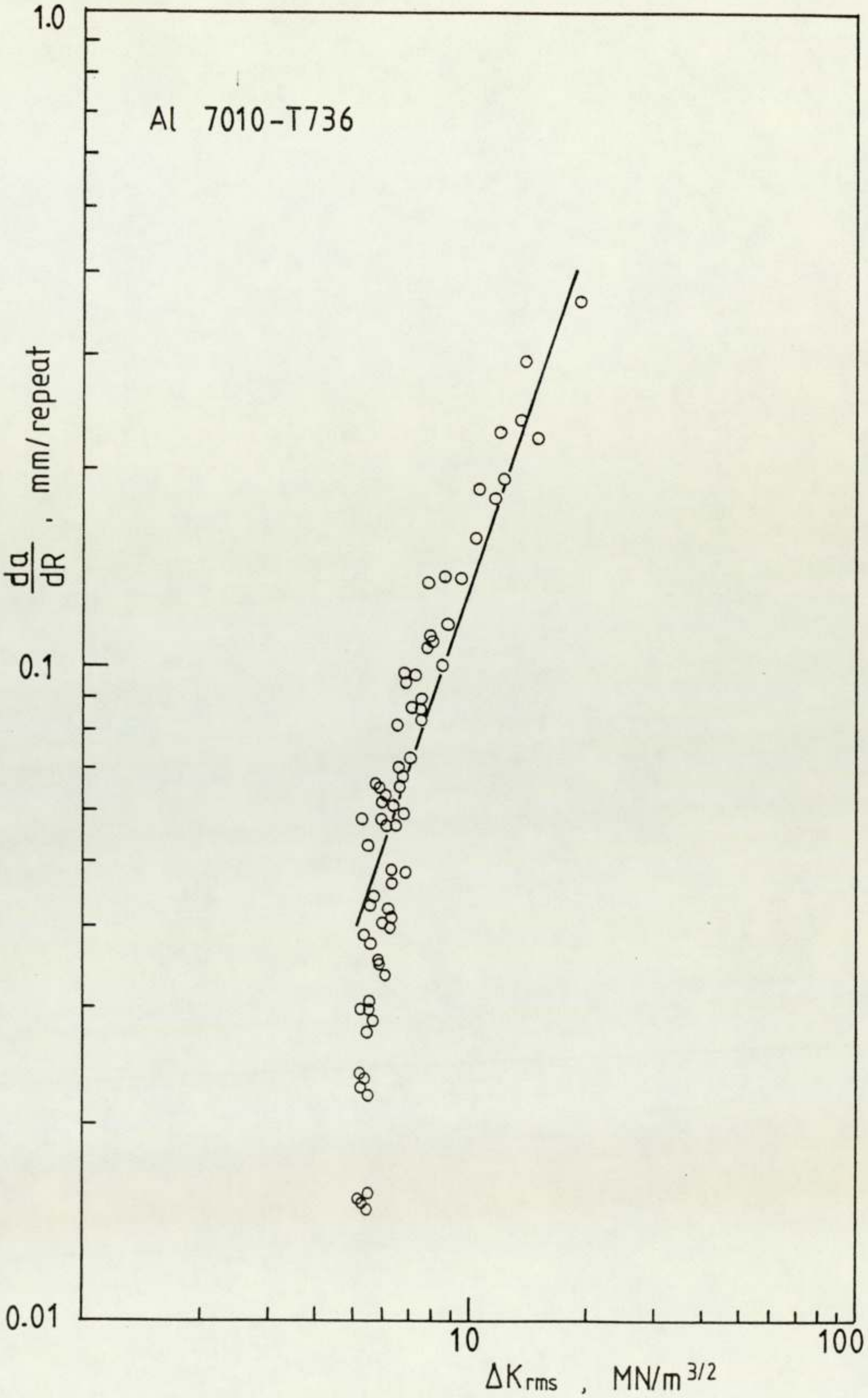

Figure 9.34 Fatigue crack growth rates (per repeat of block loading) as a function of the root-mean-square stress intensity factor range in alloy 7010 - T736

(a)

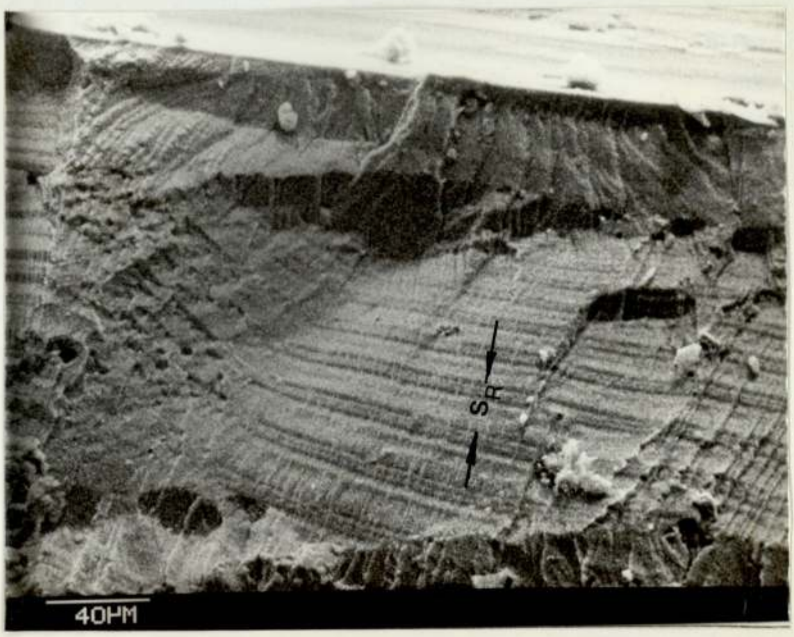

(b)

Plate 9.63 SEM fractographs showing crack initiation and its propagation in early stage in alloy 7010-T736 subject to block spectrum loading.

a) Low-magnification view showing crack initiation at multiple sites.

b) Higher-magnification view of the region outlined by the rectangle in Plate (a).

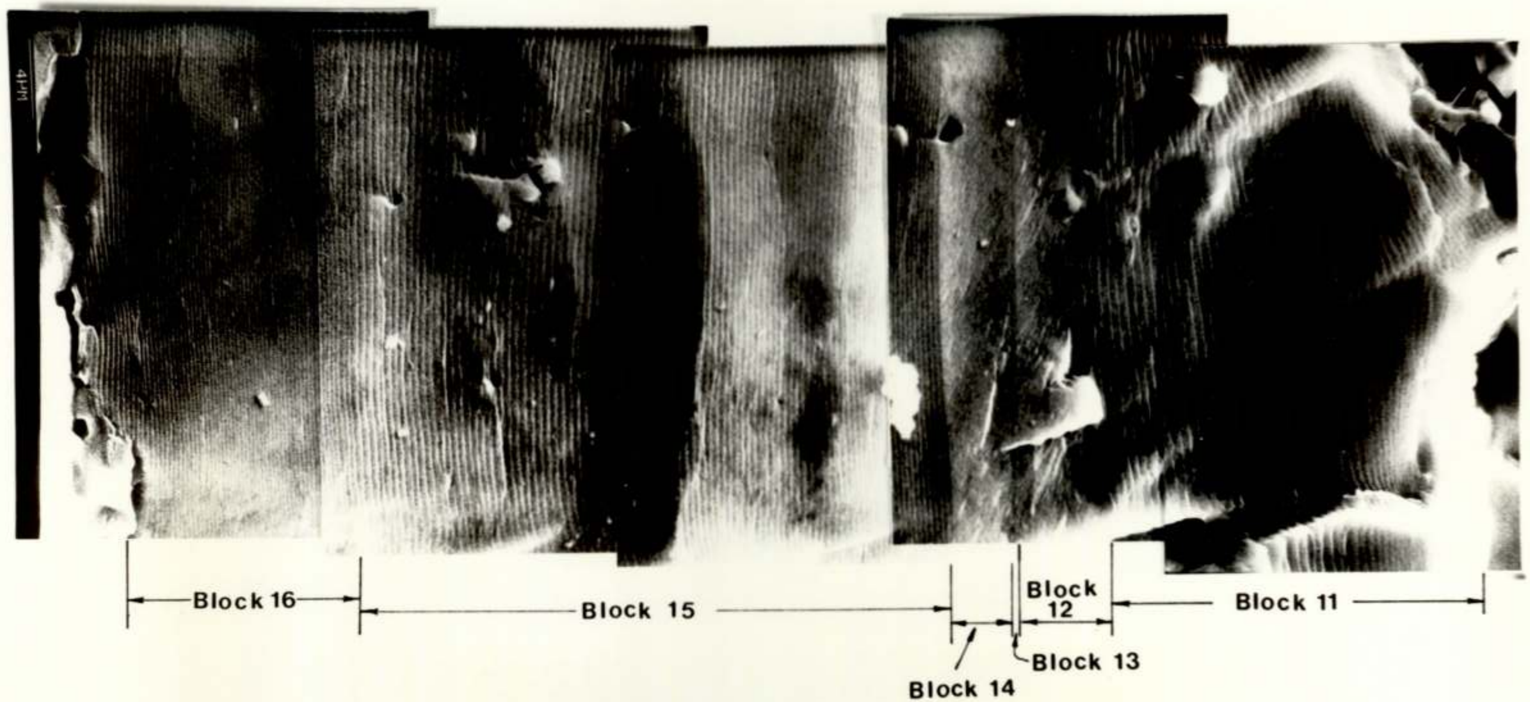

Plate 9.64 SEM fractographs showing striations from block 11 to block 16 of load programme 1 in alloy 7010 - T736.

Table 9.21

Comparison of Striation Spacings of Block 11 to Block 16 in Load Programme 1

Block No.	Average Striation Spacing $\times 10^{-4}$ mm	Stress Intensity Factor Range $MN/m^{3/2}$	Stress Ratio R	Overload Ratio R_{o1}
11	6.14	25.6	0.43	
* 12	0.37	19.04	0.46	1.17
13	-	-	-	
14	0.29	14.1	0.64	1.02
15	5.16	23.5	0.43	1.05
16	3.15	19.30	0.46	1.08

* For block 12 and block 14 no striations could be identified and, thus the average striation spacings were obtained by dividing the extensions of crack in block 12 and block 14 by their number of cycles, respectively.

It should be noted that the average crack growth rate of block 16 was larger than that of block 12 by a factor of 8. Since the two blocks have the identical load variables and the crack only extended about 0.07mm from block 12 to block 16, the change in stress intensity factors due to increase in crack length was only 0.26 $MN/m^{3/2}$ and therefore its influence on crack growth rate can be neglected. The considerable difference in crack growth rates between the two blocks can be only attributed to the effects of prior overloads. The overload ratios were 1.17 for block 11 to 12 and 1.08 for block 15 to 16 respectively. Previous investigation (127) suggested that the retardation effect of single overload with an overload ratio R_{ol} less than 1.4 was negligible in 7075 aluminium alloy. The present results demonstrate when multiple overloads were applied, even overload ratio R_{ol} less than 1.2 (R_{ol} = 1.17 for block 11 and 12), the retardation effect was still remarkable. However, when overload ratio dropped to about 1.1 no retardation effects were observed.

10 DISCUSSION

10.1 Electrical Potential Calibration.

The reliable measurement of crack length is prerequisite for the investigation of fatigue crack initiation and propagation. When the D.C. electrical potential technique is employed to monitor the crack growth the establishment of experimental potential calibration curves for the individual specimen geometry under consideration is necessary. This can be achieved by multi-specimen methods (73) or single specimen methods (128). The results can be presented by plotting the crack length against the change of potential drop, the ratio of measured potential drop to a reference potential drop against the ratio of notch depth plus crack length to the specimen width and other approaches (129).

Many factors could affect the experimental results. The plastic deformation at the starter notch root, crack closure, the multiple initiation of cracks and the thumbnail crack shape could lead some error to the calibration, particularly for short crack. For the multi-specimen method other error sources such as the effects of position of potential probes and the initial notch depth must be considered when the parameter $\frac{V_a}{V_o W}$ and $\frac{a_o+C}{W}$ are used to represent the results of experiments.

In the present experiments the effect of plastic deformation on crack measurement were neglected. It was found that although a small increase of about 1% of the total output potential did occur when a cracked specimen was loaded, no such increase was observed in uncracked specimens even if the load was raised to different levels so that different plastic deformation would be introduced at the notch root. This seems to indicate that the observed potential increments of 1% should be attributed to the crack opening under loading rather than plastic deformation in a cracked specimen.

The cracks may initiate at multiple positions around the notch root particularly for blunt notch specimens. This can affect the results of the experimental calibration in the region of early crack propagation. The initiated macrocracks glow forward parallel to each other until at a certain length the main crack forms by linking these cracks. Therefore, each crack makes a contribution to the potential increase. However, when the specimens with small cracks are broken maybe only one crack is measured because these short cracks are not initiated on same plane, whilst such a situation does not occur for long cracks as the main crack is longer and other shorter cracks stop growing and become insignificant from the potential viewpoint. The effect of crack closure during cyclic loading on the measurement of crack length was not observed at the frequency (20 HZ) used in the experiments. As the potential technique can only detect the crack area the equivalent through thickness crack length was employed and thus the influence of crack shape could be ignored.

The nominal distance of potential measurement probes was 10mm at present experiments, but the real distance was not identical for individual specimens. Although the procedure of welding the potential probes were carefully operated the distance error less than 0.8mm between two probes cannot be avoided. The machine notch depths were not the same for individual specimen. Thus, the measurements of potential drop for individual specimen before cracking are not the same. However, in the parameter $\frac{V_a}{V_o W}$, V_a includes two parts, V_{ao} and ΔV, the former is the potential drop measured before crack initiation and the latter is contributed by the growing crack. Obviously, the V_a would be considerably affected by the change of V_{ao} when crack is short, i.e. ΔV is small.

In the present investigation the average values of notch depth, the average values of V_{ao} and their standard deviations are listed in Table 10.1. It was found that reasonably good results for experimental potential calibrations were obtained for the change of V_{ao} within this range. The statistical analysis shows that the experimental results represented by Eq.(9.1) with the constants listed in Table 9.2 cause the standard deviations of 1.95%, 2.13%, 1.30% and 2.0% and the maximum percent deviation of 4%, 4%, 2.3% and 3.8% for 2XX, 35XX, 30XX, and 5XX type specimens, respectively.

10.2 Constant Amplitude Fatigue

10.2.1 Fatigue Crack Initiation

The initiation data (Table 9.7 - 9.10) show that the exponents in Eqs.(9.5) - (9.8) are almost the same for the four parameters $K_t \Delta S$, $K_f \Delta S$, $\Delta K/\rho^{\frac{1}{2}}$ and ΔK_n, but the coefficients B are different. The parameter ΔK_n gives the more similar values of coefficient B for the four

Table 10.1

Average Notch Depth and Average Potential

Drop before Crack Initiation

Specimen Type	Notch Depth		Potential Drop	
	Average mm	Standard Deviation mm	Average μv	Standard Deviation μv
2XX	5.048	0.188	147.4	2.80
35XX	4.989	0.066	176.0	1.58
5XX	5.090	0.092	202.5	2.37
30XX	9.910	0.037	308.0	3.32

groups of specimens compared with other parameters. Comparing Fig.9.3 with Fig.9.4 and Fig.9.5 with Fig.9.6, it can be seen that similar results are given by parameters $K_t\Delta S$ and $\Delta K/\rho^{\frac{1}{2}}$ and also similar results are obtained using parameters $K_f\Delta S$ and ΔK_n.

In reality, $K_t\Delta S$ and $\Delta K/\rho^{\frac{1}{2}}$ equally represent the local maximum stress at notch tip. The parameter $\Delta K/\rho^{\frac{1}{2}}$ originates from the elastic treatment of the stress at the base of a notch. For an elliptical notch with mode 1 stress , the approximate result for the stress concentration factor is $1 + 2\sqrt{a/\rho}$, where a is the axis transverse to the tension force and ρ is the radius of curvature at the end point of a. The stress amplitude at the root of notch is given by $\Delta\sigma = \Delta S\ (1 + 2\sqrt{a/\rho})$ when only elastic stresses are considered. If ρ is small then $2\sqrt{a/\rho} \gg 1$ and $\Delta\sigma \simeq 2\Delta S\sqrt{a/\rho} \simeq \Delta K/\rho^{\frac{1}{2}}$.

In fact, the local plastic deformation must occur for initiation of fatigue cracks, so the effect of local plastic deformation on initiation must be taken into account. Obviously, the local yielding will redistribute the stresses at notch tip and thus the average stress in a small volume of notch tip is more important to crack initiation than the maximum stress on the notch surface. In Fig.9.3 and Fig.9.4 the data points for sharp notch specimens exceed others because the sharp stress gradient developed in sharp notch specimens leads to the lower average stresses in the vicinity of the notch tip.

The fatigue notch factor K_f is characterised of both the mechanical notch and the material. The parameter $K_f \Delta S$ represents the redistributed stress at the notch root. The test results presented by $K_f \Delta S$ versus N_i are shown in Fig.9.5. It is noted that the results are better grouped than that presented by $K_t \Delta S$ and $\Delta K/\rho^{\frac{1}{2}}$.

As mentioned in Section 4.4.1.3 the dependence of N_i on the stress intensity factor range at the notch root is based on the analysis of the critical cumulative displacement at the notch root (76). Therefore, for an attempt at relating N_i to ΔK the physical process of the crack formation must be responded in the computation of the stress intensity factor. This was considered by Barnby, Nadkarni and Eqs.(9.3) and (9.4) were proposed to compute the stress intensity factor range at notch root. In Eq.(9.4) the grain size C_B as a material parameter was experimentally introduced under the consideration that the slip may occur initially within one grain. The experimental results represented by ΔK_n are shown in Table 9.10 and Fig.9.6. It can be seen that the data scatter band is smaller compared with others. The linear regression analysis was used to give the best-fit line to represent the all test data and the constants were presented in Section 9.2.1 ($B_4 = 3.32 \times 10^7$, $n_4 = 3.03$). The correlation coefficient was equal to 0.67. Taking C = 0, Eq.(9.4) becomes

$$a_o \tanh\left(\frac{2\, C_B \sqrt{1 + a_o/\rho}}{\sqrt{a_o \rho}}\right) + C_B - a_o\left(\frac{Y_n}{Y_L}\right)^2 = 0 \qquad (10.1)$$

and then C_B can be calculated by solving this equation. The average values of C_B deduced from the short crack growth results for the specimens of group 5XX, 35XX and 30XX are 0.39mm, 0.31mm and 0.15mm respectively. Comparing with the experimentally determined grain dimension C_B, which was 0.08mm, the difference is obvious. To solve Eq.(10.1) the minimum value of $\frac{Y_n}{Y_L}$ must be pre-determined by experiments using Eq.(9.15) and the calculated C_B will in large part depend on the value of $\frac{Y_n}{Y_L}$. However $\frac{Y_n}{Y_L}$ depends on the crack growth rate $\frac{da}{dN}$ and the constants A and m. All the three parameters have to be determined by experiments. The errors in the measurements of $\frac{da}{dN}$ will result from the electrical potential calibration and the constants A and m in Paris equation are also affected by other factors such as mean stress. Therefore, it seems that the reliable calculated value of C_B by solving Eq.(10.1) can not be expected.

10.2.2 Fatigue Crack Propagation in Notch Stress Field

The test results of Y_n/Y_L presented in Figs.9.11, 9.12 and 9.13 show that almost all experimental data points are below curve 1. Eq.(9.4) represented by curve 2 fits the results very well for shallow notch specimens (a_o = 5.00mm). However, for deep notch specimens (a_o = 10.00mm) most experimental data points lie below the curve 2 (Fig.9.13). A similar phenomenon can be observed in Fig.9.6. The diagram of Log ΔK_n versus Log N_i shows that the data points for shallow notch specimens neatly lie on one straight line, but for deep notch specimens deviation occurs. Nadkarni explained that Eq.(9.4) arises from the effect of the notch stress field on the stress intensity factor coefficient of a short crack and also includes the effect of crack shape on the stress intensity factor coefficient. As the crack shape of the short crack is similar for both shallow and deep blunt notch specimens (Section 9.2.5.3), the deviation for deep notch specimens must be attributed to the effect of notch stress field. In the present work the deep notch specimens show mild stress concentration compared to shallow notch specimens (124) (Table 8.3). According to the theory of notch stresses (130) the stress concentration factor is a function of the notch depth and the radius of curvature of notch root for shallow notches. On the other hand the stress concentration factor is a function of the radius of curvature of notch root and the width of the narrowest cross section as the disturbance of the stress variation will extend over the entire narrowest section. Since the notch stress field is dominated by different parameters with shallow notch specimen and deep notch specimen under consideration, the Equation (9.4) should be further modified so that it can hold for both shallow and deep notch geometries. This could be achieved by redefining the parameters as shown in Fig.10.1 and Eq.(9.4) could be modified to the following form

$$Y_n = Y_L[(a_o \tanh(2\sqrt{1 + a_o/\rho}\ (C + C_B) / \sqrt{a_o\rho}) \pm (C + C_B) / (a_o \pm C)]^{\frac{1}{2}} \tag{10.2}$$

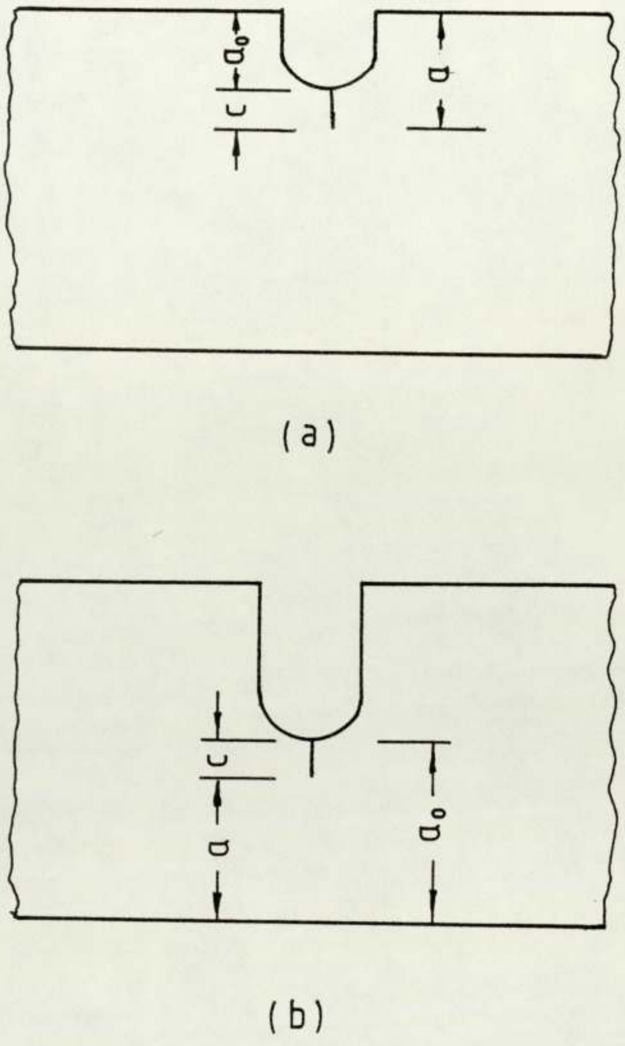

Figure 10.1 Nomenclature for notches

(a) shallow;

(b) deep.

For shallow notch the a_o is defined as the notch depth shown in Fig.10.1a and the positive sign is used. For deep notch the a_o is defined as the width of narrowest cross section shown in Fig.10.1b, and the negative sign is used. Eq.(10.2) was employed to calculate ΔK_n at initiation and the results are shown in Fig.10.2. It is noted that the data points for both shallow notch specimens and deep notch specimens close together and the smaller scatter band is given compared to Fig.9.6. The best-fit line given by linear regression analysis is in the form

$$N_i = B_4(\Delta K_n)^{n_4}$$

with the constants

$$B_4 = 2.52 \times 10^8$$

$$n_4 = -4.0$$

The linear correlation coefficient is 0.8.

In Fig.9.13 curve 3 represents Eq.(10.2) and it gives a better fit to experimental data points than that given by Eq.(9.4).

Figs.10.3, 10.4 and 10.5 show fatigue crack propagation data as a function of unmodified and modified stress intensity factor amplitude (calculated using Eqs.(9.3) and (9.4)) for blunt notch specimens. The straight lines in the figures represent long fatigue crack propagation data. Again, for shallow notch specimens the modified crack propagation data lie around the straight lines, but for deep notch specimens it lies below the straight line. Fig.10.6 presents the results of unmodified and

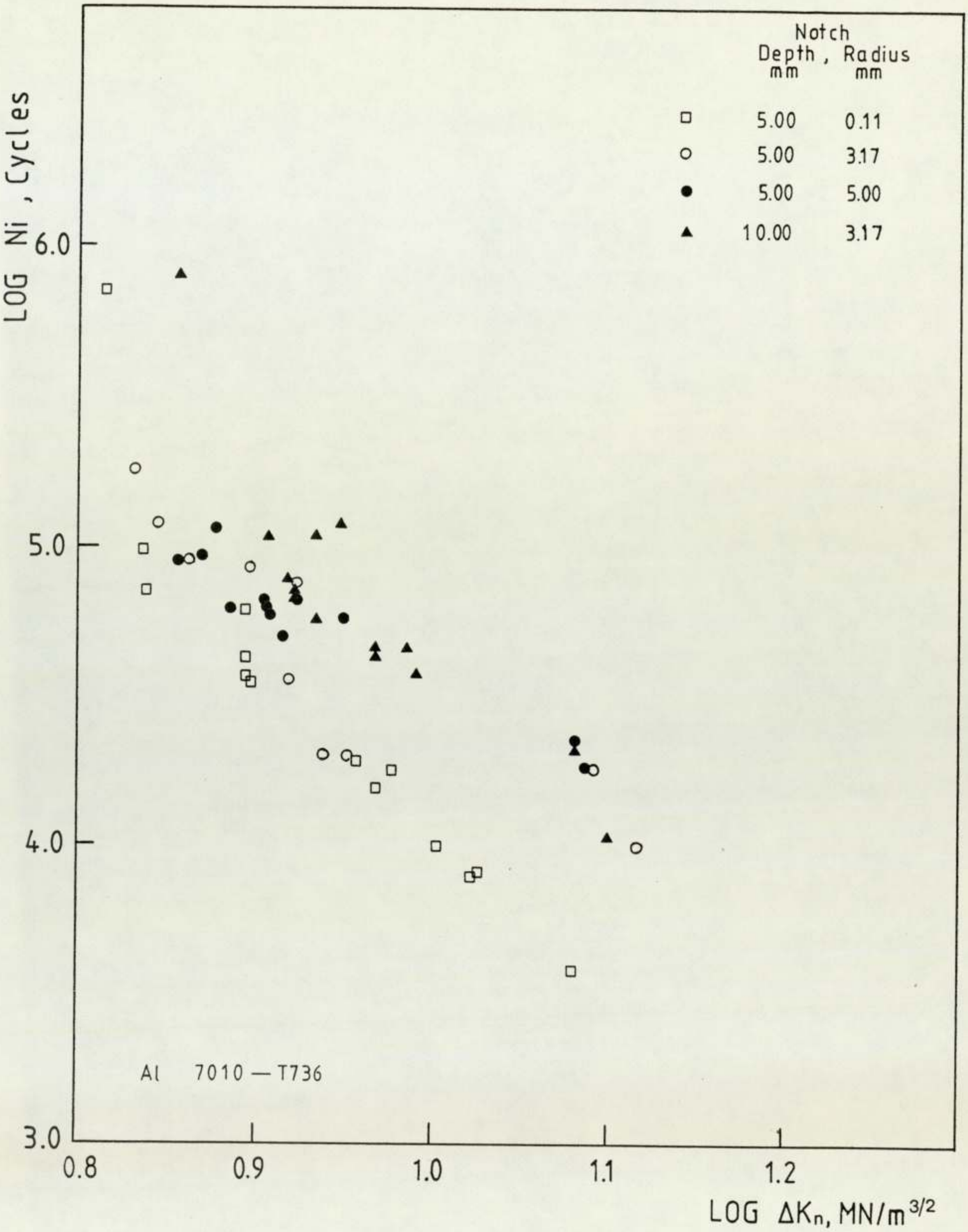

Figure 10.2 Fatigue crack initiation data for alloy 7010 - T736.
N_i versus modified ΔK_n calculated using Eqs.(9.3) and (10.2)

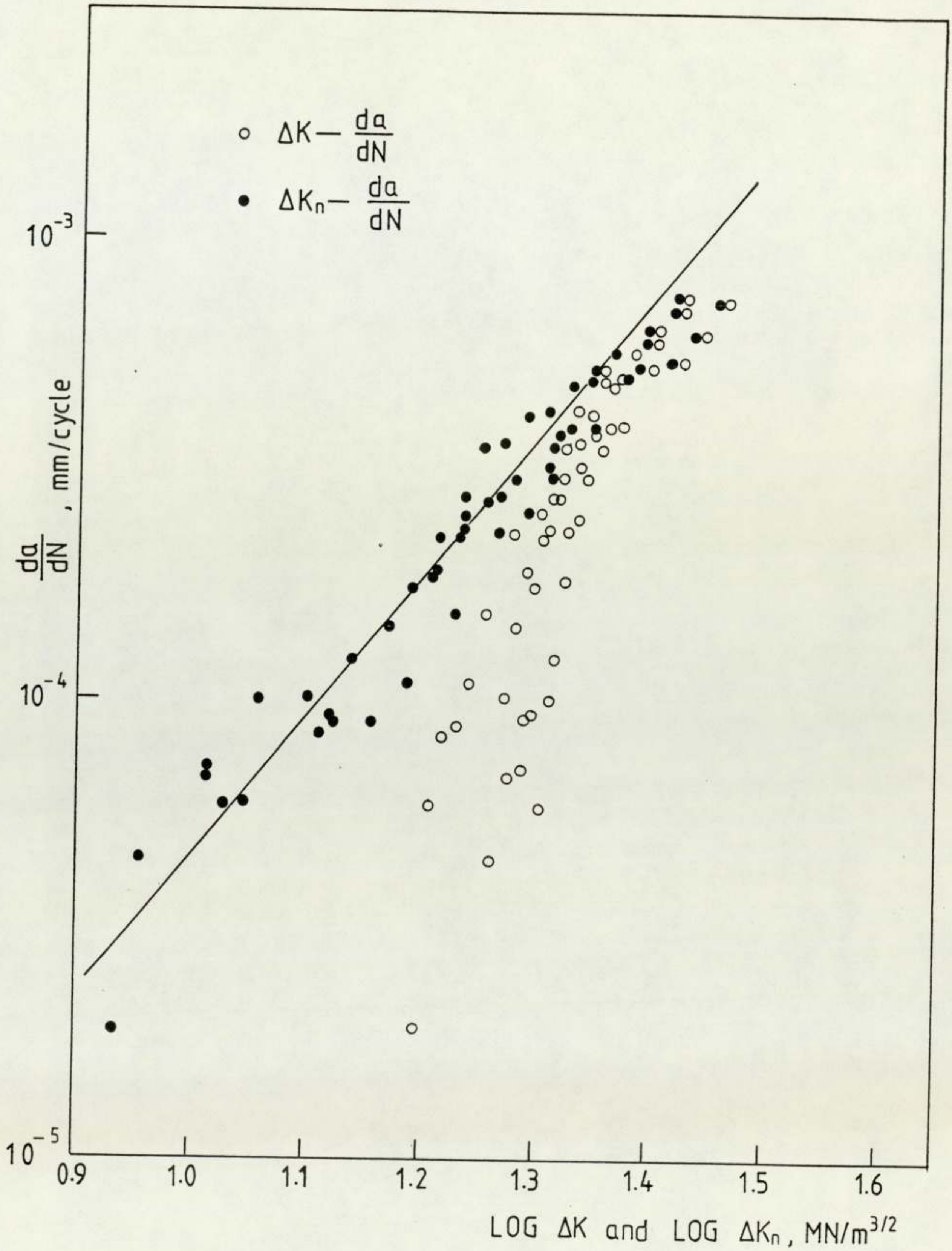

Figure 10.3 Fatigue crack growth rates in notch stress field as the function of unmodified and modified stress intensity factor range. (a_o = 5.00mm, ρ = 3.17mm)

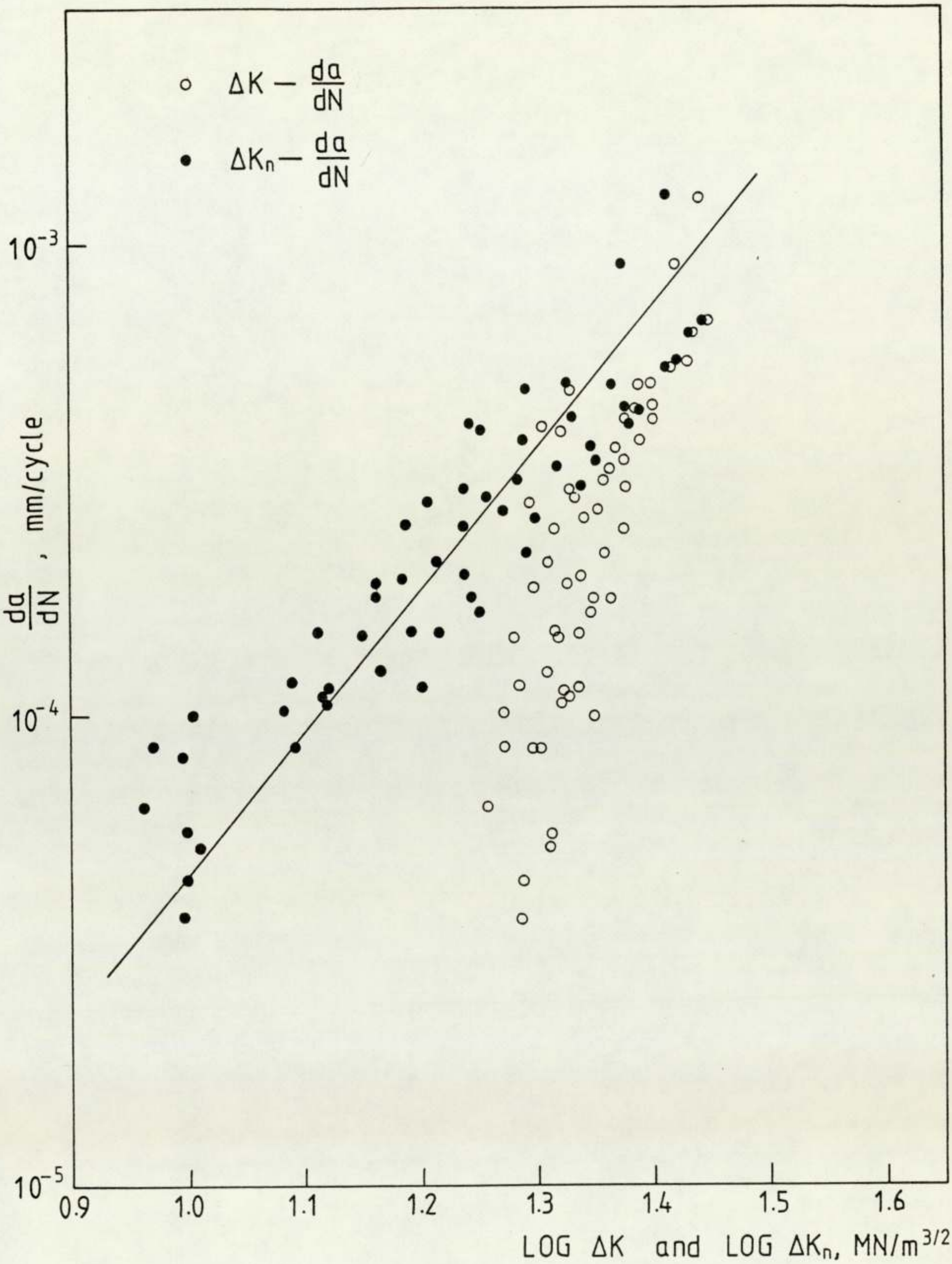

Figure 10.4 Fatigue crack growth rates in notch stress field as the function of unmodified and modified stress intensity factor range. (a_o = 5.00mm, ρ = 5.00mm).

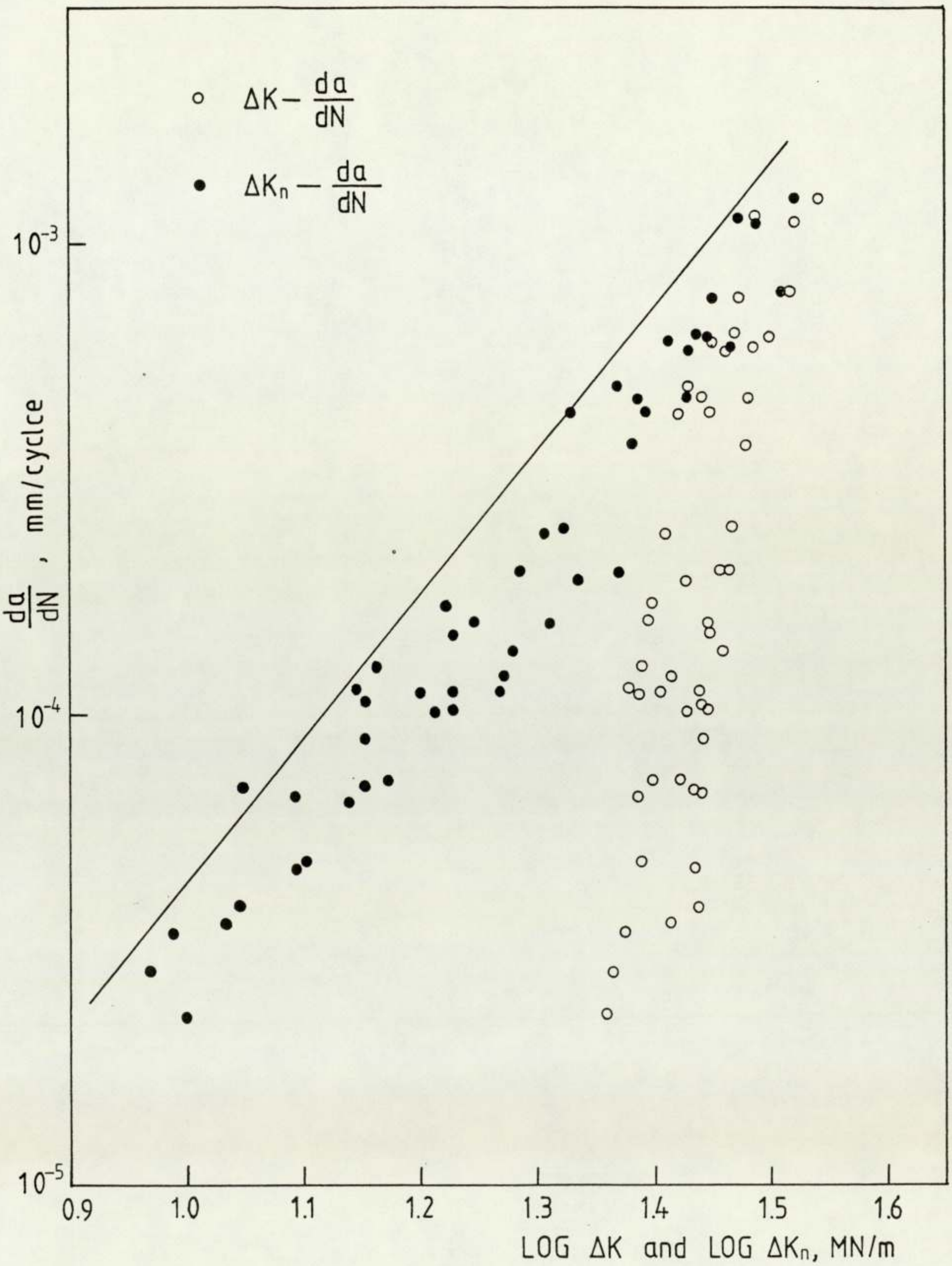

Figure 10.5 Fatigue crack growth rates in notch stress field as the function of unmodified and modified stress intensity factor range. (a_o = 10.00mm, ρ = 3.17mm).

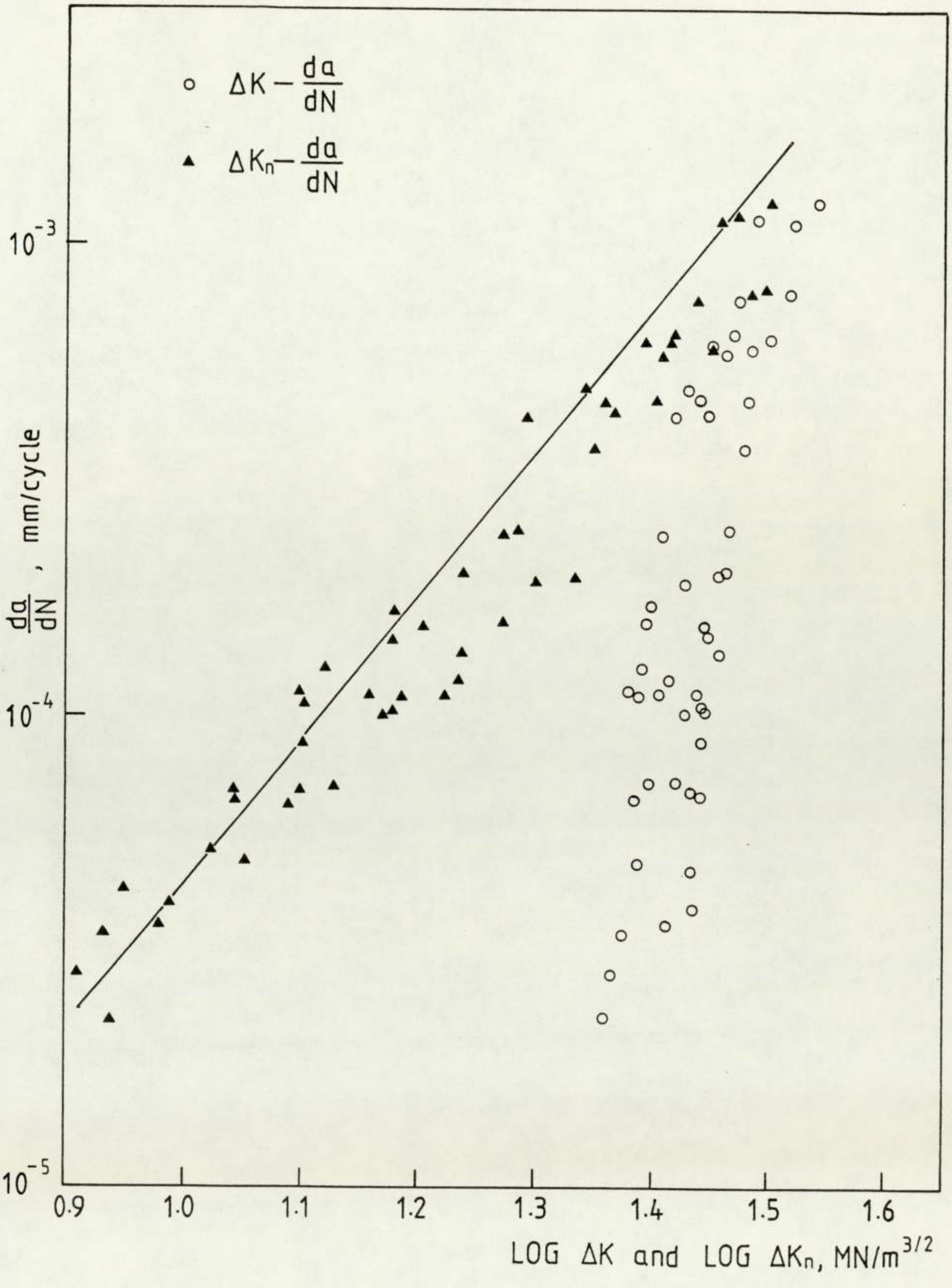

Figure 10.6 Fatigue crack growth rates in notch stress field as the function of unmodified and modified stress intensity factor range. The modified stress intensity factor was calculated using Eqs.(9.3) and (10.2) (a_o = 10.00mm, ρ = 3.17mm)

modified stress intensity factor amplitude (calculated using Eq.(10.2)) against fatigue crack propagation rate for deep notch specimens. It can be seen that like Fig. 10.3 and Fig.10.4 the data points in Fig.10.6 lie around the striaght line, This indicates that the Eq.(10.2) could give better fit to test results.

10.2.3 The Effect of Machining on Fatigue Crack Initiation

In the present investigation the specimens were machined after heat treatment. To check the influence of the residual stress introduced by machining on crack initiation two groups of specimens were employed. One of them was re-heat treated using the same procedure described previously (Section 8.1) and all parameters were carefully controlled. The measurements of hardness show the same values of hardness HB148 for the two groups of specimens. The specimens then were fatigued to initiation using the same loading variables. The test results were presented in Table 10.2. It suggests the compressive residual stress introduced by machining could increase the resistance to crack initiation by 13% to 30%.

10.2.4 The Effects of Shot-Peening on Crack Initiation and Propagation

The improvement in the resistance to fatigue crack initiation at lower load level observed in shot-peened specimens was ascribed to the compressive self-stresses in the notch root surface region induced by the peening

Table 10.2

Comparison of Initiation Data for Re-Heat Treated and Un-reheated Treated Specimens.

Specimen No.	Notch Geometries		Load Range	Stress Ratio	Re-Heat Treated	Ni
	a_o, mm	ρ, mm	ΔP, KN	R		
501	5.06	5.09	5.76	0.1	No	62700
505	5.16	5.21	5.76	0.1	No	64240
507	4.96	4.92	5.76	0.1	No	58980
514	5.14	5.10	5.76	0.1	Yes	43000
515	5.14	5.07	5.76	0.1	Yes	46860
516	5.19	5.14	5.76	0.1	Yes	51100

process. Obviously, the compressive stresses will be gradually decayed during the fatigue process. The lower the applied load is, the longer the compressive self-stresses will last and vice versa. If the local stress at the notch tip exceeds the yield stress of the material local plastic deformation will occur and the stresses at the notch surface will be re-distributed and therefore the compressive self-stresses induced by shot-peening cannot be maintained any longer, and moreover the roughened surface caused by peening process will reduce the resistance to fatigue. It should be noted that the corresponding maximum local stress ($K_t\ S_{max}$) at the intersection point in Fig.9.13 is about 470 MN/m^2. It is almost equal to the ultimate stress of the material (471 MN/m^2). If we considered that the yield stress of the material in notch root region was increased by strain hardening during shot-peening, then the intersection point should correspond to the transition from the elastic state to the plastic state at the notch root. This implies that below the transition the material at the notch tip primarily is in the elastic state and a beneficial effect of shot-peening can be expected.

It should be noted that the crack growth rate for peened specimens was higher than that for unpeened specimens until the crack grew to an equivalent crack length of about 1.2mm. This phenomenon may be due to the effect of residual stress reversal. After shot-peening the compressive stresses are developed in the peened surface layer. The equilibrium of forces requires tensile stresses in the core of the specimen. Usually the compressive stresses exist within about several one tenth millimeters in the surface layer and after that the tensile stresses prevail. In the present work the residual stress distribution was not measured due to the limitation of equipment. Hawkes measured the residual stresses after shot-peening by the x-ray technique in D.T.D 5054 aluminium alloy (Zn 6.0, Mg 2.4, Cu 0.74, Cr 0.1, Mn 0.28, balance Al). The peening intensity was 0.008 A. The results were represented in Fig.10.7 (131). It can be seen that the maximum compressive stress occurred at about 0.1mm depth and at the depth of about 0.2mm below surface the stress was reversed and at about 1.2mm the residual stress vanished. Comparing Fig.9.19 with Fig.10.7 the dependence of crack growth rates on crack length and the distribution of the residual stress were coincidence for the crack length greater than 0.2mm. No such comparison was made for the crack less than 0.2mm as the crack growth rates could not be measured by the potential technique.

10.2.5 Variability in Fatigue Crack Growth Rate (FCGR) Data

The variability in FCGR data could result from a number of factors such as the variability of material properties, crack length measurement errors, inaccuracy of load control and the method of data processing. In the present investigation the FCGR data was obtained referring to

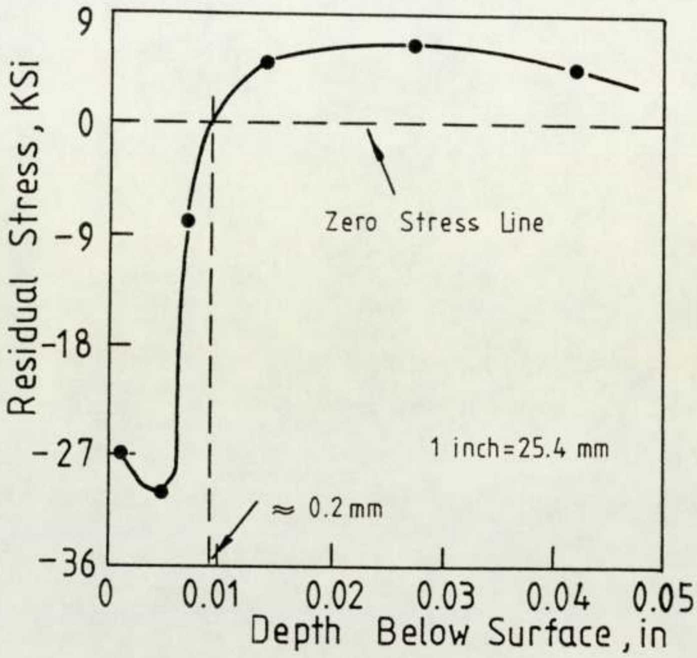

Figure 10.7 Residual stress distribution near the surface of a specimen of D.T.D 5054 alloy after shot-peening. (after Hawkes, (131))

ASTM Standard E647-78T. It was noted that the crack growth increment size could result in variation in the resulting FCGR (132, 133). Ostergaard and his co-workers analysed the data of 68 replicate fatigue crack growth tests on centre cracked panels of 2024-T3 aluminium alloy and concluded that the minimum error of calculating $\frac{da}{dN}$ was obtained for Δa between 0.8mm and 1.6mm (132). As the Δa-increment of centre crack panels is twice the Δa-increment of edge crack specimens, so the proper Δa-increments should be 0.4mm to 0.8mm for edge crack specimens. According to ASTM Standard (E647-78T) the minimum Δa should be 0.25mm or ten times crack length measurement precision which is defined as the standard deviation on the mean value of crack length determined for a set of replicate measurements. Artley et al (133) suggested that the ratio of Δa-increment to the crack length measurement precision should be greater than 15. In the present experiments the crack measurement precision can not be determined. For the procedure of calculation of FCGR described in section 8.3.1 the Δa-increments maintained at the range of 0.3mm to 0.7mm corresponding to the Δv-increments of 5 μr to 20 μv.

10.2.6 Metallography and Fractography

10.2.6.1 The Influence of Second Phases on Fatigue Crack Growth.

The effects of microstructure of high strength aluminium alloy on toughness and the resistance to fatigue crack growth were reviewed by Sanders and Starley (134). They concluded that coarse secondary intermetallic particles, intermediate size dispersoids and fine precipitates all have influence on fracture toughness and fatigue crack growth at intermediate and high levels of stress intensity under constant amplitude loading. In the present investigation the effect of microstructure on fatigue crack growth was examined. A blunt notch specimen (ρ = 5.00mm) was fatigued to initiate a crack and then the metallographic sample was cut from the notch part of the specimen. A number of sections of the sample were examined under opticalloscope. The Plate 10.1 was taken from the section of 2.57mm below the surface. It shows that the coarse secondary intermetallic particles could affect the fatigue crack propagation. The direction of the crack growth locally changed when an intermetallic particle or a cluster of particles was encountered at A, B, C and D. Plates 10.2 - 10.3 show the distribution of secondary intermetallic particles. X-ray probe micro-analysis proved that these particles were compounds of Al-Cu-Fe-Zn and Al-Cu-Zn (Figs.10.8-10.9). Most particles were of a size of less than 10 μm, but these particles may be in a cluster form with a much larger size than a single particle and therefore affected crack growth significantly.

The effect of single secondary phase particle on crack growth is shown in Plates 9.38, 9.41, 9.42 and 9.43. These particles indicated as a, b, c and d were of a size of 1.0 – 3.0 μm. It can be seen that the individual small particle gave an insignificant influence to fatigue crack

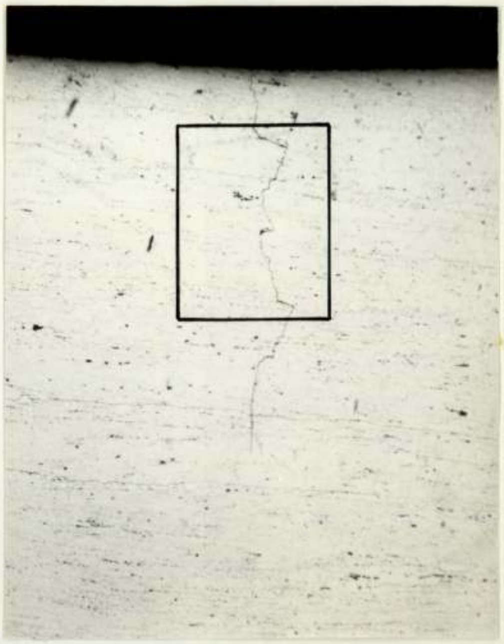

(a)

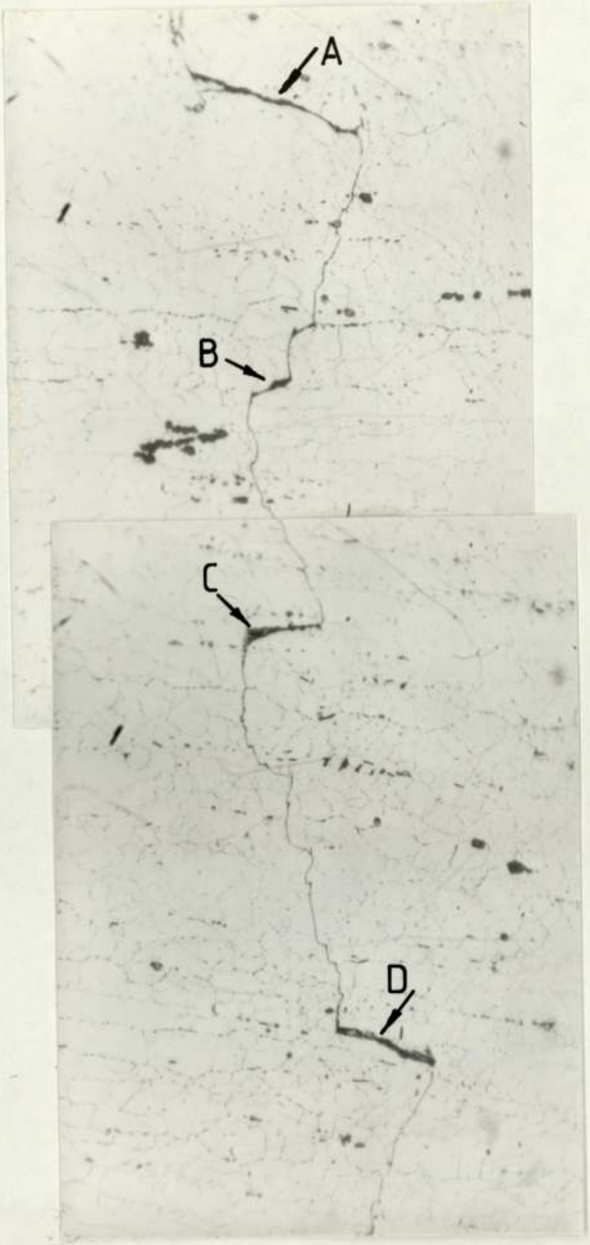

(b)

Plate 10.1 Optical micrographs showing the effect of secondary intermetallic particles on fatigue crack growth, etching in Keller's reagent.

(a) Full view of a short crack emanating from notch root, X100.

(b) Higher-magnification view of the region outlined by the rectangle in Plate (a) X600.

Plate 10.2 Microstructure of alloy 7010 - T736 on L - S section.

Plate 10.3 Microstructure of alloy 7010 - T736 on normal cross section.

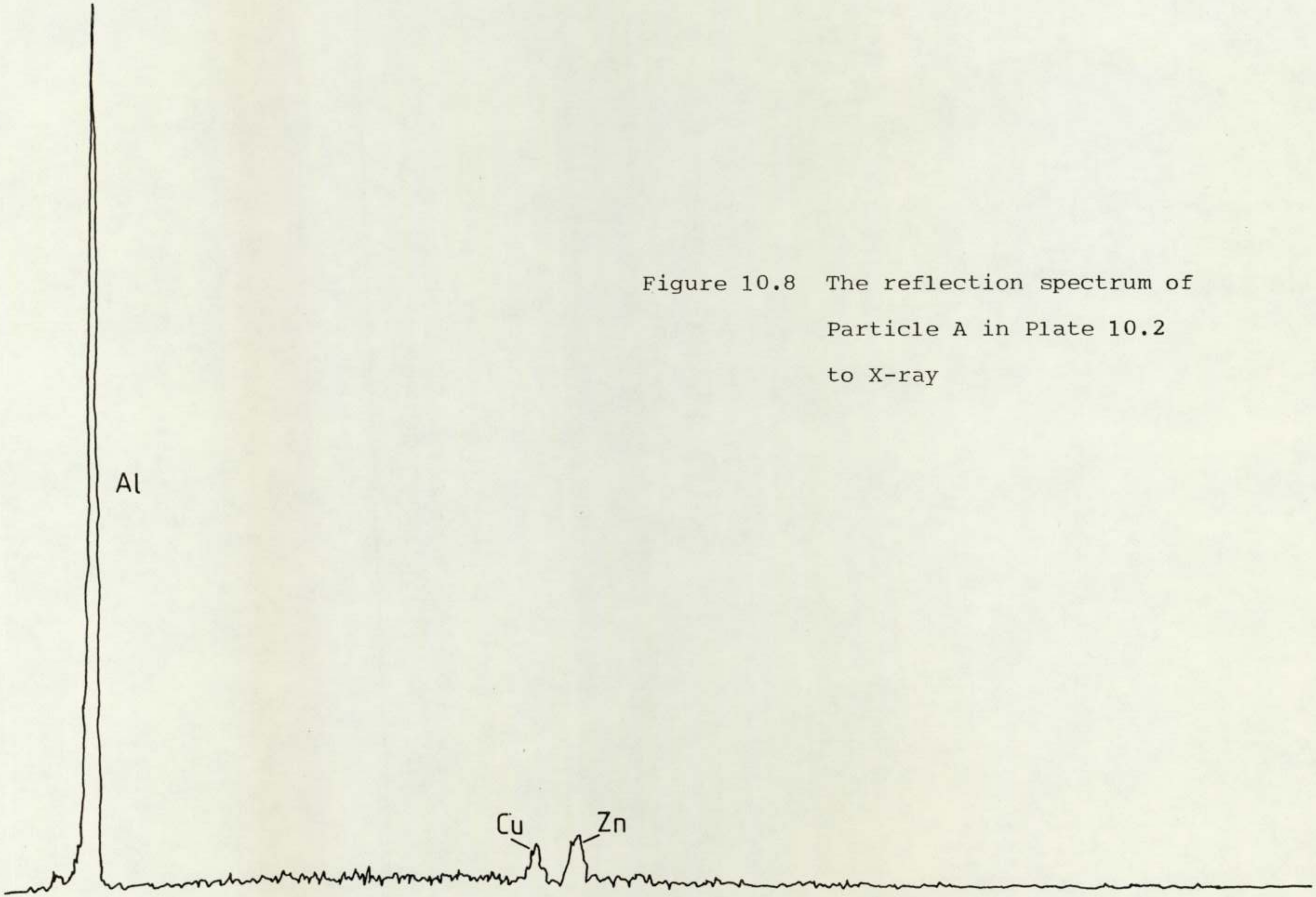

Figure 10.8 The reflection spectrum of Particle A in Plate 10.2 to X-ray

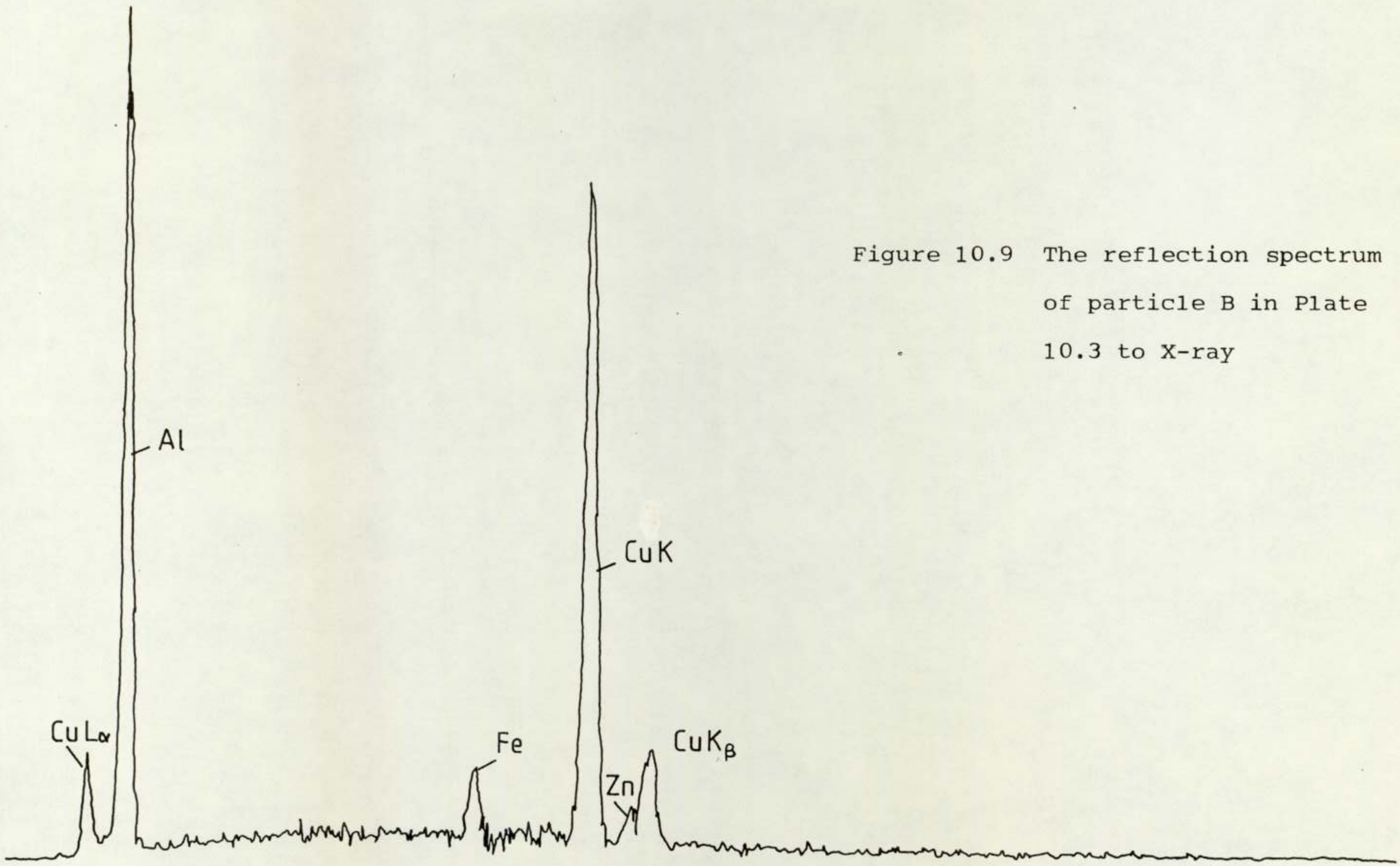

Figure 10.9 The reflection spectrum of particle B in Plate 10.3 to X-ray

growth. For example, in Plate 9.43 although the crack growth rate was accelerated at B due to the separation of the particle from the matrix the macro crack growth rate would not be changed due to the reduction of crack growth rates at A and C. Plate 10.4 suggests that the effect of the more fine dispersoids with a size of about 0.02 μm on fatigue crack growth rate could be neglected.

10.2.6.2 The Measurement of Fatigue Striation Spacings.

As mentioned previously the relationship of single striation to single-load-cycle was confirmed (38, 39, 41) within a certain range of FCGR. In present investigation this range is from 0.1 μm/cycle to 1 μm/cycle. The range could be various, and it depends on materials, environment and the resolution of the employed analysis instruments etc. Weiss and Lal (138) suggested a lower limit of 0.030 μm/cycle and according to Broek's results the lower limit is about 0.05 μm/cycle for 7075-76 and 2024-T3 aluminium alloy and the upper limit is about 1.0 μm/cycle.

Plates 9.17 - 9.22 suggest that at the lower stress intensity factor range ($\Delta K = 9.3\ MN/m^{3/2} - 12.0\ MN/m^{3/2}$) the crack fronts did not progress as an entity, but only some fractions of the crack grew small increment per load cycle and the "discontinuous striations" could not be formed until a number of redundant cycles elapsed.

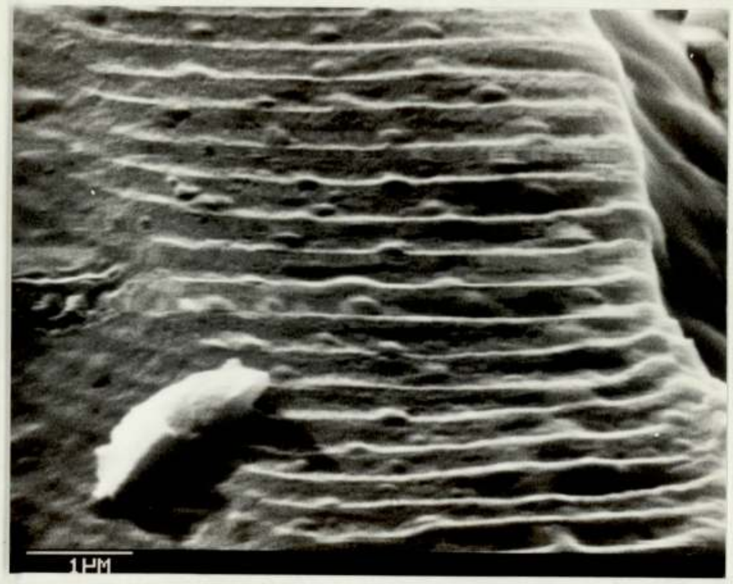

Plate 10.4 SEM micrograph showing the effect of fine dispersoids on fatigue crack growth.

At high stress intensity the fracture occured by mixed mechanisms of static fracture and fatigue striations. The mixed fracture surfaces of tearing, voids plus fatigue striations shown in Plates 9.46, 9.48 and 10.5 were taken from the sites where the corresponding stress intensity factor amplitudes were greater than 30 $MN/m^{3/2}$. As the static fracture occurred, so the measured striation spacings were less than the macrocrack growth rate at high stress intensity factor amplitudes. For example, the average striation spacing measured on Plate 9.45 and Plate 9.46 was 8.14 X 10^{-4}mm but the macrocrack growth rate was 11.12 X 10^{-4}mm/cycle.

From Fig.(9.24) it can be seen that the crack growth equation (Eq.(9.10)) fits the striation spacing data very well. Therefore, if the constants A and m in Paris equation have been determined and the fatigue striation measurements can be obtained for the material to be examined then the fractographic technique can be used to determine the local stress intensity factor range in failure analysis by the equation

$$S_p = A(\Delta K)^m \tag{10.3}$$

Unfortunately the exponent m varies with materials and loading variables and usually it has to be determined individually by experiments.

To take the response of materials into account Pearson (135) proposed a parameter $\frac{\Delta K}{E}$ to represent fatigue crack growth rate in a number of alloys, where E is Young's

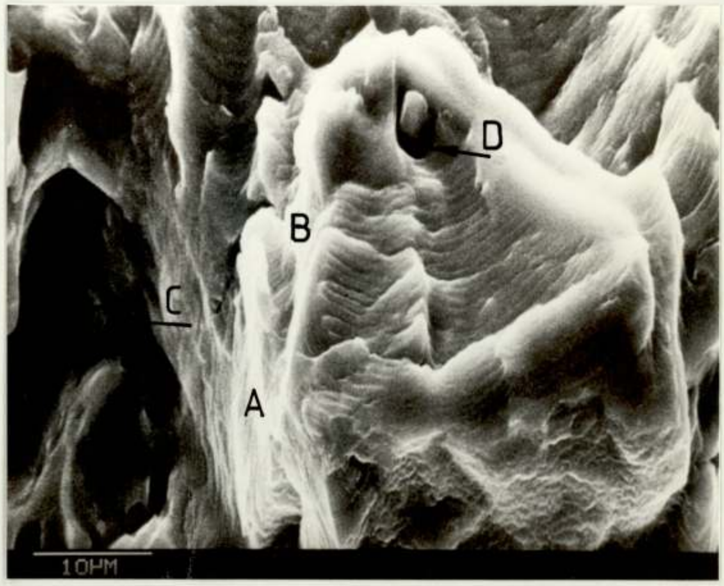

Plate 10.5 SEM fractograph showing mixed fracture mechanisms at high stress intensity factor. Fracture was occurred by the mechanism of striation formation, voids coarseness (at C and D) and tearing (at A and B).

modulus. Although the macroscopic crack growth rates were different for materials such as steel, titanium and aluminium, their crack growth rates could be normalised to a large extent by this parameter. Since the fatigue crack growth rates for the material under consideration can be represented by striation spacings, the relationship between $\frac{\Delta K}{E}$ and S_p was established, which is shown in Fig.10.10 and may be expresses by:

$$\text{Striation spacing; } S_p \simeq 4.5\left(\frac{\Delta K}{E}\right)^2 \qquad (10.4)$$

where the Young's modulus E is 10.28×10^3 KSi taken from (115). Bates and Clark (6) studied several metals and derived the similar equation shown in Eq.(10.5).

$$\text{Striation spacing; } S_p \simeq 6\left(\frac{\Delta K}{E}\right)^2 \qquad (10.5)$$

Since Eq.(10.4) was obtained under constant amplitude fatigue at R = 0.1, the effect of high stress ratio needs to be verified. The data obtained at R = 0.2, 0.4 and 0.5 shown in Fig,10.10 suggests that the simple expression of Eq.(10.4) could be used for high positive stress ratio without leading to a serious error. However, more tests are required before a more reliable expression of striation spacing versus $\frac{\Delta K}{E}$ for high stress ratio can be derived.

In the present work each data point presented in Figs. 9.23, 9.24 and 10.10 was obtained by measuring the average striation spacings on one or two micrographs which were taken in the interior region of the fracture surface using sharp notch specimens. It was found that

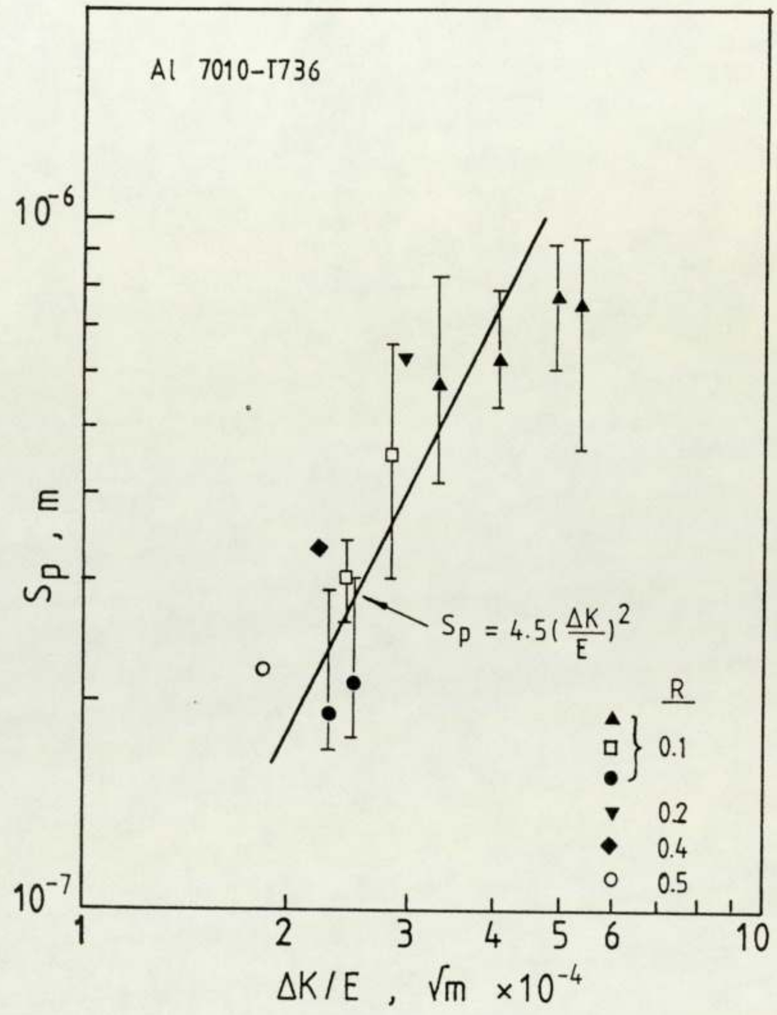

Figure 10.10 Fatigue striation spacing as a function of $\Delta K/E$ in aluminium alloy 7010 - T736

the fatigue crack grew basically uniformly through the thickness for sharp notch specimens and thus it is believed that the results were representive. The scatter bands for this method are shown in Fig.10.10, which is given in terms of the range of the striation spacings measured from ten to fifteen microscopic locations through the thickness direction at the same crack length. Scatter in these terms varies from a factor of 1.3 to 2.8 with 2 being typical.

It was found that the width of individual striation-bearing plateaux is different and Plumbridge (122) argued that this will give some variations to the measured growth rates represented by striation spacings. In the present experiments the effect of the width of striation-bearing plateaux on the measurement of striation spacings was examined. In Plate 9.41 the plateaux widths vary by up to an order of magnitude, (The narrowest one is about 0.0026mm. The widest is about 0.025mm) but the measured striation spacings on the two plateaux only vary by 20%. In Plate 9.38 the width of plateau A is twice the width of plateau B, but the measured striation spacings are almost the same. Thus, if the average value of striation spacing measured at different areas on the plates which include one or several plateaux is taken the effect of the width of plateau on the measurement of striation spacings could be neglected.

10.3 Variable Amplitude Fatigue

10.3.1 The Measurement of Crack Opening Stress Intensity Factor and Significance of the Effective Stress Intensity Factor Range on Crack Growth

For fractographic technique used in the present work it was assumed that no interaction of load sequence had to be considered when the maximum load was maintained constant (load programme 2 Fig.8.6). This assumption should be reasonable since the examination of the fracture surface showed no detectable difference in striation spacings within one block (see block 9. 10, 12 and 15 in Plates 9.49 and 9.50), indicating that no retardation or acceleration effects occurred during the transition of the application of cyclic loading for the programmed loads under consideration.

In the present investigation no attempt has been made to investigate crack closure systematically. The purpose of the measurements of K_{op} is to evaluate whether or not the applied stress intensity factor range ΔK should be replaced by the effective one, ΔK_{eff}, which was defined as $\Delta K_{eff} = K_{max} - K_{op}$, in the Paris law ($\frac{da}{dN} = A(\Delta K)^m$) under constant amplitude fatigue. The experimental results show that the ratio K_{op}/K_{max} is less than 0.2 at the stress intensity factor range 23.5 $MN/m^{3/2}$. Similar results have been obtained by Pelloux and his co-workers in 2124 - T351 aluminium alloy (114).

According to Elber's observation K_{op} was equal to 0.5 K_{max} for R = 0 loading and the ratio K_{op}/K_{max} decreased as R increased. The later results published by other investigators suggested that this was only true in the lower stress intensity region. Paris and Hermann (112, 136) found that the ratio K_{op}/K_{max} was about 0.5 at near threshold region but at higher stress intensity levels the ratio decreased to 0.23 under constant amplitude loading for stress ratio R = 0.05 in 2024 - T351 aluminium alloy. The results have been confirmed by McEvily (111, 112). In the near threshold region he found that the ratio was 0.4 to 0.5 at R = 0 loading and that it decreased to 0.1 as stress intensity factor increased. Lindley and Richards (108) tested a variety of steels and found that the crack closure vanished as the thickness of specimens increased using potential technique since the crack closure only occurred in the side, plane stress region, and thus the crack closure could not be detected by potential method.

The published results suggest that the crack closure phenomenon is a complex subject and results in great controversy over its relative importance (100, 136, 107). Experimental methods, specimen geometry and its compliance, crack length, applied stress intensity level and environment can all affect the experimental results of crack closure (107, 110, 109, 137). Considering the complex nature of crack closure and the limited results obtained it seems that K_{op} is at quite a low level for intermediate crack growth rates ($K_{op}/K_{max} < 0.2$) under constant amplitude loading. Moreover, there are some experimental difficulties with closure detection and interpretation of results obtained by different experiment methods. Thus, the application of ΔK_{eff} to Paris equation instead of ΔK is doubtful.

For lower crack growth rate (near threshold region), however, the concept of crack closure could be of importance to explain the existence of threshold and its variation affected by stress ratio and other factors. This indicates that striation spacings measured in the region of intermediate crack growth rates can be directly correlated with the applied stress intensity factor range without worrying about the effect of crack closure.

10.3.2 The Effect of Multiple Overloads on Fatigue Crack Growth

The study of retardation effects induced by multiple overloads at R_{oL} = 1.8, 1.5 and 1.2 showed that the retardation in crack growth did occur following the 20% overloads although only a moderate effect was observed. It was found that the retardation vanished within 200 - 350 cycles. The examination of fractography suggested the large stretch of material in near surface region to be responsible for the retardation in crack growth. This explained why the crack front after overload was more curved than that under constant amplitude loading.

The application of fractographic technique proved some advantages to study load sequence effects despite its limitation. No other methods can study the retardation effects following overloads cycle by cycle, for example, even if the delayed retardation phenomenon occurred within 20 cycles it still can be observed by fractographic method (Plate 9.55). The observation of fractography can clearly reveal the relative contribution of surface region and interior of the specimen to retardation effects in fatigue crack growth following the overloads.

It was noted that no significant retardation in fatigue crack growth was observed in the interior region of the specimen following the 20% multiple overloads. If the retardation effect ascribed to crack closure, this finding means that the level of crack closure in the interior of the specimen was not significantly affected by the overloads. However, in the near surface region the crack growth rates was retarded by a factor of 65%, indicating that the closure level was undoubtedly increased by the overloads.

Using potential technique Paris and Hermann (136) studied the opening load behaviour after a single overload of the order of 75% and found that two opening loads could be observed. The results are shown in Fig.10.11. They did not explain why there were two opening loads after overload. Compared with the results obtained in the present work the lower opening loads should be related to what occurs in the interior of the specimen

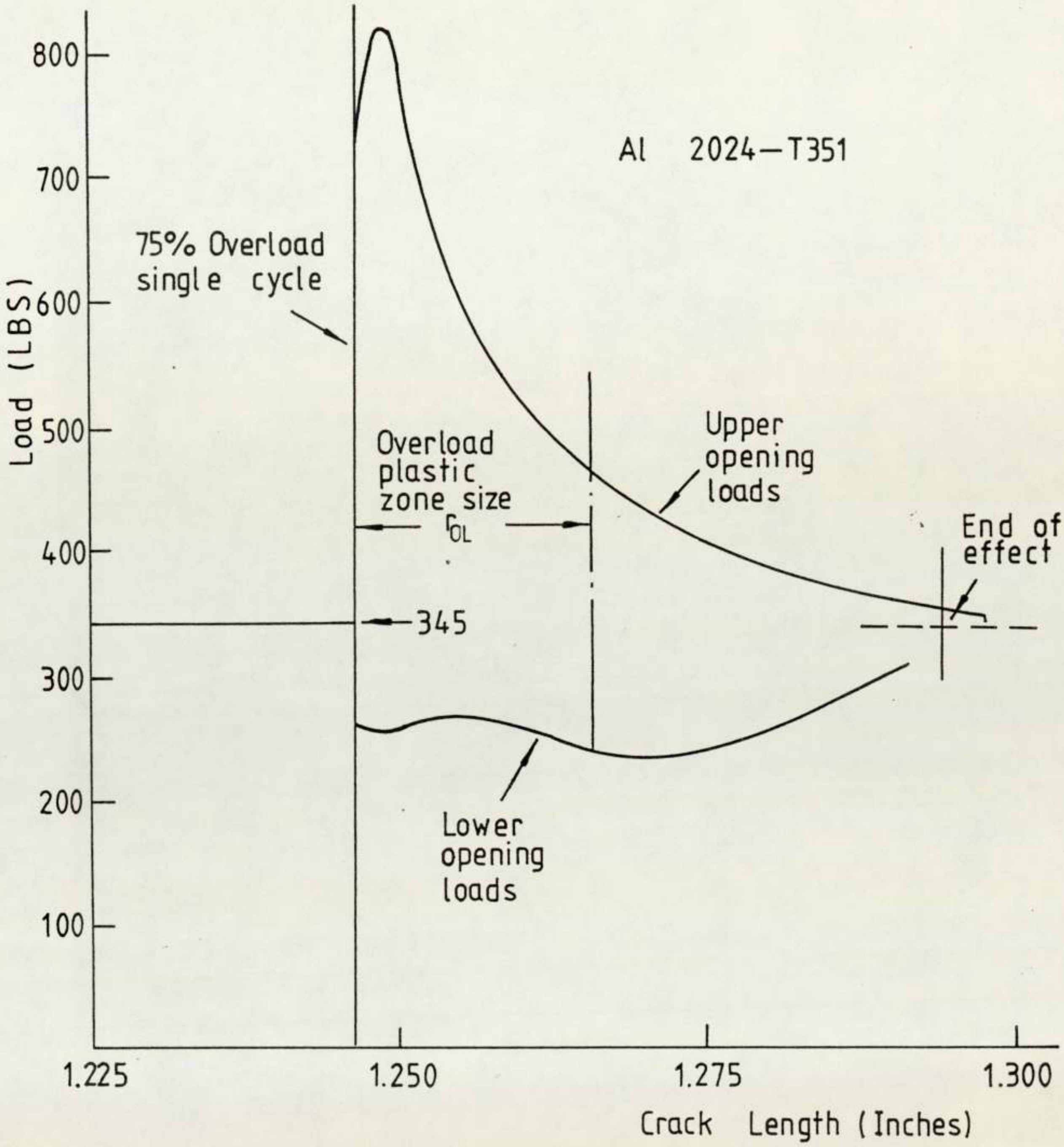

Figure 10.11 Dependence of lower and upper opening loads on crack length after 75% single overload cycle. (after Paris (136))

and the upper opening loads to what occurs in the near surface region. The limited results suggest that if an attempt was made to correlate crack growth rate with overload retardation effect the relative contribution of near surface region and interior region should be further considered.

10.3.3 Fatigue Crack Growth Under Block Spectrum Loads

The main problem for the approach of a characteristic stress intensity factor to predict the crack growth under variable amplitude fatigue is how to find such a stress intensity factor. Barsom (55, 113) studied the crack growth behaviour under various random-sequences, ordered-sequence and constant amplitude load fluctuations in a number of steels, and found that the average rate of fatigue crack growth could be represented by ΔK_{rms} using the Paris equation regardless of the order of occurrence of the cyclic load fluctuations. As far as author's knowledge no such investigation is available for aluminium alloys. The application of ΔK_{rms} for representation of the testing results in present experiments was based on the following consideration. The sequence of blocks in the programmed load spectrum (Programme 1) was random and the overload ratios for all blocks were less than 1.15 and most of them were less than 1.1 except the maximum overload ratio which was 1.17 occurred from block 11 to block 12. From the point of view of the whole programmed load spectrum it was assumed that the effect of load sequence on crack growth could be neglected without leading to serious error. However, the approach needs to be further appraised. One of the most reliable methods is to conduct experiments under constant amplitude cyclic loading with the same load variables as that of ΔK_{rms} and then the results are compared with that of realistic programmed block load spectrum. If the similar lifetimes are given by the two tests, ΔK_{rms} can be considered as an adequate equivalent characteristic parameter for prediction of fatigue crack growth; otherwise, the ΔK_{rms} can not be used.

In Figs.9.33 and 9.34 the transition point was observed for which the corresponding stress intensity factor range was about 6 $MN/m^{3/2}$. It was found that before the transition no striation can be observed on the fracture surface and after the transition the striation mechanism prevails. Probably this can be ascribed to the effect of crack closure.

From Plate 9.63 it can be seen that some patches (patch c) show striation-like marks but others (patch d) do not. The quantitative measurement confirmed the size of these patches to be of an order of grain size (S_c = 0.17mm, S_d = 0.06mm and average grain size = 0.08mm). Thus, it might be argued that the patches represented the response of the individual grain to fracture. When slip planes in the grains were oriented favourably with respect to the maximum resolved shear stresses at the advancing crack tip, the striation-like marks could be formed at the blocks with maximum load. Alternately, the striation-like marks could not be formed in the grains for which the slip planes were unfavourably oriented.

11. APPLICATION OF THE RESULTS

The results obtained in the present work suggest that the fracture mechanics approach could be used to design a notched component against fatigue failure. To predict the fatigue life for such components under constant amplitude loading three phases of the total life have to be considered as described previously.

$$N_t = N_i + N_s + N_f$$

All the three terms can be predicted by LEFM approach. To do this several pieces of information must be known as follows.

1. The stress intensity factor, K_I.
2. The fracture toughness, K_c.
3. The applicable fatigue crack initiation life expression.
4. The applicable fatigue crack growth rate expression.
5. The definition of crack initiation, a_i.
6. The critical crack size, a_c.

The K_I-expression for most configuration encountered in engineering practice can be found in literature. If the size of the component meets the plane strain condition then the K_{Ic} can also be found in references for most common engineering materials otherwise the K_c must be experimentally determined. The fatigue crack initiation life and growth rate expressions have to be established if no applicable expressions are available in literature. The definition of crack initiation is arbitrary and it is usually defined as a crack with a detectable length at lower magnification, which is 0.005 inch (0.127mm) being a typical value. The critical crack size can be estimated from K_{Ic} or K_c.

After the mentioned information is obtained then the fatigue life can be predicted as follows:

$$N_i = B\ (\Delta K)^n \qquad (11.1)$$

and N_s and N_f can be found by integrating the Paris equation:

$$\frac{da}{dN} = A\ (\Delta K)^m \qquad (11.2)$$

where ΔK is stress intensity factor range. For crack initiation and growth in the notch stress field the modified equation (Eq.(10.2)) should be used to calculate the stress intensity coefficient and beyond the notch stress field the standard expression is available. The extent of the notch stress field, C_o, can be estimated by $C_o = 0.5\ \sqrt{a_o \rho}$. For the notched member of alloy 7010 - T736 with the stress concentration factor ranged from 1.5 - 7.75 the constants in Eqs.(11.1) and (11.2) have been found as follows:

$$B = 2.25 \times 10^8$$

$$n = -4.0$$

$$A = 4.3926 \times 10^{-8}$$

$$m = 3.015$$

Using this design philosophy the fatigue life for the specimens used in the present work was calculated as follows:

$$N_t = N_i + N_s + N_f$$

$$= 2.25 \times 10^8 (\Delta K_n)^{-4} + \int_{a_i}^{a_n} \frac{da}{4.3926 \times 10^{-8} (\Delta K_n)^{3.015}}$$

$$+ \int_{a_n}^{a_f} \frac{da}{4.3926 \times 10^{-8} (\Delta K)^{3.015}}$$

where $a_i = a_o + C_i$

$a_n = a_o + C_o$

and a_f is a certain crack length. The N_s and N_f were calculated by numerical integration. The comparison between the calculated values and the experimental values is shown in Table 11.1 and Fig.11.1. It can be seen that the agreement is generally good when it is considered that all the three terms involve the experimentally determined constants.

The derived relationship between fatigue striation spacing and ΔK normalized with respect to elastic modulus, which was shown in Eq.(10.12), can be used in failure analysis to estimate local stress intensity factor range and local stress level if the K-expression is available.However, one must exercise care in using this technique. First, it is important to identify accurately the crack length position where the striation spacing measurements were made. Obviously, the stress level cannot be computed if the crack length is not known. The other problem is that the striation formation is a highly localized event, it depends on both the

Table 11.1

Comparison between the Calculated and Experimental

Fatigue Lives to a Certain Crack Length.

Specimen No.	Crack Length at Initiation C_i, mm	ΔK_n at Initiation $MN/m^{3/2}$	Final Crack Length C_f, mm	Experimental		Calculated	
				Cycles at Initiation	Cycles at C_f	Cycles at Initiation	Cycles at C_f
205	0.13	9.07	0.950	18940	37580	37237	58644
202	0.14	6.87	1.323	97200	198930	113129	182715
203	0.14	9.51	1.759	17700	42440	30809	62940
206	0.14	10.10	2.729	9888	33310	24216	62048
207	0.14	10.57	4.808	7764	34610	20188	64720
211	0.14	7.86	6.077	60800	246300	66025	183915
212	0.14	7.83	6.175	35400	194220	67043	186437
210	0.14	7.92	6.486	34700	154410	64047	180941
201	0.14	7.83	8.413	42330	177790	67043	192652
208	0.14	9.33	8.656	15520	92730	33256	107012
213	0.14	10.64	9.501	8160	45650	19662	70374
214	0.14	12.02	9.818	3792	26870	12072	46482
209	0.14	6.90	10.429	69670	352270	111174	296910

Table 11.1 (Contd.)

Specimen No.	Crack Length at Initiation C_i, mm	ΔK_n at Initiation $MN/m^{3/2}$	Final Crack Length C_f, mm	Experimental		Calculated	
				Cycles at Initiation	Cycles at C_f	Cycles at Initiation	Cycles at C_f
3506	0.12	7.29	0.451	90260	93970	89226	107238
3505	0.12	6.97	0.681	119500	131020	106775	129563
3507	0.11	7.91	1.511	85038	95050	64371	84220
3510	0.11	8.38	2.372	75560	84710	51100	69000
3511	0.12	8.97	3.504	19640	29350	38925	53957
3517	0.11	8.27	4.915	35300	49300	53874	75108
3516	0.12	6.83	5.470	182020	216350	115802	152344
3509	0.11	8.69	5.663	20160	33200	44190	62669

Table 11.1 (Contd.)

Specimen No.	Crack Length at Initiation C_i, mm	ΔK_n at Initiation $MN/m^{3/2}$	Final Crack Length C_f, mm	Experimental		Calculated	
				Cycles at Initiation	Cycles at C_f	Cycles at Initiation	Cycles at C_f
501	0.14	8.06	0.523	62700	86950	59711	74859
502	0.13	8.39	0.611	67300	72150	50857	64581
505	0.14	8.06	0.532	64240	71250	59711	73429
519	0.14	12.19	1.459	18428	19580	11413	16551
506	0.14	7.69	1.745	60120	69780	72060	93451
504	0.13	8.93	2.619	57000	64230	39627	54873
508	0.13	7.54	3.608	114400	135140	77968	93214
517	0.14	7.15	4.183	89950	105950	96422	122838
507	0.13	8.10	5.335	58980	-	58541	-

Table 11.1 (Contd.)

Specimen No.	Crack Length at Initiation C_i, mm	ΔK_n at Initiation $MN/m^{3/2}$	Final Crack Length C_f, mm	Experimental Cycles at Initiation	Experimental Cycles at C_f	Calculated Cycles at Initiation	Calculated Cycles at C_f
3004	0.13	9.77	0.898	37860	40330	27658	35857
3013	0.12	12.64	1.039	10660	11540	9872	13981
3005	0.13	9.69	1.357	45968	51830	28583	37655
3007	0.13	9.33	1.759	46060	53920	33256	43742
3016	0.12	8.44	2.250	67200	75200	49663	65176
3014	0.12	8.41	2.897	69760	79680	50375	65742
3009	0.13	8.65	2.902	110000	122500	45013	58310
3017	0.12	8.30	3.250	75880	84830	53099	69956
3010	0.13	8.12	4.112	109530	129570	57966	75191
3015	0.12	8.58	4.287	57700	67320	46500	62157

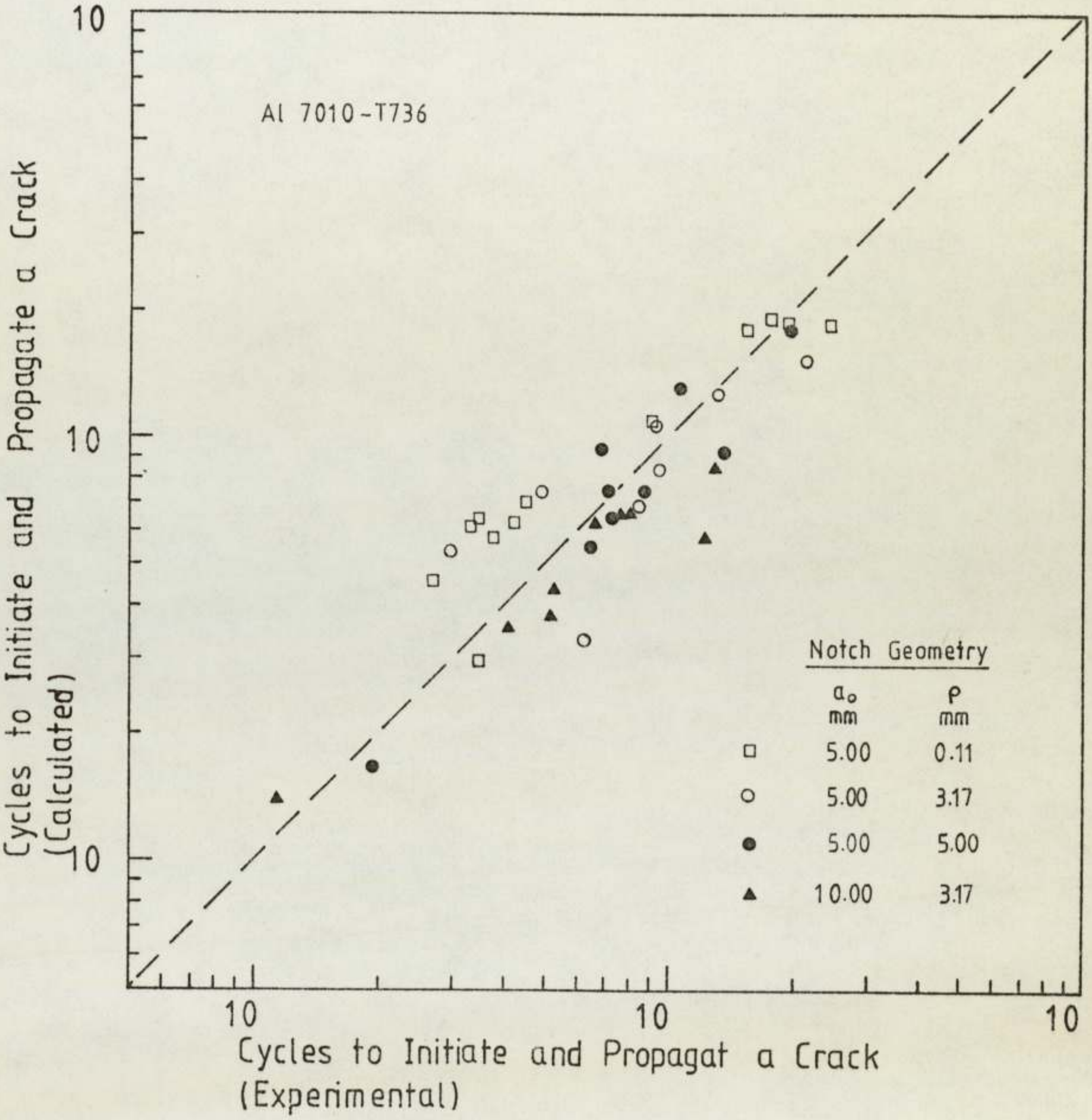

Figure 11.1 Comparison between the calculated and experimental fatigue lives to a certain crack length

stress intensity factor and metallurgical conditions. It has been found that the striation spacings in local regions may vary by a factor of 1.3 to 3. Therefore, to estimate a crack growth rate at a particular crack length many measurements of striation spacings should be made and the measurements should be further checked by measuring the striation spacings at different crack length positions.

12 CONCLUSIONS

1. The total fatigue lives of notched members may be predicted by adding up the following three quantities : number of cycles to initiate an engineering crack from the notch, N_i, the life of short crack propagation in notch stress field, N_s, and the life of long crack propagation beyond the notch stress field, N_f. All the three phases could be described by stress intensity approach.

2. The stress intensity factor coefficients for short crack were calibrated using the fatigue crack growth rates. The results could be expressed in the form

$$Y_n = Y_L \left[\frac{a_o \tanh\left(\dfrac{2\sqrt{1 + \dfrac{a_o}{\rho}(C + C_B)}}{\sqrt{a_o \rho}} \right) \pm (C + C_B)}{a_o \pm C} \right]^{\frac{1}{2}}$$

The definitions of a_o and C and the application of the positive or negative signs depend on the notch geometry.

3. The parameters $K_t \Delta S$ and $\Delta K / \sqrt{\rho}$ were not adequate for prediction of fatigue crack initiation from the notches with the stress concentration factors ranged from 1.5 to 7.75 in alloy 7010 - T736.

4. For the sharp notch specimens the cracks were initiated at multiple sites on the same fracture plane and a through thickness crack was formed at the very beginning of the crack propagation. However, the

initiated crack for blunt notch specimens was found to be in a semi-elliptical shape until the equivalent crack lengths were nearly 3mm, after which a through thickness crack was formed.

5. In alloy 7010 - T736 the coarse secondary intermetallic particle or particles could affect the fatigue crack growth significantly, especially when these particles were in a clustered form. The smaller intermetallic particles with a size of 1.0 μm - 3.0 μm generally showed the insignificant influence to fatigue crack growth at the intermediate stress intensity. The effect of fine dispersoids with a size of about 0.02 μm on stage II crack growth could be neglected.

6. The fatigue striations in alloy 7010 - T736 could be distinctly identified using SEM and TEM and it was found that the relationship of single striation to single cyclic load existed in the range of crack growth rate from 0.1 μm to 1.0 μm. The empirical equation of striation spacings and the normalized ΔK was derived and it could be represented by

$$\text{striation spacing, } S_p \approx 4.5\left(\frac{\Delta K}{E}\right)^2$$

7. Shot peening could slightly improve the resistance of alloy 7010 - T736 to initiation of cracks at lower load level but probably worse effect could be expected at higher load level. Once a crack was initiated from a peened surface, it grew more rapidly

than that for the unpeened case. The measurements of short crack growth rates could be used to estimate the distribution of residual stress induced by shot-peening and other processes.

8. The crack closure behaviour in alloy 7010 - T736 was quantitatively investigated by the fractographic technique. The measured K_{op}/K_{max} was less than 0.2. Therefore, it is concluded that in the Paris equation the application of the applied stress intensity factor range ΔK ($\Delta K = K_{max} - K_{min}$) is probably more reliable than the effective stress intensity factor range ΔK_{eff} ($\Delta K_{eff} = K_{max} - K_{op}$) under tension-tension constant amplitude cyclic loading due to the considerable low level of K_{op}/K_{max} and its complex nature.

9. The potential method is an applicable technique to study the effect of overloads on crack growth. It was found that the retardation in crack growth rates following overloads was a complex phenomenon. Besides the overload ratio many other factors such as crack length at which overloads were applied and the intervals between the occurances of the overloads could affect the retardation effects significantly. The examination of fracture surface at 20% multiple overloads suggested that the retardation effects mainly occurred in the near surface region.

10. The behaviour of alloy 7010 - T736 under the programmed block spectrum loads, which was simulated

and edited from a real service situation, was tested and the results were represented by characteristic stress intensity approach. The study of fractography suggested that the multiple overloads of 51 cycles could cause a considerable retardation effect in crack growth even if the overload ratio was only 1.17.

13 APPENDIX

Computer Programme for Processing of Fatigue Crack Growth Rate Data.

```
100 OPEN 128,4
115 CMD 128
116 LIST
118 DIM V(50),XN(50),A1(50),H(50),Q(50)
120 DIM XD(50),DADN(50),B(20),W(20),A0(20),P(20)
122 PRINT,,"****REPRESENTATION OF FATIGUE****"
123 PRINT,,"****CRACK GROWTH RATE DATA    ****"
124 PRINT
125 PRINT,," THE TYPE OF SPECIMEN IS 2XX"
126 PRINT
127 PRINT
128 PRINT"SPECIMEN NO. IS "
130 INPUT M,V0
134 C=0
136 D=0
138 E=0
140 F=0
142 G=0
144 NN=0
150 FOR J=1 TO M
170 INPUT B(J),W(J),A0(J),P(J)
171 PRINT"B(J)= ";B(J)
172 PRINT"W(J)= ";W(J)
173 PRINT"A0(J)=";A0(J)
174 PRINT"P(J)= ";P(J)
175 PRINT
176 PRINT
180 INPUT N
185 PRINT " P.D. "," NO-CLS"," LENGTH"," LENGTH"
186 PRINT " MICROV","NUMBER"," A0+C,MM","C,MM"
187 PRINT
190 FOR I=1 TO N
210 INPUT V(I),XN(I)
220 NEXT I
225 FOR I=1 TO N
250 PD=V(I)/V0/W(J)
260 AW=-0.415+1.263*PD-0.525*PD^2+0.087*PD^3
270 IF I=1 THEN 315
280 A1(I)=AW*W(J)-A1(1)+A0(J)
290 A=A1(I)-A0(J)
310 PRINT V(I),XN(I),INT(A1(I)*1000+.5)/1000,INT(A*1000+.5)/1000
312 GO TO 320
315 A1(I)=AW*W(J)
320 NEXT I
321 PRINT
322 PRINT
323 PRINT "ALENGTH","DLENGTH","DNUMBER"
324 PRINT "  MM   ","  MM   ","OF CYCLES"
325 PRINT
330 FOR I=3 TO N
340 A2=(A1(I)+A1(I-1))/2.0
350 AW=A2/W(J)
352 Y1=1.99-2.15*AW+6.08*AW^2-6.63*AW^3+2.7*AW^4
354 Y2=(1.0+2.0*AW)*(1.0-AW)^1.5
360 Y=Y1/Y2
370 BM=B(J)/1000.0
380 WM=W(J)/1000.0
390 A2=A2/1000.0
400 XD(I)=6.0*P(J)*Y*SQR(A2)/BM/WM
405 H(I)=LOG(XD(I))/2.30256
```

```
410 DD=A1(I)-A1(I-1)
420 DN=XN(I)-XN(I-1)
430 DADN(I)=DD/DN
435 Q(I)=LOG(DADN(I))/2.30256
440 A2=A2*1000.0
445 PRINT INT(A2*1000+.5)/1000,INT(DD*1000+.5)/1000,DN
450 NEXT I
451 PRINT
452 PRINT
453 PRINT " DELTK"," G-RATE"
454 PRINT
455 FOR I=3 TO N
456 PRINT INT(XD(I)*100+.5)/100,INT(DADN(I)*10E7+.5)/10E7
457 NEXT I
458 PRINT
460 PRINT
461 PRINT " LOGDK"," LOGGR"
462 PRINT
463 FOR I=3 TO N
464 PRINT INT(H(I)*1000+.5)/1000,Q(I)
465 NEXT I
470 NN=NN+N-3
472 FOR I=4 TO N
473 C=C+H(I)^2
475 D=D+Q(I)^2
480 E=E+H(I)*Q(I)
485 F=F+H(I)
490 G=G+Q(I)
495 NEXT I
496 PRINT
497 PRINT
498 PRINT
499 IF J=M THEN 504
502 PRINT"SPECIMEN NO. IS "
504 NEXT J
505 XL=C-F^2/NN
510 YL=D-G^2/NN
515 XYL=E-F*G/NN
520 XB=XYL/XL
525 XA=G/NN-XB*F/NN
530 R=XYL/(SQR(XL*YL))
540 XW=10.0^XA
550 PRINT"XB=";XB
560 PRINT"XW=";XW
570 PRINT"R= ";R
575 PRINT"NN=";NN
580 STOP
590 CLOSE 128,4
READYEND
```

14 REFERENCES

1. H.O.Fuches and R.I.Stephens, "Metal Fatigue in Engineering", John Wiley and Sons, 1980, P.1.

2. R.E.Peterson, "Discussions of a Century Ago Concerning the Nature of Fatigue, and Review of some of the Subsequent Researches Concerning the Mechanism of Fatigue", ASTM Bull. No.164, 1950, PP.50-54.

3. P.Paris and F.Erdogan, "A Critical Analysis of Crack Propagation Laws", J. bas. Eng. Trans., ASME, Ser. D. 85(4), 1963, PP.528-534.

4. J.T.Barnby and R.Holder, "Fatigue from Notches in Cast Steels", Met. Sci. Vol.11, 1977, PP.11-15.

5. V.B.Livesey and J.E.Knott, "The Initiation of Fatigue Cracks at Notches", Strength of Metals and Alloys, Vol.2, ICSMA 5, 1980, PP.1137-1144.

6. R.C.Bates and W.G.Clark, "Fractography and Fracture Mechanics", Trans. ASM., Vol.62, 1969, P.380.

7. R.W.Hertzberg and E.F.J.Von Euiv, "Crack Closure and Fatigue Striations in 2024-T3 Aluminium Alloy", Metallurgical Transaction of the American Institute of Mining, Metallurgical and Petroleum Engineers, Vol.4, 1973, PP.887-889.

8. J.Y.Mann, "Fatigue of Materials", Melbourne University Press, 1967, P.5.

9. J.Bauchinger, "On the Change of the Position of the Elastic Limit of Iron and Steel Under Cyclic Variations of Stress", English Abstract, J. Inst. Civil Engrs., 2, 1886-7, P.463.

10. J.A.Ewing and J.C.W.Humfrer, "The Fracture of Metals under Repeated Alternations of Stress", Phil. Trans. Roy. Soc. A200, 1903, P.241.

11. H.J.Gough and D.Hansen, "Behaviour of Metals Subjected to Repeated Stresses", Proc. Roy. Soc., A104, 1923, P.539.

12. A.A.Griffith, "The Phenomena of Rupture and Flow in Solids", Phil. Trans. Roy. Soc. (London), Series A., 221, 1920, PP.163-198.

13. H.Neuber, "Theory of Notches", J.W.Edwards, Am. Arbor, Mi., 1946.

14. M.A.Miner, "Cumulative Damage in Fatigue", Trans. ASME, J.Appl. Mech., Vol.67, 1945, P.A159.

15. G.R.Irwin, "Analysis of Stresses and Strains Near the End of Crack Traversing a Plate", Trans. ASME, J. Appl. Mech., Vol.24, 1957, P.361.

16. J.E.Travernelli and L.F.Coffin, Jr., "Experimental Support for Generalized Equation Predicting Low Cycle Fatigue", Trans. ASME, J. Bas. Eng., Vol.84, 1962, P.533.

17. S.S.Manson, Discussion of Ref.16., ibid, P.537.

18. A.S.Tetelman and A.J.McEvily, Jr., "Fracture of Structural Materials", John Wiley and Sons, 1967, PP. 347-400.

19. David Broek, "Elementary Engineering Fracture Mechanics", Noordhoff Int. Pub., 1974, PP.69-71.

20. Fracture Toughness Testing and Its Applications. ASTM STD 381, 1965.

21. H.Tada, P.Paris and G.Irwin, The Stress Analysis of Cracks Handbook, Del Research Corporation, 1977, P.2.16.

22. G.C.Sih, Handbook of Stress Intensity Factors, Bethlehem, Pennsylvania, Lehigh University, 1973.

23. C.E.Ingles, "Stresses in a Plate Due to the Presence of Cracks and Sharp Corners", Proc. Institute of Naval Architects, 1913, P.60.

24. J.T.Branby, "An Introduction to Fracture Toughness", Welding and Metal Fabrication, 1969, PP.71-75.

25. J.R.Rice, "Fatigue Crack Propagation", ASTM STP 415, 1967, PP.247-311.

26. F.A.McClintock and G.R.Irwin, "Fracture Toughness Testing and Its Applications", ASTM STP 381, 1965 PP.84-113.

27. G.R.Irwin, "Plastic Zone Near a Crack and Fracture Toughness", Proc., 7th Sagamore Conf., 1960, P.IV-63.

28. J.T.Barnby, Lectures, Univ. of Aston in Birmingham, 1981.

29. J.Lankford, D.L.Davidson and T.S.Cook, "Fatigue Crack Tip Plasticity", ASTM STP 637, 1977, PP.36-55.

30. M.R.Mitchell, "Fundamentals of Modern Fatigue Analysis for Design", Fatigue and Microstructure, ASM Mat. Sci. Seminar, 1978, PP.385-437.

31. David Broek, "Elementary Engineering Fracture Mechanics", Noordhoff Int. Pub., 1974, P.8.

32. W.J.Plumbridge and D.A.Ryder, "The Metallography of Fatigue", Metallurgical Reviews, Vol.136, 1969, PP.119-142.

33. Campbell Laird, "Mechanisms and Theories of Fatigue", Fatigue and Microstructure, ASM Mat. Sci. Seminar, 1978, PP.149-203.

34. H.O.Fuchs and R.I.Stephens, "Metal Fatigue in Engineering", John Wiley and Sons, 1980, PP.27-35.

35. W.Wood, "Fine Slip in Fatigue", Bull. Inst. Met., Vol.3, 1955, PP.5-6.

36. P.J.E.Forsyth , "The Physical Basis of Metal Fatigue", Blaklie and Son Limited, 1969, P.61.

37. M.E.Fine and R.O.Ritchie, "Fatigue Crack Initiation and Near Threshold Crack Growth", Fatigue and Microstructure, ASM Mat. Sci. Seminar, 1978, PP.250-251.

38. P.J.E.Forsyth, "Fatigue Damage and Crack Growth in Aluminium Alloys", Acta Metallurgical, Vol.11, 1963, PP.703-715.

39. D.Broek, "Some Contributions of Electron Fractography to the Theory of Fracture", Int. Met. Reviews, 185, Vol.19, 1974, PP.135-155 .

40. Metal Handbook, ASM, Vol.9, PP.64-78.

41. D.W.Hoeppner and W.E.Krupp, "Prediction of Component Life by Application of Fatigue Growth Knowledge", Eng. Fract. Mech., Vol.6, 1974, PP.47-70.

42. J.Weertman, "Fatigue Crack Propagation Theories", Fatigue and Microstructure, 1978, PP.279-306.

43. C.Laird and G.C.Smith, "Crack Propagation in High Stress Fatigue", Phil. Mag., 1962, PP.847-857.

44. P.Neumann, "The Geometry of Slip Processes at a Propagating Fatigue Crack - II", Acta. Met. 22, 1974, PP.1167-1178.

45. R.M.N.Pelloux, "Mechanisms of Formation of Ductile Fatigue Striations", Trans. ASM, 62, 1969, PP.281-285.

46. D.Broek and C.W.Bowles, "The Study of Fracture Surface Profiles in the Electron Microscope", Int. J. Fract. Mech., Vol.6, 1970, PP.321-322.

47. I.Lemay, "Failure Mechanisms and Metallography", Metallography in Failure Analysis, New York and London, 1977, PP.1-31.

48. H.O.Fuchs and R.I.Stephens, "Metal Fatigue in Engineering", John Wiley and Sons, 1980, P.67.

49. T.Duggan and J.Byrne, "Fatigue as a Design Criterion", The Macmillan Press Ltd., 1977, P.51.

50. A.S.Nadkarni, Ph.D. Thesis, 1981, University of Aston in Birmingham.

51. S.Pearson, "Fatigue Crack Initiation and Propagation in Half Inch (12.7mm) Thick Specimens of an Aluminium Alloy", Roy. Air. Estab., Tech. Report, 1971.

52. O.H.Basquin, "The Experimental Law of Endurance Tests", Proc. ASTM, Vol.10, Part II, 1919, P.625.

53. S.S.Manson, "Fatigue A Complex Subject, Some Simple Approximations", Exp. Mech., Vol.5, 1965, PP.192-226.

54. D.W.Hoeppner and W.E.Krupp, "Prediction of Component Life by Application of Fatigue Crack Growth Knowledge", Eng. Fract. Mech., Vol.6, 1974, PP.47-70.

55. S.T.Rolfe and J.M.Barsom, "Fracture and Fatigue Control in Structure", Prentice-Hall, Inc., 1977, PP.237-240.

56. H.O.Fuchs and R.I.Stephens, "Metal Fatigue in Engineering", John Wiley and Sons, 1980, PP.56-99.

57. R.G.Forman, V.E.Kearney and R.M.Engle, "Numerical Analysis of Crack Propagation in Cyclic-Loaded Structures", Trans. ASME., J. Bas. Eng., Vol.89, No.3, 1967, P.459.

58. T.C.Lindley and L.N.McCartney, "Mechanics and Mechanisms of Fatigue Crack Growth", Developments in Fracture Mechanics - 2, Appl. Sci. Pub., 1981, PP.292-293.

59. H.O.Fuchs and R.I.Stephens, "Metal Fatigue in Engineering", John Wiley and Sons, 1980, P.301.

60. P.E.Irving and L.N.McCartney, "Prediction of Fatigue Crack Growth Rates : Theory, Mechanisms and Experimental Results", Met. Sci., Aug. and Sept., 1977, P.351.

61. R.M.Wetzel, "Smooth Specimen Simulation of Fatigue Behaviour of Notches", J. Mat., Vol.3, 1968, PP.647-657.

62. T.H.Topper, R.M.Wetzel and Dean Morrow, "Neuber's Rule Applied to Fatigue of Notched Specimens", J. Mat., Vol.4, No.1, 1969, PP.200-209.

63. M.R.Mitchell, "Fundamentals of Modern Fatigue Analysis for Design", Fatigue and Microstructure, ASM Mat. Sci. Seminar, 1978, PP.385-437.

64. D.F.Socie, "Fatigue Life Estimates for Bluntly Notched Members", J. Eng. Mat. Tech., Vol.102, 1980, PP.153-157.

65. J.Morrow and D.F.Socie, "The Evolution of Fatigue Crack Initiation Life Prediction Methods", Proc. Fatig. '81, Mat. Exp. Des. Fatig., 1981, PP.3-21.

66. N.Dowling, "Notched Member Fatigue Life Predictions Combining Crack Initiation and Propagation", Fatigue of Engineering Materials and Structure, Vol.2, 1979, PP.129-138.

67. J.T.Barnby and R.Holder, "Fatigue from Notches in Cast Steels", Mat. Sci., Vol.11, 1977, PP.11-15.

68. A.R.Jack and A.T.Price, "The Initiation of Fatigue Cracks from Notches in Mild Steel Plates", Int. J. Fract. Mech., Vol.6, 1970, PP.401-409.

69. R.G.Forman, "Study of Fatigue Crack Initiation from Flaws Using Fracture Mechanics Theory", Eng. Fract. Mech., 6, 1972, P.333.

70 Y.Yamamoto, "Stress Intensity Factors for Cracks in Notch Bend Specimens for Three-Point Bending", Int. J. Fract., Vol.12, 1976, PP.495-497.

71. H.A.Jergeus, "A Simple Formula for the Stress Intensity Factors of Cracks in Side Notches", Int. J. Fract., Vol.14, 1978, PP.R113-116.

72. S.T.Rolfe and J.M.Barsom, "Fracture and Fatigue Control in Structures", Prentice-Hall Inc., 1977, PP.208-229.

73. R.Holder, "Fatigue Crack Initiation from Stress Concentrations in Cast Steels", Ph.D. Thesis, 1976, University of Aston in Birmingham.

74. R.E.Peterson, "Stress Concentration Factors", John Wiley and Sons, New York, 1974.

75. H.J.Grover, "Fatigue of Aircraft Structures", NAVAIR 01 - 1A - 13 Department of the Navy, 1966.

76. B.A.Bilby and P.T.Heald, "Crack Growth in Notch Fatigue", Proc. Roy. Soc., A. 305, 1968, PP.429-439.

77. J.M.Barsom and R.C.McNicol, "Effect of Stress Concentration on Fatigue Crack Initiation in HY - 130 Steel", ASTM STP 559, ASTM, Philadelphia, 1974.

78. Y.H.Kim, T.Mura and M.E.Fine, "Fatigue Crack Initiation and Microcrack Growth in 4140 Steel", Met. Trans. A, ASM, Vol.9A, 1978, PP.1679-1683.

79. J.T.Barnby and A.S.Nadkarni, "Fatigue Crack Growth from Notches", to be published.

80. R.A.Smith, "A Simplified Method of Predicting the Rates of Growth of Cracks Initiated at Notches", Fracture Mechanics in Engineering Practice, 1976, PP.173-182.

81. R.A.Smith and K.J.Miller, "Prediction of Fatigue Regimes in Notched Components", Int. J. Mech. Sci., Vol.20, 1978, PP.201-206.

82. R.A.Smith and K.J.Miller, "Fatigue Cracks at Notches", Int. J. Mech. Sci., Vol.19, 1977, PP.11-22.

83. S.Novak and J.Barsom, "Brittle Fracture (K_{Ic}) Behaviour of Cracks Emanating from Notches", ASTM STP 601, ASTM 1976, PP.409-447.

84. "Metal Handbook", American Society for Metals, Vol.2, 8th Edition, PP.402.

85. G.E.Nordmark, "Peening Increase Fatigue Strength of Welded Aluminium", Metal Progress, Nov.,1963, PP.101-103.

86. J.E.Campbell, "Shot Peening for Improved Fatigue Properties and Stress-Corrosion Resistance", MCIC Report, Metals and Ceramics Information Centre, 1971, PP.28-31.

87. G.S.Was and R.M.Pelloux, "The Effect of Shot-Peening on the Fatigue Behaviour of Alloy 7075-T6", AIME, Vol.10A, May, 1979, P.3.

88. D.O.Sprowls and R.H.Brown, "What Every Engineer Should Know About Stress Corrosion of Aluminium", Metal Progress, Vol.81, May, 1962.

89. R.A.Paulkner, "The Effects of Various Peening Processes on the Axial Fatigue Properties of Light Alloys", Report, Hawker Siddeley Aviation Ltd., 1971.

90. SAE Standard, "Test Strip, Holder and Gauge for Shot-Peening - SAE J442 Aug. 79", SAE Handbook, Part 1, 1982, P.9.05.

91. M.A.Miner, "Cumulative Damage in Fatigue", Trans. ASME, J. Appl. Mech., Vol.67, Sept., 1945, PP.A159-A164.

92. R.W.Landgraf, F.D.Richards and Lapointe, "Fatigue Life Predictions for a Notched Member Under Complex Load Histories", Fatigue Under Complex Loading, SAE 1977, PP.97-106.

93. D.V.Nelson and H.O.Fuchs, "Predictions of Cumulative Fatigue Damage Using Condensed Load Histories", ibid, PP.147-163.

94. BSI, BS5400 : Part 10 : 1980, Steel, Concrete and Composite Bridges, Part 10, Code of Practice for Fatigue, British Standards Institution, Gr.9.

95. D.F.Socie and P.J.Artwohl, "Effect of Spectrum Editing on Fatigue Crack Initiation and Propagation in a Notched Member", Effect of Load Spectrum Variables on Fatigue Crack Initiation and Propagation, ASTM STP 714, D.F.Bryan and J.M.Potter, Eds., 1980, PP.3-23.

96. J.R.Carroll, Jr., "Time Dependent Changes in Notch Stress/Notch Strain and Their Effects on Crack Initiation", ibid, PP.24-40.

97. R.C.Rice and R.I.Stephens, "Overload Effects on Subcritical Crack Growth in Austenitic Manganese Steels," Progress in Flaw Growth and Fracture Toughness Testing, ASTM STP 536, ASTM 1973, PP.95-114.

98. J.Schijve,"Prediction Methods for Fatigue Crack Growth in Aircraft Material", Fracture Mechanics, ASTM STP 700, ASTM 1980, PP.3-34 .

99. P.R.Abelkis, "Use of Microfractography in the Study of Fatigue Crack Propagation under Spectrum Loading", Fractography in Failure Analysis, ASTM STP 645, ASTM 1978, PP.213-234.

100. W.Schutz, "The Prediction of Fatigue Life in the Crack Initiation and Propagation Stages - A State of the Art Survey", Eng. Fract. Mech., Vol.11, 1979, PP.405-421.

101. J.B.Chang, R.M.Engle and J.Stolpested, "Fatigue Crack Growth Behaviour and Life Predictions for 2219-T851 Aluminium Subjected to Variable-Amplitude Loadings", Fracture Mechanics, ASTM STP 743, ASTM 1981, PP.3-27.

102. A.U.de Koning, "A Simple Crack Closure Model for Prediction of Fatigue Crack Growth Rates under Variable-Amplitude Loading", ibid, PP.63-85.

103. R.Sunder, "A Mathematical Model of Fatigue Crack Propagation under Variable Amplitude Loading", Eng. Fract. Mech. Vol.12, 1979, PP.155-165.

104. O.E.Wheeler, "Spectrum Loading and Crack Growth", Trans. ASME, J. Basic Eng., Vol.94, 1972, PP.181-186.

105. J.Willenborg, R.M.Engle and H.A.Wood, "A Crack Growth Retardation Model Using an Effective Stress Concept", WPAFB, TM-71-1-FBR, 1971.

106. W.Elber, "The Significance of Fatigue Crack Closure", Damage Tolerance in Aircraft Structures, ASTM STP 486, ASTM 1971, P.230.

107. K.D.Unangst, T.T.Shih and R.P.Wei, "Crack Closure in 2219-T851 Aluminium Alloy", Eng. Fract. Mech., Vol.9, 1977, PP.725-734.

108. T.C.Lindley and C.E.Richards, "The Relevance of Crack Closure to Fatigue Crack Propagation", Mat. Sci. Eng., 14, 1974, PP.281-293.

109. V.Bachmann and D.Munz, "Fatigue Crack Closure Evaluation with the Potential Method", Eng. Fract. Mech., Vol.11, 1979, PP.61-71.

110. G.R.Chanani and M.J.Mays, "Observation of Crack-Closure Behaviour after Single Overload Cycles in 7075-T6 Single-Edge-Notched Specimens", ibid, Vol.9, 1977, PP.65-73.

111. A.J.McEvily, "On Crack Closure in Fatigue Crack Growth", Fracture, Vol.4, ICF4, 1977. PP.39-42.

112. A.J.McEvily, "Current Aspects of Fatigue", Met. Sci., Aug/Sept., 1977, PP.274-283.

113. J.M.Barsom, "Fatigue Crack Growth under Variable-Amplitude Loading in ASTM A514-B Steel", ASTM STP 536, ASTM 1973, PP.147-162.

114. R.M.Pelloux, M.Faral and W.M.McGee, "Fractographic Measurements of Crack-Tip Closure", Fracture Mechanics, ASTM STP 700, ASTM 1980, PP.35-48.

115. P.E.Fitzsimmons, "A Review of the Properties of Alcan 7010 Plate", Alcan Plate Ltd., 1979.

116. J.G.Harris, "Aluminium Alloy 7010 Plate", Alcan Booth Sheet Ltd., 1976.

117. H.H.Johnson, "Calibrating the Electric Potential Method for Studying Slow Crack Growth", Material Research Standards, Vol.5, 1965, PP.442-445.

118. C.Li and R.P.Wei, "Calibrating the Electrical Potential Method for Studying Slow Crack Growth", ibid, Vol.6, 1966, PP.392-394.

119. D.M.Gilbey and S.Pearson, "Measurement of the Length of a Central or Edge Crack in a Sheet of Metal by an Electrical Resistance Method", RAE Technical Report No.66402, 1966.

120. R.J.Cooke and J.L.Robinson, "Some Further Consideration of the Potential Drop Method for Measuring Crack Length", Internal Report, Dept. of Physical Metallurgy and Science of Materials, Univ. of Birmingham.

121. G.Clark and J.F.Knott, "Measurement of Fatigue Crack in Notched Specimens by Means of Theoretical Electrical Potential Calibrations", J. Mech. Phys. Solids, Vol.23, 1975, PP.265-276.

122. W.J.Plumbridge, "Problems Associated with Early Stage Fatigue Crack Growth", Met. Sci., Vol.12, 1978, PP.251-256.

123. Standard Test Methods for Plane-Strain Fracture Toughness of Metallic Materials , E399-80, Annual Book of ASTM Standards, ASTM, 1981.

124. P.Wood and T.Richards, "Stress Concentration Factors for Some Blunt Notched Three Point Bend Fracture Specimens", Internal Report, Univ. of Aston in Birmingham, 1977.

125. J.E.Srawley, "Wide Range Stress Intensity Factor Expression for ASTM E399 Standard Fracture Toughness Specimens," Int. J. Fract., Vol.12, June 1976, PP.475-476.

126. H.Tada, P.C.Paris and G.R.Irwin, "The Stress Analysis of Crack Handbook", Development Research Corporation, Hellertown, 1973 .

127. R.J.Bucci, A.B.Thakker, T.H.Sanders, R.R.Sawtell and J.T.Staley, "Ranking 7XXX Aluminium Alloy Fatigue Crack Growth Resistance under Constant Amplitude and Spectrum Loading", Effect of Load Spectrum Variables on Fatigue Crack Initiation and Propagation, ASTM STP 714, 1980, PP.41-78.

128. R.O.Ritchie and K.J.Bathe, "On the Calibration of the electrical potential technique for monitoring crack growth using finite element methods", Int. J. Fract., Vol.15, 1979, PP.47-55.

129. R.P.Wei and R.L.Brazill, "An assessment of A-C and D-C potential systems for monitoring fatigue crack growth", Fatigue Crack Growth Measurement and Data Analysis, ASTM STP 738, 1981, PP.103-119.

130. H.Neuber, "Theory of Notch Stresses", Springer Publishers, 1958, PP.19-22.

131. J.E.Campbell, "Shot Peening for Improved Fatigue Properties and Stress-Corrosion Resistance", MCIC Report, Metals and Ceramics Information Centre, 1971, PP.41-43.

132. D.F.Ostergaard, J.R.Thomas and B.M.Hillberry, "Effect of Δa-increment on calculating $\frac{da}{dN}$ from a versus N data", Fatigue Crack Growth Measurement and Data Analysis, ASTM STP 738, 1981, PP.194-204.

133. M.E.Artley, J.P.Gallagher and H.D.Stalnaker, "Variations in Crack Grwoth Rate Behaviour", Fracture Mechanics, ASTM STP 677, 1979, PP.54-67.

134. T.H.Sanders, Jr., and J.T.Saley, "Review of Fatigue and Fracture Research on High-Strength Aluminium Alloys", Fatigue and Microstructure, ASM Mat. Sci. Seminar, 1978, PP.467-522.

135. S.Pearson, "Fatigue Crack Propagation in Metals", Nature, Vol.211, 1966, P.1077.

136. P.C.Paris, "Twenty Years of Reflection on Questions Involving Fatigue Crack Growth".

137. T.C.Lindley and L.N.McCartney, "Mechanics and Mechanisms of Fatigue Crack Growth", Developments in Fracture Mechanics - 2, Appl. Sci. Pub., 1981, PP.275-290.

138. D.N.Lai and V.Weiss, 'A notch analysis of fracture approach to fatigue crack propagation, 'Metall. Trans. Vol.94, March 1978, pp.413-425